

Electronic Thesis and Dissertation Repository

3-7-2022 2:30 PM

Small Molecule Activation and Catalysis by Low Valent Group 14 Compounds

Sarah Louise McOnie, *The University of Western Ontario*

Supervisor: Baines, Kim M., *The University of Western Ontario*

A thesis submitted in partial fulfillment of the requirements for the Doctor of Philosophy degree in Chemistry

© Sarah Louise McOnie 2022

Follow this and additional works at: <https://ir.lib.uwo.ca/etd>

Recommended Citation

McOnie, Sarah Louise, "Small Molecule Activation and Catalysis by Low Valent Group 14 Compounds" (2022). *Electronic Thesis and Dissertation Repository*. 8434.
<https://ir.lib.uwo.ca/etd/8434>

This Dissertation/Thesis is brought to you for free and open access by Scholarship@Western. It has been accepted for inclusion in Electronic Thesis and Dissertation Repository by an authorized administrator of Scholarship@Western. For more information, please contact wlsadmin@uwo.ca.

Abstract

The work described in this thesis focuses on three main themes: small molecule activation by ditetrelenes, the Lewis acidity assessment of low valent germanium(II) and tin(II) crown ether complexes and catalysis by low valent germanium(II) and tin(II) crown ether complexes. The activation of ammonia and amines using tetramesityldisilene and digermene was explored synthetically and the lowest energy path to ammonia activation by tetramesityldisilene was computed. The results of the mechanistic analysis have implications for the reactions of disilenes and digermenes with nucleophiles. Subsequent functionalization of the ditetrelene-amine adducts with electrophilic alkynes was attempted, highlighting the significant challenges in the area of secondary functionalization using ditetrelenes.

The Lewis acidities of selected germanium(II) and tin(II) crown ether complexes were examined both synthetically and computationally. In the addition of triethylphosphine oxide to the germanium(II) and tin(II) crown ether complexes following the Gutmann-Beckett method, mixtures of species derived from the coordination of multiple phosphine oxide equivalents and displacement of the crown ether were observed. These results have implications for the standard procedure of the Gutmann-Beckett method in which exclusively one equivalent of phosphine oxide is assumed to coordinate. The Lewis acidity of Ge^{2+} was found to be higher than that of Sn^{2+} .

Lewis acid-catalyzed hydrosilylation of carbonyl compounds was explored using the germanium(II) and tin(II) crown ether complexes as catalysts. Only the germanium(II) crown ether complexes were found to selectively reduce aldehydes efficiently and selectively to one product. The scope of aldehyde reduction was explored using $[\text{Ge}([\mathbf{12}]\text{crown-4})_2][\text{OTf}]_2$

revealing tolerance of the reaction for a number of functional groups, excluding those containing nitrogen. Lower conversions to reduced products was observed in ketone hydrosilylation using $[\text{Ge}(\text{[12]crown-4})_2][\text{OTf}]_2$ as a catalyst. Preliminary studies on the mechanism of addition revealed the first step is consistent with hydrosilylation and that the catalysis is derived from the germanium(II) centre. This study includes the first extensive substrate scope of hydrosilylation by a cationic germanium(II) compound.

The mechanism of aldehyde reduction catalyzed by $[\text{Ge}(\text{[12]crown-4})_2][\text{OTf}]_2$ was probed using a number of experimental techniques including the stoichiometric addition of silane and aldehyde, deuterium labelling studies, a Hammett analysis and Variable Time Normalization Analysis. The results of the experiments were consistent with carbonyl-activation and is the first study to implement Linear Free Energy Relationships to examine the reduction of aldehydes catalyzed by low valent Group 14 compound.

Keywords

Germanium • Tin • Lewis Acidity • Lewis Acid Catalysis • Crown ether • Group 14 • Hydrosilylation • Mechanistic analysis • Ditetrelenes • Small molecule activation

Summary for Lay Audience

Catalysis is an important field of chemistry, implemented heavily in industry, which uses a catalyst to enable the efficient, cost-effective and high-yielding production of important chemicals, such as pharmaceuticals, in reactions. Most catalysts are composed of transition-metals; however, their low abundance in the Earth's crust and high cost of extraction has prompted investigations into alternative catalysts to transition metals.

One alternative to transition metals are Lewis acids, which have been shown to catalyze similar reactions. Although many examples of catalysis by compounds composed of elements in Group 13 of the periodic table have been reported, fewer investigations into compounds containing Group 14 elements have been reported. One underexplored area of Group 14 compounds are compounds of germanium and tin, which have not been used extensively as catalysts. This thesis focuses on catalysis by the germanium and tin compounds.

The ability of the germanium and tin compounds to act as catalysts was assessed using a common reaction. In this reaction, a carbon-oxygen double bond is reduced to a carbon-oxygen single bond. The germanium compounds were shown to catalyze this reaction, while the analogous tin compounds were not effective catalysts. Using a number of chemical methods, a mechanism, the description of individual steps in a reaction, was proposed.

Co-Authorship Statement

This thesis includes work from two previously published manuscripts in Chapter 2.

The first article presented in Chapter 2 was coauthored by S. L. McOnie, G. A. Özpınar, J. L. Bourque, T. Müller and K. M. Baines, *Dalton Trans.*, **2021**, *50*, 17734-17750. SLM performed all synthetic experiments and NMR characterization in this work. JLB collected and solved the X-ray crystallographic data. GAO performed all theoretical calculations. The manuscript was prepared and edited by SLM, GAO, TM and KMB.

The second article presented in Chapter 2 was coauthored by S. L. McOnie and K. M. Baines, *Phosphorus Sulfur*, **2022**, *197*, 7-12. SLM performed all synthetic experiments and characterization work. SLM and KMB contributed to the preparation and editing of the manuscript.

The computational work presented in Chapter 3 was performed in collaboration with Andrew T. Henry.

Acknowledgments

First and foremost, I would like to thank my supervisor, Kim Baines. I am extremely grateful for the support and guidance she has provided throughout the course of my PhD. Nothing seemed to be straight forward in the projects I undertook during my PhD and so Kim's knowledge and expertise was invaluable. I am also very grateful for the opportunities Kim has allowed me to experience including presenting at national and international conferences, developing course materials and lecturing which have undoubtedly allowed for me to develop into a well-rounded scientist. The thorough and thoughtful editing of this thesis by Kim has certainly improved my writing skills and shaped this thesis into something of which I am very proud. Thank you Kim for always being kind and helpful and for allowing me to complete a PhD in your research group.

Secondly, I would like to thank the past and present members of the Baines group. I would like to thank Andrew and Zahra for listening to me rant all the time, for all the good laughs and also for being supportive during the trying times that have happened over the course of the chaotic year and a half plus of COVID. I wish both of you the best of luck in the completion of your theses. I would also like to thank Bahar Farhadpour for her help and training at the beginning of my PhD which got me started in the right direction. I would also like to thank Jeremy Bourque for being a great labmate and friend even beyond his time in the Baines group.

I would like to especially thank Mat Willans for his technical support, NMR expertise and for the many conversations about NMR and life in general. My thesis relied heavily on NMR experiments and Mat has always been willing and able to set up and test all the

'unusual' experiments I wanted to try. Throughout my PhD, I have encountered nearly every possible spectrometer issue which Mat was always able to fix. I would also like to thank Doug Hairsine for his assistance with mass spectrometry and Paul Boyle for his assistance with X-ray crystallography.

Finally, I would like to thank my parents and grandparents for supporting me in pursuing my dreams. None of this would have been possible without your love and support.

Table of Contents

Abstract.....	ii
Summary for Lay Audience.....	iv
Co-Authorship Statement.....	v
Acknowledgments.....	vi
Table of Contents.....	viii
List of Tables.....	xiv
List of Figures.....	xvi
List of Schemes.....	xx
List of Figures and Tables in the Appendices.....	xxiii
List of Abbreviations.....	xxix
Chapter 1.....	1
1 Introduction.....	1
1.1 Main Group Lewis Acids of Group 13 and 14.....	2
1.2 Small Molecule Activation by Ditetrelenes.....	5
1.2.1 Structure and Bonding in Ditetrelenes.....	5
1.2.2 Reactivity of Ditetrelenes.....	8
1.3 Lewis Acid Catalysis by Tetrylenes.....	10
1.3.1 Structure and Bonding of Tetrylenes.....	10
1.3.2 Lewis Acid Catalysis by Tetrylenes.....	12
1.3.3 Structure and Bonding in Crown Ether Complexes of Germanium(II) and Tin(II).....	13
1.4 Scope of Thesis.....	20
1.5 References.....	22
Chapter 2.....	31

2	Amine Functionalization by Ditetrelenes.....	31
2.1	Introduction.....	31
2.2	The Addition of Amines to Ditetrelenes.....	39
2.2.1	Experimental Results and Discussion.....	39
2.2.2	Computational Results and Discussion.....	43
2.2.3	Comparison to Previously Proposed Mechanisms.....	51
2.3	Silylation Using Disilylamines.....	56
2.3.1	Experimental Results of Discussion.....	56
2.4	Conclusions.....	63
2.5	Experimental.....	65
2.5.1	General Experimental.....	65
2.5.2	Preparation of Disilylamines 2.3-2.7	66
2.5.3	Preparation of Digermylamines 2.8 and 2.9	69
2.5.4	X-ray Crystallographic Details for 2.3	70
2.5.5	Computational Details.....	71
2.5.6	General Procedure for Silylated Enamine Synthesis.....	72
2.6	References.....	75
	Chapter 3.....	83
3	Lewis Acidity Assessment of Group 14 Crown Ether Complexes.....	83
3.1	Introduction.....	83
3.2	Gutmann-Beckett Results for Group 14 Crown Ether Complexes.....	86
3.3	Analysis of the Solution-State Structures of the Tin(II) Crown Ether-TEPO Adducts.....	89
3.3.1	[Sn([12]crown-4)₂][OTf]₂	89
3.3.2	Sn(OTf)₂	93
3.3.3	[Sn([18]crown-6)][OTf]₂	95

3.3.4	[SnCl([18]crown-6)][SnCl ₃]	99
3.4	Analysis of the Solution-State Structures of the Germanium(II) Crown Ether-TEPO Adducts	105
3.4.1	[Ge([12]crown-4) ₂][OTf] ₂	105
3.4.2	[Ge([18]crown-6)][OTf] ₂	108
3.4.3	[GeCl([18]crown-6)][GeCl ₃]	110
3.5	Discussion of Gutmann-Beckett Results	112
3.6	Comparisons of the Lewis Acidities of Ge(II) and Sn(II) Species and Literature Results	117
3.7	Litchenberg-Modified Gutmann-Beckett Method	122
3.8	Fluoride Ion Affinity Method	126
3.8.1	Computational Results	126
3.8.2	Comparison of FIA and Gutmann-Beckett Results	131
3.9	Other Lewis Acidity Assessments	132
3.10	Preliminary Studies of Lewis Acid Catalysis of the Ge(II) and Sn(II) Crown Ether Triflate Salts	132
3.11	Summary and Conclusions	134
3.12	Experimental	135
3.12.1	General Experimental	135
3.12.2	Synthesis of New Complexes	136
3.12.3	Lewis Acidity Assessment of Ge (II) and Sn(II) Crown Ether Complexes using the Gutmann-Beckett Method (Table 3.1)	138
3.12.4	The 2:1 Additions of TEPO to Ge(II) and Sn(II) Crown Ether Complexes for VT-NMR	139
3.12.5	Titration of [SnCl([18]crown-6)][OTf] ₂	139
3.12.6	Lewis Acidity Assessment of Ge(II) and Sn(II) Crown Ether Complexes using Litchenberg-Modified Gutmann-Beckett (Table 3.4)	140
3.12.7	Lewis Acidity Assessment of Ge(II) and Sn(II) Crown Ether Complexes using Child's Method	140

3.12.8	Lewis Acidity Assessment of Germanium(II) and Tin(II) crown ether complexes using the Fluorobenzonitrile Method.....	140
3.12.9	Computational Details	141
3.13	References.....	143
Chapter 4	150
4	Carbonyl Reduction by Group 14 Crown Ether Complexes.....	150
4.1	Introduction.....	150
4.2	Aldehyde Reduction Results.....	153
4.2.1	Aldehyde Reduction by Group 14 Crown Ether Triflate Salts	153
4.2.2	Aldehyde Reduction by Group 14 Crown Ether Trichlorometallate Salts	156
4.2.3	Optimization of Aldehyde Etherification by $[\text{Ge}(\mathbf{12}\text{crown-4})_2][\text{OTf}]_2$	160
4.2.4	Substrate Scope for Aldehyde Etherification Catalyzed by $[\text{Ge}(\mathbf{12}\text{crown-4})_2][\text{OTf}]_2$	164
4.2.5	Comparisons of the Performances of Other Main Group Catalysts in Hydrosilylation/Etherification Reactions.....	168
4.3	Ketone Reduction.....	171
4.3.1	Ketone Reduction Catalyzed by Group 14 Crown Ether Triflate Salts ..	171
4.4	Preliminary Mechanistic Studies into Aldehyde Hydrosilylation by $[\text{Ge}(\mathbf{12}\text{crown-4})_2][\text{OTf}]_2$	176
4.4.1	Etherification of Silyl Ether IIb	176
4.4.2	Ruling out Brønsted Acid Catalysis in the Etherification of Aldehydes by $[\text{Ge}(\mathbf{12}\text{crown-4})_2][\text{OTf}]_2$	177
4.4.3	Ruling out Silyl Cation Catalysis in the Etherification of Aldehydes by $[\text{Ge}(\mathbf{12}\text{crown-4})_2][\text{OTf}]_2$	179
4.5	Summary and Conclusions	180
4.6	Experimental	181
4.6.1	General Experimental	181
4.6.2	General Catalytic Methods for the Etherification of Aldehydes	182

4.6.3	General Catalytic Method for the Reduction of Ketones (Tables 4.7 & 4.8)	183
4.6.4	NMR Data for Synthesized Compounds	184
4.6.5	Conversion of Silyl Ether IIIb to Symmetric Ether I	185
4.6.6	Test for Brønsted Acid Catalysis	186
4.7	References	187
Chapter 5		192
5	Mechanistic Study on the Etherification of Aldehydes by $[\text{Ge}([\text{12crown-4}]_2)[\text{OTf}]_2]$	192
5.1	Introduction	192
5.2	Results and Discussion	197
5.2.1	Stoichiometric Additions to $[\text{Ge}([\text{12crown-4}]_2)[\text{OTf}]_2]$	197
5.3	Crown Ether Coordination in the Active Catalyst	201
5.4	Hammett Analysis and Proposed Mechanism	203
5.5	Deuterium Labelling and Kinetic Isotope Effect	210
5.6	Reaction Order Determination Using Visual Kinetic Analysis	212
5.7	Comparison to Silane-Activated Mechanism by Group 13 Catalysts	214
5.8	Summary and Conclusions	216
5.9	Experimental	217
5.9.1	General Experimental	217
5.9.2	Stoichiometric Additions to $[\text{Ge}([\text{12crown-4}]_2)[\text{OTf}]_2]$	218
5.9.3	Stoichiometric Additions to $\text{B}(\text{C}_6\text{F}_5)_3$	219
5.9.4	Hammett Study	220
5.9.5	Deuterium Labelling Experiments	221
5.9.6	Visual Kinetic Analysis	221
5.10	References	226
Chapter 6		228

6	Summary, Conclusions and Future Work	228
6.1	Summary and Conclusions	228
6.2	Future Work	231
6.2.1	Experimental Determination of <i>Anti</i> or <i>Syn</i> Ammonia Addition to a Disilene	231
6.3	Lewis Acidity Assessments	232
6.4	Other Lewis Acid Catalysis	234
6.5	Kinetic Isotope Effect Studies	235
6.6	Mechanistic Study on the Hydrosilylation and Etherification of Aldehydes by Group 14 Crown Ether Trichlorometallate Salts	235
6.7	References	236
	Appendices.....	238
	Appendix A : Supplementary Materials for Chapter 2	238
	Appendix B: Supplementary Material for Chapter 3	256
	Appendix C: Supplementary Material for Chapter 4	273
	Appendix D: Supplementary Material for Chapter 5	274
	Appendix E: Copyright Permissions for Articles/Figures	277
	Curriculum Vitae	304

List of Tables

Table 2.1 Silylamination of electrophilic alkynes.	58
Table 3.1 The Gutmann-Beckett Acceptor number (AN) and ³¹ P NMR chemical shifts for the addition of TEPO to main group Lewis acids in DCM.	87
Table 3.2 The Gutmann-Beckett ANs of the germanium(II)- and tin(II)-TEPO complexes generated from the addition of TEPO to germanium(II) and tin(II) crown ether complexes.	113
Table 3.3 ANs for the the coordination of one and two equivalents of TEPO to bis(catecholato)silanes and -germanes.....	119
Table 3.4 The Litchenberg-Modified Gutmann-Beckett Acceptor Number (AN ^{LM}) and ³¹ P NMR chemical shifts for the addition of TMPS to main group Lewis acids in DCM.	123
Table 3.5 The FIAs of various germanium(II) and tin(II) crown ether species calculated at B3LYP D3(BJ)/def2-TZVPP level of theory	127
Table 3.6 Reduction of 4-methylbenzaldehyde with pentamethyldisiloxane catalyzed by germanium(II) and tin(II) crown ether complexes.....	133
Table 3.7 Calculated data for the determination of the FIA values of the germanium(II) and tin(II) crown ether complexes.	142
Table 3.8 The anchor point data used in the determination of FIA values.	142
Table 4.1 Etherification of 4-methylbenzaldehyde by germanium(II) or tin(II) triflate salts in the presence of silane.	155
Table 4.2 Etherification of 4-methylbenzaldehyde in the presence of silane catalyzed by tin(II) or germanium(II) trichlorogermanate salts.....	158
Table 4.3 The influence of catalyst loading and time on the etherification of 4-methylbenzaldehyde in the presence of silane catalyzed by germanium(II) triflate complexes.	161

Table 4.4 The influence of solvent on the yield of I in the etherification of 4-methylbenzaldehyde in the presence of silane catalyzed by $[\text{Ge}([\mathbf{12}]\text{crown-4})_2][\text{OTf}]_2$	162
Table 4.5 The influence of silane on the yield of I in the etherification of 4-methylbenzaldehyde catalyzed by $[\text{Ge}([\mathbf{12}]\text{crown-4})_2][\text{OTf}]_2$	164
Table 4.6 Summary of aldehyde reduction using silanes as the reducing agent catalyzed by main group catalysts.	169
Table 4.7 Aldehyde reduction catalyzed by germanium(II) and tin(II) triflate salts.	173
Table 4.8 Ketone reduction catalyzed by $[\text{Ge}([\mathbf{12}]\text{crown-4})_2][\text{OTf}]_2$	174

List of Figures

Figure 1.1 Lewis acid-base adduct formation with Group 13 complexes.	2
Figure 1.2 3-centre-4-electron bonding in bis(catecholato)silanes and -germanes	4
Figure 1.3 The general structures of a) cations of Group 14 b) tetrylenes and c) ditetrelenes. The orbital available for reactivity is shown.....	5
Figure 1.4 The structures of <i>trans</i> -bent and twisted ditetrelenes and planar alkenes.	6
Figure 1.5 Bonding in alkenes and one interpretation of the bonding in ditetrelenes as dimers of tetrylenes.....	7
Figure 1.6 Interactions of the π and σ^* orbitals in ditetrelenes.	8
Figure 1.7 Reactivity of ditetrelenes.	9
Figure 1.8 The addition of ammonia and hydrogen to a bis(imino)bis(silyl)disilene.	10
Figure 1.9 Examples of the different structures of tetrylenes: a) a diarylstannylene b) a germylene stabilized by a β -diketiminate ligand and c) an N-heterocyclic carbene-stabilized silylene	11
Figure 1.10 a) The ambiphilic character of tetrylenes b) an anionic silylene and c) a cationic germylene.....	12
Figure 1.11 Structure of some cationic crown ether complexes: a) the first reported cationic tin(II) crown ether complex b) a dicationic germanium(II) crown ether complex and c) a dicationic tin(II) crown ether complex	14
Figure 1.12 Displacement ellipsoid plots of a) [Ge([12]crown-4)₂][GeCl₃]₂ , b) [Sn([12]crown-4)₂][OTf]₂ and c) [Sn([15]crown-5)₂][OTf]₂ . Ellipsoids are drawn at the 50% probability.....	16
Figure 1.13 Displacement ellipsoid plots of a) [Ge([18]crown-6)][OTf]₂ b) [Ge([15]crown- 5)][OTf]₂ and c) [Sn([18]crown-6)][OTf]₂ . Ellipsoids are drawn at the 50% probability. ..	17

Figure 1.14 a) Displacement ellipsoid plot of [GeCl([15]crown-5)][GeCl₃] . b) The solid-state structure of [SnCl([18]crown-8)][SnCl₃]	18
Figure 2.1 Displacement ellipsoid plot of 2.3	42
Figure 2.2 Newman projections for species along Path A and Path B.	45
Figure 2.3 Relative free energies (in kcal/mol, at 298 K and 1 atm) for Path 4	48
Figure 2.4 Energetics of Path 4 computed using the dimer of ammonia.....	50
Figure 2.5 NOESY correlations observed in a) 2.13 <i>E</i> -c confirming formation of the <i>E</i> isomer and b) 2.14c confirming the formation of the <i>E</i> -enamine.....	60
Figure 3.1 Germanium(II) and tin(II) crown ether-stabilized complexes studied in this work.	86
Figure 3.2 ¹¹⁹ Sn{ ¹ H} and ³¹ P{ ¹ H} NMR spectra of the addition of two equivalents of TEPO to [Sn([12]crown-4)₂][OTf]₂ at room temperature (a/b) and -80 °C (c/d).....	91
Figure 3.3 The solid-state structures of a) [Sn([12]crown-4)₂][OTf]₂ and b) [Sn([15]crown-5)₂][OTf]₂	93
Figure 3.4 ¹¹⁹ Sn{ ¹ H} NMR spectra and ³¹ P{ ¹ H} NMR spectra of the addition of TEPO to Sn(OTf) ₂ at room temperature (a/b) and -80 °C (c/d).....	94
Figure 3.5 ¹¹⁹ Sn{ ¹ H} and ³¹ P{ ¹ H} NMR spectra of the addition of two equivalents of TEPO to [Sn([18]crown-6)][OTf]₂ at room temperature (a/b) and -80 °C (c/d).....	96
Figure 3.6 The solid state structure of [Sn([18]crown-6)][OTf]₂	97
Figure 3.7 ¹¹⁹ Sn{ ¹ H} NMR spectra of the addition of two equivalents of TEPO to [SnCl([18]crown-6)][SnCl₃] at room temperature (a/b) and -80 °C (c/d).....	100
Figure 3.8 a) Stack plot of the ¹¹⁹ Sn{ ¹ H} NMR spectra for additions in which the ratio of SnCl ₂ : [SnCl₂(TEPO)₂] is varied. b) Stack plot of the ³¹ P{ ¹ H} NMR spectra for additions in which the ratio of SnCl ₂ : [SnCl₂(TEPO)₂] is varied.....	103

Figure 3.9 Two possible dimers of $[\text{SnCl}_2(\text{TEPO})_2]$	104
Figure 3.10 The solid state structures of a) $[\text{Ge}(\text{[15]crown-5})][\text{OTf}]_2$ b) $[\text{Ge}(\text{[18]crown-6})][\text{OTf}]_2$	109
Figure 3.11 Summary of reactivity with TEPO and germanium(II) and tin(II) species at room temperature.	115
Figure 3.12 Cationic Lewis acids and their corresponding Gutmann-Beckett AN.	120
Figure 3.13 Silicon dications assessed using the FIA method.....	130
Figure 3.14 Plot of the Gutmann-Beckett Method AN and FIAs for the cationic germanium(II) and tin(II) crown ether complexes.....	132
Figure 3.15 The change in ^{31}P NMR chemical shift when TEPO is added to $[\text{SnCl}(\text{[18]crown-6})][\text{SnCl}_3]$	139
Figure 4.1 Germanium(II) and tin(II) crown ether-stabilized complexes studied in this work.	153
Figure 4.2 Substrate scope for the etherification of aldehydes with TES catalyzed by $[\text{Ge}(\text{[12]crown-4})_2][\text{OTf}]_2$	166
Figure 5.1 The Lewis acid-catalyzed hydrosilylation of carbonyl compounds through a) a carbonyl-activated pathway and b) through a silane-activated pathway.	193
Figure 5.2 ^1H NMR spectra (600 MHz, CD_2Cl_2) for a) 4-dimethylaminobenzaldehyde, b) the addition of 4-dimethylaminobenzaldehyde to $[\text{Ge}(\text{[12]crown-4})_2][\text{OTf}]_2$, c) the addition of 4-dimethylaminobenzaldehyde to $[\text{Sn}(\text{[12]crown-4})_2][\text{OTf}]_2$	198
Figure 5.3 a) The ^1H NMR (400 MHz, CD_2Cl_2) spectrum 4-dimethylaminobenzaldehyde and b) the ^1H NMR (400 MHz, CD_2Cl_2) spectrum for the addition of 4-dimethylaminobenzaldehyde to $\text{B}(\text{C}_6\text{F}_5)_3$	200
Figure 5.4 a) The ^1H NMR (400 MHz, CD_2Cl_2) spectrum of <i>N,N</i> -dimethylaniline, b) the ^1H NMR (400 MHz, CD_2Cl_2) spectrum for the addition of <i>N,N</i> -dimethylaniline to $\text{B}(\text{C}_6\text{F}_5)_3$ and	

c) the ^1H NMR (400 MHz, CD_2Cl_2) spectrum for the addition of <i>N,N</i> -dimethylaniline to $[\text{Ge}([\text{12}]\text{crown-4})_2][\text{OTf}]_2$	201
Figure 5.5 The change in the ^1H NMR chemical shift of a) the signals assigned to the crown ether hydrogens in $[\text{Ge}([\text{12}]\text{crown-4})_2][\text{OTf}]_2$ over time and b) the signals assigned to the methylene hydrogens of 1,1'-[oxybis(methylene)]bis[4-methyl-benzene].	203
Figure 5.6 Hammett plot for the hydrosilylation of benzaldehydes catalyzed by $[\text{Ge}([\text{12}]\text{crown-4})_2][\text{OTf}]_2$	204
Figure 5.7 Proposed mechanism for the hydrosilylation of aldehyde catalyzed by $[\text{Ge}([\text{12}]\text{crown-4})_2][\text{OTf}]_2$	208
Figure 5.8 a) LUMO of $[\text{Ge}([\text{12}]\text{crown-4})_2]^{2+}$ and b) LUMO+1 of $[\text{Ge}([\text{12}]\text{crown-4})_2]^{2+}$. Geometries were optimized using PBEh-3c/def2-mSVP.	210
Figure 5.9 The VTNA plots for aldehyde etherification with the best visual correlations for a) triethylsilane, b) 4-methylbenzaldehyde and c) $[\text{Ge}([\text{12}]\text{crown-4})_2][\text{OTf}]_2$	213
Figure 5.10 Proposed mechanism for the formation of the silyl ether and symmetric ether using $\text{Ga}(\text{OTf})_3$	215
Figure 5.11 The VTNA plots for aldehyde etherification for 4-methylbenzaldehyde.	223
Figure 5.12 The VTNA plots for aldehyde etherification for triethylsilane.	224
Figure 5.13 The VTNA plots for aldehyde etherification for $[\text{Ge}([\text{12}]\text{crown-4})_2][\text{OTf}]_2$	225
Figure 6.1 a) The structures of some disilenes with known stereochemistry. b) Possible reaction pathway for the addition of ammonia to a disilenes I-Z showing both possible donor adducts and the two possible reaction products.	232
Figure 6.2 Proposed FIA calculations with the germanium(II) and tin(II) crown ether complexes.	233

List of Schemes

Scheme 1.1 a) Hydrosilylation of alkenes by $[\text{SiCp}^*][\text{B}(\text{C}_6\text{F}_5)_4]$, b) hydrosilylation of aldehydes and ketones by $[\text{GeCp}^*][\text{B}(\text{C}_6\text{F}_5)_4]$ c) hydroboration of aldehydes by $[\text{GeNN}][\text{OTf}]$	13
Scheme 1.2 The addition of ammonia and water to $[\text{Ge}(\text{15crown-5})][\text{OTf}]_2$	19
Scheme 2.1 N-H Bond activation of ammonia by a) disilenes I, II, III and b) VII to yield silylated amines.....	32
Scheme 2.2 Suggested mechanisms for E-H (E = N, O) bond activations of disilenes.....	34
Scheme 2.3 Reversible addition of acetonitrile to tetramesityldigermene	37
Scheme 2.4 Plausible pathway for the step-wise functionalization of amines by tetramesityldisilene.	37
Scheme 2.5 a) Silyl- and germylation of diethyl acetylenedicarboxylate b) Silylation of dimethyl acetylenedicarboxylate.....	39
Scheme 2.6 Addition of amines to ditetrelenes.	40
Scheme 2.7 Summary of Paths 1 – 4 examined in this work.....	44
Scheme 2.8 Attempted silylation of diethylacetylene dicarboxylate with disilylamine adducts 2.3-2.7	56
Scheme 2.9 Addition of $\text{Ph}_3\text{GeNMe}_2$ to dimethylacetylene dicarboxylate. The yields reported are NMR yields.	63
Scheme 3.1 The addition of TEPO to $[\text{Sn}(\text{12crown-4})_2][\text{OTf}]_2$ at room temperature.	91
Scheme 3.2 The reaction of $[\text{Sn}(\text{12crown-4})_2][\text{OTf}]_2$ and TEPO at room temperature and -80 °C.	93
Scheme 3.3 The addition of TEPO to $\text{Sn}(\text{OTf})_2$ at room temperature or -80 °C.....	95

Scheme 3.4 The addition of TEPO to $[\text{Sn}([\mathbf{18}\text{crown-6}][\text{OTf}]_2]$ at room temperature.	97
Scheme 3.5 The reaction of $[\text{Sn}([\mathbf{18}\text{crown-6}][\text{OTf}]_2]$ and TEPO at room temperature and -80 °C.	98
Scheme 3.6 The addition of TEPO to $[\text{SnCl}([\mathbf{18}\text{crown-6}][\text{SnCl}_3])]$	100
Scheme 3.7 Proposed mechanism for the formation of $[\text{SnCl}_2(\text{TEPO})_2]$ from two equivalents of TEPO and $[\text{SnCl}([\mathbf{18}\text{crown-6}][\text{SnCl}_3])]$	100
Scheme 3.8 The addition of TEPO to I to form $[\text{SnCl}_2(\text{TEPO})_2]$ and relevant chemical shift data.	101
Scheme 3.9 The reaction of $[\text{Ge}([\mathbf{12}\text{crown-4}]_2)[\text{OTf}]_2]$ and TEPO.	107
Scheme 3.10 The addition of TEPO to $[\text{Ge}([\mathbf{18}\text{crown-6}][\text{OTf}]_2)]$ at RT and -80 °C.	109
Scheme 3.11 The addition of TEPO to a) $[\text{GeCl}([\mathbf{18}\text{crown-6}][\text{GeCl}_3])]$ and b) GeCl₂·dioxane	110
Scheme 3.12 The addition of one equivalent of TEPO to tris(imidazolyl)amine complexes of germanium(II) and tin(II).	121
Scheme 4.1 a) The crosslinking of polysiloxane chains using a platinum catalyst and b) hydrosilylation of alkenes by $[\text{SiCp}^*][\text{B}(\text{C}_6\text{F}_5)_4]$ and c) hydrosilylation of aldehydes by $[\text{GeCp}^*][\text{B}(\text{C}_6\text{F}_5)_4]$	151
Scheme 4.2 Representative synthesis of the germanium(II) and tin(II) crown ether complexes	152
Scheme 4.3 The formation of $[\text{MCl}_2(\text{TEPO})_2]$ (M = Ge, Sn) through chloride displacement.	160
Scheme 4.4 The hydrosilylation of paraldehyde using $[\text{GeCp}^*][\text{B}(\text{C}_6\text{F}_5)_4]$ as a catalyst and either dimethylphenylsilane or triisopropylsilane as the silane source.	164

Scheme 4.5 Conversion of 4-methylbenzyl triethylsilyl ether to 1,1'-[oxybis(methylene)]bis[4-methyl-benzene] in the presence of [Ge([12]crown-4) ₂][OTf] ₂	177
Scheme 4.6 Etherification of 4-methylbenzaldehyde with PMDS in the presence of 2,6-di-tert-butylpyridine. Mole percent is relative to the aldehyde concentration.	178
Scheme 4.7 Proposed coordination of 2,6-di-tert-butylpyridine to [Ge([12]crown-4) ₂][OTf] ₂	178
Scheme 5.1 Etherification of an aldehyde by a germanium(II) crown ether catalyst.	194
Scheme 5.2 Proposed pathway for the formation of silyl ethers from aldehydes and silanes catalyzed by [Si(cat ^F) ₂]	195
Scheme 5.3 Proposed pathway for the formation of symmetric ethers from aldehydes and silanes catalyzed by [MCp*][B(C ₆ F ₅) ₄]	196
Scheme 5.4 The coordination of triethylsilane to a boraindene.....	196
Scheme 5.5 Competition experiment in the hydrosilylation of benzaldehyde and substituted benzaldehydes.	204
Scheme 5.6 The three elementary steps in carbonyl-activated hydrosilylation.....	206
Scheme 5.7 Incorporation of deuterium into 1,1'-[oxybis(methylene)]bis[4-methyl-benzene].	211
Scheme 6.1 a) The influence of AlCl ₃ on the Diels alder reaction between 2-methyl-1,3-butadiene and methyl acrylate and b) the mechanism of Lewis acid Diels alder catalysis. .	234
Scheme 6.2 The reaction of <i>para</i> -substituted benzaldehydes and triethylsilane- <i>d</i>	235

List of Figures and Tables in the Appendices

AA Table 1 Summary of crystal data for 2.3	238
AA Figure 1 ^1H NMR spectrum (600 MHz, C_6D_6) of 2.3	239
AA Figure 2 $^{13}\text{C}\{^1\text{H}\}$ NMR spectrum (151 MHz, C_6D_6) of 2.3	240
AA Figure 3 ^1H - ^{29}Si gHMBC spectrum (C_6D_6) of 2.3	240
AA Figure 4 ^1H NMR spectrum (600 MHz, C_6D_6) of 2.4	241
AA Figure 5 $^{13}\text{C}\{^1\text{H}\}$ NMR spectrum (151 MHz, C_6D_6) of 2.4	241
AA Figure 6 ^1H - ^{29}Si gHMBC spectrum (C_6D_6) of 2.4	242
AA Figure 7 ^1H NMR spectrum (600 MHz, C_6D_6) of 2.5	242
AA Figure 8 $^{13}\text{C}\{^1\text{H}\}$ NMR spectrum (151 MHz, C_6D_6) of 2.5	243
AA Figure 9 ^1H - ^{29}Si gHMBC spectrum (C_6D_6) of 2.5	243
AA Figure 10 ^1H NMR spectrum (600 MHz, C_6D_6) of 2.6	244
AA Figure 11 $^{13}\text{C}\{^1\text{H}\}$ NMR spectrum (151 MHz, C_6D_6) of 2.6	244
AA Figure 12 ^1H - ^{29}Si gHMBC spectrum (C_6D_6) of 2.6	245
AA Figure 13 ^1H NMR spectrum (600 MHz, C_6D_6) of 2.7	245
AA Figure 14 $^{13}\text{C}\{^1\text{H}\}$ NMR spectrum (151 MHz, C_6D_6) of 2.7	246
AA Figure 15 ^1H - ^{29}Si gHMBC spectrum (C_6D_6) of 2.7	246
AA Figure 16 ^1H NMR spectrum (600 MHz, C_6D_6) of crude 2.8	247
AA Figure 17 $^{13}\text{C}\{^1\text{H}\}$ NMR spectrum (151 MHz, C_6D_6) of crude 2.8	247
AA Figure 18 ^1H NMR spectrum (600 MHz, C_6D_6) of crude 2.9	248

AA Figure 19 ^1H NMR spectrum of the reaction of N, N-dimethyl(trimethylsilylamine) and dimethyl acetylenedicarboxylate	248
AA Figure 20 $^{13}\text{C}\{^1\text{H}\}$ NMR spectrum for the reaction of N, N-dimethyl(trimethylsilylamine) and dimethyl acetylenedicarboxylate	249
AA Figure 21 ^1H - ^{29}Si HMBC NMR spectrum of the reaction of N, N-dimethyl(trimethylsilylamine) and dimethyl acetylenedicarboxylate	249
AA Figure 22 ^1H NMR spectrum of the reaction of N, N-dimethyl(trimethylsilylamine) and diethyl acetylenedicarboxylate.....	250
AA Figure 23 $^{13}\text{C}\{^1\text{H}\}$ NMR spectrum for the reaction of N, N-dimethyl(trimethylsilylamine) and diethyl acetylenedicarboxylate.....	250
AA Figure 24 ^1H - ^{29}Si HMBC NMR spectrum of the reaction of N, N-dimethyl(trimethylsilylamine) and diethyl acetylenedicarboxylate	251
AA Figure 25 ^1H NMR spectrum of the reaction of N, N-dimethyl(trimethylsilylamine) and methyl propiolate	251
AA Figure 26 $^{13}\text{C}\{^1\text{H}\}$ NMR spectrum for the reaction of N, N-dimethyl(trimethylsilylamine) and methyl propiolate	252
AA Figure 27 ^1H - ^{29}Si HMBC NMR spectrum of the reaction of N, N-dimethyl(trimethylsilylamine) and methyl propiolate	252
AA Figure 28 ^1H NMR spectrum of the reaction of N, N-dimethyl(trimethylsilylamine) and ethyl propiolate	253
AA Figure 29 $^{13}\text{C}\{^1\text{H}\}$ NMR spectrum for the reaction of N, N-dimethyl(trimethylsilylamine) and ethyl propiolate	253
AA Figure 30 ^1H - ^{29}Si HMBC NMR spectrum of the reaction of N, N-dimethyl(trimethylsilylamine) and ethyl propiolate	254

AA Figure 31 ^1H NMR spectrum of the reaction of N, N-dimethyl((dimethylphenylsilyl)amine) and ethyl propiolate	254
AA Figure 32 $^{13}\text{C}\{^1\text{H}\}$ NMR spectrum for the reaction of N, N-dimethyl((dimethylphenylsilyl)amine) and ethyl propiolate	255
AA Figure 33 Upfield portion of the ^1H - ^{29}Si HMBC NMR spectrum of the reaction of N, N-dimethyl((dimethylphenylsilyl)amine) and ethyl propiolate	255
AB Figure 1 ^1H NMR spectrum (400 MHz, CDCl_3) of $[\text{GeCl}_2(\text{dibenzo}[18]\text{crown-6})]$	256
AB Figure 2 ^1H NMR spectrum (400 MHz, $\text{ACN-}d_3$) of $[\text{SnCl}(\text{dibenzo}[18]\text{crown-6})][\text{SnCl}_3]$	256
AB Figure 3 ^1H NMR spectrum (400 MHz, CDCl_3) of $[\text{SnCl}(\text{benzo}[15]\text{crown-5})][\text{SnCl}_3]$	257
AB Figure 4 Stacked plot of the $^{31}\text{P}\{^1\text{H}\}$ NMR spectra (243 MHz, CD_2Cl_2 , 25 to $-80\text{ }^\circ\text{C}$) of the addition of TEPO to $[\text{Ge}(\text{18-crown-6})][\text{OTf}]_2$ at different temperatures.	257
AB Figure 5 Stacked plot of the ^1H NMR spectra (600 MHz, CD_2Cl_2 , 25 to $-80\text{ }^\circ\text{C}$) for the addition of two equivalents of TEPO to $[\text{Ge}(\text{18-crown-6})][\text{OTf}]_2$	258
AB Figure 6 Stacked plot of the $^{31}\text{P}\{^1\text{H}\}$ NMR spectrum (243 MHz, CD_2Cl_2 , 25 to $-90\text{ }^\circ\text{C}$) for the addition of TEPO to $\text{GeCl}_2\cdot\text{dioxane}$	258
AB Figure 7 Stacked plot of the ^1H NMR spectra (600 MHz, CD_2Cl_2 , 25 to $-90\text{ }^\circ\text{C}$) for the addition of two equivalents of TEPO to $\text{GeCl}_2\cdot\text{dioxane}$	259
AB Figure 8 Stacked plot of the $^{31}\text{P}\{^1\text{H}\}$ NMR spectrum (243 MHz, CD_2Cl_2 , 25 to $-90\text{ }^\circ\text{C}$) for the addition of TEPO to $[\text{Ge}([\text{12}]\text{crown-4})_2][\text{OTf}]_2$	259
AB Figure 9 Stacked plot of the ^1H NMR spectra (600 MHz, CD_2Cl_2 , 25 to $-80\text{ }^\circ\text{C}$) for the addition of two equivalents of TEPO to $[\text{Ge}([\text{12}]\text{crown-4})_2][\text{OTf}]_2$	260
AB Figure 10 $^{31}\text{P}\{^1\text{H}\}$ NMR spectrum (162 MHz, CD_2Cl_2 , $25\text{ }^\circ\text{C}$) for the addition of two equivalents of TEPO to SnCl_2	260

AB Figure 11 ^1H NMR spectrum (400 MHz, CD_2Cl_2 , 25 °C) for the addition of two equivalents of TEPO to SnCl_2	261
AB Figure 12 ^{119}Sn NMR spectrum (149 MHz, CD_2Cl_2 , 25 °C) of the addition of two equivalents of TEPO to SnCl_2 . $\text{Cr}(\text{acac})_3$ was used as a relaxation agent.	261
AB Figure 13 Stacked plot of the $^{31}\text{P}\{^1\text{H}\}$ NMR spectrum (243 MHz, CD_2Cl_2 , 25 to -90 °C) for the addition of two equivalents of TEPO to $\text{Sn}(\text{OTf})_2$	262
AB Figure 14 $^{119}\text{Sn}\{^1\text{H}\}$ NMR spectrum (224 MHz, CD_2Cl_2 , -80 °C) for the addition of two equivalents of TEPO to $\text{Sn}(\text{OTf})_2$	262
AB Figure 15 Stacked plot of the $^{31}\text{P}\{^1\text{H}\}$ NMR spectrum (243 MHz, CD_2Cl_2 , 25 to -90 °C) for the addition of two equivalents of TEPO to $\text{Sn}(\text{OTf})_2$ and 5 mg of $\text{Cr}(\text{acac})_3$	263
AB Figure 16 $^{119}\text{Sn}\{^1\text{H}\}$ NMR spectrum (224 MHz, CD_2Cl_2 , -80 °C) for the addition of two equivalents of TEPO to $\text{Sn}(\text{OTf})_2$ and 5 mg of $\text{Cr}(\text{acac})_3$	263
AB Figure 17 $^{119}\text{Sn}\{^1\text{H}\}$ NMR spectrum (189 MHz, CD_2Cl_2 , -80 °C) for the addition of two equivalents of TEPO to $\text{Sn}(\text{OTf})_2$ and 5 mg of $\text{Cr}(\text{acac})_3$	264
AB Figure 18 $^{119}\text{Sn}\{^1\text{H}\}$ NMR spectrum (224 MHz, CD_2Cl_2 , -80° C) for the addition of two equivalents of TEPO to $[\text{Sn}([\text{12}]\text{crown-4})_2][\text{OTf}]_2$	264
AB Figure 19 Stacked plot of the $^{31}\text{P}\{^1\text{H}\}$ NMR spectrum (243 MHz, CD_2Cl_2 , 25 to -90 °C) for the addition of two equivalents of TEPO to $[\text{Sn}([\text{12}]\text{crown-4})_2][\text{OTf}]_2$	265
AB Figure 20 Stacked plot of the ^1H NMR spectra (600 MHz, CD_2Cl_2 , 25 to -80 °C) for the addition of two equivalents of TEPO to $[\text{Sn}([\text{12}]\text{crown-4})_2][\text{OTf}]_2$	265
AB Figure 21 ^1H - ^1H COSY spectrum (600 MHz, CD_2Cl_2 , -90 °C) of $[\text{Sn}([\text{12}]\text{crown-4})_2][\text{OTf}]_2$ and two equivalents of TEPO	266
AB Figure 22 ^1H - ^1H EXSY spectrum (600 MHz, CD_2Cl_2 , -50 °C) of $[\text{Sn}([\text{12}]\text{crown-4})_2][\text{OTf}]_2$ and two equivalents of TEPO.	266

AB Figure 23 Stacked plot of the $^{31}\text{P}\{^1\text{H}\}$ NMR spectrum (243 MHz, CD_2Cl_2 , 25 to $-90\text{ }^\circ\text{C}$) for the addition of two equivalents of TEPO to $[\text{Sn}(\mathbf{18}\text{crown-6})][\text{OTf}]_2$.	267
AB Figure 24 Stacked plot of the ^1H NMR spectra (600 MHz, CD_2Cl_2 , 25 to $-80\text{ }^\circ\text{C}$) for the addition of two equivalents of TEPO to $[\text{Sn}(\mathbf{18}\text{crown-6})][\text{OTf}]_2$.	267
AB Figure 25 ^1H - ^1H EXSY spectrum (600 MHz, CD_2Cl_2 , $-50\text{ }^\circ\text{C}$) of $[\text{Sn}(\mathbf{18}\text{crown-6})][\text{OTf}]_2$ and two equivalents of TEPO	268
AB Figure 26 $^{119}\text{Sn}\{^1\text{H}\}$ NMR spectrum (224 MHz, CD_2Cl_2 , $-80\text{ }^\circ\text{C}$) for the addition of two equivalents of TEPO to $[\text{Sn}(\mathbf{18}\text{crown-6})][\text{OTf}]_2$.	268
AB Figure 27 $^{119}\text{Sn}\{^1\text{H}\}$ NMR spectrum (149 MHz, CD_2Cl_2 , $25\text{ }^\circ\text{C}$) for the addition of two equivalents of TEPO to $[\text{Sn}(\mathbf{18}\text{crown-6})][\text{OTf}]_2$.	269
AB Figure 28 Stacked plot of the $^{31}\text{P}\{^1\text{H}\}$ NMR spectrum (243 MHz, CD_2Cl_2 , 25 to $-90\text{ }^\circ\text{C}$) for the addition of two equivalents of TEPO to $[\text{SnCl}(\mathbf{18}\text{crown-6})][\text{SnCl}_3]$.	269
AB Figure 29 Stacked plot of the ^1H NMR spectra (600 MHz, CD_2Cl_2 , 25 to $-80\text{ }^\circ\text{C}$) for the addition of two equivalents of TEPO to $[\text{SnCl}(\mathbf{18}\text{crown-6})][\text{SnCl}_3]$.	270
AB Figure 30 $^{119}\text{Sn}\{^1\text{H}\}$ NMR spectrum (224 MHz, CD_2Cl_2 , $-80\text{ }^\circ\text{C}$) for the addition of two equivalents of TEPO to $[\text{SnCl}(\mathbf{18}\text{crown-6})][\text{SnCl}_3]$.	270
AB Figure 31 $^{119}\text{Sn}\{^1\text{H}\}$ NMR spectrum (149 MHz, CD_2Cl_2 , $25\text{ }^\circ\text{C}$) for the addition of two equivalents of TEPO to $[\text{SnCl}(\mathbf{18}\text{crown-6})][\text{SnCl}_3]$.	271
AB Figure 32 Stacked plot of the ^1H NMR spectra (600 MHz, CD_2Cl_2 , 25 to $-80\text{ }^\circ\text{C}$) for the addition of two equivalents of TEPO a) $[\text{Sn}(\mathbf{12}\text{crown-4})_2][\text{OTf}]_2$ b) $\text{Sn}(\text{OTf})_2$ c) $[\text{Sn}(\mathbf{18}\text{crown-6})][\text{OTf}]_2$ and d) $[\text{SnCl}(\mathbf{18}\text{crown-6})][\text{SnCl}_3]$.	271
AB Figure 33 Stacked plot of the ^1H NMR spectra (600 MHz, CD_2Cl_2 , 25 to $-80\text{ }^\circ\text{C}$) for the addition of two equivalents of TEPO a) $[\text{Ge}(\mathbf{12}\text{crown-4})_2][\text{OTf}]_2$ b) $[\text{Ge}(\mathbf{18}\text{crown-6})][\text{OTf}]_2$ and c) $\text{GeCl}_2 \cdot \text{dioxane}$.	272
AC Figure 1 ^1H NMR spectrum (400 MHz, CDCl_3) of bis(naphthyl) ether.	273

AC Figure 2 $^{13}\text{C}\{^1\text{H}\}$ NMR spectrum (101 MHz, CDCl_3) of bis(naphthyl) ether.	273
AD Figure 1 ^1H NMR spectrum (400 MHz, CD_2Cl_2) of the addition of <i>N,N</i> -dimethylaniline to $[\text{Ge}([\mathbf{12}\text{crown-4}]_2)[\text{OTf}]_2$	274
AD Figure 2 ^1H NMR spectrum (400 MHz, CD_2Cl_2) of the addition of <i>N,N</i> -dimethylaniline to $\text{B}(\text{C}_6\text{F}_5)_3$	274
AD Figure 3 ^1H NMR spectrum (400 MHz, CD_2Cl_2) of the addition of <i>N,N</i> -dimethylaniline to $[\text{Ge}([\mathbf{12}\text{crown-4}]_2)[\text{OTf}]_2$	275
AD Figure 4 ^1H NMR spectrum (400 MHz, CD_2Cl_2) of the addition of <i>N,N</i> -dimethylaniline to $\text{B}(\text{C}_6\text{F}_5)_3$	275
AD Figure 5 ^2H NMR spectrum (92 MHz, C_6H_6) of the 1,1'-[oxybis(methylene)]bis[4-methyl-benzene].	276

List of Abbreviations

°	degrees
~	approximately
12c4	[12]crown-4
18c6	[18]crown-6
Å	angstrom, 10^{-10} m
acac	acetylacetone
ACN	acetonitrile
ACN- <i>d</i> ₃	trideuteroacetonitrile
AN	Acceptor Number
AN ^{LM}	Lichtenberg-Modified Gutmann-Beckett Acceptor Number
Ar	aryl group
BDE	bond dissociation energy
br	broad
C	Celsius
calc.	calculated
cat	catecholato
CCDC	Cambridge Crystallographic Data Centre
Cp*	pentamethylcyclopentadienyl
CPCM	conductor-like polarization model
δ	chemical shift
d	doublet
D	donor
DCM	dichloromethane

DCM- <i>d</i> ₂	dideuterodichloromethane
dioxane	1,4-dioxane
Dipp	2,6-diisopropylphenyl
DMAP	4-dimethylaminopyridine
DMSO	dimethylsulfoxide
DN	donor number
dq	doublet of quartets
dtbc	<i>ditert</i> -butylcatecholato
Dur	2,3,5,6-tetramethylphenyl
dt	doublet of triplets
E	element
EDG	electron-donating group
EWG	electron-withdrawing group
equiv.	molar equivalents
ESI-MS	electrospray ionization mass spectrometry
Et	ethyl
eV	electron volts
FIA	Fluoride Ion Affinity
FT	Fourier transform
FWHM	full width at half maximum
g	grams
G	Gibb's free energy
GC-MS	gas chromatography mass spectrometry
gCOSY	gradient homonuclear correlation spectroscopy

[Ge1]	[Ge([12]crown-4) ₂][OTf] ₂
[Ge2]	[Ge([12]crown-4)] ²⁺
gHSQC	gradient heteronuclear single-quantum correlation spectroscopy
gHMBC	gradient heteronuclear multiple-bond correlation spectroscopy
h	hour
HOMO	highest occupied molecular orbital
HR	high resolution
Hz	hertz
<i>i</i>	<i>ipso</i>
IEF-PCM	Integral Equation Formalism-Polarizable Continuum Model
<i>i</i> Pr	<i>iso</i> -propyl
IR	infrared
IRC	intrinsic reaction coordinate
<i>J</i>	coupling constant
K	Kelvin
KIE	kinetic isotope effect
kJ	kilojoules
LMGB	Litchenberg-Modified Gutmann-Beckett Method
LUMO	lowest unoccupied molecular orbital
μ	bridging (molecular formula)
μL	microlitre
LA	Lewis acid
LB	Lewis base
<i>m/z</i>	mass to charge ratio

m	multiplet
M	metal; concentration
<i>m</i>	meta
Me	methyl
Mes	mesityl, 2,4,6-trimethylphenyl
mg	milligram
MHz	megahertz
mL	millilitre
MO	molecular orbital
mmol	millimoles
mol	moles
Ni ^t Bu	bis(<i>t</i> -butyl)imidazolin-2-imino
NMR	nuclear magnetic resonance
NOESY	Nuclear Overhauser Enhancement Spectroscopy
<i>o</i>	<i>ortho</i>
OTf	triflate, trifluoromethanesulfonate
<i>p</i>	para
Ph	phenyl
PMDS	pentamethyldisiloxane
ppm	parts per million
Pr	propyl
q	quartet
R	organic ligand/substituent
RC	reactant complex

RLS	rate-limiting step
RT	room temperature
s	singlet
SSNMR	solid-state nuclear magnetic resonance
t	triplet
<i>t</i> Bu	<i>tert</i> -butyl
TCPO	tricyclohexylphosphine oxide
TEPO	triethylphosphine oxide
Terpy	2,6-bis(2-pyridyl)pyridine
TES	triethylsilane
THF	tetrahydrofuran
Tipp	2,4,6-triisopropylphenyl
TLC	thin layer chromatography
TMOP	2,4,6-trimethoxyphenyl
TMPO	trimethylphosphine oxide
TMPS	trimethylphosphine sulfide
TMS	trimethylsilyl
TOF	time of flight
VT-NMR	variable temperature nuclear magnetic resonance
X	halide, or halogen

Chapter 1

1 Introduction

The functionalization and activation of small molecules have been of industrial and academic interest for decades. The demand for diverse chemicals in the agricultural, pharmaceutical and manufacturing industries has grown exponentially over time, and thus, the demand for catalysts to facilitate chemical transformations has also increased. Small molecule activation and catalysis have been traditionally facilitated by transition metals.¹ Industrially, palladium is used as a catalyst in a number of carbon-carbon bond formation reactions² and platinum is the primary metal utilized in the formation of cross-linked polysiloxanes.³ However, there are a number of drawbacks associated with using precious metals including these platinum-group metals: 1) platinum and palladium are typically expensive due to the mining and purifications processes,⁴ 2) they have a low abundance in the Earth's crust (less than 0.01 ppm⁵) and 3) obtaining these metals can be unreliable due to supply chain issues in the countries of origin.⁶ As there are a number of drawbacks to precious metals, interest in alternatives to these metals as catalysts is growing. First row transition metals⁷ and *s*-block metals⁸ have been proposed as alternatives as well as the main group elements⁹ in the *p*-block.

Historically, research into the chemistry of *p*-block elements was focused on the discovery of stable low valent main group complexes and investigations into their structures and bonding. In the last few decades, a shift to application-based research has led to a substantial increase in the use of main group compounds in small molecule activation

and catalysis due to early successes in the activation of important small molecules such as dihydrogen¹⁰ and ammonia.¹¹ In addition to these reactions, low valent *p*-block compounds have also been utilized in the activation of carbon dioxide¹² and as catalysts for reduction, cyclization and polymerization reactions.¹³ The reactivities of these main group complexes are comparable to that of transition metals⁹ which has further shifted the focus of research to the development of new complexes for small molecule activation and catalysis.

1.1 Main Group Lewis Acids of Group 13 and 14

Within the *p*-block, catalysis and small molecule activation by Group 13 complexes has been, perhaps, the most extensively explored.¹⁴ With an empty *p*-orbital, Group 13 compounds in the 3+ oxidation can coordinate small molecules through the acceptance of an electron pair (Lewis base) generating a Lewis-acid base adduct (Figure 1.1).¹⁵ Through the modification of the substituents on the central atom of the Lewis acid, the Lewis acidity of the complex can be adjusted. For some complexes, polarization of the Lewis base upon coordination to the Lewis acid is sufficient for catalysis. For most main group complexes, including those of Group 13, Lewis acid catalysis is the primary method for catalytic transformations,^{14d} although frustrated Lewis pair catalysis has also been documented.¹⁶

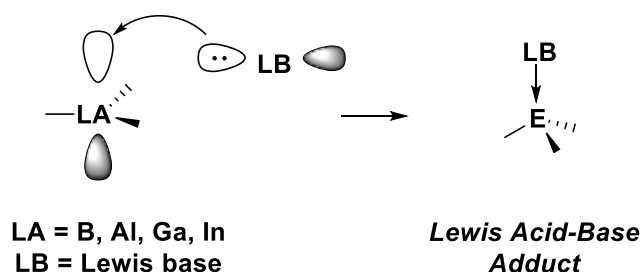


Figure 1.1 Lewis acid-base adduct formation with Group 13 complexes.

In Group 14 of the periodic table, the preference for the 4+ oxidation number for silicon, germanium and tin can make Lewis acid-base adduct formation more challenging due to the absence of an energetically-accessible empty orbital. Although catalysis by SiCl_4 , GeCl_4 and SnCl_4 has been reported,¹⁷ these species are less effective catalysts in comparison to the Group 13 analogues, BCl_3 and AlCl_3 .¹⁸ To increase the Lewis acidity of the Group 14 centre, three methods have been developed. One method is via orbital engineering,¹⁹ in which the use of multidentate ligands on the main group centre forces a unique geometry and electronic structure. Recent developments in octahedral silicon(IV)²⁰ and germanium(IV)²¹ complexes with bidentate catecholato ligands (Figure 1.2) have demonstrated that orbital engineering is a viable method for increasing the Lewis acidity of the central atom. For example, the placement of two catechol ligands with electron-withdrawing substituents on germanium or silicon changes the bonding and allows for the formation of a hexacoordinate complex, rather than the more common tetrahedral complexes. In these octahedral complexes, the bonding can be described as 3-centre-4 electron bonding between the oxygen ligands and metal centre (Figure 1.2). The remaining orbitals on the Group 14 element are two *sp*-hybridized orbitals in the axial positions of the octahedral complex which can accept electron density from a Lewis base to facilitate catalysis.

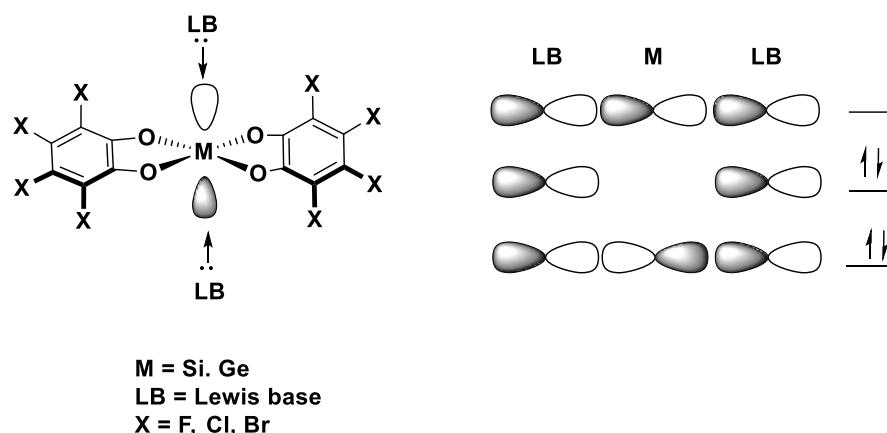


Figure 1.2 3-centre-4-electron bonding in bis(catecholato)silanes and -germanes.²⁰⁻²¹

Another method to increase the Lewis acidity of the Group 14 centre is to form cationic complexes, MR_3^+ . Cationic complexes of Group 14 elements in the 4^+ oxidation number contain an empty orbital that can accept electron density from a Lewis base (Figure 1.3a) and are isoelectronic to BX_3 ($X = F, Cl, Br$). Notably, catalysis by cationic silylium ions has been reported.²² The electron deficiency at the Group 14 centre in the cationic complexes results in a greater Lewis acidity in comparison to the analogous neutral Group 13 species.²³ The final method to increase the Lewis acidity of a Group 14 centre is to lower the oxidation number from $+4$ to $+2$. The change in oxidation number generates an accessible orbital for Lewis base coordination. Divalent species, or tetrylenes (Figure 1.3b), the heavier main group analogues of carbenes, have been reported to activate small molecules and catalyze reactions.²⁴ Ditetrelenes, the heavier main group analogue of alkenes and dimers of tetrylenes (Figure 1.3c), have been shown to activate a number of small molecules including H_2 , NH_3 and CO_2 ;²⁵ however, catalysis by ditetrelenes has not yet been realized. The π^* orbital on the ditetrelene enables reactivity with small molecules.

Compared to tetravalent Group 14 Lewis acids, applications of divalent Group 14 complexes in catalysis, especially cationic derivatives, have been relatively unexplored, and thus, the focus of this thesis will be on the applications of divalent Group 14 complexes in catalysis.

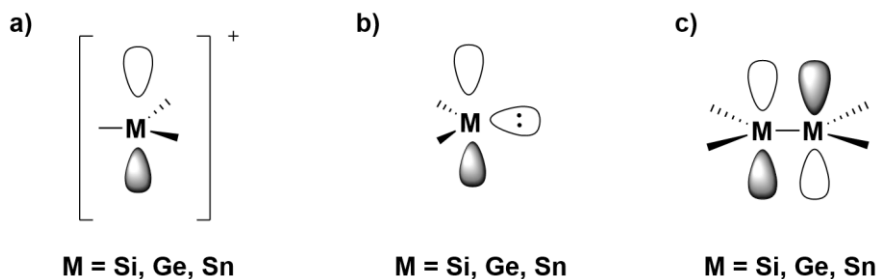


Figure 1.3 The general structures of a) cations of Group 14 b) tetrelenes and c) ditetrelenes. The orbital available for reactivity is shown.

1.2 Small Molecule Activation by Ditetrelenes

1.2.1 Structure and Bonding in Ditetrelenes

Unlike planar alkenes, the heavier main group analogue ditetrelenes can be twisted and/or *trans*-bent about the double bond (Figure 1.4). The twisting in ditetrelenes, typically between 0-25°, is a result of the bulky substituents required to kinetically-stabilize the molecule and has also been observed in alkenes bearing bulky-substituents.²⁶ The degree of twisting is highly dependent on the nature of the substituents²⁷ and is also influenced by solvation in the solid-state.²⁸

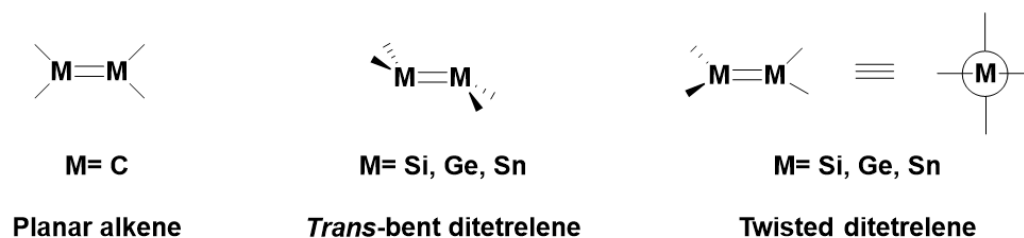


Figure 1.4 The structures of *trans*-bent and twisted ditetrelenes and planar alkenes.

Two different theories on the bonding in ditetrelenes can be used to account for the unique *trans*-bent geometry about the M=M bond. One theory considers the association of two tetrylene units to form a doubly-bonded species. The ground-state of the carbon in carbenes is a triplet, resulting in the formation of a classic covalent σ and a π bond between the singly-filled p -orbitals (Figure 1.5). However, for tetrylenes of silicon, germanium and tin, the ground-state electron arrangement is a singlet. As a result, Pauli repulsion between the two filled singlet orbitals prevents the formation of a classic sigma bond between the tetrylene units. Donation of the lone pair of electrons from tetrylene unit to the empty p -orbital on the other forms a non-classical donor-acceptor double bond. Due to the necessary orientation for the mutual overlap of the orbitals, a *trans*-bent geometry occurs.

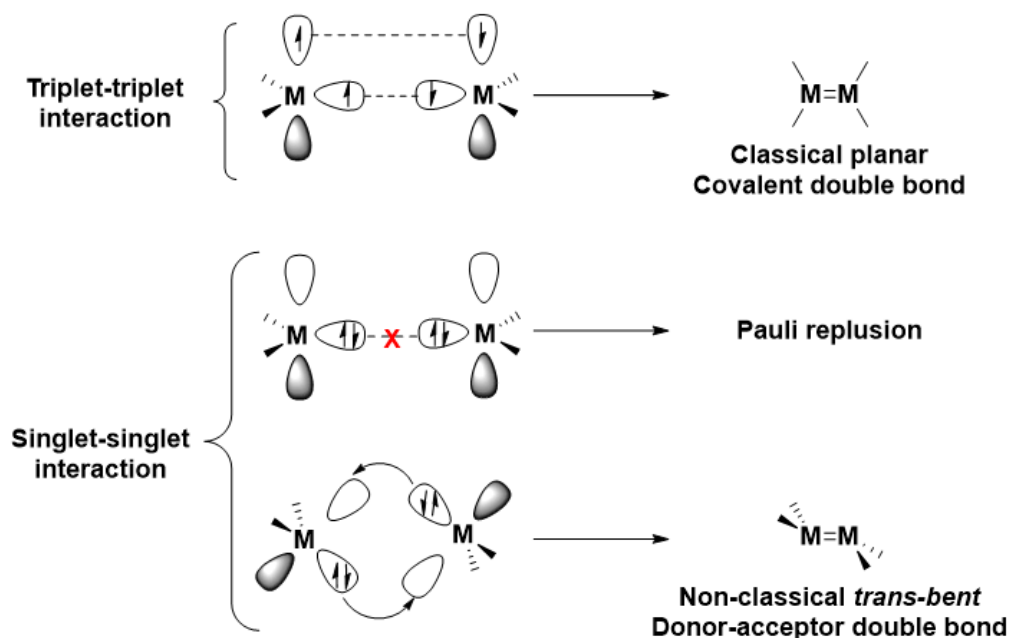


Figure 1.5 Bonding in alkenes and one interpretation of the bonding in ditetrelenes as dimers of tetrylenes.

The second theory considers an interaction between a classic π bond and the σ^* orbital of the M-M interaction (Figure 1.6). The mixing of these orbitals results in the *trans*-bent geometry at the main group centre. The magnitude of the interaction between the π and σ^* is dependent on the energy difference between these two orbitals. As the Group 14 element increases in size down the group, the energy difference between the π and the σ^* orbitals decreases, increasing the degree of *trans*-bending observed in ditetrelenes. The presence of electron-withdrawing groups on the ditetrelene can also increase the degree of *trans*-bending observed²⁹ as well as the energy of the π^* orbital.

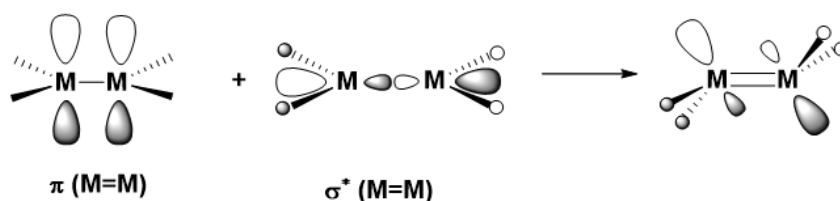


Figure 1.6 Interactions of the π and σ^* orbitals in ditetrelenes.

1.2.2 Reactivity of Ditetrelenes

The twisted and *trans*-bent geometry at the Group 14 element in ditetrelenes results in a longer bond and a weaker interaction between the atoms. Compared to carbon, the strengths of the Si=Si bond and Ge=Ge bond (as measured by BDE) are 100 kJ/mol lower.³⁰ The HOMO-LUMO gap in ditetrelenes is small as a result of the high-lying HOMO and low-lying LUMO, allowing for facile activation and reaction with polar and polarizable small molecules compared to carbon.

Ditetrelenes undergo a number of different reactions including 1,2-addition,³¹ cycloaddition³² and polymerization³³ (Figure 1.7). Thermal $[2\pi_s + 2\pi_s]$ cycloadditions are forbidden in carbon; however, ditetrelenes readily react with doubly-bonded reagents, highlighting one of the differences in reactivity compared to alkenes. One of the most common reactions of ditetrelenes are 1,2-additions. Previous experimental and computational studies on the addition of water and alcohols to disilenes have demonstrated that water and alcohols undergo nucleophilic addition to the double bond of disilenes and digermenes^{31a,34} in contrast to the electrophilic addition of water and alcohols observed for alkenes.

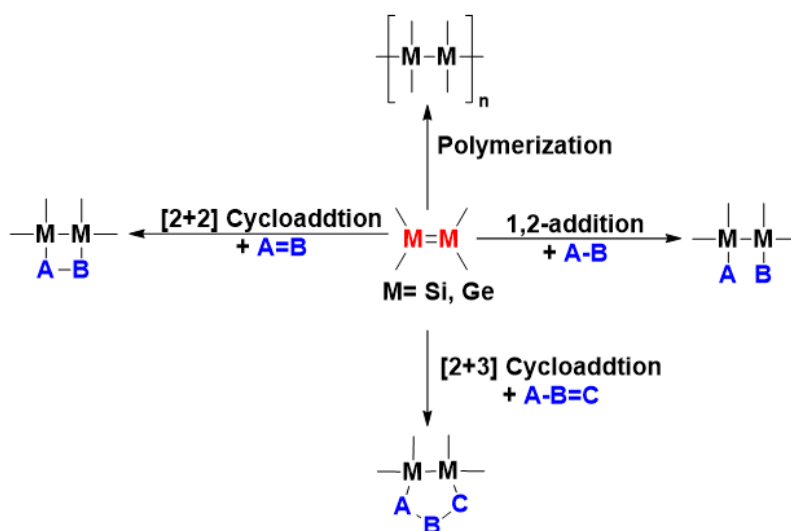


Figure 1.7 Reactivity of ditetrelenes.

One of the most exciting recent developments in the 1,2-addition reactions of ditetrelenes is the N-H activation of ammonia. Ammonia is a common precursor in the pharmaceutical industry for the synthesis of nitrogen-containing drugs. However, as the N-H bond of ammonia is strong (BDE 99.4 kJ/mol³⁵), methods to activate or break the N-H bond have been of significant interest. Traditionally, ammonia has been activated by transition metals; however, N-H activation has been reported by a tetrasilabutadiene³⁶ and later by an asymmetrically substituted disilene.³⁷ The activation of ammonia^{25b} and dihydrogen^{25c} by a highly twisted iminodisilyldisilene has also been recently reported (Figure 1.8). However, investigations into the addition of ammonia to simple symmetrically-substituted tetraarylditetrelenes has not been conducted.

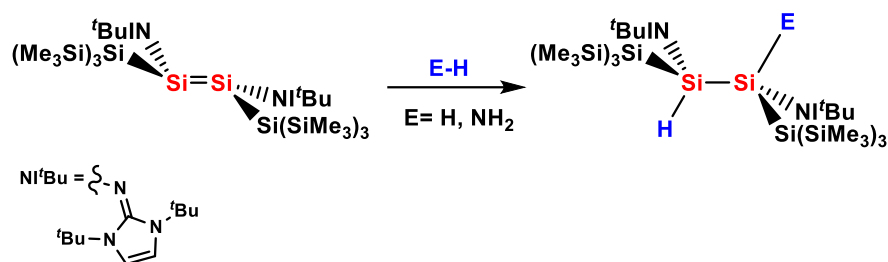


Figure 1.8 The addition of ammonia and hydrogen to a bis(imino)bis(silyl)disilene.^{25b-c}

1.3 Lewis Acid Catalysis by Tetrylenes

1.3.1 Structure and Bonding of Tetrylenes

The singlet ground state of silicon, germanium and tin-based tetrylenes has an empty, unhybridized orbital on the metal centre in addition to a lone pair (Figure 1.3b). Some of the first reported stable tetrylenes featured two bulky aryl substituents preventing dimerization;³⁸ however, the variety of ligands utilized to stabilize tetrylenes has been expanded to include many different types of ligands including heteroatom-containing ligands, such as 1,3-diketimines.³⁹ In addition, Lewis bases can be used to stabilize transient tetrylenes, enabling the use of less bulky ligands on the central atom, such as chloride or hydrogen.⁴⁰ Selected examples of the different ligand types utilized in the stabilization of tetrylenes are shown in Figure 1.9.

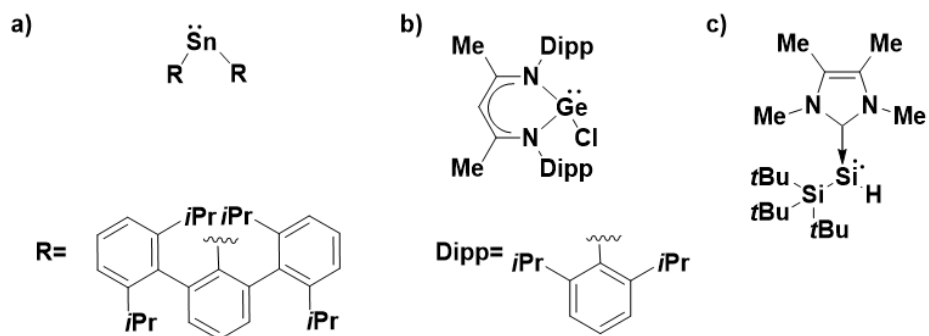


Figure 1.9 Examples of the different structures of tetrylenes: a) a diarylstannylene³⁸ b) a germylene stabilized by a β -diketiminato ligand³⁹ and c) an N-heterocyclic carbene-stabilized silylene.⁴⁰

Tetrylenes are ambiphilic being both electrophilic, as a consequence of the empty p orbital on the Group 14 centre, and nucleophilic, as a consequence of the lone pair (Figure 1.10). The ambiphilic reactivity of tetrylenes, most well-documented in silylenes,⁴¹ is highly dependent on the substituents of the stabilizing ligands. σ -Electron-withdrawing substituents increase the electrophilicity of the Group 14 centre favoring reactivity as a Lewis acid, while π -donating substituents increase the electron density at the Group 14 centre favoring reactivity as a nucleophile. Furthermore, the presence of charge on the Group 14 centre can also influence the reactivity. Cationic tetrylenes⁴² are less electron dense than their neutral counterparts and typically act as Lewis acids, while anionic tetrylenes,⁴³ with more electron density than a neutral derivative, react as nucleophiles.

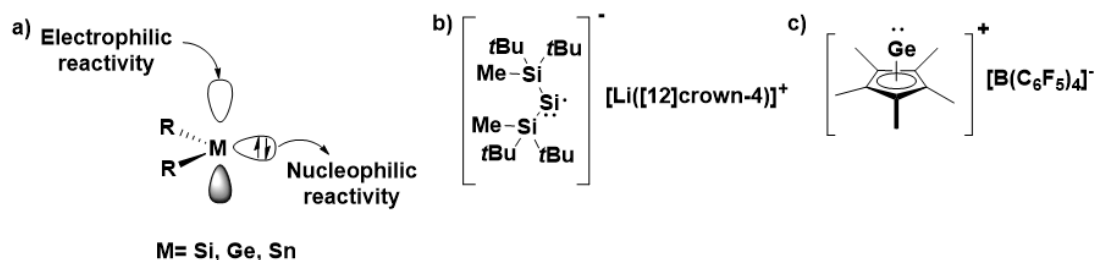
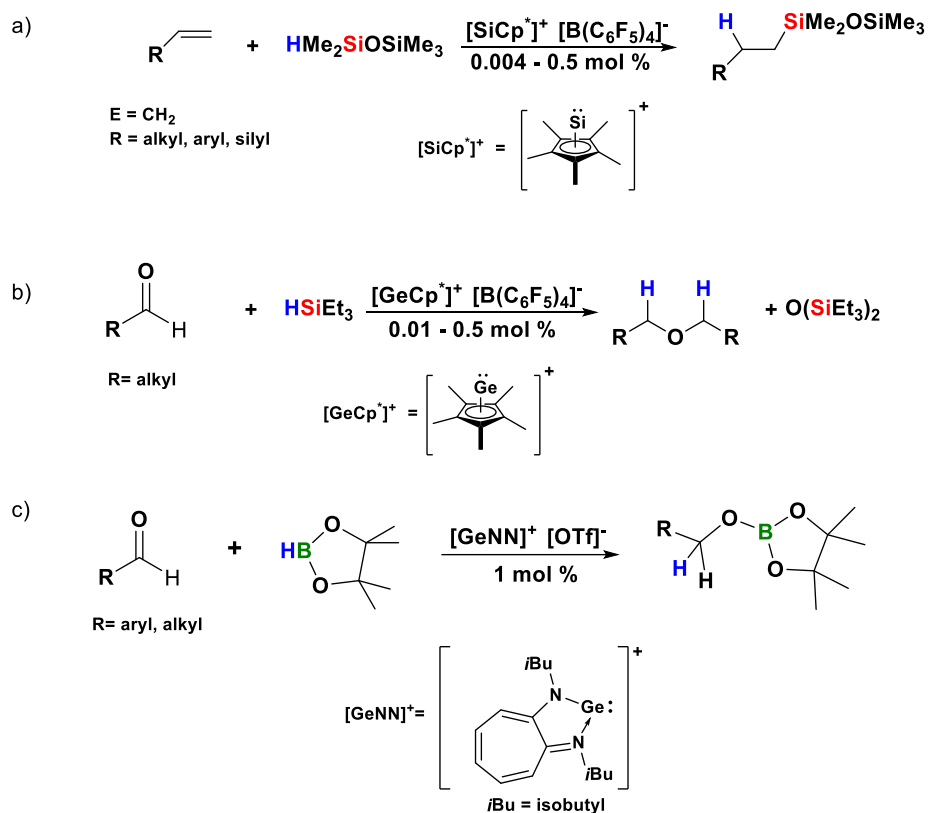


Figure 1.10 a) The ambiphilic character of tetrylenes b) an anionic silylene⁴³ and c) a cationic germylene.^{42b}

1.3.2 Lewis Acid Catalysis by Tetrylenes

When utilized as catalysts, tetrylenes typically exhibit Lewis acid behavior. As Lewis acids, silylenes,⁴⁴ germynes^{24b,45} and stannylens^{24b} have been demonstrated to catalyze the hydrosilylation and hydroboration of doubly-bonded compounds, such as carbonyl compounds and alkenes. In one exciting development, the monocationic salt [SiCp*][B(C₆F₅)₄]^{42a} was shown to catalyze the hydrosilylation of alkenes at the parts per million catalyst loading level (Scheme 1.12a). The analogous germanium(II) species, [GeCp*][B(C₆F₅)₄], was also shown to efficiently facilitate aldehyde and ketone hydrosilylation at comparable catalyst loadings (Scheme 1.12b).^{42b} The hydroboration of aldehydes can be catalyzed by a troponimine-substituted germanium(II) cation^{45a} (Scheme 1.1c) or a siloxy-substituted germylene.^{45b} To the best of our knowledge, there are only four known examples of Lewis acid catalysis by cationic tetrylenes.



Scheme 1.1 a) Hydrosilylation of alkenes by [SiCp*]⁺[B(C₆F₅)₄]⁻,^{42a} b) hydrosilylation of aldehydes and ketones by [GeCp*]⁺[B(C₆F₅)₄]⁻,^{42b} c) hydroboration of aldehydes by [GeNN]⁺[OTf]⁻.⁴⁵

1.3.3 Structure and Bonding in Crown Ether Complexes of Germanium(II) and Tin(II)

One unique class of tetraenes are the crown ether-stabilized germanium(II) and tin(II) cations. The first reported cationic crown ether complexes of tin(II) was described in 1986⁴⁶ (Figure 1.10) and, since then, several examples have been reported.⁴⁷ Dicationic crown ether complexes of germanium(II) were first reported in 2009⁴⁸ (Figure 1.10). The analogous dicationic tin(II) species⁴⁹ were reported the next year and exhibit similar structures to the germanium(II) species.

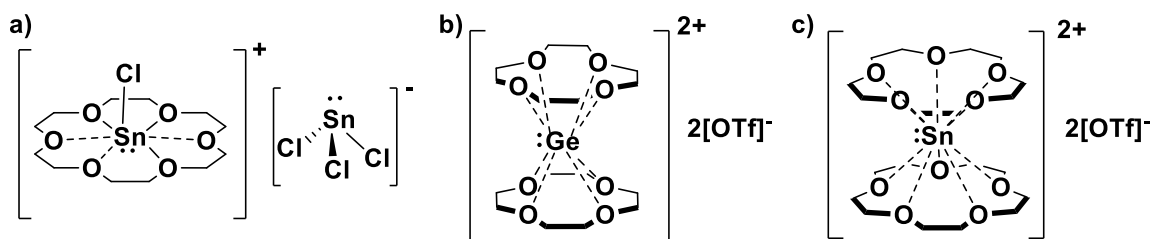


Figure 1.11 Structure of some cationic crown ether complexes: a) the first reported cationic tin(II) crown ether complex⁴⁶ b) a dicationic germanium(II) crown ether complex⁴⁸ and c) a dicationic tin(II) crown ether complex.⁴⁹

The structures germanium(II) and tin(II) crown ether complexes are unique in comparison to the structures of other tetrylenes. Most tetrylenes are stabilized by two bulky substituents through covalent bonds to nitrogen,⁵⁰ silicon,^{40,43} carbon-based⁵¹ or oxygen-based ligands.⁵² However, in the structures of the germanium(II) and tin(II) crown ether complexes, the Group 14 centre is stabilized through 3-10 oxygen contacts from the crown ether ligand to the metal centre. There are three typical structural environments for these complexes: a sandwich complex in which the metal lies between two crown ether ligands, an enveloped complex in which the metal centre lies within the crown ether cavity and a chloride complex in which an MCl^+ fragment lies within the crown ether cavity.

The structures of $[Ge([12]crown-4)_2][GeCl_3]_2$, $[Ge([12]crown-4)_2][OTf]_2$ and $[Sn([12]crown-4)_2][OTf]_2$ and $[Sn([15]crown-5)_2][OTf]_2$ are sandwich-type complexes (Figure 1.13). Eight oxygen-germanium contacts are present in the structure of $[Ge([12]crown-4)_2][GeCl_3]_2$ which range in distance from 2.383(6) to 2.489(7) Å.⁴⁸ The Ge-O interactions are significantly longer (~30%) than typical covalent Ge-O bond lengths of 1.75 to 1.85 Å.⁵³ No interaction with the counterion, $[GeCl_3]^-$, is observed, indicating

that the germanium(II) is dicationic. The data quality of the crystals obtained of $[\text{Ge}([\mathbf{12}\text{crown-4}]_2)[\text{OTf}]_2]$ was poor, however comparable connectivity of the cationic fragment to $[\text{Ge}([\mathbf{12}\text{crown-4}]_2)[\text{GeCl}_3]_2]$ was observed. In the analogous tin(II) crown ether complex, $[\text{Sn}([\mathbf{12}\text{crown-4}]_2)[\text{OTf}]_2]$, the two crown ethers are tilted with respect to one another (Figure 1.12b).⁴⁹ Eight oxygen contacts from the crown ether ligands to the tin(II) centre are present; however, four are significantly shorter ranging from 2.474(4) to 2.495(3) Å while four are longer ranging from 2.629(3) to 2.813(3) Å. All Sn-O contacts are longer than those found on other representative complexes, such as the tin(II) coordination complexes $[\text{Sn}(\text{DMSO})_5]^{2+}$ (DMSO = dimethylsulfoxide) (mean of 2.204(9) Å) and $[\text{Sn}(\text{OH}_2)_3]^{2+}$ (mean of 2.206(2) Å)⁵⁴ and also tin(II) bis(2,6-di-*tert*-butylphenoxide) (1.995(4) and 2.022(4) Å).^{52a} The structure of $[\text{Sn}([\mathbf{15}\text{crown-5}]_2)[\text{OTf}]_2]$ closely resembles the structure of $[\text{Ge}([\mathbf{12}\text{crown-4}]_2)[\text{OTf}]_2]$, although ten, rather than eight, Sn-O interactions between the tin centre and crown ether ligands are present.⁴⁹ In all complexes, the M-O (M = Ge, Sn) contact distances are significantly longer than reported covalent M-O bonds for M(II) complexes suggesting that the interactions between the oxygen atoms of the crown ether and the Group 14 centre are weaker than covalent bonds.

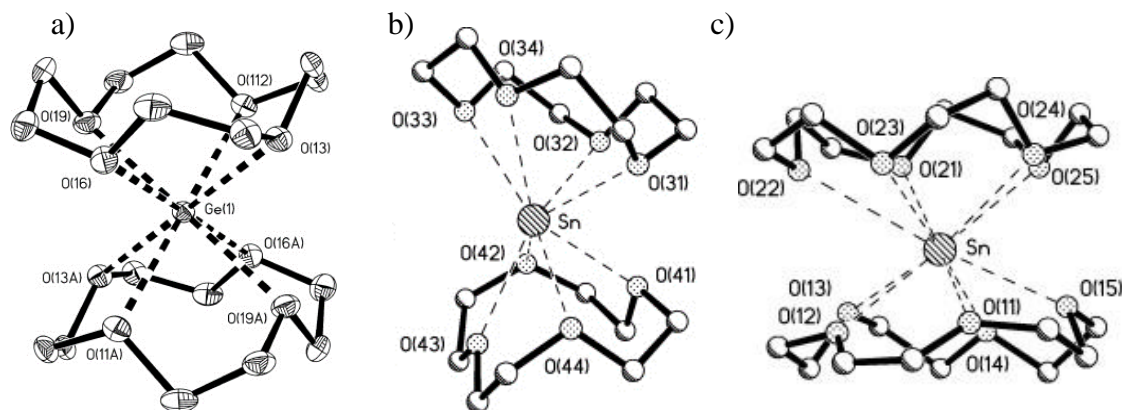


Figure 1.12 Displacement ellipsoid plots of a) $[\text{Ge}([\mathbf{12}\text{crown-4}]_2)[\text{GeCl}_3]_2$,⁴⁸ b) $[\text{Sn}([\mathbf{12}\text{crown-4}]_2)[\text{OTf}]_2$ ⁴⁹ and c) $[\text{Sn}([\mathbf{15}\text{crown-5}]_2)[\text{OTf}]_2$.⁴⁹ Ellipsoids are drawn at the 50% probability. The anions have been omitted for clarity. Reprinted with permission from Elsevier and John Wiley & Sons.⁵⁵

The solid-state structures of $[\text{Ge}([\mathbf{15}\text{crown-5}]_2)[\text{OTf}]_2$, $[\text{Ge}([\mathbf{18}\text{crown-6}]_2)[\text{OTf}]_2$ and $[\text{Sn}([\mathbf{18}\text{crown-6}]_2)[\text{OTf}]_2$ feature metal centres that lie within the central cavity of the crown ether and are directly coordinated to the triflate anions.⁴⁸⁻⁴⁹ Both $[\text{Ge}([\mathbf{15}\text{crown-5}]_2)[\text{OTf}]_2$ and $[\text{Ge}([\mathbf{18}\text{crown-6}]_2)[\text{OTf}]_2$ show six germanium-oxygen contacts in the solid-state, although $[\text{Ge}([\mathbf{15}\text{crown-5}]_2)[\text{OTf}]_2$ is designated as monocationic due to the central fragment GeOTf^+ with one associated triflate while $[\text{Ge}([\mathbf{18}\text{crown-6}]_2)[\text{OTf}]_2$ features the neutral $\text{Ge}(\text{OTf})_2$ fragment.⁴⁸ In $[\text{Ge}([\mathbf{15}\text{crown-5}]_2)[\text{OTf}]_2$, the Ge-O interactions between the germanium and crown ether oxygen range from 2.233(5) to 2.349(6) Å, again longer than typical covalent Ge-O bonds and the Ge-O interaction between the germanium centre and triflate anion is significantly shorter at 2.015(3) Å. In $[\text{Ge}([\mathbf{18}\text{crown-6}]_2)[\text{OTf}]_2$, four interactions between the oxygen of the crown ether ligands and the germanium(II) centre are present with similar bond distances between the germanium and oxygen atoms compared to those of $[\text{Ge}([\mathbf{15}\text{crown-5}]_2)[\text{OTf}]_2$. Notably, the germanium in

$[\text{Ge}([\mathbf{18}\text{crown-6})][\text{OTf}]_2$ is asymmetrically placed within the ring. The structure of $[\text{Sn}([\mathbf{18}\text{crown-6})][\text{OTf}]_2$ is very similar to that of $[\text{Ge}([\mathbf{15}\text{crown-5})][\text{OTf}]_2$, although two triflate anions are closely associated with the tin(II) centre.

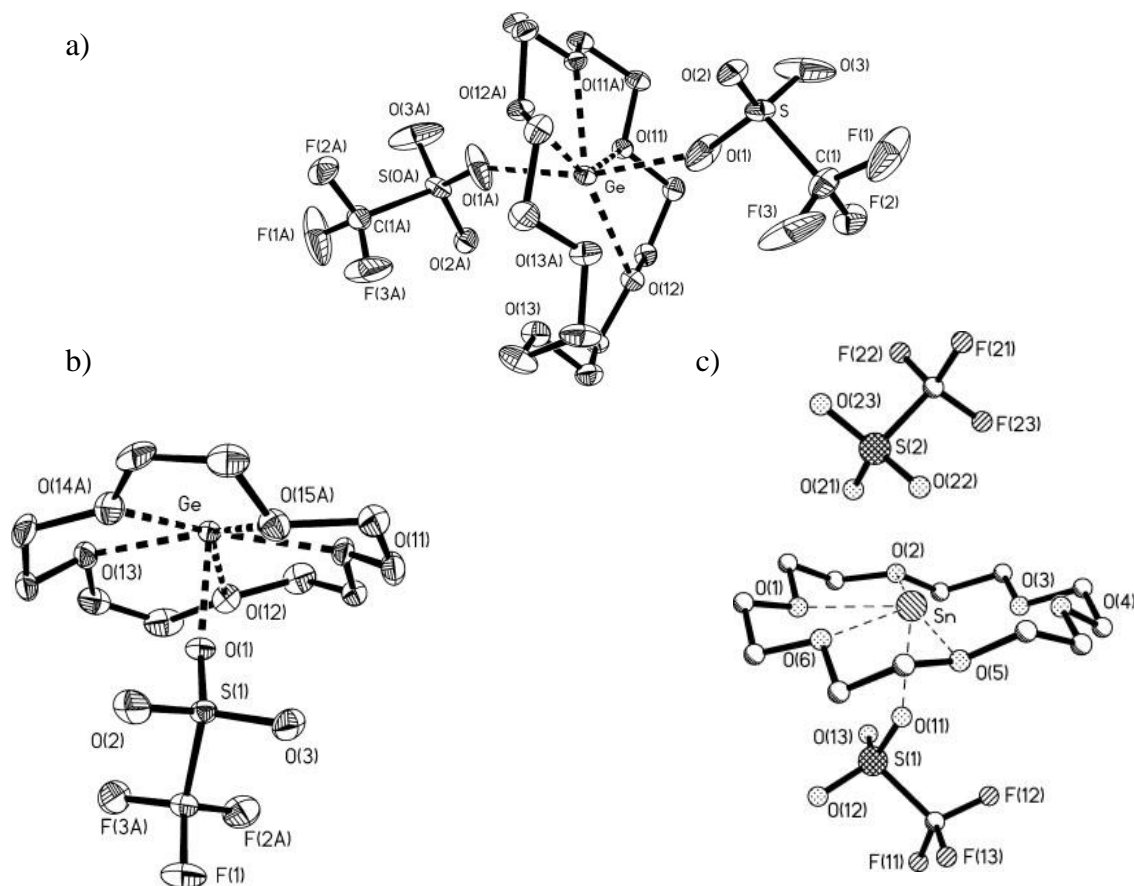


Figure 1.13 Displacement ellipsoid plots of a) $[\text{Ge}([\mathbf{18}\text{crown-6})][\text{OTf}]_2$ ⁴⁸ b) $[\text{Ge}([\mathbf{15}\text{crown-5})][\text{OTf}]_2$ ⁴⁸ and c) $[\text{Sn}([\mathbf{18}\text{crown-6})][\text{OTf}]_2$.⁴⁹ Ellipsoids are drawn at the 50% probability. Reprinted with permission from Elsevier and John Wiley & Sons.⁵⁵

The final class of structures of the tin(II) and germanium(II) crown ether complexes feature an additional chloride ligand on the Group 14 centre, as observed in the solid-state structures of $[\text{GeCl}([\mathbf{18}\text{crown-6})][\text{GeCl}_3]$ and $[\text{SnCl}([\mathbf{18}\text{crown-6})][\text{SnCl}_3]$ (Figure 1.14).

Both complexes are monocationic due to the presence of the MCl^+ fragment within the ring. In $[GeCl([18]crown-6)][GeCl_3]$, four oxygen contacts between the crown ether and germanium centre are present with one very short Ge-O interaction at 2.195(3) Å. The remaining distances range from 2.359(4)-3.237(4) Å, making the germanium centre asymmetrically placed within the crown ether ring. In the analogous tin(II) complex, six oxygen contacts are present ranging from 2.428(2)-2.883(7)⁴⁶ with the tin(II) symmetrically placed within the crown ether.

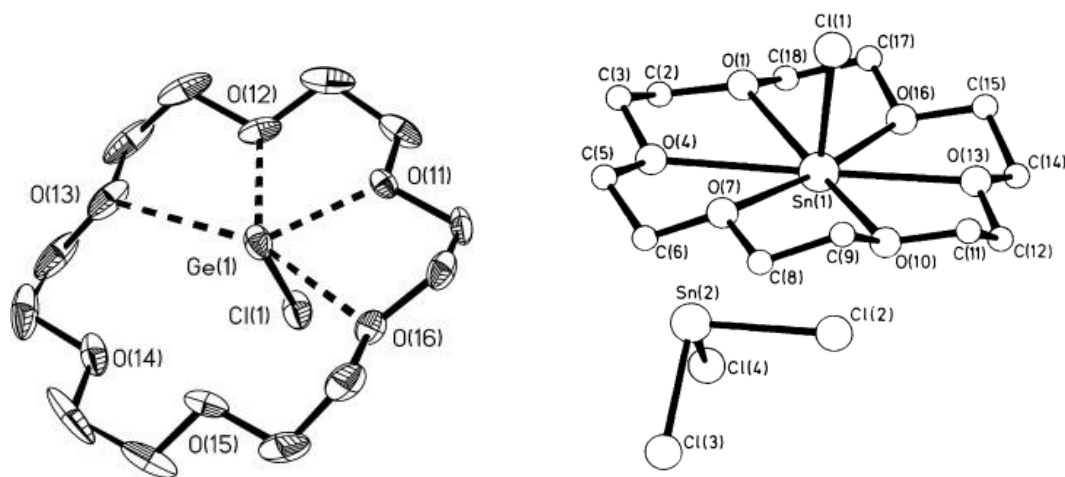
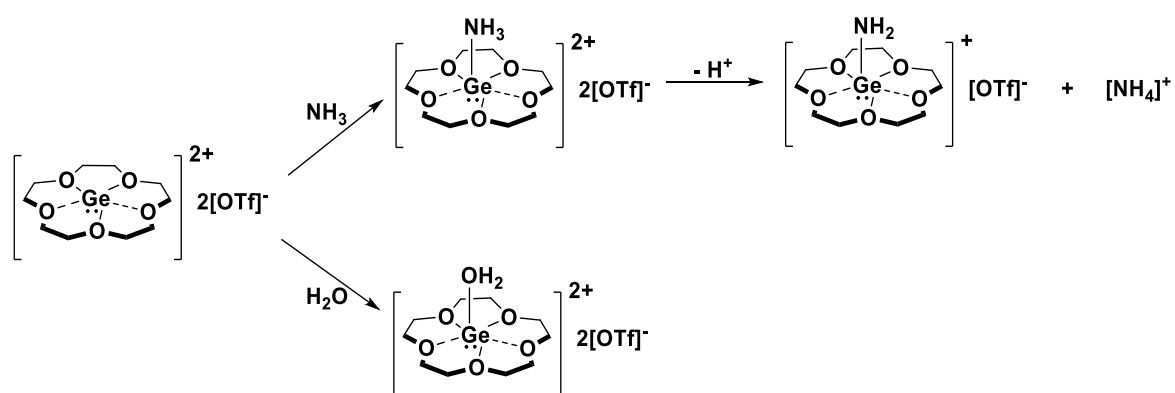


Figure 1.14 a) Displacement ellipsoid plot of $[GeCl([15]crown-5)][GeCl_3]$.⁴⁸ Ellipsoids are drawn at the 50% probability. The $[GeCl_3]^-$ has been omitted for clarity. b) The solid-state structure of $[SnCl([18]crown-8)][SnCl_3]$.⁴⁶ Reprinted with permission from John Wiley & Sons and the Royal Society of Chemistry.⁵⁵

The solid-state structures of the Group 14 crown ether complexes highlight the various coordination environments accessible to the Group 14 centre, varying with both counterion and crown ether size. With different structural environments around the germanium and tin centres, it is anticipated that the reactivity of these complexes will

differ; however, only one study on the reactivity of a germanium crown ether complex has been conducted. The coordination of Lewis bases, ammonia and water, was observed for $[\text{Ge}([\text{15crown-5})][\text{OTf}]_2$ (Scheme 1.2),⁵⁸ illustrating the Lewis acidity of the germanium(II) centre. Although, typically, the activation of small molecules such as water and ammonia by tetraenes is achieved through oxidative addition,^{11b} oxidative addition was not observed in the water or ammonia germanium(II) complex. However, the presence of NH_4^+ was detected in solution by ^1H NMR spectroscopy when ammonia was added to $[\text{Ge}([\text{15crown-5})][\text{OTf}]_2$. Presumably, coordination of ammonia to the germanium(II) centre increases the acidity of the hydrogens of the coordinated ammonia to facilitate the formation of NH_4^+ . This increased acidity is another type small molecule activation different from the typical oxidative addition and highlights the Lewis acidity of the germanium(II) centre. An examination into the coordination of Lewis bases to a series of Group 14 crown ether complexes would enable a more comprehensive understanding of the Lewis acidity and reactivity of Group 14 crown ether complexes.



Scheme 1.2 The addition of ammonia and water to $[\text{Ge}([\text{15crown-5})][\text{OTf}]_2$.⁵⁸

Although the bonding in neutral tetrelenes has been explored extensively,⁵⁶ only one computational study has examined the bonding environments in cationic Group 14 crown ether complexes.⁵⁷ Analysis of the frontier molecular orbitals of **[SnCl([18]crown-6)]⁺** and **[SnOTf([18]crown-6)]⁺** revealed that the HOMOs of the complexes are located primarily on the tin centre and correspond to the lone pair. The LUMOs are also centred on the tin atoms highlighting the potential for ambiphilic reactivity at tin. From the Wiberg bond indices, the sum of the tin-oxygen interactions was consistent with a single bond between the tin and crown ether ligand. Given the similarities in the structures of tin(II) species studied computationally, and the analogous germanium complexes, **[Ge([18]crown-6)][OTf]₂** and **[GeCl([18]crown-6)][GeCl₃]**, a similar electronic structure is expected in the germanium(II) species.

1.4 Scope of Thesis

The thesis herein focuses on the activation of small molecules and Lewis acid catalysis by low valent Group 14 compounds. The goals of this thesis are to 1) to investigate small molecule activation by ditetrelenes, 2) to assess the Lewis acidity of low valent Group 14 complexes and 3) to investigate and understand their catalytic activity in Lewis acid catalysis. The activation of ammonia by a tetraarylditetrelene will be presented and aldehyde reduction by germanium(II) and tin(II) crown ether complexes will be explored.

Chapter 2 describes the activation of ammonia and amines by tetramesityldisilene and -digermene, prototypical ditetrelenes. In addition, through collaboration, computational

studies into the mechanism of the addition of ammonia were carried out, revealing critical stereochemical implications for each step in the N-H bond activation. The lowest energy pathway for the reaction will be presented. Attempts to further functionalize the disilene-amine adducts with alkynes will be described. Model reactions of silylamines with electrophilic alkynes will be explored to re-examine the stereoselectivity of silylation reactions.

Chapter 3 focuses on the quantification of the Lewis acidity of neutral and cationic germanium(II) and tin(II) crown ether complexes. Both experimental and computational methods are employed to assess both the hard and soft Lewis acidities of these species. Multinuclear NMR spectroscopic studies of the solution-state structures of the Lewis acid-base adducts of triethylphosphine oxide and the germanium(II) and tin(II) crown ether complexes are described.

With information regarding the catalytic potential of germanium(II) and tin(II) crown ether complexes, the hydrosilylation of carbonyl compounds catalyzed by these complexes will be explored in Chapter 4. The scope of aldehyde hydrosilylation by $[\text{Ge}([\mathbf{12}]\text{crown-4})_2][\text{OTf}]_2$ will be investigated by varying both the carbonyl and silane sources.

The mechanism of aldehyde reduction by $[\text{Ge}([\mathbf{12}]\text{crown-4})_2][\text{OTf}]_2$ will be explored using a number of experimental techniques and is described in Chapter 5. Deuterium-labelling studies, Linear Free Energy Relationships and stoichiometric addition

experiments will be used to formulate the mechanism of activation and to determine the rate-limiting step.

A summary of this thesis is presented in Chapter 6 along with the major conclusions drawn from this work. Future studies in the area of chemistry explored in this thesis will be suggested.

1.5 References

- [1] a) Mason, R. *Nature*, **1968**, *217*, 543-545. b) Zhang, W.; La, W.; Cao, R. *Chem. Rev.*, **2017**, *117*, 3717-3797. c) Trowbridge, A.; Walton, S. M.; Gaunt, M. J. *Chem. Rev.*, **2020**, *120*, 2613-2692. d) Lang, X.; Zhao, J.; Cheb, X. *Chem. Soc. Rev.*, **2016**, *45*, 3026-3038.
- [2] Chiusoli, G. P.; Maitlis, P. M. *In Metal-catalysis in Industrial Organic Processes*; RSC Publishing: Cambridge, 2019; pp 163–200.
- [3] Lewis, L. N.; Stein, J.; Gao, Y.; Colborn, R. E.; Hutchins, G. *Platinum Metals Rev.*, **1997**, *41*, 66-75.
- [4] Nansai, K.; Nakajima, K.; Suh, S.; Kagawa, S.; Kondo, Y.; Takayanagi, W.; Shugetomi, Y. *Econ. Sys. Res.*, **2017**, *29*, 335-356.
- [5] a) Rehkämper, M.; Halliday, A. N.; Barford, D.; Fitton, J. G.; Dawson, J. B. *Science*, **1997**, *278*, 1595-1598. b) Park, J. W.; Hu, Z.; Gao, S.; Campbell, I. H.; Gong, H. *Geochim. Cosmochim. Ac.*, **2012**, *93*, 63-76.

- [6] Garg, A. K.; Van Tonder, R.; Joubert, R. J. O. *Int. J. Indian Culture and Business Management*, **2007**, *1*, 174-204.
- [7] a) Wen, J.; Wang, F.; Zhang, X. *Chem. Soc. Rev.*, **2021**, *50*, 3211-3237. b) Elsby, M. R.; Baker, R. T. *Chem. Soc. Rev.*, **2020**, *49*, 8933-8987. c) Zweig, J. E.; Kim, D. E.; Newhouse, T. R. *Chem. Rev.*, **2017**, *117*, 11680-11752.
- [8] Harder, S. *Early main group metal catalysis concepts and reactions*; Wiley-VCH: Weinheim, Germany, 2020.
- [9] Power, P. P. *Nature*, **2010**, *463*, 171-177.
- [10] a) Spikes, G. H.; Fettinger, J. C.; Power, P. P. *J. Am. Chem. Soc.*, **2005**, *127*, 12232-12233. b) Welch, G. C.; San Juan, R. R.; Masuda, J. D.; Stephan, D. W. *Science*, **2006**, *314*, 1124-1126. c) Peng, Y.; Ellis, B. D.; Wang, X. Power, P. P. *J. Am. Chem. Soc.*, **2008**, *130*, 12268-12269.
- [11] a) Jana, A.; Schulzke, C.; Roesky, H. W. *J. Am. Chem. Soc.*, **2009**, *131*, 4600-4601. b) Wang, W.; Inoue, S.; Yao, S.; Dreiss, M. *Organometallics*, **2011**, *30*, 6490-6494. c) Power, P. P. *Chem. Rec.*, **2012**, *12*, 238-255.
- [12] a) Thompson, B. L.; Heiden, Z. M. *Tetrahedron*, **2019**, *75*, 2099-2105. b) Peuser, I.; Neu, R. C.; Zhao, X.; Ulrich, M.; Schirmer, B.; Tannert, J. A.; Kehr, G.; Fröhlich, R.; Grimmer, S.; Kerker, G.; Stephan, D. W. *Chem. Eur. J.*, **2011**, *17*, 9640-9650.

- [13] a) Yadav, S.; Saha, S.; Sen, S. S. *Chem. Cat. Chem.*, **2016**, *8*, 486-501. b) Hong, M.; Chen, J.; Chen, E. X.-Y. *Chem. Rev.*, **2018**, *118*, 10551-10616. c) Gao, S.; Blum, S. A. *Trends in Chemistry*, **2021**, *3*, 645-659.
- [14] a) Lawson, J. R.; Melen, R. L. Recent developments and applications of Lewis acidic boron reagents. *Organometallic Chemistry: Volume 41*; Royal Society of Chemistry: Cambridge, UK, 2017. b) Hatano, M.; Ishihara, K. Lewis Acids. *Boron Reagents in Synthesis*, 2016, 27–66. c) Ganesamoorthy, C.; Matthias, M.; Bläser, D.; Wölper, C.; Schulz, S. *Dalton Trans.*, **2016**, *45*, 11437-11444. d) Sagorne, S.; Wehmschulte, R. *Chem. Cat. Chem.*, **2018**, *10*, 2509-2520.
- [15] Jensen, W. B. *Chem. Rev.*, **1978**, *78*, 1-22.
- [16] a) Stephan, D. W. *J. Am. Chem. Soc.*, **2021**, *143*, 20002-20014. b) Paradies, J. *Eur. J. Org. Chem.*, **2018**, *2*, 283-294. c) Erker, G.; Stephan, D. W. *Frustrated Lewis Pairs*; Springer: Heidelberg, Germany, 2013.
- [17] a) Denmark, S. E.; Beutner, G. L. ; Wynn, T.; Eastgate, M. D. *J. Am. Chem. Soc.*, **2005**, *127*, 3774-3789. b) Zhang, Z.; Liu, B.; Zhao, Z. *Carbohydr. Polym.*, **2012**, *88*, 891-895. c) Nair, V.; Sethumadhavan, D.; Nair, S. M.; Rath, N. P.; Eigendorf, G. K. *J. Org. Chem.*, **2002**, *67*, 7533-7536. d) Enslow, K. R.; Bell, A. T. *Catal. Sci. Technol.*, **2015**, *5*, 2839-2847.

[18] MCl_4 ($M = Si, Ge, Sn$) require substrates with oxygen atoms to facilitate coordination and catalysis while BCl_3 and $AlCl_3$ can catalyze reactions with alkenes, more challenging substrates. See references [17c] and [17d].

[19] a) Kindervater, M. B.; Marczenko, K. M.; Werner-Zwanziger, U.; Chitnis, S. S. *Angew. Chem. Int. Ed.*, **2019**, *58*, 7850-7855. b) Marczenko, K. M.; Zurakowski, J.; Bamford, K. L.; MacMillan, J. W. M.; Chitnis, S. S. *Angew. Chem. Int. Ed.*, **2019**, *58*, 18096-18101. c) Marczenko, K. M.; Zurakowski, J. A.; Kindervater, M. B.; Jee, S.; Hynes, T.; Roberts, N.; Park, S.; Werner-Zwanziger, U.; Lumsden, M.; Langelaan, D. N.; Chitnis, S. S. *Chem. Eur. J.*, **2019**, *25*, 16414-16424.

[20] a) Liberman-Martin, A. L.; Bergman, R. G.; Tilley, T. D. *J. Am. Chem. Soc.*, **2015**, *137*, 5328-5331. b) Tschernuth, F. S.; Thorwart, T.; Greb, L.; Hanusch, F.; Inoue, S. *Angew. Chem. Int. Ed.*, **2021**, *60*, 25799-25803. c) Hartmann, D.; Braner, S.; Greb, L. *Chem. Commun.*, **2021**, *57*, 8572-8575. d) Thorwart, T.; Roth, D.; Greb, L. *Chem. Eur. J.* **2021**, *27*, 10422–10427.

[21] a) Roth, D.; Wadepohl, H.; Greb, L. *Angew. Chem. Int. Ed.*, **2020**, *59*, 20930-20934. b) Henry, A. T.; Cosby, T. P. L.; Boyle, P. D.; Baines, K. M. *Dalton Trans.*, **2021**, *50*, 15906-15913.

[22] a) Klare, H. F. T.; Albers, L.; Süsse, L.; Keess, S.; Müller, T.; Oestreich, M. *Chem. Rev.*, **2021**, *121*, 5889-5985. b) Walker, J. C. L.; Klare, H. F. T.; Oestreich, M. *Nat. Rev. Chem.*, **2019**, *4*, 54-62.

- [23] Fluoride ion affinity for BPh₃ 164 kJ/mol, fluoride ion affinity for SiMes₃+ 407 kJ/mol. From: Großekappenberg, H.; Reißmann, M.; Schmidtman, M.; Müller, T. *Organometallics*, **2015**, *34*, 4952-4958; Erdmann, P.; Leitner, J.; Shhwarz, J.; Greb, L. *Chem. Phys. Chem.*, **2020**, *21*, 987-994.
- [24] a) Hadlington, T. J.; Dreiss, M.; Jones, C. *Chem. Soc. Rev.*, **2018**, *47*, 4176-4197. b) Dasgupta, R.; Das, S.; Hiwase, S.; Pati, S. K.; Khan, S. *Organometallics*, **2019**, *38*, 1429-1435. c) Fujimori, S.; Inoue, S. *Eur. J. Inorg. Chem.*, **2020**, *33*, 3131-3142.
- [25] a) Hanusch, F. ; Groll, L.; Inoue, S. *Chem. Sci.*, **2021**, *21*, 2001-2015. b) Wendel, D.; Szilvási, T.; Henschel, D.; Altmann, P. J.; Jandl, C.; Inoue, S.; Rieger, B. *Angew. Chem. Int. Ed.*, **2018**, *57*, 14575-14579. c) Wendel, D.; Szilvási, T.; Jandl, C.; Inoue, S.; Rieger, B. *J. Am. Chem. Soc.*, **2017**, *139*, 9156-9159.
- [26] Jutzi, P.; Schubert, U. *Silicon Chemistry: From the atom to Extended Systems*; Wiley-VCH: Weinheim, Germany, 2003.
- [27] Kira, M. *Proc. Jpn. Acad. Ser. B*, **2012**, *88*, 167-191.
- [28] a) Wind, M.; Powell, D. R.; West, R. *Organometallics*, **1996**, *15*, 5772-5773. b) Fink, M. J.; Michalczyk, M. J.; Haller, K. J.; West, R.; Michl, J. *J. Chem. Soc, Chem. Commun.*, **1983**, 1010-1011.
- [29] a) Shepherd, B. D.; Campana, C. F.; West, R. *Heteroat. Chem.*, **1990**, *1*, 1-7. b) Izod, K.; Evans, P.; Waddell, P. G. *Angew. Chem. Int. Ed.*, **2017**, *56*, 5593.

- [30] a) Grev, R. S.; Schaefer, H.F.; Baines, K. M. *J. Am. Chem. Soc.*, **1990**, *112*, 9458.
b) Schmidt, M. W.; Truong, P. N.; Gordon, M. S. *J. Am. Chem. Soc.*, **1987**, *109*, 5217.
- [31] a) Budaraju, J.; Powell, D.; West, R. *Main Group Met. Chem.*, **1996**, *19*, 531-538 b)
De Young, D. J.; Fink, M. J.; West, R. Michl, J. *Main Group Met. Chem.*, **1987**, *10*, 19-43.
- [32] a) Milnes, K. K.; Pavelka, L. C.; Baines, K. M. *Chem. Rev. Soc.*, **2016**, *45*, 1019-1035. b) Tashkandi, N. Y. ; Parsons, F. ; Guo, J. ; Baines, K. M. *Angew. Chem. Int. Ed.*, **2015**, *54*, 1612-1615.
- [33] Majumdar, M.; Bejan, I.; Huch, V.; White, A. J. P.; Whittell, G. R.; Schäfer, A.; Manners, I.; Scheschkewitz, D. *Chem Eur. J.*, **2014**, *20*, 9225-9229.
- [34] a) McOnie, S. L.; Özpınar, G. A.; Bourque, J. L.; Müller, T.; Baines, K. M. *Dalton Trans.*, **2021**, *50*, 17734-17750. b) Apeloig, Y.; Nakash, M. *Organometallics*, **1998**, *17*, 1260-1265.
- [35] Warren, J. J.; Tronic, T. A.; Mayer, J. M. *Chem. Rev.*, **2010**, *110*, 6961-7001.
- [36] Boomgaarden, S.; Saak, W.; Weidenbruch, M. *Z. Anorg. Allg. Chem.*, **2001**, *627*, 349-352.
- [37] Meltner, A.; Majumdar, M.; White, A. J. P.; Huch, V.; Scheschkewitz, D. *Organometallics*, **2013**, *32*, 6844-6850.
- [38] Simons, R. S.; Pu, L.; Olmstead, M. M.; Power, P. P. *Organometallics*, **1997**, *16*, 1920-1925.

- [39] Ding, Y.; Roesky, H. W.; Noltemeyer, M.; Schmindt, H.G.; Power, P. P. *Organometallics*, **2001**, *20*, 1190-1194.
- [40] Eisenhut, C.; Szilvsi, T.; Breit, N. C.; Inoue, S.; *Chem. Eur. J.*, **2015**, *21*, 1949-1954.
- [41] Krahfuss, M. J.; Radius, U. *Dalton Trans.*, **2021**, *50*, 6752-6765.
- [42] a) Fritz-Langhals, E. *Org. Process. Res. Dev.*, **2019**, *23*, 2369-2377. b) Fritz-Langhals, E.; Werge, S.; Kneissl, S.; Piroutek, P. *Org. Process. Res. Dev.*, **2020**, *24*, 1484-1495.
- [43] Inoue, S.; Ichinohe, M.; Sekiguchi, A. *J. Am. Chem. Soc.*, **2007**, *129*, 6096-6097.
- [44] Hu, C.; Zhang, J.; Yang, H.; Guo, L.; Cui, C. *Inorg. Chem.*, **2021**, *60*, 14038-14046.
- [45] a) Sinhababu, S.; Singh, D.; Sharma, M. K.; Kumar, S.; Mahawar, P.; Nagendran, S. *Dalton Trans.*, **2019**, *48*, 4904-4100. b) Roy, M. M. D.; Fujimori, S.; Ferguson, M. J.; McDonald, R.; Tokitoh, N.; Rivard, E. *Chem. Eur. J.*, **2018**, *24*, 14392-14399.
- [46] Drew, M. G. B.; Nicholson, D. G. *J. Chem. Soc., Dalton Trans.*, **1986**, 1543-1549.
- [47] Swidan, A.; Macdonald, C. L. B., *Chem. Soc. Rev.*, **2016**, *45*, 3883-3915.
- [48] Rugar, P. A.; Bandyopadhyay, R.; Copper, B. F. T.; Stinchombe, M. R.; Ragogna, P. J.; Macdonald, C. L. B.; Baines, K. M. *Angew. Chem. Int. Ed.*, **2009**, *48*, 5155-5158.

- [49] Bandyopadhyay, R.; Copper, B. F. T.; Rossini, A. J.; Schurko, R. W.; Macdonald, C. L. B. *J. Organomet. Chem.*, **2010**, *695*, 1012-1018.
- [50] a) Sen, S. S.; Roesky, H. W.; Stern, D.; Henn, J.; Stalke, D. *J. Am. Chem. Soc.*, **2010**, *132*, 1123-1126. b) Dreiss, M.; Yao, S.; Brym, M.; van Wüllen, C.; Lenta, D. *J. Am. Chem. Soc.*, **2006**, *128*, 9628-9629.
- [51] a) Li, W.; Köhler C.; Yang, Z.; Stalke, D.; Herbst-Irmer, R. Roesky, H. W. *Chem. Eur. J.*, **2019**, *25*, 1193-1197. b) Kira, M.; Ishida, S.; Iwamoto, T.; Kabuto, C. *J. Am. Chem. Soc.*, **1999**, *121*, 9722-9723.
- [52] a) Çetinkaya, B.; Gümrükçü, I.; Lappert, M. F.; Atwood, J. L.; Shakir, R. *J. Am. Chem. Soc.*, **1980**, *102*, 2088-2089. b) Loh, Y. K.; Ying, L.; Fuentes, Á.; Do, D. C. H.; Aldridge, S. *Angew. Chem. Int. Ed.*, **2019**, *58*, 4847-4851.
- [53] Baines, K. M.; Stibbs, W. G. *Coord. Chem. Rev.*, **1995**, *145*, 157-200.
- [54] Persson, I.; D'Angelos, P.; Lundberg, D. *Chem. Eur. J.*, **2016**, *22*, 18583-18592.
- [55] Copyright permission for the reprinting of the figures from John Wiley & Sons, Elsevier, and the Royal Society of Chemistry are given in Appendix E.
- [56] a) Shan, C.; Yao, S.; Dreiss, M. *Chem. Rev. Soc.*, **2020**, *49*, 6733-6754. b) Eisenhut, C.; Szilvási, T.; Dubek, G.; Breit, N. C.; Inoue, S. *Inorg. Chem.*, **2017**, *56*, 10061-10069.

- [57] Macdonald, C. L. B.; Bandyopadhyay, R.; Cooper, B. F. T.; Friedl, W.; Rossini, A. J.; Schurko, R. W.; Eichhorn, S. H.; Herber, R. H. *J. Am. Chem. Soc.*, **2012**, *134*, 4332-4345.
- [58] Bandyopadhyay, R.; Nguyen, J. H.; Swidan, A.; Macdonald, C. L. B. *Angew. Chem. Int. Ed.*, **2013**, *125*, 3553-3556.

Chapter 2

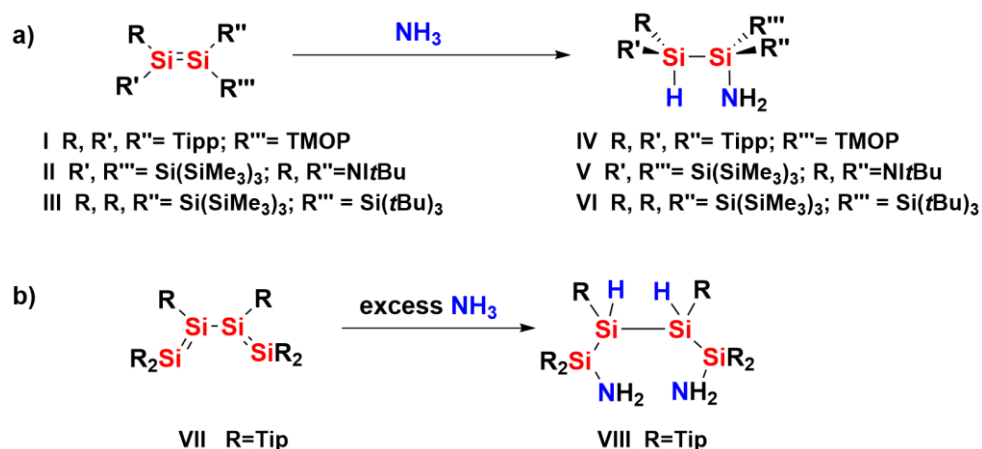
2 Amine Functionalization by Ditetrelenes

2.1 Introduction

Amines are key functional groups in pharmaceuticals, and thus, the development of new approaches for the activation and functionalization of the primary feedstock, ammonia, is of continued interest. Although several examples of the activation of the NH bond in ammonia by transition metal complexes have been reported,¹ the coordination of ammonia to the transition metal centre often competes, hindering oxidative addition. In contrast, low valent main group compounds have been found to activate ammonia under mild conditions leading to the exclusive formation of N-H bond activated products,² and thus, may be promising alternatives to transition metal complexes in the functionalization of amines. Although research currently focuses on the NH bond activation of ammonia by main group species, the end goal is to further react the activated species in a catalytic fashion to generate functionalized amines.³

Low valent group 14 compounds have been found to be promising in the area of amine activation, yielding only the N-H activated species under mild or ambient conditions.³ Although several examples of ammonia activation by tetrylenes, the heavier Group 14 analogue of carbenes, have been reported,⁴ only a few ditetrelenes, the heavier Group 14 analogue of alkenes, have been shown to react with ammonia or amines. In the case of disilenes, the addition of ammonia to asymmetrically-substituted disilenes^{5,6} (**I**, **III**, Scheme 2.1a), a highly twisted imino(silyl)disilene⁷ (**II**, Scheme 2.1a) and a

tetrasilabutadiene⁸ (**VII**, Scheme 2.1b) have been reported. The reaction of diethylamine or butylamine with transient arylated digermenes has also been investigated although the products were not isolated.⁹ Given the interest in the chemistry of ditetrelenes, it is unclear if a polarized,^{5,6} highly twisted⁷ or a conjugated⁸ Si-Si π system is required to activate ammonia or if it is possible to activate ammonia with a simple, symmetrically-substituted tetraaryldisilene and -digermene. Thus, the reaction of ammonia and amines with tetramesityldisilene and -digermene, prototypical, symmetrically-substituted ditetrelenes was examined.



Scheme 2.1 N-H Bond activation of ammonia by a) disilenes **I**, **II**, **III**⁵⁻⁷ and b) **VII**⁸ to yield silylated amines. Tipp = 2,4,6-trimethylphenyl; TMOP = 2,4,6-trimethoxyphenyl; NI*t*Bu = bis(*t*-butyl)imidazolin-2-imino.

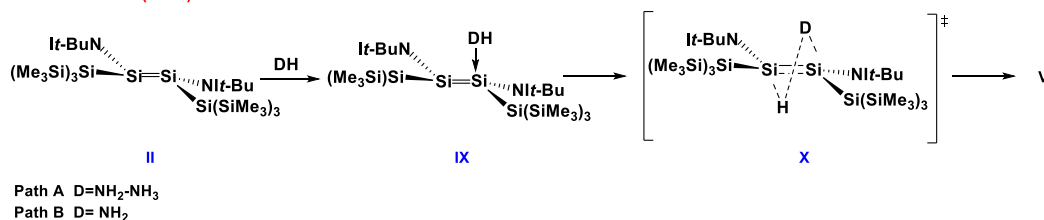
The addition of ammonia to disilene **II** is stereospecific giving the *anti* isomer of the addition product, **V** (Scheme 2.1a). The mechanism of the reaction was examined computationally by Wendel *et al.*;⁷ two reaction paths were explored using either monomeric or dimeric ammonia as the reagent (Scheme 2.2a). Path A, utilizing dimeric

ammonia, was found to be more energetically favourable ($\Delta G^\ddagger = 14.4$ kcal/mol) compared to Path B, utilizing monomeric ammonia ($\Delta G^\ddagger = 20.5$ kcal/mol). Both paths, with only one transition state in each, are single step mechanisms. The authors referred to the transition state as an “*anti*-transition state”.

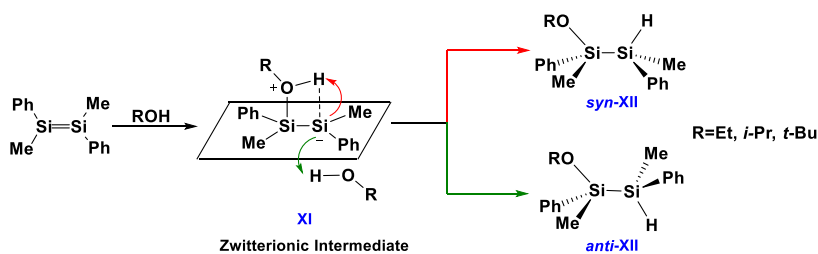
The addition of water and alcohols to disilenes, the prototypical 1,2-addition reaction of disilenes, is one of the few reactions of disilenes for which the mechanism has been extensively studied both experimentally¹⁰ and computationally¹¹ and provides a comparator for the 1,2-addition of ammonia. On the basis of kinetic studies and the influence of the concentration of alcohol on the diastereoselectivity of the reaction, Sekiguchi *et al.* suggested a two-step nucleophilic addition mechanism (Scheme 2.2b) to account for the formation of both the *syn* and *anti* isomers.^{10e} At low alcohol concentrations, intramolecular proton transfer on the same plane of the disilene in the zwitterionic intermediate, **XI**, predominates giving the *syn*-product (*syn*-**XII**) whereas at high concentrations of alcohol, intermolecular proton transfer resulted in the formation of the *anti*-products (*anti*-**XII**). Apeloig and Nakash^{10b} studied the kinetics of the addition reaction of substituted phenols to a bulkier disilene (see Scheme 2.2c) and, in contrast to Sekiguchi *et al.*,^{10e} noted that the stereochemistry of product was *independent* of alcohol concentration. In addition, the stereospecificity of the addition was influenced by the solvent of the reaction, as had been observed previously by West.^{10d} Although a similar mechanism was given to account for the formation of the *syn*-isomer of the product (*syn*-**XV**), to account for the formation of the *anti*-product (*anti*-**XV**), bond rotation about Si-Si bond of the zwitterionic intermediate (**XIII**) was proposed (Scheme 2.2c) followed by

protonation of the backside of the formally negatively charged silicon atom instead of intermolecular proton transfer.

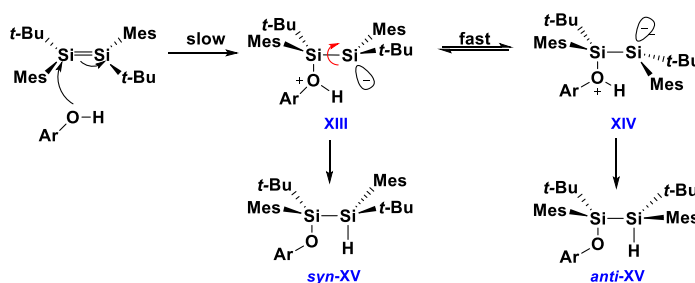
a. Wendel *et al.*⁷ (2018)



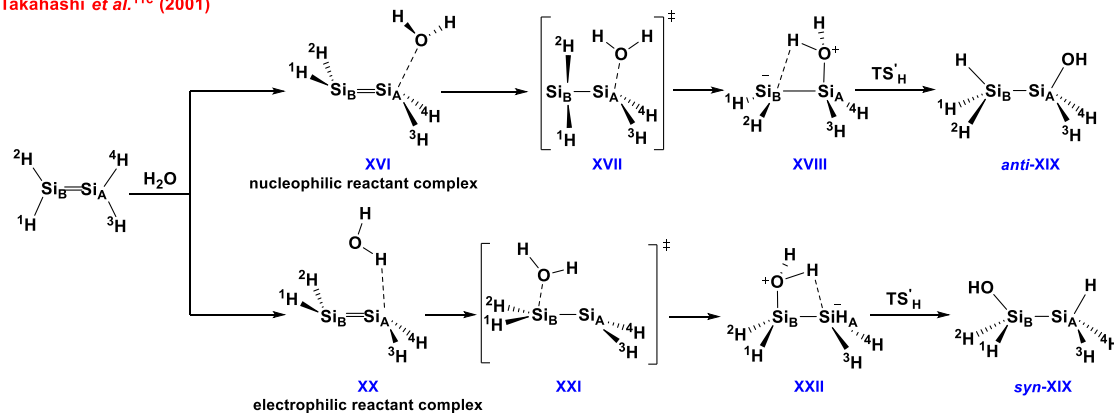
b. Sekiguchi, Maruki and Sakurai^{10e} (1993)



c. Apeloig and Nakash^{10b} (1998)



d. Takahashi *et al.*^{11c} (2001)



Scheme 2.2 Suggested mechanisms for E-H (E = N, O) bond activations of disilenes.

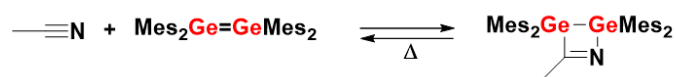
The only computational study which considers the formation of both stereoisomers in the reaction of water with the parent disilene ($\text{H}_2\text{Si}=\text{SiH}_2$) was carried out by Takahashi *et al.* and published in a series of papers.^{11a-d} Two reaction pathways were found starting with either a weakly-bonded nucleophilic (**XVI**) or an electrophilic (**XX**) reactant complex (Scheme 2.2d) which the authors emphasized were key in setting the reaction path. Complex **XVI** is formed by the lone pair (HOMO) of water interacting with the LUMO of the disilene.^{11c} The structural metrics of **XVI** are not significantly different from those of the individual components and there is no significant energetic difference between the complex and the individual starting materials. The O–Si_A bond formation and Si_A–Si_B bond rotation occurs simultaneously in the transition state of the first elementary step of the mechanism (**XVII**) derived from the nucleophilic reactant complex allowing proton transfer to the opposite face of the disilene in intermediate **XVIII** giving the *anti*-isomer of the product (*anti*-**XIX**; the stereochemistry was tracked by numbering the hydrogen substituents on the disilene). The electrophilic reactant complex **XX** is formed by interaction between the hydrogen of the water molecule (LUMO) and the HOMO of the disilene (Scheme 2.2d). Complex **XX**, again, has minimal changes in its structural metrics compared to the individual reactants. After formation of **XX**, the oxygen associates with Si_B of the disilene undergoing nucleophilic addition, forming the Si–O bond and generating the zwitterionic species, **XXII** through transition state **XXI**. Finally, hydrogen transfer from the oxygen to the silicon results in the *syn*-addition product, *syn*-**XIX**. Although the two paths differ in the orientation of the water-disilene complex and the structures of the

transition states leading to **XVIII/XXII**, the hydrogen transfer steps from the water moiety are nearly identical.

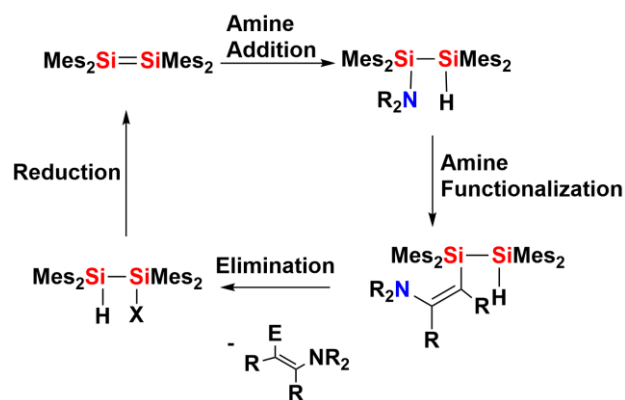
Bulky substituents are necessary to stabilize disilenes; the use of a disilene with small substituents such as hydrogen in the computations ignores the steric factors that may affect the course of the mechanism. On the basis of calculations with $\text{H}_2\text{Si}=\text{SiH}_2$, Takahashi *et al.* predicted that in the addition of water to disilenes with bulky substituents, the *anti*-product will be favoured due to the less-crowded approach of the nucleophile to the disilene.^{11d} Although there are additional computational studies of the mechanism of the addition of water or alcohols to disilenes,^{11e-h} and, in some cases, a one-step mechanism was found,^{11f-h} the focus of the studies was not understanding the stereochemistry of the reaction.

Despite being one of the most studied and fundamental reactions of disilenes, there are many unanswered questions regarding the mechanism of the 1,2-addition reactions. Does intermolecular proton transfer and/or Si-Si bond rotation in the putative zwitterionic intermediate play a role in the stereochemistry of the reaction? What are the key factors which influence the stereochemical outcome of the reaction? The polarity of the solvent? The bulk of the substituents? The formation of initial reactant complexes? To better understand the NH bond activation of ammonia by disilenes and digermenes, and indeed 1,2-additions in general, the stereochemistry and mechanism of the reaction of the addition of ammonia to tetramesityldisilene was examined computationally.

Although many examples of the small molecule activation by ditetrelenes have been reported, ditetrelenes have not been used as catalysts in any chemical transformation. A general catalytic pathway has three steps: activation of substrate, transformation of substrate to product and elimination of product. Although there are several examples of ditetrelenes being used to activate molecules (*vide supra*), only one example of elimination to give a ditetrelene, the release of acetonitrile from a 1,2,3-azadigermetine to yield tetramesityldigermene (Scheme 2.3), has been documented.¹² No examples of the further functionalization of substrates activated by ditetrelenes have been reported. Herein the reaction of disilylamines with electron-deficient alkynes to give silylenamines was investigated as a proof-of-concept example for the functionalization of a disilene-activated substrate (Scheme 2.4).



Scheme 2.3 Reversible addition of acetonitrile to tetramesityldigermene.¹²

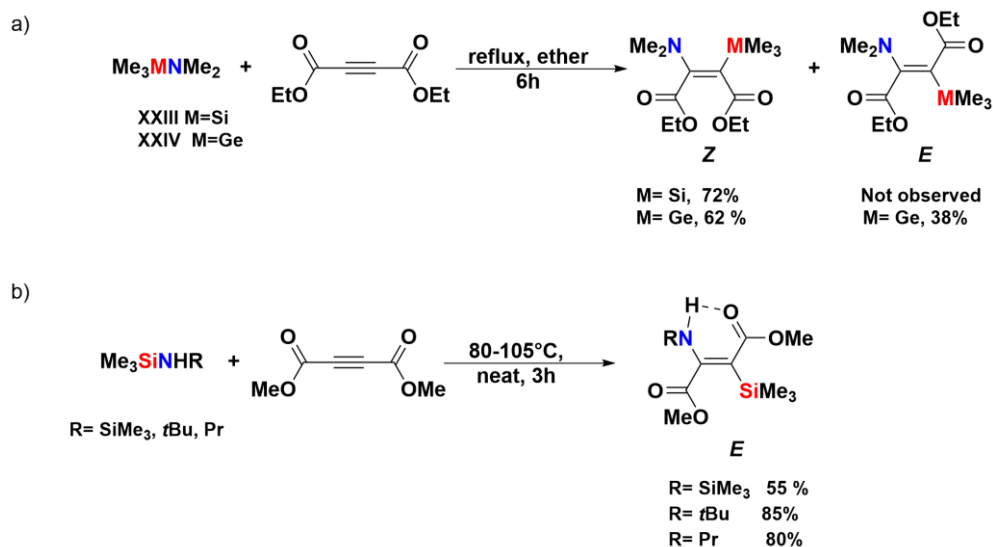


Scheme 2.4 Plausible pathway for the step-wise functionalization of amines by tetramesityldisilene. Amine addition and functionalization will be presented in this Chapter.

Two investigations of the stereoselectivity and mechanism of the silylamination of electron deficient alkynes have been reported^{13,14} and a number of silylamination reactions have been described.¹⁵ The first report of silylamination was the reaction of *N,N*-dimethyl(trimethylsilyl)amine, **XXVIII**, and diethyl acetylenedicarboxylate which was found to yield *Z*-silylenamines stereoselectively by George and Lappert (Scheme 2.5a).¹³ The stereochemistry about the double bond was proposed on the basis of the stereochemistry of the addition of secondary amines to dimethyl acetylenedicarboxylate.¹⁶ In analogous germylamination reactions, Satgé observed the formation of both *E*- and *Z*-germylenamines (Scheme 2.5a),¹⁷ indicating that this reaction is not as stereoselective as the silylamination reactions reported by George and Lappert. The *E* stereochemistry of the products was assigned by a detailed analysis of the IR data and on the basis of the deshielded chemical shift of the N-H of the silylenamines in the ¹H NMR spectra of the adducts which was attributed to hydrogen bonding with the *cis*-carbomethoxy group. The formation of predominantly *E*-silylenamines is in contrast to the observation of only the *Z*-silylenamine as reported by Lappert and George and may be a consequence of the ability to form a hydrogen bond between the NH bond and the *cis*-oriented carbomethoxy group. A subsequent investigation of the stereoselectivity of the silylamination of electron deficient alkynes by Srivastava also showed selectivity towards one silylenamine isomer.¹⁴ Using silylamines with the general formula Me₃SiNHR, the formation of exclusively *E*-silylenamines was observed (Scheme 2.5b).

To evaluate the possibility to further functionalize the amine moiety activated by a ditetrelene, silylamination of acetylene carboxylates will be investigated using silylamines

derived from disilenes. In addition, the work of George and Lappert will be reinvestigated to confirm the difference in stereoselectivity observed in silylamination and germylamination reactions.

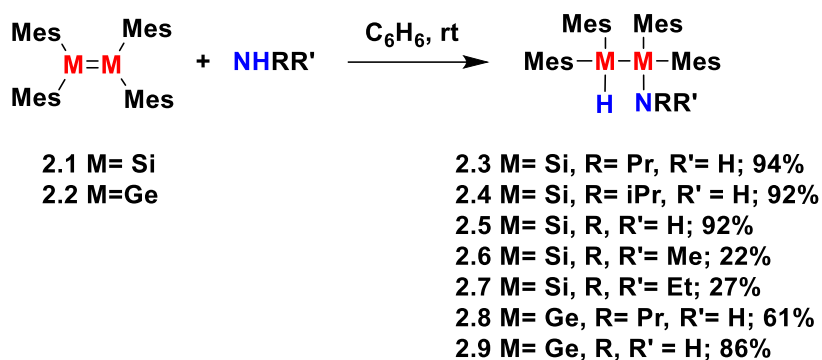


Scheme 2.5 a) Silyl- and germylamination of diethyl acetylenedicarboxylate.^{13,17} Isolated yields are given. b) Silylamination of dimethyl acetylenedicarboxylate. Isolated yields are given.¹⁴

2.2 The Addition of Amines to Ditetrelenes

2.2.1 Experimental Results and Discussion

The reactivity of ditetrelenes towards amines was explored using tetramesityldisilene, **2.1**, and tetramesityldigermene, **2.2**, prototypical tetraarylditetrelenes selected for their ease of synthesis.¹⁸ Dissolution of **2.1** or **2.2** in benzene afforded a yellow solution to which an equivalent of amine was added (Scheme 2.6). Once the bright yellow colour of the solution had dissipated, the solvent was removed under vacuum to yield clear or light-yellow oils, **2.3-2.9**.



Scheme 2.6 Addition of amines to ditetrelenes. Isolated yields of the products are reported for **2.3-2.7**. NMR yields of **2.8** and **2.9** are reported.

The ^1H NMR spectra of the products derived from the addition of ammonia or a primary amine to disilene **2.1** showed quantitative conversion to the expected products of hydroamination, disilylamines (**2.3-2.5**). In the addition of secondary amines to **2.1**, low conversion (approximately 40-50%) to the products (**2.6** and **2.7**) was observed by ^1H NMR spectroscopy. Thin layer chromatography was utilized to separate the product from 1,1,2,2-tetramesityldisilanol, formed from the exposure of unreacted disilene to wet solvents after the reaction, leading to low isolated yields for **2.6** and **2.7**. In the reaction of tetramesityldisilene with dimethylamine, trace amounts of other amine-containing products were evident in the ^1H NMR spectrum of the crude product; however, these species could not be isolated or identified. The ^1H NMR spectra of the products derived from the addition of propylamine or ammonia to digermene **2.2** revealed a mixture of products including compounds **2.8** and **2.9**, respectively. The purification of the crude reaction mixtures by TLC was attempted; no amine-derived products were recovered from the plate. Huck *et al.*

noted that digermene **2** does not react with butylamine or diethylamine in THF after 2 days at 4 °C.^{9c}

¹H-²⁹Si HMBC NMR spectroscopy was useful in the identification of adducts **2.3-2.7**. Two signals were present in the ¹H-²⁹Si HMBC spectra of **2.3-2.7**; the high field signal with a large splitting (~180 Hz) was assigned to the Si with a directly bound H. The low field signal showed correlations to the signals assigned to the NH moiety in adducts **2.3** and **2.4**, the NCH₃ moiety in **2.6** and the NCH₂ moiety in **7** confirming the assignment of these signals to the Si bearing the N. The ²⁹Si NMR chemical shifts of approximately -56 ppm for the Si-H and approximately -15 ppm for the Si-N in **2.3-2.7** are similar to those of **IV** (Scheme 2.1; -57 and -21 ppm, respectively).⁵ As further evidence for the formation of **2.3-2.7**, the ¹H-¹⁵N HMBC NMR spectra of **2.3-2.7** were recorded. Only one signal was observed in the ¹⁵N dimension, which showed a correlation to the signal assigned to the Si-H moiety in the ¹H dimension. In the case of **2.3**, the molecular structure was determined using X-ray crystallography (Figure 2.1). The bond lengths and bond angles are comparable to those of **IV**⁵ and are within the expected ranges.

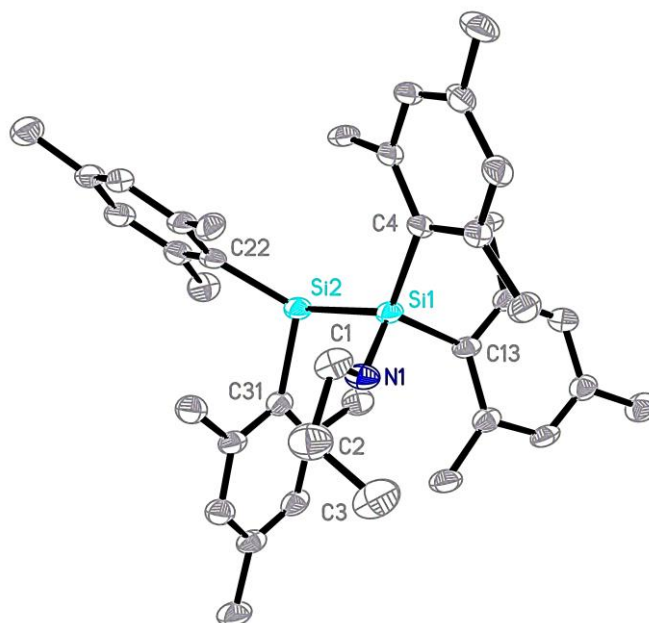


Figure 2.1 Displacement ellipsoid plot of **2.3**. Ellipsoids are drawn at the 50% probability level. Hydrogen atoms are omitted for clarity. Selected parameters (bond lengths in Å; bond angles in °): Si1-N1 1.738(3), Si1-Si2 2.386(2), N1-C1 1.474(5), Si1-C13 1.916(4), Si2-C22 1.901(4) ; N1-Si1-C4 105.30(16), N1-Si1-C13 111.29(15), C4-Si1-C13 109.55(16), N1-Si1-Si2 106.54(13).

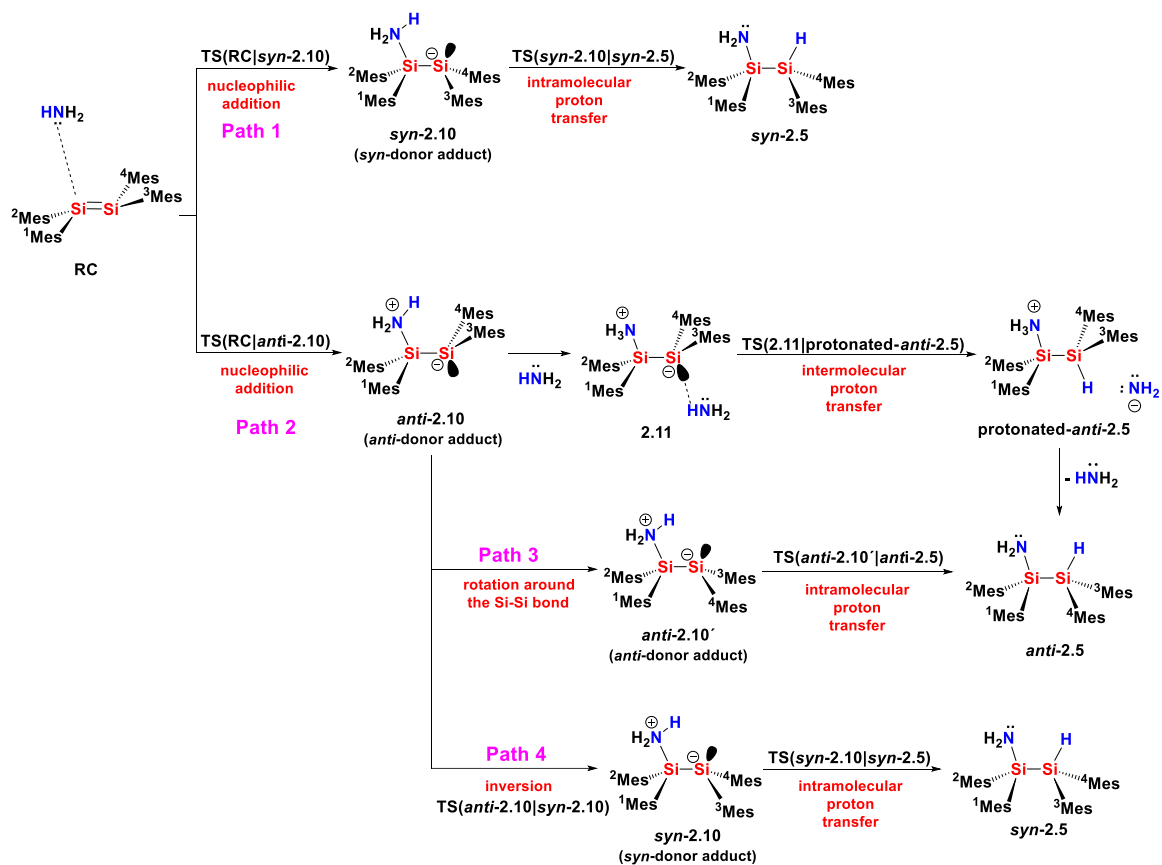
In the addition of primary amines to **2.1**, the yellow colour of the disilene decolourized over a period of 10 minutes at room temperature. The addition of an excess of amine was found to increase the rate of reaction, as evidenced by the rapid disappearance of the yellow colour (in less than 2 minutes). For reactions with secondary amines, little colour change was observed upon the addition of the amines to the disilene, with no notable increase in the qualitative rate of the disappearance of the colour of the solution when excess amine was utilized. As the secondary amines contain an additional alkyl group, steric bulk of the amine evidently decreases the rate of addition. When the steric

bulk is increased even further, such as in *tert*-butylamine, diisopropylamine and dibenzylamine, no reaction with **2.1** was observed. Amine cone angles, analogous to Tolman cone angles for phosphines, quantify the steric bulk of amine ligands.¹⁹ Ammonia and propylamine, with cone angles of 94° and 106°, respectively, react faster than the secondary amines, dimethylamine and diethylamine, with cone angles of 119° and 125°, respectively. Although the cone angles of *tert*-butylamine and diethylamine are similar (123° and 125°, respectively), the increased nucleophilicity of secondary amines compared to primary amines evidently facilitates the reaction. When the steric bulk of the amine is increased even further, such as in diisopropylamine (137°) and dibenzylamine (140°), it is unsurprising that no reaction was observed. The formation of **2.3-2.9** indicates that a symmetrically-substituted disilene (or digermene) with electronically benign aryl substituents is able to activate ammonia as well as amines to give the product of hydroamination; an asymmetric ligand substitution pattern or specialized substituents are not required.

2.2.2 Computational Results and Discussion

Four distinct paths for the mechanism of ammonia addition to disilene **2.1** have been examined. All paths were modelled using M06-2X/6-311+G(d,p) model chemistry; an overview of the approaches is given in Scheme 2.7. With a symmetrically-substituted disilene (**2.1**), the *syn/anti* products (*syn-2.5/anti-2.5*) cannot be distinguished experimentally; however, for the purposes of this computational study, the mesityl substituents have been numbered to be able to track the stereochemistry of the steps along the reaction path. In addition to paths involving monomeric ammonia, the energetics of the

key steps of the most plausible path involving a dimer of ammonia was examined, as ammonia forms hydrogen-bonded clusters in non-polar solvents.²⁰ Similar pathways involving dimeric ammonia was previously examined by Wendel *et al.*⁷ and by others in the examination of the addition of water and methanol to disilenes.^{11e-f}



Scheme 2.7 Summary of Paths 1 – 4 examined in this work.

Path 1. Path 1 depicts the formation of the *syn*-ammonia-2.1 donor adduct, *syn*-2.10, via a reactant complex (RC), followed by a *syn* transfer of a proton to give *syn*-2.5 (Scheme 2.7). Notably, the reactant complex is nucleophilic in nature, in contrast to the electrophilic complex **XX** that gave rise to the *syn* product of the addition of water to

H₂Si=SiH₂, *syn*-**XIX**. The transition state structure of **TS**(*syn*-**2.10**|*syn*-**2.5**) in the second step of Path 1 resembles that of **X** (D=NH₂)⁷ (Scheme 2.2a). The computed N – Si – Si ...H dihedral angles for **TS**(*syn*-**2.10**|*syn*-**2.5**) (-2°) and **X** (D = NH₂, -20°; Figure 2.2) indicate that intramolecular proton transfer occurs in a *syn* fashion in *both* cases, and thus, it is misleading to refer to **X** as an “*anti*-addition transition state”.⁷

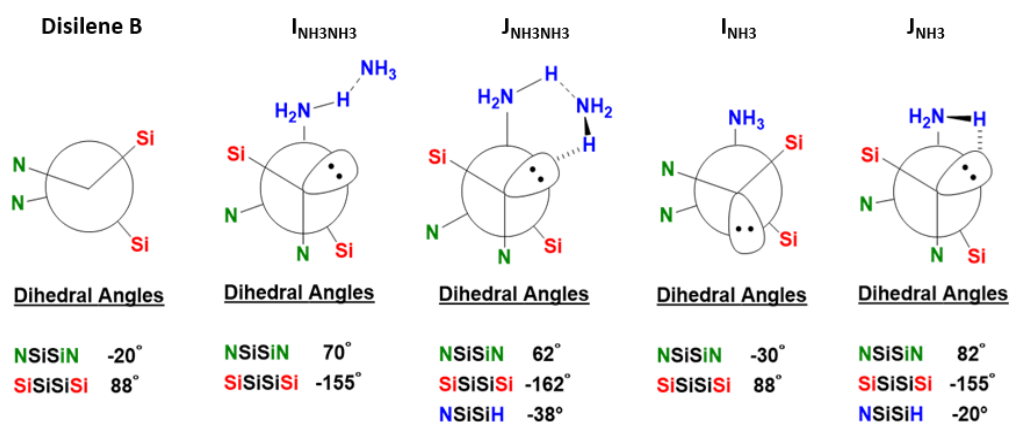


Figure 2.2 Newman projections for species along Path A and Path B (Scheme 2.2a).⁷

The computed Gibbs activation barrier for the formation of *syn*-**2.10**, the rate determining step, in both the gas phase and benzene is approximately 18 kcal/mol, which is too high for a reaction to proceed at room temperature within the short reaction times (10 minutes for ammonia/primary amines). Therefore, Path 1 is not a plausible explanation accounting for the hydroamination reactions of disilene **2.1**. Due to the sizeable barrier for the formation of the *syn*-ammonia-disilene donor adduct in the system under study, only reaction pathways involving the formation of the *anti*-donor adduct (*vide infra*) were considered further. Notably, in previous experimental studies of the addition of water and

alcohols to disilenes, which pre-date the computational work, the possibility of an *anti*-water/alcohol-disilene donor adduct was not mentioned, presumably due to the preponderance of the formation of the *syn*-products.¹⁰

Path 2. The initial step (a nucleophilic addition) of Path 2 is the formation of the *anti*-ammonia-**2.1** adduct (*anti*-**2.10**) via **TS(RC|*anti*-2.10)** (Scheme 2.7). The formation of the *anti*-ammonia-**2.1** donor adduct, *anti*-**2.10** has a barrier of 7.7 kcal/mol; the formation of *anti*-**2.10** is kinetically more favourable at room temperature by 9.9 kcal/mol compared to the formation of *syn*-**2.10**. Close examination of the reported structures of the initially formed ammonia or dimeric ammonia complexes of disilene **II**⁷ (**IX**, Scheme 2.2d and Figure 2.2) reveals an *anti*-orientation between the donor and the lone pair on the β -silicon. Notably, **IX** (D = NH₂NH₃) is significantly rotated about the Si-Si bond compared to the core structure of the starting disilene, whereas **IX** (D = NH₂) with monomeric ammonia is not (Figure 2.2).

After the formation of *anti*-**2.10** and hydrogen-bonding of a second molecule of ammonia to give **11**, intermolecular proton transfer takes place through **TS(2.11|protonated-*anti*-2.5)** to *anti*-**2.5** (Scheme 2.7). A barrier of activation of 47.8 kcal/mol (37.6 kcal/mol relative to **2.11**) for the intramolecular proton transfer indicates that this step is rate-determining and is not kinetically favourable. Due to the rather high free energy and barrier height, Path 2 is likely not followed at room temperature.

Intermolecular proton transfer from a second equivalent of alcohol was proposed by Budaraju *et al.*^{10d} and Sekiguchi *et al.*^{10e} to account for the formation of the *anti*-isomer of

the product derived from the addition of alcohols to disilenes at high concentrations of alcohol. In contrast, Apeloig and Nakash^{10b} found that the stereochemistry of the products derived from the addition of phenols to *E*-1,2-di-*tert*-butyl-1,2-dimesityldisilene is independent of the phenol concentration suggesting that intermolecular proton transfer (from a second molecule of phenol) does not occur, consistent with our computational result.

Path 3. Due to the high activation barrier of intermolecular proton transfer (37.6 kcal/mol), other steps to proton transfer were considered. From *anti*-**2.10**, the lone pair and ammonium group must achieve a *syn* conformation to achieve intramolecular proton transfer. In Path 3, bond rotation about the Si1–Si2 (similar to the suggestion of Apeloig and Nakash^{10b}) to give *anti*-**2.10'**, an eclipsed conformation of *anti*-**2.10**. The computed rotational barrier from *anti*-**2.10** to *anti*-**2.10'** is about 20 kcal/mol which is high relative to the Si – Si bond rotation in simple disilanes.²¹ The large rotational barrier in *anti*-**2.10** is due to the steric strain in the eclipsed conformation where repulsive interactions between the mesityl group (¹Mes) and the lone pair at Si2 and between mesityl groups, ²Mes and ⁴Mes, occurs. The free energy of activation of the intramolecular proton transfer in *anti*-**2.10'** is the same as that in *syn*-**2.10**, 5.6 kcal/mol and consequently, the rate-determining step of Path 3 is the rotation about Si–Si bond (from *anti*-**2.10** to *anti*-**2.10'**). In contrast to suggestion of Apeloig and Nakash,^{10b} with this barrier, the reaction will not proceed at a reasonable rate at room temperature, and thus, Path 3 can also be excluded.

Path 4. Another method to achieve a *syn* conformation of the ammonium and lone pair in *anti*-2.10 is inversion. The inversion barriers of anionic silicon species with small substituents (such as H or Me)²² are large (>25 kcal/mol) and the inversion barriers of oligosilyl anions carrying bulky substituents (such as -Ph, -SiMe₃, -SiMe₂(*t*Bu)) are in the range of 13–18 kcal/mol²³ indicating that inversion barriers of silyl anions significantly depend on the nature of the substituents. On the basis of these data, in Path 4, the formation of an *anti*-donor adduct (*anti*-2.10) step and intramolecular proton transfer with inversion of configuration at the formally negatively-charged silicon atom are combined (Figure 2.3).

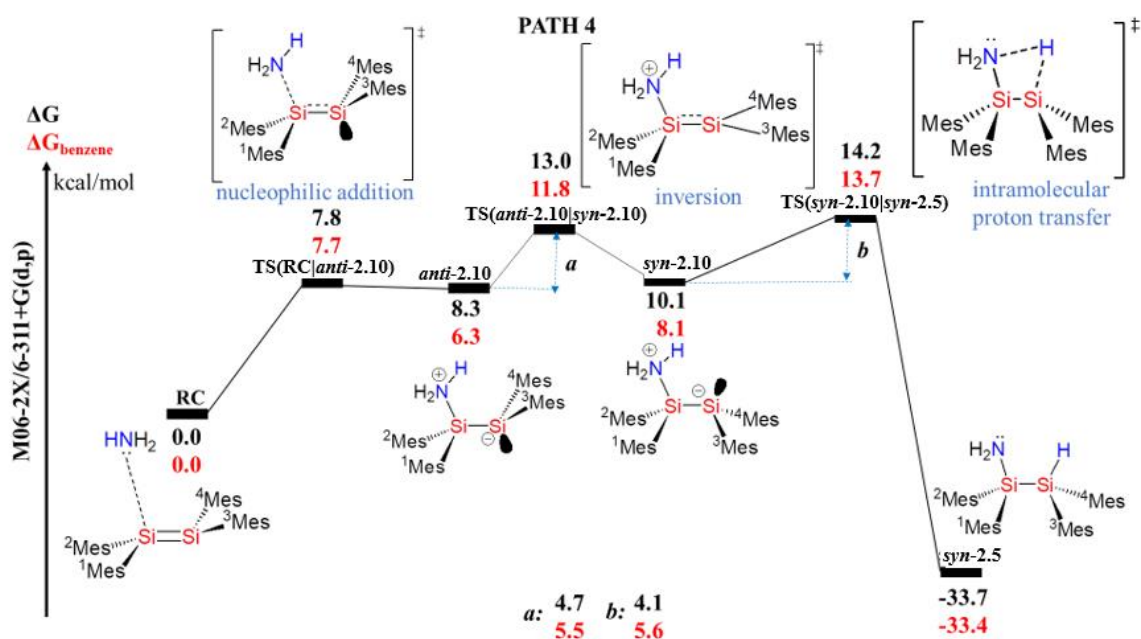


Figure 2.3 Relative free energies (in kcal/mol, at 298 K and 1 atm) for Path 4 in the gas phase (black) and in benzene (red).

Path 4 starts with the formation of *anti*-10 via TS(RC|*anti*-2.10) but results in the formation of *syn*-2.5 via TS(*syn*-2.10|*syn*-2.5) due to inversion from *anti*-2.10 to *syn*-2.10

via **TS(anti-2.10|syn-2.10)**. The Gibbs activation barrier for the inversion step (from **anti-2.10** to **syn-2.10**) is only 5.5 kcal/mol, indicating that inversion is energetically more favourable by 14.5 kcal/mol compared to rotation. The magnitude of the inversion barrier agrees well with the results of Marschner and co-workers²³ and can be attributed to the strong interaction between lone pair (LP) of silicon centre and σ^* Si-R antibonding orbital of silyl substituent, stabilizing the transition state for inversion and decreasing its barrier. Thus, the low inversion barrier found for the interconversion of **anti-2.10** to **syn-2.10** is not unreasonable and is key to understanding the stereochemical outcome of the reaction.

As Path 4 is kinetically very efficient; it can be concluded that it is the most plausible path among those examined (Scheme 2.7), clarifying the mechanism of ammonia addition to disilene **2.1**. The rate-determining step of Path 4 is the intramolecular proton transfer with a Gibbs activation energy of 13.7 kcal/mol relative to the reactant complex, **RC**. On the other hand, the highest single step barrier height (relative to the corresponding reactant complex or intermediates) is that of the formation of the *anti*-donor adduct at 7.27 kcal/mol.

The nucleophilic addition of ammonia to disilene **2.1** occurs in a nonpolar solvent (benzene), and therefore, a proton shuttle may be involved in the proton transfer step. Proton shuttles play an important role in many reactions, including proton transfers in nonpolar solvents and their inclusion is known to significantly influence the activation energy of the reaction.²⁰ Indeed, Wendel *et al.*⁷ found that using the ammonia dimer as the donor in the reaction with disilene **II** had a significant effect on the energetics of the proton

transfer and similar observations have been made when dimers or trimers of water or alcohols add to disilenes.^{11e-f} In benzene, the formation of oligomeric ammonia clusters, which can serve as proton shuttles, is very likely. Accordingly, Path 4 was modelled using an ammonia dimer as the nucleophile to investigate the influence of having a proton shuttle on the energetics of these steps.

Path 4 (ammonia dimer). The energetics of the remodelled steps of Path 4 using the ammonia dimer as the nucleophile is shown in Figure 2.4. The addition of the ammonia dimer to disilene **2.1** gives *anti*-**2.12** and then inversion at the anionic silicon centre of *anti*-**2.12** occurs to form *syn*-**2.12**. Proton transfer on *syn*-**2.12**, using the proton shuttle, leads the formation of the *syn* product, *syn*-**2.5** (Figure 2.4).

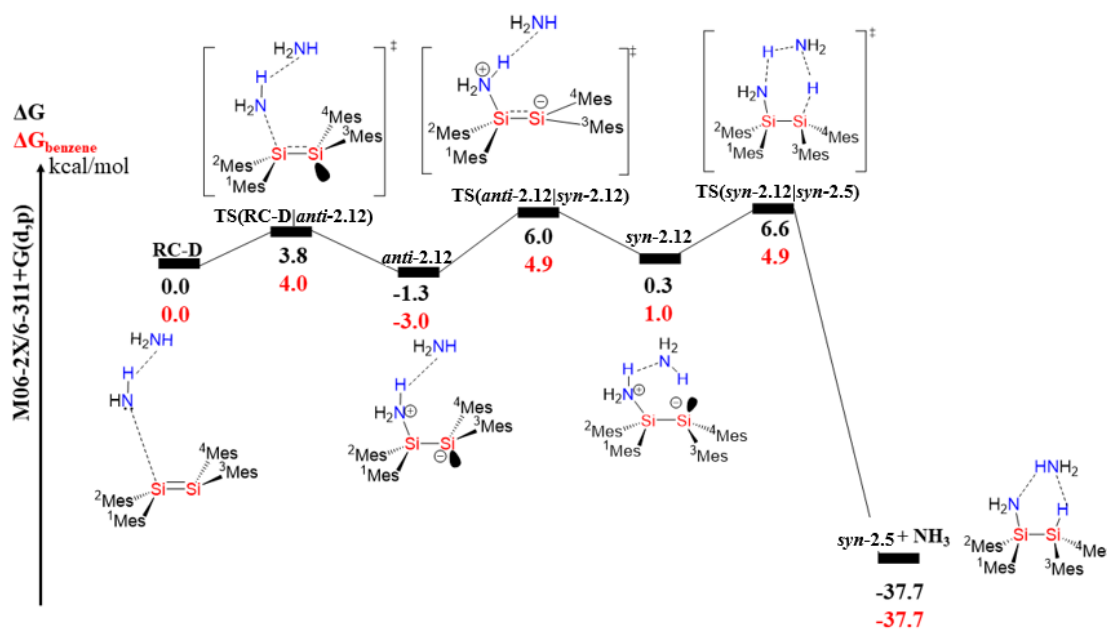


Figure 2.4 Energetics of Path 4 computed using the dimer of ammonia.

The use of the ammonia dimer in the formation of the *anti*-donor adduct, inversion and proton transfer steps results in a decrease in the free energy of activation of about 4, 7 and 9 kcal/mol, respectively, compared to that of monomeric ammonia (Figure 2.3) in Path 4. However, the presence of the second hydrogen-bonded ammonia does not remarkably influence the optimized geometry of the structures. As expected, the involvement of the dimer of ammonia in the mechanism causes a significant decrease in activation free energy. However, from the relative free activation energies computed in benzene, it is difficult to come to an unambiguous conclusion about which is the rate-determining step of the addition reaction of ammonia to disilene **2.1**, since there is little difference between the activation energies (4.0, 4.9 and 4.9 kcal/mol) of each elementary step.

In summary, the most energetically-favoured reaction mechanism for the addition of ammonia to disilene **2.1** involves three steps: formation of the *anti*-ammonia-disilene adduct, inversion at the β -silicon, and *syn*-transfer of the proton to give the *syn*-product and utilizes the ammonia dimer as a proton shuttle.

2.2.3 Comparison to Previously Proposed Mechanisms

Previous studies have shown that the stereochemistry of the 1,2-addition of alcohols to disilenes is influenced by the concentration of the alcohol and the polarity of the solvent for the reaction. The ratio of the *syn:anti* isomers of the addition of ethanol to *E*-1,2-dimethyl-1,2-diphenyldisilene decreased at high concentrations of ethanol.^{10e} Due to the lower acidity of hydroxy hydrogen in the ethanol donor adduct (EtO⁺H(Si)) compared to the propanol derivative,^{10e} at elevated concentrations intermolecular proton transfer from a

second equivalent of alcohol was proposed to be competitive with intramolecular proton transfer enabling the formation of the *anti*-product derived from ethanol. Notably, phenols, with a greater acidity, show no dependence of the *syn:anti* ratio on concentration^{10b} and the results herein have now shown that intermolecular proton transfer is energetically inaccessible. Regarding the influence of the polarity of the solvent, reactions conducted in benzene led to almost exclusive formation of the *syn* product while reactions conducted in a more polar solvent, THF, led to increasing amounts of the *anti* addition product.^{10b,d} THF, with a greater dielectric constant, was proposed to stabilize the donor adduct which is zwitterionic in nature, extending its lifetime and allowing rotation about the Si-Si bond to occur and protonation from the backside of the β -silicon to give the *anti*-isomer (Scheme 2.2b). Rotation about the central Si-Si bond in a donor adduct with bulky substituents has a rather high barrier (Path 3); protonation from the backside of the β -silicon also seems unreasonable. However, Takahashi *et al.*^{11c} have stated that the dependence of the ratio of *syn:anti* isomers on the polarity of the solvent can be accounted for by the dipole moments of the two transition states of the rate-determining steps in the addition of water to the parent disilene. They found that the transition state for the rate-determining step of the path leading to the *anti*-product (**XVII**) is more polar than that leading to the *syn*-product (**XXI**) (6.56 D vs 3.51 D, respectively), and thus, solvents with a higher dielectric constant should give more of the *anti*-isomer (as observed). Notably, the energy difference between the two transition states **XVII** and **XXI** is just 2.3 kcal/mol in the absence of solvent; in a solvent with a high dielectric constant, the different dipole moments of the transition states will decrease this energy difference. This provides a reasonable explanation of the influence of

the polarity of the solvent on the stereochemistry of the reaction, and it requires an understanding of the dipole moments of the relevant transition states to predict the influence of solvent on the stereochemistry of the reaction.

The influence of alcohol concentration on the *syn:anti* ratio,^{10e} can also be understood when the polarity of the two transition states is, once again, considered. Small alkyl alcohols have large dielectric constants (e.g. $\epsilon = 24.3$ for ethanol²⁴), and thus, at a high concentration of alcohol, the polarity of the solution is increased, favouring the *anti*-product. In contrast, the dielectric constants of phenols are smaller ($\epsilon = 13.4$ for phenol; 11.05 for *p*-methoxyphenol (60 °C))²⁴. High concentrations of phenols would have a negligible effect on the polarity of the solution, and thus, the *syn:anti* ratio is unaffected.

Apeloig and Nakash^{10b} proposed a unique route to an *anti*-product, namely, formation of a *syn*-donor adduct, rotation about the Si-Si bond in the adduct and then proton transfer from back side of the β -silicon bearing the lone pair (Scheme 2.2c); the formation of an *anti*-donor adduct was not considered. Their proposal was also based on the assumption that the rotational barrier about the central Si-Si bond in the *syn*-phenol-disilene donor adduct would be less than that of the inversion barrier (estimated to be 24 kcal/mol for *i*-Pr₂PhSi:⁻)²² at the silicon bearing the lone pair in the donor adduct. Given the results herein, the most probable mechanism for the formation of the *syn*-isomer in the addition of *p*-methoxyphenol to *E*-1,2-*t*-butyl-1,2-dimesityldisilene is *anti*-donor adduct formation, inversion and *syn* transfer of the proton, whereas the *anti*-isomer is obtained by initial formation of the *anti*-donor adduct followed by *syn*-transfer of the proton after

rotation about the Si-Si bond (either during the formation of or after the formation of the donor adduct).

In computational studies of the nucleophilic addition of water to the parent disilene (Si_2H_4), the structure of an *initial reactant complex* was stated to be key in setting the stereochemistry of the product; a nucleophilic reactant complex lead to the formation of the *anti*-disilanol and an electrophilic reactant complex lead to the formation of the *syn*-disilanol (Scheme 2.2d).^{11c} However, the nucleophilic and electrophilic reactant complexes lead to the formation of *anti*- and *syn*-water-disilene donor adducts, respectively, en route to the *anti*- and *syn*-products although the stereochemistry of the intermediate donor adducts was not discussed in detail in the original publication. The proton transfer is *syn* in both pathways. Upon re-examination of the structure of transition state **XXI** using the published coordinates and constructing the intrinsic reaction coordinate (IRC) of the reaction path,^{11c} the starting structure of the IRC reveals an apparent nucleophilic complex rather than an electrophilic complex. Thus, the formation of both the *syn*- and *anti*-products is proposed to depend *on the stereochemistry of the addition of the nucleophile* as governed by the path of the approach of the water molecule to the parent disilene and *not* the formation of two different types of reactant complexes. For the formation of the *anti*-product (***anti*-XIX**), the water approaches the apex of pyramidal Si_A where the hydrogen atoms are bent away from the approaching water molecule. Simultaneous rotation about the Si-Si bond takes place resulting in the formation of an *anti*-water-disilene donor adduct, **XVIII**. *Syn* transfer of the hydrogen yields the *anti*-product. In contrast, if the water approaches from the base of pyramidal Si_B where the hydrogen atoms are bent *towards* the

approaching water molecule, Si_B will undergo inversion and give the *syn* donor adduct, **XXII**. *Syn* proton transfer to the adjacent Si_B gives the *syn* product.

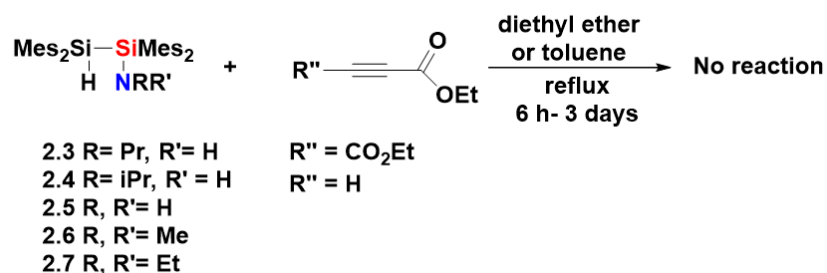
In the only published study of the stereochemistry of the addition of ammonia to a disilene, that of Wendel *et al.*,⁷ the *anti*-isomer of the product, **V**, was isolated (Scheme 2.2a). The authors attributed the stereochemical outcome to an “*anti*-addition transition state” and did not comment on the nature of the species preceding the transition state (although it was located). As an alternate interpretation, the formation of the *anti*-product is instead a consequence of the initial formation of an *anti*-ammonia-disilene **II intermediate** (**IX**, D=NH₂NH₃) the transition state to which was not located. From the calculations on this system, significant rotation about the Si-Si bond occurs *during* the formation of the *anti*-donor adduct as is evident from the structure of complex **IX** (D = NH₂NH₃), Scheme 2.2a) which shows significant rotation about the Si-Si bond in comparison to the starting disilene. The *anti*-donor adduct is then already positioned for the *syn* transfer of the proton from a *gauche* conformation. Thus, the *anti*-stereochemistry of the hydroamination product can be the result of a first elementary step of the reaction, the formation of the *anti*-donor adduct, and not because of an “*anti*-addition” of the N-H bond to the disilene as originally stated.⁷ The formation of an *anti*-donor adduct accompanied by significant rotation is analogous to that observed by Takahashi *et al.* in their study of the stereochemistry of the addition of water to the parent disilene (**XVII**, Scheme 2.2d).^{11c} An examination of the factors which may attribute to the formation of an *anti*-donor adduct with little change in structure compared to the starting disilene, as reported herein (*anti*-**10/12**), or a significant

change in structure compared to the starting disilene may be key to predicting the stereochemical outcomes of the reaction.

2.3 Silylamination Using Disilylamines

2.3.1 Experimental Results of Discussion

As N-H activation was found to be possible with tetramesityldisilene, further functionalization of the amine through Si-N bond activation in silylamination was investigated. Disilylamines **2.3-2.7** were subjected to the same conditions reported by Lappert and George (Scheme 2.8).¹³ No changes to the ¹H NMR or ²⁹Si NMR spectra were observed after 6 hours, indicating no reaction occurred. When the time of the reaction was extended to 3 days, again, no changes to the ¹H NMR or ²⁹Si NMR spectra of the reaction mixtures were observed. Due to the bulky mesityl groups, access to the Si-N bond may be hindered, and thus, further optimizations were conducted using **2.5**, containing the least bulky amine group (NH₂). Even when the reaction was carried out at a higher temperature (100 °C), or for longer time periods (3 days), no changes to the NMR spectra were observed.



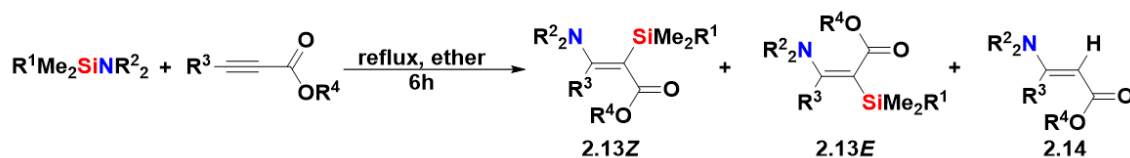
Scheme 2.8 Attempted silylamination of diethylacetylene dicarboxylate with disilylamine adducts **2.3-2.7**.

In an attempt to further reduce the sterics of the system, singly-substituted alkynes, methyl and ethyl propiolate, were selected for silylamination with **2.3-2.5** (Scheme 2.8). Under the same conditions, no evidence of a reaction was observed by ^1H NMR or ^{29}Si NMR spectroscopy. Evidently there is a steric limitation to the silylamination of electron-deficient alkynes which has not been recognized previously. To understand the steric limitations of the silylamination reaction, experiments featuring less bulky alkyl-substituted silylamines were investigated in detail. In addition, the identities of the products were also investigated using 2D-NMR spectroscopic methods not previously available to confirm the stereoselectivities of the reactions.

The reactions of *N, N*-dimethyl(trimethylsilyl)amine, **XXIII**, and diethyl acetylenedicarboxylate was re-examined under the same reaction conditions reported by George and Lappert¹³ (Table 2.1, Entry 2). The ^1H NMR spectrum of the crude product revealed three sets of signals which were assigned to the *Z/E* isomers of the silylated enamine, **2.13Z-b** and **2.13E-b**, and enamine **2.14b**. Attempts to separate the mixture by thin layer chromatography were unsuccessful. Only enamine **2.14b** was recovered from the plate in yields greater than expected on the basis of the ratios of the products in the crude reaction mixture as determined by ^1H NMR spectroscopy suggesting that hydrolysis of both **2.14E-b** and **2.14Z-b** during chromatography had occurred. Assignment of the signals to specific isomers of **2.14** could not be done using 2D NMR experiments, and thus, were assigned on the basis of the ^1H NMR chemical shift of the signals assigned to the SiMe_3 group. The isomer with the larger chemical shift of the SiMe_3 group was assigned the *E* configuration; similar arguments were employed by Satgé.¹⁷ The stereochemistry of

enamine **2.14b** was assigned as *E* using NMR chemical shift comparisons²⁵ and confirmed using Nuclear Overhauser Enhancement Spectroscopy (NOESY) where correlations between the signal assigned to the dimethylamino group and the signal assigned to the vinylic hydrogen were observed. Similar stereochemical results were also observed for the silylation of dimethyl acetylenedicarboxylate and **XXIII** (Table 2.1, Entry 1).

Table 2.1 Silylation of electrophilic alkynes.



Entry ^a	Silylamine	Product Identifier	Alkyne	Ratios of Products ^b		
				2.13Z	2.13E	2.14
1	R ¹ = Me R ² = Me	a	R ³ = C(O)OMe, R ⁴ = Me	6	12	1
2		b	R ³ = C(O)OEt, R ⁴ = Et	2	4	1
3		c	R ³ = H, R ⁴ = Me	Trace	0.2	1
4		d	R ³ = H, R ⁴ = Et	0.1	2	1
5	R ¹ = Me R ² = Et	e	R ³ = C(O)OMe, R ⁴ = Me	-	-	1
6		f	R ³ = C(O)OEt, R ⁴ = Et	-	-	1
7		g	R ³ = H, R ⁴ = Me	-	-	1
8		h	R ³ = H, R ⁴ = Et	-	-	1
9	R ¹ = Ph R ² = Me	i	R ³ = C(O)OMe, R ⁴ = Me	-	-	1
10		j	R ³ = C(O)OEt, R ⁴ = Et	-	-	1
11		k	R ³ = H, R ⁴ = Me	-	-	1
12		l	R ³ = H, R ⁴ = Et	-	0.2	1

^a Reactions were also conducted for a 48h time period; comparable *Z/E* ratios were obtained. ^b All reactions went to full conversion by ¹H NMR spectroscopy; all products were identified.

The formation of two stereoisomers of the silylated enamines, **2.13E-b** and **2.13Z-b** (Table 2.1, Entry 2), is inconsistent with the report by George and Lappert where the

2.13Z-b isomer was identified as the only stereoisomer formed in the reaction between **2.1** and diethyl acetylenedicarboxylate. Though a ^1H NMR spectroscopic analysis of the product identified as **2.13Z-b** was alluded to in the previous work, no NMR spectroscopic data were provided, and thus, the formation of exclusively **2.13Z-b** cannot be confirmed. Our results demonstrate that the silylamination of diethyl acetylenedicarboxylate with **XXIII** is not as stereoselective as originally reported. The selectivity for silylamination is consistent with the non-stereoselective reactions observed in the germylamination of diethyl or dimethyl acetylenedicarboxylate.¹⁷

Reactions of **XXIII** with terminal alkynes, methyl propiolate and ethyl propiolate, were also examined (Table 2.1, Entries 3 and 4). Mixtures of the *Z/E* silylated enamines and **2.14c-d** were observed, although, the mixture could not be separated by thin layer chromatography. The stereochemistry of the major product was established using NOESY, where correlations between the signals assigned to the trimethylsilyl and dimethylamino groups and the signal assigned to the vinylic hydrogen were observed, consistent with the formation of the *E* isomers, **2.13E-c** or **2.13E-d** (Figure 2.5a). NOESY correlations between the two signals assigned to the vinylic hydrogens and the signal assigned to the dimethylamino group lead to the assignment of enamines **2.14c/2.14d** as *E*-enamines (Figure 2.5b). The reactions of methyl and ethyl propiolate with **2.1** are regioselective; the amino group adds exclusively on the terminal carbon, similar to the regioselectivity of the hydroamination of propiolates.¹⁶ These results show that the silylamination of alkynes can be achieved with an alkyne featuring a single electron withdrawing group and that the absence of reaction with methyl and ethyl propiolate and disilylamines **2.3-2.7** is not

related to the electronics of the alkyne, further suggesting the steric limitation in these systems.

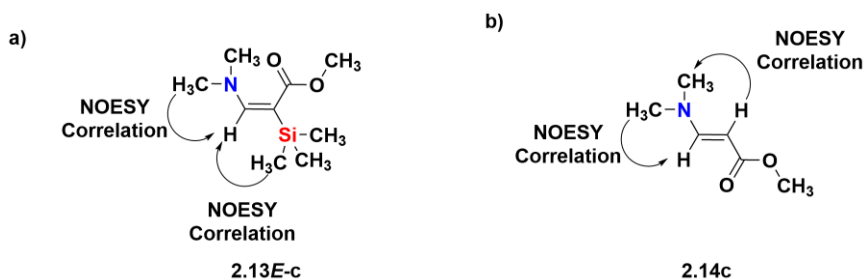


Figure 2.5 NOESY correlations observed in a) **2.13E-c** confirming formation of the *E* isomer and b) **2.14c** confirming the formation of the *E*-enamine.

Despite rigorous attempts, including distillations of all solvents and reagents, and the use of molecular sieves, hydrolysis of **2.13Z** and **2.13E** to form **2.14** could not be avoided. Although the acid-catalyzed hydrolysis of vinylsilanes is stereospecific,²⁶ the hydrolysis of **2.13Z/2.13E** to form **2.14** is not. As there is no known source of acid in the reaction, it is proposed that hydrolysis occurs through direct cleavage of the silyl group by water. A different pathway to the desilylated enamine accounts for the lack of stereospecificity observed in the hydrolysis of silylenamines. However, hydrolysis of silylenamines **2.13Z/2.13E** enables the reliable and high-yielding formation of one enamine isomer, **2.14**.

Only methylaminosilanes were investigated by George and Lappert.¹³ The influence of substituents with additional steric bulk on nitrogen on the outcome of the silylation reaction was investigated. Larger substituents on the nitrogen would allow for synthesis of more diverse silylenamines if disilenes were implemented as amine functionalization

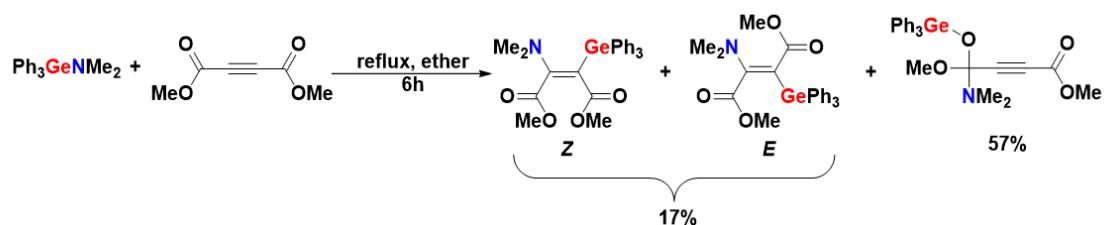
catalysts. The reactions of the acetylenecarboxylates and *N,N*-diethyl(trimethylsilyl)amine were investigated. Under the standard reaction conditions (Table 2.1), **2.14e-h** were the only products observed in all cases (Table 2.1, Entries 5-8). Using NOESY experiments, correlations between the signal assigned to the NCH₂ groups to the signal assigned to the singular vinylic hydrogen in **2.14e** and **2.14f**, or both vinylic hydrogens in **2.14g** and **2.14h** confirmed the stereochemistry of **2.14e-h** as *E*-enamines. Further attempts to observe the *E*- or *Z*-silylenamines through reaction optimization were unsuccessful.²⁷ Evidently, steric bulk at nitrogen does not reduce the susceptibility of silylenamines to hydrolysis.

Similarly, only silylation featuring methyl groups on the silyl substituent were previously investigated,¹³ in contrast to the triethylgermyl- and triphenylgermylamines studied by Satgé.¹⁷ As disilenes require bulky substituents to stabilize the double bond, if tetramesityldisilene were to be used as a catalyst, the reaction must be tolerant of significant bulk around the Si-N bond. The effect of increasing the steric bulk of the substituents at silicon was examined by using *N,N*-dimethyl(dimethylphenylsilyl)amine in reactions with dimethyl or diethyl acetylenedicarboxylate (Table 2.1, Entries 9-10). Once again, **2.14i-j** were the only alkyne-derived products observed. The chemical shifts of **2.14i-j** are identical to those assigned to **2.14c-d** and are consistent with the loss of the dimethylphenylsilyl substituent from **2.13Z-i/j** or **2.13E-i/j**. However, other signals derived from the silylamine were noted in the ¹H NMR spectrum. In the ¹H-²⁹Si HMBC spectrum of the crude product from each reaction, a signal was observed in the ²⁹Si dimension at -0.4 ppm and was assigned to 1,1,2,2-tetramethyl-1,2-diphenyldisiloxane,²⁸ a by-product of hydrolysis.²⁹ Reactions of *N,N*-dimethyl(dimethylphenylsilyl)amine with methyl and ethyl

propiolate were investigated (Table 2.1, Entries 11-12). In addition to the formation of **2.14k-1**, a small amount (~15% of the mixture) of the *E*-silylenamine was observed in the reaction of *N,N*-dimethyl(dimethylphenylsilyl)amine and ethyl propiolate (Table 2.1, Entry 12), though not in the reaction with methyl propiolate. The ^1H - ^{29}Si HMBC spectrum of the reaction mixture for the reaction of *N,N*-dimethyl(dimethylphenylsilyl)amine and ethyl propiolate revealed a signal at -6.7 ppm in the ^{29}Si dimension which showed correlation to the signal assigned to the vinylic hydrogen at 6.18 ppm in the ^1H dimension, consistent with the formation of the silylenamine. In the NOESY spectrum, the signal assigned to the dimethylsilyl group and the signal assigned to the dimethylamino group both showed correlations to the signal assigned to the vinylic hydrogen which confirmed the formation of the silylenamine as well as confirmed the stereochemistry as *E*. The formation of the silylenamine provides direct evidence for the silylation of the alkyne with bulkier silylamines.

Satgé observed the germylamination of dimethylacetylene dicarboxylate using $\text{Ph}_3\text{GeNMe}_2$, a bulkier tetramine than $\text{PhMe}_2\text{SiNMe}_2$.¹⁷ After 5 hours 17% of the germyl enamine was observed. Notably, the carbonyl-addition product was observed in a 57% yield and is presumed to have formed due to rearrangement of the alkyne-addition products (Scheme 2.6). Approximately 26% of the alkyne remained unreacted after 5 hours, compared to the quantitative addition of $\text{Me}_3\text{GeNMe}_2$ to the alkyne observed in the same time frame suggesting that the phenyl substituents slow the reaction down. As our results have now confirmed the similarities in selectivity between the germyl and silylamine additions to electron-deficient alkynes, with an even bulkier tetramine, such as

disilylamines **2.3-2.7**, the bulky substituents would slow the reaction down and evidently in this case, prevent reaction altogether. Furthermore, the decomposition of the triphenylgermylenamines suggest that if silylamination had occurred with **2.3-2.7**, a similar decomposition pathway could be anticipated generating a mixture of products.



Scheme 2.9 Addition of $\text{Ph}_3\text{GeNMe}_2$ to dimethylacetylene dicarboxylate. The yields reported are NMR yields.

2.4 Conclusions

In conclusion, investigations into the addition of amines and ammonia to tetramesityldisilene and digermene have shown the facile formation of 1,2-addition products, disilyl- or digermylamines. These results show that the hydroamination of disilenes is a general reaction and does not require unusual structural features of the disilene to take place under ambient conditions. The mechanism of the addition of ammonia to tetramesityldisilene was computed and revealed a three-step reaction pathway: formation of the *anti*-ammonia-disilene adduct, inversion at the β -silicon, and *syn*-transfer of the proton to give the *syn*-product, where each step follows a distinct stereochemical course. This work underlines critical aspects of the stereochemistry of nucleophilic additions to disilenes, and presumably, digermenes, that has not been fully realized in previous studies in this area: 1) that the stereochemistry of the addition relies on an

understanding of the stereochemical implications of *all* elementary steps of the reaction mechanism: addition of the nucleophile and transfer of the proton as well as the possibility of inversion at the silicon bearing the lone pair or rotation about the Si-Si bond during the reaction, 2) that intermolecular proton transfer in non-polar solvents is not energetically feasible, 3) that all activation barriers may decrease with the involvement of dimers (oligomers) of the nucleophile, and 4) that the bulk and/or electronic effects of the substituents can have a profound effect on the stereochemical course of the reaction, particularly their influence on the barrier to rotation and inversion in the donor adduct.

Attempts to further functionalize the disilylamines generated from the hydroamination of tetramesityldisilene through silylamination of electron-deficient alkynes were unsuccessful. The results of the attempted silylamination of electron-deficient alkynes have highlighted a significant challenge when using kinetically-stabilized ditetrelenes: sterics. The bulky substituents required to stabilize ditetrelenes can hinder subsequent reactivity, such as the functionalization of a silylamine derived from the ditetrelene. This secondary reactivity is necessary for catalysis, and thus, less bulky ditetrelenes, may be required for catalytic applications; however, the use of less bulky ditetrelenes will be challenging due to their short lifetimes.

Reinvestigation of the addition of silylamines to acetylenecarboxylates demonstrated that the formation of both *E* and *Z* silylenamines occurs, correcting a previous report. The reactions are stereoselective towards the *E* isomer. Although selectivity for only the *E* isomer was observed in the addition of secondary silylamines to

dimethyl acetylenedicarboxylate,¹⁴ for tertiary silylamines, the reaction is not as selective. The silylamination reactions were found to be extremely sensitive to moisture, and thus, have limited synthetic utility if the silylenamines are the desired product. However, the hydrolysis of both isomers does give a high yield of the *E*- isomer of the formal hydroamination product. Steric bulk at both silicon and nitrogen was shown to increase the susceptibility of the silylenamines to hydrolysis demonstrating that the addition of steric bulk does not stabilize the enamine towards hydrolysis. Given the steric limitations on both silicon and nitrogen as well as the high susceptibility of silylenamines towards water, the silylamination of electron-deficient alkynes is not a viable step in an amine functionalization pathway using disilenes.

2.5 Experimental

2.5.1 General Experimental

All manipulations were performed under an inert atmosphere of argon using Schlenk techniques or under an atmosphere of nitrogen in an MBraun glovebox. Solvents were purified using an Innovative Technologies 400-5 Solvent Purification System and were stored over activated 4 Å molecular sieves. C₆D₆ was dried over activated 4 Å molecular sieves. Liquid amines were degassed and stored over 4 Å molecular sieves prior to use. Ammonia was purchased as a 0.4 M solution in THF and dimethylamine was purchased as a 2.0 M solution in THF and used as received. (Me₃Si)₂SiMes₂^{18a} and Ge₃Mes₆³⁰ were synthesized according to the literature procedure. Tetramesityldisilene, **2.1**,^{18a} and tetramesityldigermene, **2.2**,³⁰ were synthesized prior to each reaction in quantitative yield.

The volatiles were removed and **2.1** or **2.2** were dissolved in the reaction solvent. All other chemicals were purchased from commercial sources and used without further purification.

All new compounds were characterized by ^1H , ^{13}C , ^1H - ^1H gCOSY, ^1H - ^{13}C gHSQC, ^1H - ^{13}C gHMBC NMR spectroscopy, ESI mass spectrometry and in some cases ^1H - ^{29}Si gHMBC and ^1H - ^{15}N gHMBC NMR spectroscopy and X-ray diffraction. NMR spectra were recorded on an Inova 600 MHz NMR spectrometer using C_6D_6 as the solvent at room temperature. The NMR standards used are as follows: ^1H NMR spectra were referenced to residual $\text{C}_6\text{D}_5\text{H}$ (7.15 ppm); ^{13}C NMR spectra were referenced to the central transition of C_6D_6 (128.06 ppm); ^{29}Si NMR spectra were referenced to external TMS; and CH_3NO_2 was used as the external standard for ^{15}N NMR spectra. All NMR assignments were confirmed using two-dimensional techniques (gCOSY, gHSQC, gHMBC). NMR spectra for new compounds synthesized can be found in Appendix A. Electrospray ionization mass spectra were collected using a Bruker micrOTOF II spectrometer. Mass spectral data are reported in mass-to-charge units (m/z).

2.5.2 Preparation of Disilylamines **2.3-2.7**

Ammonia (0.3 mL of a 0.4 M solution in THF, 0.12 mmol) was added to was added to a bright yellow solution of tetramesityldisilene, **2.1**, (64 mg, 0.12 mmol) dissolved in benzene (3 mL) at room temperature. After 10 minutes, the colour of the solution had faded to pale yellow and the solvent was evaporated to yield a pale, yellow oil. Dimethylamine (0.1 mL of a 2.0 M solution in THF, 0.2 mmol) was added to a bright yellow solution of tetramesityldisilene, **2.1**, (64 mg, 0.12 mmol) dissolved in benzene (3 mL) at room temperature. The solution was allowed to stir for 2 days, after which time the colour of the

solution had faded to pale yellow. The product was purified by thin layer chromatography using a silica plate with a fluorescent indicator and a mixture of hexanes and DCM (70:30) as the eluent. The remaining amines (0.12 mmol) were added directly to a bright yellow solution of tetramesityldisilene, **2.1**, (64 mg, 0.12 mmol) dissolved in benzene (3 mL) at room temperature. Once the colour of the solution had faded to pale yellow (10 minutes for primary amines, 2 days for secondary amines), the solvent was evaporated to yield a pale-yellow oil. Attempts were made to purify the products by thin layer chromatography using a silica plate with a fluorescent indicator and a mixture of hexanes and DCM (70:30) as the eluent; however, only **2.6** and **2.7** could be isolated cleanly from the plates.

$$\begin{array}{c} \text{Mes}_2\text{Si}-\text{SiMes}_2 \\ | \quad | \\ \text{H} \quad \text{NHPr} \end{array}$$
2.3: Pale, yellow oil (67 mg, 94%) ^1H NMR (600 MHz, C_6D_6) 6.75 (s, 4H, *m*-H), 6.69 (s, 4H, *m*-H), 5.64 (s, 1H, Si-H), 2.79 (dt, 2H, $^3J = 6$ Hz, 6 Hz, N-CH₂), 2.41 (br s, 12H, *o*-CH₃), 2.30 (s, 12H, *o*-CH₃), 2.13 (s, 6H, *p*-CH₃), 2.11 (s, 6H, *p*-CH₃), 1.45 (tq, 2H, $^3J = 6$ Hz, 6 Hz, CH₂), 0.84 (t, 1H, $^3J = 6$ Hz, N-H), 0.78 (t, 3H, $^3J = 6$ Hz, CH₃); $^{13}\text{C}\{^1\text{H}\}$ (151 MHz, C_6D_6) 145.32 (*o*-C), 144.61 (*o*-C), 138.62 (*p*-C), 138.46 (*p*-C), 134.21 (*i*-C), 132.50 (*i*-C), 129.69 (*m*-C), 129.13 (*m*-C), 46.32 (N-C), 27.26 (CH₂), 24.70 (*o*-CH₃), 24.48 (*o*-CH₃), 21.12 (*p*-CH₃), 21.04 (*p*-CH₃), 11.88 (CH₃), ^{29}Si (C_6D_6) -56.1 ($^1J = 180$ Hz) Si-H), -15.6 ($^3J = 8$ Hz, Si-N); ^{15}N (C_6D_6) -354.7 ($^1J = 72$ Hz) ppm. High resolution ESI-MS m/z for $\text{C}_{39}\text{H}_{53}\text{NNaSi}_2^+$ calc. 614.3614, found 614.3604.

$$\begin{array}{c} \text{Mes}_2\text{Si}-\text{SiMes}_2 \\ | \quad | \\ \text{H} \quad \text{NHPr} \end{array}$$
2.4: Pale yellow oil (65 mg, 92 %) ^1H NMR (600 MHz, C_6D_6) 6.75 (s, 4H, *m*-H), 6.69 (s, 4H, *m*-H), 5.65 (s, 1H, Si-H), 3.23 (d of sept, $^3J = 8$ Hz, 6 Hz, N-CH), 2.43 (s, 12H, *o*-CH₃), 2.27 (s, 12H, *o*-CH₃), 2.13 (s, 6H, *p*-CH₃), 2.11 (s,

6H, *p*-CH₃), 1.02 (d, 6H, ³*J* = 6 Hz, -CH₃), 0.69 (d, 1H, ³*J* = 8 Hz, NH), ¹³C{¹H} (151 MHz, C₆D₆) 145.25 (*o*-C), 144.21 (*o*-C), 138.45 (*p*-C), 138.39 (*p*-C), 135.24 (*i*-C), 132.54 (*i*-C), 129.62 (*m*-C), 129.09 (*m*-C), 45.09 (NCH), 27.89 (CH-CH₃), 25.24 (*o*-CH₃), 24.96 (*o*-CH₃), 21.12 (*p*-CH₃), 21.06 (*p*-CH₃); ²⁹Si (C₆D₆) -54.2 (¹*J* = 176 Hz, Si-H), -17.0 (¹*J* = 8 Hz, Si-N); ¹⁵N (C₆D₆) -332.7 (¹*J* = 75 Hz) ppm. High resolution ESI-MS *m/z* for C₃₉H₅₃NNaSi₂⁺ calc. 614.3614, found 614.3613.

$$\begin{array}{c} \text{Mes}_2\text{Si}-\text{SiMes}_2 \\ | \quad | \\ \text{H} \quad \text{NH}_2 \end{array}$$
2.5: Pale yellow oil (61 mg, 92 %) ¹H NMR (600 MHz, C₆D₆) 6.73 (s, 4H, *m*-H), 6.68 (s, 4H, *m*-H) 5.67 (s, 1H, Si-H), 2.36, 2.30 (each s, 24H, *o*-CH₃), 2.12 (s, 6H, *p*-CH₃), 2.10 (s, 6H, *p*-CH₃), 0.93 (s, 2H, N-H); ¹³C{¹H} (151 MHz, C₆D₆) 145.39 (*o*-C), 144.45 (*o*-C), 138.56 (*p*-C), 138.54 (*p*-C), 135.50 (*i*-C), 132.16 (*i*-C), 129.76 (*m*-C), 129.17 (*m*-C), 24.63 (*o*-CH₃), 24.44 (*o*-CH₃), 21.12 (*p*-CH₃), 21.02 (*p*-CH₃), ²⁹Si (C₆D₆) -54.8 (¹*J* = 176 Hz, Si-H), -17.0 (¹*J* = 8 Hz, Si-N); ¹⁵N (C₆D₆) -362.9 (¹*J* = 72 Hz) ppm. High resolution ESI-MS *m/z* for C₃₆H₄₇NNaSi₂⁺ calc. 572.3145, found 572.3155.

$$\begin{array}{c} \text{Mes}_2\text{Si}-\text{SiMes}_2 \\ | \quad | \\ \text{H} \quad \text{NMe}_2 \end{array}$$
2.6: Isolated using TLC (70:30 hexane:DCM). Clear oil (15 mg, 22%). ¹H NMR (600 MHz, C₆D₆) 6.74 (s, 4H, *m*-H), 6.69 (s, 4H, *m*-H), 5.85 (s, 1H, Si-H), 2.59 (s, 6H, N-CH₃), 2.31, 2.29 (each s, 24H, *o*-CH₃), 2.11, 2.10 (each s, 12H, *p*-CH₃); ¹³C{¹H} (151 MHz, C₆D₆) 145.22 (*o*-C), 144.34 (*o*-C), 138.40 (*p*-C), 138.36 (*p*-C), 137.35 (*i*-C), 133.22 (*i*-C), 129.74 (*m*-C), 129.40 (*m*-C), 42.57 (N-C), 25.02 (*o*-CH₃), 24.43 (*o*-CH₃), 21.07 (*p*-CH₃), 20.96 (*p*-CH₃); ²⁹Si (C₆D₆) -55.5 (¹*J* = 180 Hz, Si-H), -9.8 (³*J* = 8 Hz, Si-N) ppm; ¹⁵N (C₆D₆) No signal observed. High resolution ESI-MS C₃₈H₅₁NNaSi₂⁺ calc. 600.3458, found 600.3454.

$$\begin{array}{c} \text{Mes}_2\text{Si}-\text{SiMes}_2 \\ | \quad | \\ \text{H} \quad \text{NEt}_2 \end{array}$$
2.7: Isolated using TLC (70:30 hexanes:DCM). Clear oil (20 mg, 27 %)
 ¹H NMR (600 MHz, C₆D₆) 6.72 (s, 4H, *m*-H), 6.71 (s, 4H, *m*-H), 5.97 (s, 1H, Si-H), 3.21 (q, ³*J* = 6 Hz, 4H, CH₂), 2.35 (s, 24H, *o*-CH₃), 2.11 (s, 6H, *p*-CH₃), 2.09 (s, 6H, *p*-CH₃), 0.83 (t, ³*J* = 6 Hz, 6H, -CH₃); ¹³C{¹H} (151 MHz, C₆D₆) 145.20 (*o*-C), 144.79 (*o*-C), 138.27 (*p*-C), 138.25 (*p*-C) 136.89 (*i*-C), 134.38 (*i*-C), 129.87 (*m*-C), 129.03 (*m*-C), 41.69 (N-C), 25.40 (*o*-CH₃), 25.32 (*o*-CH₃), 21.06 (*p*-CH₃), 20.95 (*p*-CH₃), 12.67 (-CH₃); ²⁹Si (C₆D₆) -53.2 (Si-H), -10.8 (Si-N); ¹⁵N (C₆D₆) -354.8 ppm. High resolution ESI-MS *m/z* for C₄₀H₅₅NNaSi₂⁺ calc. 628.3771, found 628.3772.

2.5.3 Preparation of Digermylamines **2.8** and **2.9**

The amine (0.3 mL of a 0.4 M solution of ammonia in THF or 2 drops of propylamine) was added to a yellow solution of tetramesityldigermene, **2.2**, (20 mg, 0.03 mmol) dissolved in benzene (3 mL) at room temperature. Once the colour of the solution had faded to pale yellow (10 minutes in each case), the solvent was evaporated to yield a pale-yellow oil. Purification of the crude products by thin layer chromatography using 70:30 hexane:DCM as the eluent was attempted; however, only 1,1,2,2-tetramesityldigermanol³¹ was recovered from the plate in both reactions. NMR spectra were recorded on the crude products.

$$\begin{array}{c} \text{Mes}_2\text{Ge}-\text{GeMes}_2 \\ | \quad | \\ \text{H} \quad \text{NHPr} \end{array}$$
2.8: ¹H NMR (600 MHz, C₆D₆) 6.76 (s, 4H, *m*-H), 6.70 (s, *m*-H), 5.86 (s, 1H, Ge-H), 2.83 (dt, ³*J* = 6 Hz, 6 Hz, 2H, N-CH₂), 2.42 (s, *o*-CH₃), 2.34 (s, *o*-CH₃), 2.12 (s, *p*-CH₃), 2.09 (s, *p*-CH₃), 1.52 (tq, ³*J* = 6 Hz, 6 Hz, 2H, CH₂), 0.87 (t, ³*J* = 6 Hz, 3H, CH₃), 0.77 (br, 1H, N-H); ¹³C{¹H} (151 MHz, C₆D₆) 144.00 (*o*-C),

143.56 (*o*-C), 138.35 (*p*-C), 138.02 (*p*-C), 137.19 (*i*-C), 136.29 (*i*-C), 129.58 (*m*-C), 129.02 (*m*-C), 47.74 (N-CH₂), 28.02 (-CH₂-), 24.85 (*o*-CH₃), 24.21 (*o*-CH₃), 21.06 (*p*-CH₃), 20.99 (*p*-CH₃), 11.89 (-CH₃) ppm. High resolution ESI-MS *m/z* for C₃₉H₅₃NNa⁷²Ge⁷⁴Ge⁺ calc. 704.2508, found 704.2514.

$$\begin{array}{c} \text{Mes}_2\text{Ge}-\text{GeMes}_2 \\ | \quad | \\ \text{H} \quad \text{NH}_2 \end{array}$$
2.9: sample is contaminated with 1,1,2,2-tetramesityldigermanol (5:1 ratio); ¹H NMR (600 MHz, C₆D₆) 6.73 (s, 4H, *m*-H), 6.69 (s, *m*-H), 5.88 (s, 1H, Ge-H), 2.36 (s, *o*-CH₃), 2.34 (s, *o*-CH₃), 2.12 (s, 6H, *p*-CH₃), 2.10 (s, *p*-CH₃), 0.78 (s, 2H, N-H) ppm. High resolution ESI-MS *m/z* for C₃₆H₄₇NNa⁷²Ge⁷⁴Ge⁺ calc. 662.2039, found 662.2017.

2.5.4 X-ray Crystallographic Details for **2.3**

Data Collection and Processing: The sample was mounted on a Mitegen polyimide micromount with a small amount of Paratone N oil. All X-ray measurements were made on a Bruker Kappa Axis Apex2 diffractometer at a temperature of 110 K. The unit cell dimensions were determined from a symmetry constrained fit of 2497 reflections with 4.9° < 2θ < 44.0°. The data collection strategy was a number of ω and φ scans which collected data up to 48.84° (2θ). The frame integration was performed using SAINT.³³ The resulting raw data were scaled and absorption corrected using a multi-scan averaging of symmetry equivalent data using SADABS.³⁴

Structure Solution and Refinement: The structure was solved by using a dual space methodology using the SHELXT program.³⁵ All non-hydrogen atoms were obtained from the initial solution. The hydrogen atoms were introduced at idealized positions and were

treated in a mixed fashion. The hydrogen atoms attached to Si2 and N1 were found in the difference map and were allowed to refine isotropically. The structural model was fit to the data using full matrix least-squares based on F^2 . The calculated structure factors included corrections for anomalous dispersion from the usual tabulation. The structure was refined using the SHELXL-2014 program from the SHELXTL suite of crystallographic software.³⁶ Graphic plots were produced using the XP program suite.³⁷ Additional information and other relevant literature references can be found in the reference section of this website (<http://xray.chem.uwo.ca>). The table of crystallographic data for **2.3** can be found in Appendix A.

2.5.5 Computational Details

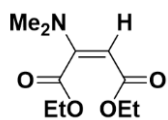
All calculations were carried out in collaboration with Gül Altınbaş Özpınar. Calculations were done using Gaussian 16³⁸ program package. The geometries of all stationary points and transition states on the potential energy surfaces of the proposed pathways were optimized with M062X/6-311+G(d,p) computational level. Transition states were located by executing traditional transition optimizations using Berny algorithm. Frequency computations were performed to characterize the nature of transition states (one imaginary frequency) and the local minima (no imaginary frequency) at the same computational level. Intrinsic reaction coordinate (IRC)³⁹ calculations for the transition states optimized with traditional method were also carried out at the same level to connect the transition states to the reactants and products. The solvent effect was investigated by performing single point energy computations at the same computational level using the Integral Equation Formalism-Polarizable Continuum Model (IEF-PCM)⁴⁰ and benzene as

solvent. In order to compute zero-point corrected electronic energy and Gibbs energy values in the solvent phase, thermodynamic corrections at 298 K obtained from the frequency calculations were added to the electronic energy obtained from single point IEF-PCM computations.

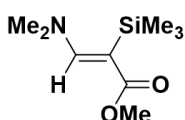
2.5.6 General Procedure for Silylated Enamine Synthesis

The acetylenecarboxylate (7.11 mmol) and silylamine (8.53 mmol) were dissolved in diethyl ether (5 mL). The solution was refluxed for 6 hours under argon. The solvent was evaporated yielding a yellow or brown oil. Products were characterized without further purification. The product ratios can be found in Table 2.1. All reactions went to full conversion by ^1H NMR spectroscopy.

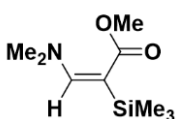
Given the mixtures obtained, the structures were elucidated using a combination of ^1H , ^{13}C , ^1H - ^{15}N and ^1H - ^{29}Si HMBC NMR spectroscopy. In a few cases, some of the components of the mixture were independently synthesized to verify their identity. ^{15}N chemical shifts could not be obtained for reactions with dimethyl acetylenedicarboxylate as no correlations were observed between the nitrogen and *N*-methyl protons. ^{15}N chemical shifts and occasionally ^{13}C chemical shifts could not be obtained for products in low proportions. High-resolution mass spectral data for the new silylated enamines could not be obtained due to their formation primarily as a minor component in a mixture and their extreme sensitivity to hydrolysis which precluded their isolation. Although the enamines have been previously reported, the NMR data here is listed as some of the NMR data for the compounds was missing, incomplete or given in a different solvent. Chemical shifts for the signals denoted with * were extracted from the ^1H - ^{13}C HMBC NMR spectrum.



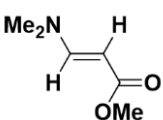
2.14b/2.14j:⁴¹ ^1H (400 MHz, C_6D_6) 4.64 (s, 1H, =CH), 4.32 (q, 2H, $^3J = 6$ Hz, OCH_2), 4.12 (q, 2H, $^3J = 6$ Hz, OCH_2), 2.17 (s, 6H, N- CH_3), 1.13 (t, 3H, $^3J = 6$ Hz, CH_3), 1.04 (t, 3H, $^3J = 6$ Hz, CH_3); $^{13}\text{C}\{^1\text{H}\}$ (101 MHz, C_6D_6) 170.23 (C=O), 165.46 (C=O), 159.20 (=CN), 61.02 (CH_2), 59.89 (OCH_2), 38.94 (N CH_3), 14.39 (CH_3), 14.08 (CH_3); ^{15}N (C_6D_6) -283.4 ppm.



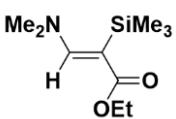
2.13Z-c: ^1H NMR (C_6D_6) 7.96 (s, =CH), 3.60 (s, OCH_3), 2.57 (s, N CH_3), 0.34 (s, SiCH_3); $^{13}\text{C}\{^1\text{H}\}$ (101 MHz, C_6D_6) 173.3* (C=O), 43.3* (N- CH_3); ^{29}Si (C_6D_6) -9.5 ppm.



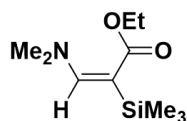
2.13E-c: 6.19 (s, 1H, =CH), 3.51 (s, 3H, OCH_3), 2.44 (s, 6H, N CH_3), 0.27 (s, 9H, SiCH_3); $^{13}\text{C}\{^1\text{H}\}$ (101 MHz, C_6D_6) 169.49 (C=O), 153.98 (=CH), 91.43 (=CSi), 49.96 (OCH_3), 43.05 (N CH_3), 0.23 (SiCH_3); ^{29}Si (C_6D_6) -3.3 ppm; ^{15}N (C_6D_6) -294.7 ppm.



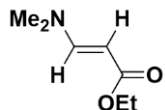
2.14c/2.14k:⁴² ^1H (400 MHz, C_6D_6) 7.44 (d, 1H, $^3J = 12$ Hz, = CHNMe_2), 4.67 (d, 1H, $^3J = 12$ Hz, = CHCO_2Me), 3.63 (s, 3H, OCH_3), 2.04 (s, 6H, N CH_3); $^{13}\text{C}\{^1\text{H}\}$ (400 MHz, C_6D_6) 169.52 (C=O), 152.90 (=CN), 84.93 (=CCO $_2$ Me), 67.14 (OCH_3), 50.26 (N CH_3); ^{15}N (C_6D_6) -307.7 ppm.



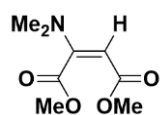
2.13Z-d: ^1H (400 MHz, C_6D_6) 8.01 (s 1H, =C-H), 4.20 (q, 2H, $^3J = 6$ Hz, OCH_3), 2.23 (s, 3H, N CH_3), 0.39 (s, 9H, SiCH_3); $^{13}\text{C}\{^1\text{H}\}$ (100 MHz, C_6D_6) 172.8* (C=O), 163.3* (=CN), 43.4* (N CH_3), 3.1* (SiMe); ^{29}Si (C_6D_6) -9.6 ppm.



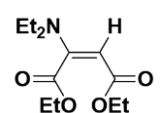
2.13E-d: ^1H (400 MHz, C_6D_6) 6.19 (s, 1H, =C-H), 4.13 (q, 2H, $^3J = 8$ Hz, OCH₂), 2.44 (s, 6H, NCH₃), 1.11 (t, 3H, $^3J = 8$ Hz, CH₃), 0.33 (s, 9H, SiCH₃); $^{13}\text{C}\{^1\text{H}\}$ (101 MHz, C_6D_6) 169.04 (C=O), 153.84 (=CH), 91.95 (=CSi), 58.90 (SiCH₃), 43.08 (NCH₃), 14.73 (CH₃), 0.42 (SiCH₃); ^{29}Si (C_6D_6) -3.5 ppm.



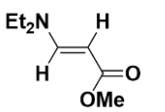
2.14d/2.14l:⁴³ ^1H (400 MHz, C_6D_6) 7.44 (s, 1H, $^3J = 12$ Hz, =CH), 4.71 (s, 1H, $^3J = 12$ Hz, =CH), 4.26 (q, 2H, $^3J = 8$ Hz, OCH₂), 1.98 (s, 6H, NCH₃), 1.16 (t, 3H, $^3J = 8$ Hz, CH₃); $^{13}\text{C}\{^1\text{H}\}$ (101 MHz, C_6D_6) 169.09 (C=O), 152.65 (=CN), 85.67 (=CH), 58.76 (OCH₂), 43.08 (NCH₃), 15.02 (CH₃).



2.14e:^{44,45} ^1H (400 MHz, C_6D_6) 4.74 (s, 1H, =CH), 3.70 (s, 3H, OCH₃), 3.51 (s, 3H, OCH₃), 2.60 (q, 4H, $^3J = 8$ Hz, NCH₂), 0.70 (t, 6H, $^3J = 8$ Hz, CH₃); $^{13}\text{C}\{^1\text{H}\}$ 168.01 (C=O), 165.99 (C=O), 154.21 (=CN), 83.92 (=CH), 52.44 (OCH₃), 50.30 (OCH₃), 44.67 (br, NCH₂), 12.56 (br, NCH₂CH₃); ^{15}N (C_6D_6) -282.6 ppm.

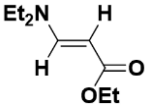


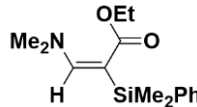
2.14f:⁴⁵ ^1H (400 MHz, C_6D_6) 4.67 (s, 1H, =CH), 4.29 (q, 2H, $^3J = 6$ Hz, OCH₂), 4.05 (q, 2H, $^3J = 6$ Hz, OCH₂), 2.73 (q, $^3J = 6$ Hz, 4H, NCH₂), 1.13 (t, 3H, $^3J = 6$ Hz, CH₃), 1.04 (t, 3H, $^3J = 6$ Hz, CH₃), 0.75 (t, 6H, $^3J = 6$ Hz, CH₃); $^{13}\text{C}\{^1\text{H}\}$ (101 MHz, C_6D_6) 167.58 (C=O), 165.54 (C=O), 154.30 (=CN), 84.37 (=CH), 61.79 (OCH₂), 58.98 (OCH₂), 44.62 (br, NCH₂), 14.76 (CH₃), 13.96 (CH₃), 12.63 (br, NCH₂CH₃); ^{15}N (C_6D_6) -283.6 ppm. Structure confirmed by independent synthesis.



2.14g:⁴³ ^1H (400 MHz, C_6D_6) 7.43 (s, 1H, $^3J = 12$ Hz), 4.82 (s, 1H, $^3J = 12$ Hz), 3.68 (s, 3H, OCH₃), 2.42 (q, 4H, $^3J = 8$ Hz, NCH₂), 0.57 (t, 6H, $^3J = 8$

Hz, CH₃); ¹³C{¹H} (400 MHz, C₆D₆) 169.75 (C=O), 150.74 (=CN), 84.45 (=CH), 50.18 (OCH₃), 45.6 (br s, N-CH₂), 12.9 (br s, CH₃); ¹⁵N (C₆D₆) -279.3 ppm. Structure confirmed by independent synthesis.


2.14h: ⁴³ ¹H (400 MHz, C₆D₆) 7.48 (d, 1H, ³J = 12 Hz, =CH), 4.73 (d, 1H, ³J = 12 Hz, =CH), 4.20 (q, 2H, ³J = 8 Hz, OCH₂), 2.54 (q, 4H, ³J = 8 Hz, NCH₂), 1.13 (t, 3H, ³J = 8 Hz, OCH₂CH₃), 0.64 (t, 6H, ³J = 8 Hz, NCH₂CH₃); ¹³C{¹H} (101 MHz, C₆D₆) 169.28 (C=O), 150.84 (=CN), 84.62 (=CH), 58.58 (OCH₂), 46 (br, NCH₂), 15.03 (CH₃), 13 (br, CH₃); ¹⁵N (C₆D₆) -279.5 ppm. Structure confirmed by independent synthesis.


2.13E-I: ¹H (400 MHz, C₆D₆) 7.68- 7.74 (m, 2H, Ph), 7.20-7.31 (m, 3H, Ph), 6.17 (s, 1H, =CH), 4.04 (q, 2H, ³J = 8 Hz, OCH₂), 2.37 (s, 6H, NCH₃), 0.98 (t, 3H, ³J = 8 Hz), 0.58 (s, 6H, SiCH₃); ¹³C{¹H} (101 MHz, C₆D₆) 168.9* (C=O), 155.41 (=C-H), 140.8* (*i*-C), 134.4* (*o*-C), 128.9* (*p*-C), 127.9* (*m*-C), 90.1* (=CSi), 58.98 (OCH₂), 43.13 (NCH₃), 14.51 (CH₃), -0.64 (SiCH₃); ²⁹Si (C₆D₆) -6.6 ppm.

2.6 References

[1] Recent examples: a) Marguleiux, G. W.; Bezdek, M. J.; Turner, Z. R.; Chirik, P. J. *J. Am. Chem. Soc.*, **2017**, *139*, 6110-6113. b) Brown, R. M.; Garcia, J. B.; Valjus, J.; Roberts, C. J.; Tuononen, H. M.; Parvez, M.; Roesler, R. *Angew. Chem. Int. Ed.*, **2015**, *54*, 6274-6277. c) Morgan, E.; MacLean, D. F.; McDonald, R.; Turculet, L. *J. Am. Chem. Soc.*, **2009**, *131*, 14234-14236. d) For a review: van der Vlugt, J. I. *Chem. Rev.*, **2010**, *39*, 2302-2322.

[2] a) Protchenko, A. V.; Bates, J. I.; Saleh, L. M. A.; Blake, M. P.; Schwarz, A. D.; Kolychev, E. L.; Thompson, A. L.; Jones, C.; Mountford, P.; Aldridge, S. *J. Am. Chem. Soc.*, **2016**, *138*, 4555-4564. b) Abdalla, J. A. B.; Riddlestone, I. M.; Tirfoin, R.; Aldridge, S. *Angew. Chem. Int. Ed.*; **2015**, *54*, 5098-5102. c) Robinson, T. P.; De Rosa, D. M.; Aldridge, S.; Goicoechea, J. M. *Angew. Chem. Int. Ed.*, **2015**, *54*, 13758-13763. d) McCarthy, S. M.; Lin, Y. C.; Devarajan, D.; Chang, J. W.; Yennawar, H. P.; Rioux, R. M.; Ess, D. H.; Radosevich, A. T. *J. Am. Chem. Soc.*, **2014**, *136*, 4640-4650. e) Cui, J.; Li, Y.; Ganguly, R.; Inthirarajah, A.; Hirao, H.; Kinjo, R. *J. Am. Chem. Soc.*, **2014**, *136*, 16764-16767. f) Xiong, Y.; Yao, S.; Muller, R.; Kaupp, M.; Driess, M. *J. Am. Chem. Soc.*, **2010**, *20*, 6912-6913. g) Zhu, Z.; Wang, X.; Peng, Y.; Lei, H.; J.; Fettinger, J. C.; Rivard, E.; Power, P. P. *Angew. Chem. Int. Ed.*, **2009**, *48*, 2031-2034. h) Beachley, O. T.; Pazik, J. C.; Noble, M. J.; *Organometallics*, **1998**, *17*, 2121-2123.

[3] Hanusch, F.; Groll, L.; Inoue, S. *Chem. Sci.*, **2021**, *12*, 2001-2015.

[4] a) Wang, W.; Inoue, S.; Yao, S.; Driess, M. *Organometallics*, **2011**, *30*, 6490-6494. b) Jana, A.; Schulzke, C.; Roesky, H. W. *J. Am. Chem. Soc.*, **2009**, *131*, 4600-4601. c) Jana, A.; Objartel, I.; Roesky, H. W.; Stalke, D. *Inorg. Chem.*, **2009**, *48*, 798-800. d) Peng, Y.; Guo, J.; Ellis, B. D.; Zhu, Z.; Fettinger, J. C.; Nagase, S.; Power, P. P. *J. Am. Chem. Soc.*, **2009**, *131*, 16272-16282. e) Peng, Y.; Ellis, B. D.; Wang, X.; Power, P. P. *J. Am. Chem. Soc.*, **2008**, *130*, 12268-12269.

[5] Meltner, A.; Majumdar, M.; White, A. J. P.; Huch, V.; Scheschkewitz, D. *Organometallics*, **2013**, *32*, 6844-6850.

- [6] Reiter, D.; Holzner, R.; Porzelt, A.; Altmann, P. J.; Frisch, P.; Inoue, S. *J. Am. Chem. Soc.*, **2019**, *141*, 13536–13546.
- [7] Wendel, D.; Szilvási, T.; Henschel, D.; Altmann, P. J.; Jandl, C.; Inoue, S.; Rieger, B. *Angew. Chem. Int. Ed.*, **2018**, *57*, 14575–14579.
- [8] Boomgaarden, S.; Saak, W.; Weidenbruch, M. *Z. Anorg. Allg. Chem.*, **2001**, *627*, 349-352.
- [9] a) Leigh, W. J.; Dumbrava, I. G.; Lollmahomed, F. *Can. J. Chem.*, **2006**, *84*, 934-948. b) Leigh, W. J.; Harrington, C. R.; Vargas-Baca, I. *J. Am. Chem. Soc.*, **2004**, *126*, 16105-16116. c) Huck, L. A.; Leigh, W. J. *Organometallics*, **2007**, *26*, 1339-1348.
- [10] a) Apeloig, Y.; Nakash, M. *Organometallics*, **1998**, *17*, 2307-2312. b) Apeloig, Y.; Nakash, M. *Organometallics*, **1998**, *17*, 1260-1265. c) Apeloig, Y.; Nakash, M. *J. Am. Chem. Soc.*, **1996**, *118*, 9798-9799. d) Budaraju, J.; Powell, D. R.; West, R. *Main Group Met. Chem.*, **1996**, *19*, 531-537. e) Sekiguchi, A.; Maruki, I.; Sakurai, H. *J. Am. Chem. Soc.*, **1993**, *115*, 11460-11466. f) De Young, D. J.; Fink, M. J.; West, R. *Main Group Met. Chem.*, **1987**, *10*, 19-43.
- [11] a) Takahashi, M.; Veszprémi, T.; Kira, M. *Int. J. Quantum Chem.*, **2001**, *84*, 192–197. b) Veszprémi, T.; Takahashi, M.; Hajgató, B.; Kira, M. *J. Am. Chem. Soc.*, **2001**, *123*, 6629-6638. c) Takahashi, M.; Veszprémi, T.; Hajgató, B.; Kira, M. *Organometallics*, **2000**, *19*, 4660-4662. d) Takahashi, M.; Veszprémi, T.; Kira, M. *Organometallics*, **2004**, *23*, 5768–5778. e) Wang, Y.; Zeng, X. *Russ. J. Phys. Chem. A*, **2020**, *94*, 800-805. f) Yamabe,

- S.; Mizukami, N.; Tsuchida, N.; Yamazaki, S. *J. Organomet. Chem.*, **2008**, *693*, 1335-1345. g) Li, B.-Y.; Sheu, J.-H.; Su, M.-D. *Organometallics*, **2011**, *30*, 4862-4872. h) Li, B.-Y.; Su, M.-D. *J. Phys. Chem. A*, **2012**, *116*, 4222-4232.
- [12] Hardwick, J. A.; Baines, K. M. *Angew. Chem. Int. Ed.*, **2015**, *54*, 6600-6603.
- [13] George, T. A.; Lappert, M. F. *J. Organomet. Chem.*, **1968**, *14*, 327-337.
- [14] Srivastava, G. *J. Organomet. Chem.*, **1978**, *152*, 39-44.
- [15] a) Makoto, H.; Masayuki, N.; Atsuko, F.; Toshiharu, Y.; Naruyasu, I.; Katsukiyo, M.; Akira, H. *Chem. Lett.*, **1994**, *23*, 719-722. b) Saidi, M. R.; Heydari, A.; Ipaktschi, J. *Chem. Ber.*, **1994**, *127*, 1761-1764. c) Corriu, R. J. P.; Lanneau, G. F.; Mehta, V. D. *J. Organomet. Chem.*, **1991**, *419*, 9-26. d) Cragg, R. H.; Lappert, M. F. *J. Chem. Soc. A*, **1966**, 82-85.
- [16] a) Dolfini, J. E. *J. Org. Chem.*, **1965**, *30*, 1298-1300. b) Winterfeldt, E.; Preuss, H. *Angew. Chem. Int. Ed.*, **1965**, *4*, 689. c) Huisgen, R.; Herbig, K.; Siegl, A.; Huber, H. *Chem. Ber.*, **1966**, *99*, 2526-2545. d) Herbig, K.; Huisgen, R.; Huber, H. *Chem. Ber.*, **1966**, *99*, 2546-2555. e) Alaimo, R. J.; Farnum, D. G. *Can. J. Chem.*, **1965**, *43*, 700-701.
- [17] Rivière-Baudet, M.; Satgé, J. *J. Organomet. Chem.*, **1973**, *56*, 159-166.
- [18] a) Fink, M. J.; Michalczyk, M. J.; Haller, K. J.; Michl, J.; West, R. *Organometallics*, **1984**, *3*, 793. b) Hurni, K. L.; Rupar, P. A.; Payne, N. C.; Baines, K. M. *Organometallics*, **2007**, *26*, 5569 – 5575.

- [19] Seligson, A. L.; Trogler, W. C. *J. Am. Chem. Soc.*, **1991**, *113*, 2520–2527.
- [20] a) Pardo, L.; Osman, R.; Weinstein, H.; Rabinowitz, J. R. *J. Am. Chem. Soc.*, **1993**, *115*, 8263-8269. b) Smith, N. E.; Bernskoetter, W. H.; Hazari, N. *J. Am. Chem. Soc.*, **2019**, *115*, 17350-17360. c) Mitra, A.; Wojcik, J. P.; Lecoanet, D.; Müller, T.; West, R. *Angew. Chem. Int. Ed.*, **2009**, *48*, 4069-4072. d) Strehl, J.; Kahrs, C.; Müller, T.; Hilt, G.; Christoffers, J. *Chem. Eur. J.*, **2020**, *26*, 3222-3225.
- [21] a) Pophristic, V.; Goodman, L.; Wu, C. T. *J. Chem. Phys. A*, **2001**, *105*, 7454-7459. b) Cho, S. G.; Rim, O. K.; Park, G. *J. Comput. Chem.*, **1997**, *18*, 1523-1533. c) Valencia, F.; Romero, A. H.; Kiwi, M.; Ramírez, R.; Toro-Labbé, A. *Chem. Phys. Lett.*, **2003**, *371*, 267-275.
- [22] a) Lambert Jr., J. B.; Schultz, W. J. In *The Chemistry of Organic Silicon Compounds*; Patai, S.; Rappoport, Z. Eds.; Wiley: New York, 1989; p 1007. b) Ramondo, F. *J. Organomet. Chem.*, **1992**, *434*, 19-33.
- [23] a) Fischer, R.; Marschner C. In *Organosilicon Chemistry V*, 2003, Eds. Auner, N.; Weis, J. WILEY-VCH Verlag GmbH & Co. KGaA, Weinheim, 190-194. b) Flock, M.; Marschner, C. *Chem. Eur. J.*, **2002**, *8*, 1024-1030.
- [24] Landolt-Börnstein - Group IV Physical Chemistry, Vol. 6 (Static Dielectric Constants of Pure Liquids and Binary Liquid Mixtures):
http://materials.springer.com/lb/docs/sm_lbs_978-3-540-47619-1_3; 10.1007/10047452_3
(Springer-Verlag Berlin Heidelberg © 1991) Accessed: 08-02-2021.

- [25] Liu, F.; Zhang, Z.; Bao, Z.; Su, B.; Xing, H.; Yang, Q.; Ren, Q. *Synlett*, **2017**, 28, 1116-1120.
- [26] a) Brook, M. A. *Silicon in organic, organometallic, and polymer chemistry*; John Wiley & Sons: New York, 2000. b) Colvin, E. W. *Silicon in organic synthesis*; Robert E. Krieger: Malabar, FL, 1985.
- [27] The solvent, temperature, concentration, molar ratios and time of the reaction were all varied in attempts to observe the silylenamine.
- [28] Scheim, U.; Lehnert, R.; Porzel, A.; Rühlmann, K. *J. Organomet. Chem.*, **1988**, 356, 141-149.
- [29] Hexamethyldisiloxane is the presumed by-product of hydrolysis for Table 1, Entries 1-8, though it is likely removed, along with the solvent, under vacuum.
- [30] a) Ando, W.; Tsumuraya, T. *J. Chem. Soc., Chem. Commun.*, **1987**, 1514 – 1515. b) Tsumuraya, T.; Kabe, Y.; Ando, W. *J. Organomet. Chem.*, 1994, **482**, 131 – 138.
- [31] Hurni, K. L.; Rupar, P. A.; Payne, N. C.; Baines, K. M. *Organometallics*, 2007, **26**, 5569 – 5575.
- [32] Baines, K. M.; Cooke, J. A.; Dixon, C. E.; Liu, H. W.; Netherton, M. R. *Organometallics*, **1994**, 13, 631 – 634.
- [33] Bruker-AXS, SAINT version 2013.8, 2013, Bruker-AXS, Madison, WI 53711, USA.

- [34] Bruker-AXS, SADABS version 2012.1, 2012, Bruker-AXS, Madison, WI 53711, USA.
- [35] Sheldrick, G. M. *Acta Cryst.* **2015**, *A71*, 3 –8.
- [36] Sheldrick, G. M. *Acta Cryst.* **2015**, *C71*, 3 – 8.
- [37] Bruker-AXS, XP version 2013.1, 2013, Bruker-AXS, Madison, WI 53711, USA.
- [38] Frisch, M. J.; Trucks, G. W. ; Schlegel, H. B.; Scuseria, G. E.; Robb, M. A.; Cheeseman, J. R.; Scalmani, G.; Barone, V.; Petersson, G. A.; Nakatsuji, H.; Li, X.; Caricato, M.; Marenich, A. V.; Bloino, J.; Janesko, B. G.; Gomperts, R.; Mennucci, B.; Hratchian, H. P.; Ortiz, J. V.; Izmaylov, A. F.; Sonnenberg, J. L.; Williams-Young, D.; Ding, F.; Lipparini, F.; Egidi, F.; Goings, J.; Peng, B.; Petrone, A.; Henderson, T.; Ranasinghe, D.; Zakrzewski, V. G.; Gao, J.; Rega, N.; Zheng, G.; Liang, W.; Hada, M.; Ehara, M.; Toyota, K.; Fukuda, R.; Hasegawa, J.; Ishida, M.; Nakajima, T.; Honda, Y.; Kitao, O.; Nakai, H.; Vreven, T.; Throssell, K.; Montgomery Jr., J. A.; Peralta, J. E.; Ogliaro, F.; Bearpark, M. J.; Heyd, J. J.; Brothers, E. N.; Kudin, K. N.; Staroverov, V. N.; Keith, T. A.; Kobayashi, R.; Normand, J.; Raghavachari, K.; Rendell, A. P.; Burant, J. C.; Iyengar, S. S.; Tomasi, J.; Cossi, M.; Millam, J. M.; Klene, M.; Adamo, C.; Cammi, R.; Ochterski, J. W.; Martin, R. L.; Morokuma, K.; Farkas, O.; Foresman, J. B.; Fox, D. J. Gaussian, Inc., Wallingford CT, 2016.
- [39] a) Fukui, K. *Acc. Chem. Res.*, **1981**, *14*, 363-68. b) Hratchian, H. P.; Schlegel, H. B. *In Theory and Applications of Computational Chemistry: The First 40 Years*, Ed. Dykstra,

C. E.; Frenking, G.; Kim K. S.; Scuseria, G. Elsevier: Amsterdam, Netherlands, 2005, 195-249.

[40] Scalmani, G.; Frisch, M. J. *J. Chem. Phys.*, **2010**, *132*, 114110.

[41] Kozmin, S. A.; Iwama, T.; Huang, Y.; Rawal, V. H. *J. Am. Chem. Soc.*, **2002**, *124*, 4628-4641.

[42] Navarro-Vázquez, A.; García, A.; Domínguez, D. *J. Org. Chem.*, **2002**, *67*, 3213-3220.

[43] Lee, K. Y.; Lee, C. G.; Na, J. E.; Kim, J. N. *Tetrahedron Lett.*, **2005**, *46*, 69-74.

[44] Winterfeldt, E.; Preuss, H. *Angew. Chem. Int. Ed.*, **1965**, *4*, 689.

[45] Liu, F.; Zhang, Z.; Bao, Z.; Su, B.; Xing, H.; Yang, Q.; Yang, Y.; Ren, Q. *Synlett*, **2017**, *28*, 1116-1120.

Chapter 3

3 Lewis Acidity Assessment of Group 14 Crown Ether Complexes

3.1 Introduction

Main group Lewis acids have been utilized as catalysts in chemical transformations for decades.¹ In recent years, the development of novel ligands and frameworks, including the use of electron-withdrawing substituents,^{2,3} as well as the generation of cationic,⁴ or low valent⁵ systems has led to the synthesis of an extensive variety of main group Lewis acids with differing catalytic abilities. To understand the influence of the main group element and ligand framework on Lewis acidity, a quantitative comparison of the Lewis acidity is required. Such a comparison between the diverse range of main group Lewis acids enables the assessment of the potential reactivity or catalytic activity of a Lewis acid.⁶

Both experimental and computational methods have been developed to quantitatively assess Lewis acidity. Typically, a judiciously selected common Lewis base is added to a variety of Lewis acids and some metric about the Lewis acid-base adduct is measured, such as an NMR chemical shift,⁷ or computed, such as an enthalpy of adduct formation.⁸ The hardness or softness of the chosen Lewis base can influence the strength of the interaction with the Lewis acid,⁹ and thus, no reported method is able to accurately scale all soft and hard Lewis acids. As a consequence, multiple methods are often employed to assess the Lewis acidity of a compound. The Gutmann-Beckett method, involving the measurement

of the ^{31}P NMR chemical shift upon the coordination of triethylphosphine oxide (TEPO) to a Lewis acid,^{7a,b} is one of the most commonly employed experimental methods for the assessment of Lewis acidity due to its ease of operation. The chemical shift can be converted into an Acceptor Number (AN), a unitless scale, to facilitate comparisons between Lewis acids. In this method, a more downfield chemical shift is indicative of a strong Lewis acid. Computationally, fluoride ion affinity (FIA) is widely employed and measures the enthalpy of reaction between a fluoride ion and Lewis acid, typically in the gas phase.⁸ FIA values can also be obtained experimentally. Other Lewis acidity assessment methods included Child's method where coordination of crotonaldehyde to a Lewis acid is observed by ^1H NMR spectroscopy,^{7c} a modified Gutmann-Beckett method employing trimethylphosphine sulfide,¹⁰ a phosphole fluorescence-based method, where the fluorescence of the phosphole-Lewis acid adduct is measured¹¹ a fluorobenzonitrile method, where the ^{19}F NMR spectrum of a fluorobenzonitrile-Lewis acid adduct is measured^{7d} and the Global Electrophilicity Index (GEI), a computational method that measures "the ability of a molecule to take up electrons" using the chemical potential and chemical hardness of a given molecule.¹²

In recent years, a number of Group 14-based Lewis acid-catalyzed systems have been developed. Although Lewis acid catalysis by group 14 halides has been known for decades,¹³ a quantitative assessment of their Lewis acidities,^{14,15} as well as the Lewis acidities of other group 14 species, has only recently been performed. Many group 14 Lewis acids with an oxidation number of 4^+ are significantly stronger Lewis acids compared to the parent Group 14 halides, SiCl_4 and GeCl_4 .^{3b-d} In contrast, the Lewis

acidity of only a few examples of Group 14 species with an oxidation number of 2⁺ have been assessed and those that have been examined have been examined exclusively using the Gutmann-Beckett method.^{16,17}

We now report, the first quantitative investigation of the Lewis acidities of a series of low valent Group 14 species. A number of crown ether-stabilized complexes of germanium(II)^{18,19} and tin(II)^{20,21} have been synthesized.²² Coordination of water and ammonia to **[Ge([15]crown-5)][OTf]₂**²³ demonstrates the Lewis acidity of the germanium(II) centre; however, a quantitative assessment of the Lewis acidity of the crown ether complexes, including **[Ge([15]crown-5)][OTf]₂**, has not been done. In this chapter, the Lewis acidities of a series of neutral and cationic tin(II) and germanium(II) crown ether complexes (Figure 3.1) have been assessed using the Gutmann-Beckett and FIA methods, enabling insight into the influence of oxidation number, charge and ligands on the Lewis acidity of the complexes and the formation of Lewis acid-base adducts. The results have allowed for an evaluation of the potential for Lewis acid catalysis by germanium(II) and tin(II) crown ether complexes.

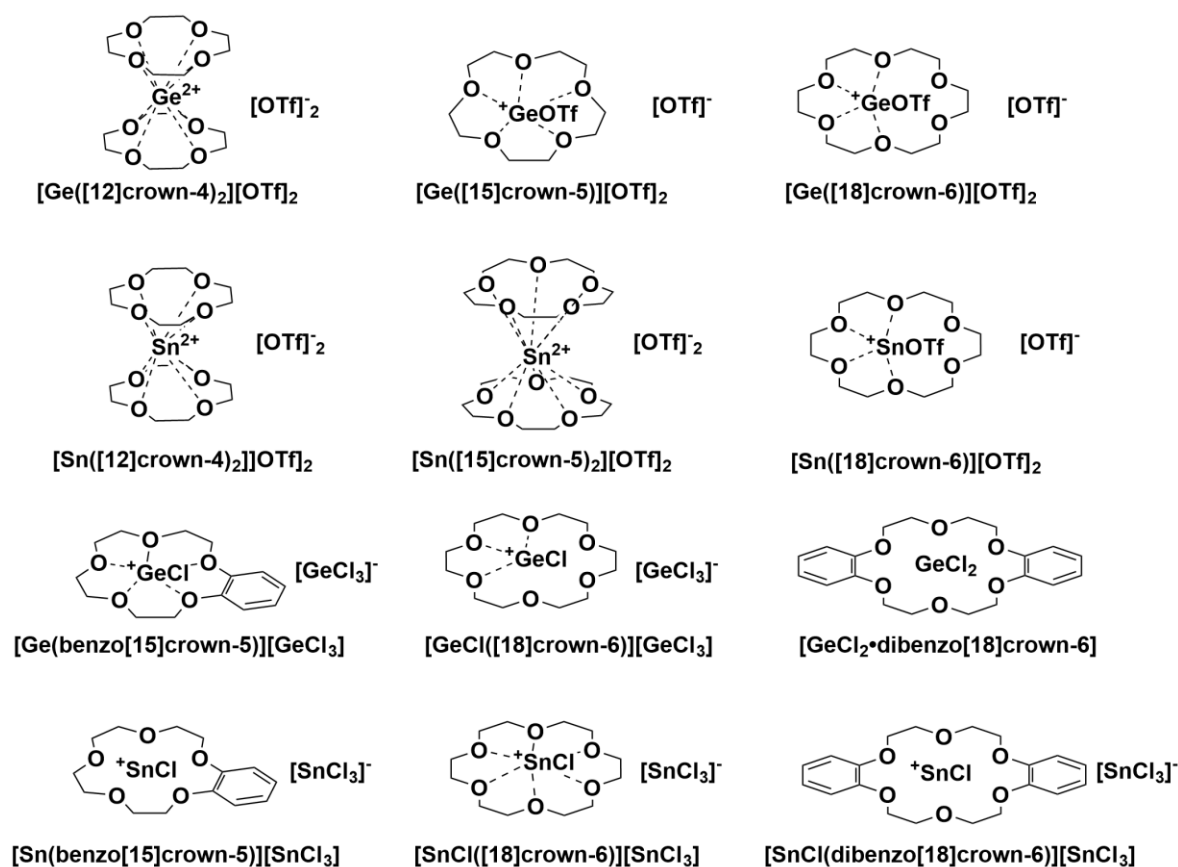


Figure 3.1 Germanium(II) and tin(II) crown ether-stabilized complexes studied in this work. Oxygen contacts are depicted with dashed lines for compounds with published solid-state X-ray diffraction data.¹⁸⁻²¹

3.2 Gutmann-Beckett Results for Group 14 Crown Ether Complexes

The addition of TEPO to germanium(II) and tin(II) crown ether complexes in a 1:1 ratio in DCM resulted in a downfield shift of the ³¹P NMR signal of TEPO in all cases (Table 3.1). To evaluate the influence of the ligand and charge on the Lewis acidity of the germanium(II) and tin(II) complexes, the Lewis acidities of the precursors to the complexes were also evaluated.

Table 3.1 The Gutmann-Beckett Acceptor number (AN) and ^{31}P NMR chemical shifts for the addition of TEPO to main group Lewis acids in DCM.

Entry ^a	Compound	Acceptor Number (1 Equiv.)	1 Equiv. ^c OPET ₃ (ppm)	2 Equiv. OPET ₃ (ppm)
1	[Ge([12]crown-4) ₂][OTf] ₂	92	82.6 ^b	82.4
2	[Ge([15]crown-5)][OTf] ₂	92	82.5	76.4
3	[Ge([18]crown-6)][OTf] ₂	90	81.8	80.6
4	[GeCl([15]crown-5)][GeCl ₃]	87	80.2	71.2
5	[GeCl(benzo[15]crown-5)][GeCl ₃]	87	80.1	74.6
6	[GeCl([18]crown-6)][GeCl ₃]	87	80.2	73.0
7	[GeCl ₂ ·dibenzo[18]crown-6)]	87	80.1	74.6
8	GeCl ₂ ·dioxane	87	80.1	74.2
9	[Sn([12]crown-4) ₂][OTf] ₂	79	76.9	71.9
10	[Sn([15]crown-5) ₂][OTf] ₂	79	76.6	73.0
11	[Sn([18]crown-6)][OTf] ₂	72	73.8	72.9
12	[SnCl(benzo[15]crown-5)][SnCl ₃]	78	76.5	68.1
13	[SnCl([15]crown-5)][SnCl ₃]	76	75.5	73.0
14	[SnCl([18]crown-6)][SnCl ₃]	74	74.3	69.0
15	Sn(OTf) ₂	81	77.7	75.1
16	SnCl ₂	77	75.8	-
18	B(C ₆ F ₅) ₃ ²⁴	82	78.0	-

^a Samples were externally referenced to an 85% phosphoric acid in water. ^b A small signal was observed at 85.7 ppm but was ~5 times less intense than the signal at 82.6 ppm. ^c Equiv. = equivalent(s).

From Table 3.1, the ANs of the germanium(II) crown ether complexes are all higher than the tin(II) crown ether complexes indicating that germanium(II) centre is more Lewis acidic than the tin(II) centre. Higher ANs are observed for the triflate salts (Table 3.1, Entries 1-3, 9-11) in comparison to their analogous trichlorometallate salts (Table 3.1, Entries 4-6, 12-14), presumably due to the presence of the chloride ligand on the metal centre. The three germanium(II) triflate salts (Table 3.1, Entries 1-3) have similar ANs as do the three chloride-containing germanium(II) species (Table 3.1, Entries 4-8). Analogous trends are also observed in the case of the tin(II) complexes, suggesting that identical

species are being formed in the reaction of the metal crown ether complexes and TEPO for complexes containing similar anions and/or chloride ligands.

From Table 3.1, variations of up to 1 ppm in the ^{31}P NMR chemical shifts were observed between the ^{31}P chemical shifts of either the germanium(II) crown ether triflate salts or the germanium(II) complexes containing chloride ligands (Table 3.1). The dependence of the ^{31}P NMR chemical shift of TEPO at various concentrations has been investigated by Gutmann^{7a} and revealed a variation in the ^{31}P NMR chemical shift of up to 2 ppm in hexanes. Thus, the variation in the ^{31}P chemical shifts between compounds exhibiting similar chemical shifts (Table 3.1, Entries 1-3, Entries 4-8, Entries 9-10 & 15, Entries 12-14 & 16) are likely due to different concentrations of the same Lewis acid-base adduct in solution. Attempts to crystallize the adducts from the reaction mixtures to identify the species in solution were unsuccessful resulting only in the precipitation of either the TEPO or the starting crown ether complexes.

Although the additions of TEPO to the crown ether complexes were performed stoichiometrically in 1:1 molar ratio (Table 3.1) as is standard in the Gutmann-Beckett method, the size of the central atom may allow for the coordination of multiple TEPO equivalents as observed previously.^{3b} Thus, two equivalents of TEPO were added to the crown ether complexes. Very similar ^{31}P NMR chemical shifts, with a less than one ppm difference, were observed in the addition of 1 or 2 equivalents of TEPO to **[Ge([12]crown-4)₂][OTf]₂** (Table 3.1, Entry 1) and **[Sn([18]crown-6)][OTf]₂** (Table 3.1, Entry 11) which

suggests that coordination of multiple TEPO equivalents is occurring, even when a 1:1 ratio of Lewis acid to TEPO is used.

The structures of the Group 14 crown ether-TEPO complexes, including the number of coordinated TEPO equivalents, cannot be easily identified from the ^{31}P chemical shift alone. Thus, multinuclear NMR spectroscopy was used to elucidate the structures of the complexes. For this study, a few crown ether salts were selected to represent the different solid-state coordination environments for both tin(II) and germanium(II) of the 15 complexes surveyed in Table 3.1. The complexes of TEPO with the following crown ether salts were examined in detail: $[\text{Sn}([\text{12}]\text{crown-4})_2][\text{OTf}]_2$, $[\text{SnCl}([\text{18}]\text{crown-6})][\text{SnCl}_3]$, $[\text{Sn}([\text{18}]\text{crown-6})][\text{OTf}]_2$, $\text{Sn}(\text{OTf})_2$, $[\text{Ge}([\text{12}]\text{crown-4})_2][\text{OTf}]_2$, $[\text{GeCl}([\text{18}]\text{crown-6})][\text{GeCl}_3]$, and $[\text{Ge}([\text{18}]\text{crown-6})_2][\text{OTf}]_2$ and $\text{GeCl}_2 \cdot \text{dioxane}$.

3.3 Analysis of the Solution-State Structures of the Tin(II) Crown Ether-TEPO Adducts

3.3.1 $[\text{Sn}([\text{12}]\text{crown-4})_2][\text{OTf}]_2$

As the tin nucleus can be probed directly with ^{119}Sn NMR spectroscopy, the tin(II) crown ether-TEPO complexes were examined first. To identify the potential for multiple TEPO equivalent coordination to the tin(II) species in solution, the ^1H and $^{31}\text{P}\{^1\text{H}\}$ NMR spectra for the 1:1 and 2:1 mixtures of TEPO and $[\text{Sn}([\text{12}]\text{crown-4})_2][\text{OTf}]_2$ were recorded at room temperature. The ^1H NMR spectra for both reactions were identical and no free TEPO was observed. A downfield shift of ~ 25 ppm from free TEPO was observed in the $^{31}\text{P}\{^1\text{H}\}$ NMR spectra in both additions although no tin-phosphorus coupling was observed. As identical spectra were observed for the 1:1 and 2:1 mixtures of TEPO and

[Sn([12]crown-4)₂][OTf]₂, the coordination of multiple phosphine oxide equivalents is probable, and thus, a 2:1 ratio of TEPO to Lewis acid was used in all additional experiments.

The ¹¹⁹Sn{¹H} NMR spectrum of the solution containing a 2:1 mixture of TEPO to **[Sn([12]crown-4)₂][OTf]₂** revealed one signal at room temperature at -865 ppm (Figure 3.2a), significantly more downfield than the ¹¹⁹Sn SSNMR chemical shift of **[Sn([12]crown-4)₂][OTf]₂** (-1405 ppm).²⁰ Although a downfield shift in the ¹¹⁹Sn{¹H} NMR spectrum for tin(IV) species is consistent with a decrease in coordination number, for tin(II) species, a downfield shift often correlates to a species with a higher coordination number.^{3b} In a related study of the addition of phosphine oxides to Sn(SbF₆)₂ a signal in the ¹¹⁹Sn NMR spectrum at -899 ppm (-60 °C) for a mixture of tricyclohexylphosphine oxide, TCPO, and Sn(SbF₆)₂, was assigned to the doubly-coordinated phosphine oxide complex [Sn(TCPO)₂]²⁺.²⁵ Thus, the formation of **[Sn(TEPO)₂]²⁺** from the addition of TEPO to **[Sn([12]crown-4)₂][OTf]₂** is proposed on the basis of chemical shift (Scheme 3.1). A coupling constant of 251 Hz was observed for [Sn(TCPO)₂]²⁺ (²J_{Sn-P}); however, the broad signal of **[Sn(TEPO)₂]²⁺** (FWHM ~ 700 Hz) precludes the observation of any coupling at room temperature in the ¹¹⁹Sn{¹H} NMR spectrum. In the ³¹P NMR spectrum of [Sn(TCPO)₂]²⁺, a shift of +15 ppm from the free phosphine oxide was observed,²⁵ similar to the change of +26 ppm observed for **[Sn(TEPO)₂]²⁺** (Figure 3.2b) derived from **[Sn([12]crown-4)₂][OTf]₂** and TEPO.

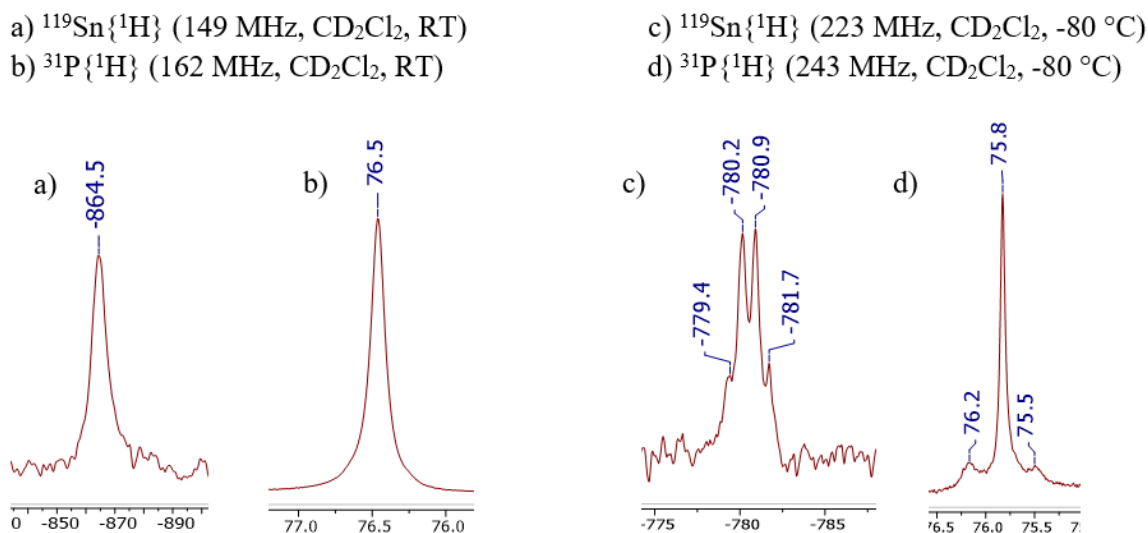
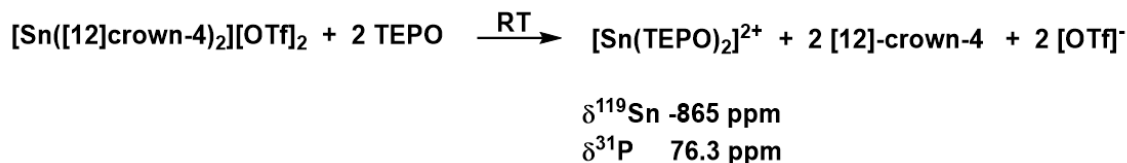


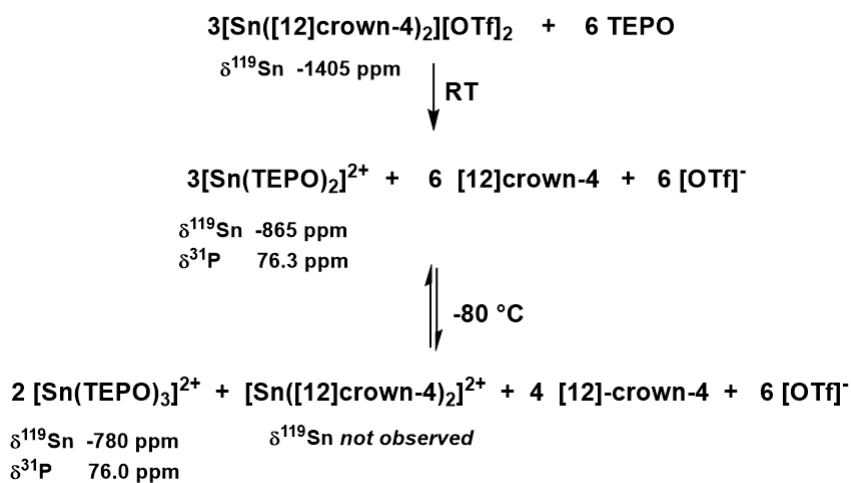
Figure 3.2 $^{119}\text{Sn}\{^1\text{H}\}$ and $^{31}\text{P}\{^1\text{H}\}$ NMR spectra of the addition of two equivalents of TEPO to $[\text{Sn}([\text{12}]\text{crown-4})_2][\text{OTf}]_2$ at room temperature (a/b) and -80°C (c/d).



Scheme 3.1 The addition of TEPO to $[\text{Sn}([\text{12}]\text{crown-4})_2][\text{OTf}]_2$ at room temperature.

In an attempt to observe Sn-P coupling, the 2:1 mixture of TEPO and $[\text{Sn}([\text{12}]\text{crown-4})_2]^{2+}$ was cooled to -80°C . Upon gradual cooling, the signal visible in the $^{31}\text{P}\{^1\text{H}\}$ NMR spectrum at room temperature decreased in intensity and a new signal emerged upfield. The relative intensities of the signals are consistent with the conversion of one species to another. The ^{31}P signal observed at -80°C , had satellites with a coupling constant of ~ 170 Hz which was assigned to coupling between the tin and phosphorus ($^2J_{\text{P-Sn}}$) (Figure 3.2d). In the ^1H NMR spectrum at -80°C , a signal at 3.57 ppm was observed, consistent with free [12]crown-4 indicating that displacement of the crown ether by TEPO

had occurred. The $^{119}\text{Sn}\{^1\text{H}\}$ NMR spectrum at $-80\text{ }^\circ\text{C}$ exhibited a quartet at -780 ppm ($^2J_{\text{P-Sn}} = 171\text{ Hz}$) (Figure 3.2c), consistent with the coordination of 3 TEPO equivalents. A ^{119}Sn shift of -780 ppm is similar to that of the tri-coordinated phosphine oxide species $[\text{Sn}(\text{TCPO})_3]^{2+}$ (-720 ppm),²⁵ which suggests that the species observed at $-80\text{ }^\circ\text{C}$ in the addition of TEPO to $[\text{Sn}([\mathbf{12}]\text{crown-4})_2][\text{OTf}]_2$ is $[\text{Sn}(\text{TEPO})_3]^{2+}$. The coupling constant of 171 Hz is smaller than the coupling constant observed for $[\text{Sn}(\text{TCPO})_3]^{2+}$ ($^2J_{\text{Sn-P}} = 237\text{ Hz}$). The change in coordination from two at room temperature to three at $-80\text{ }^\circ\text{C}$ could account for the conversion of one species into another observed in the $^{31}\text{P}\{^1\text{H}\}$ NMR spectrum as the temperature was decreased. Heating the sample back to room temperature resulted in identical spectra as those previously acquired at room temperature, indicating that the conversion is reversible. A summary of the coordination chemistry of $[\text{Sn}([\mathbf{12}]\text{crown-4})_2][\text{OTf}]_2$ and TEPO is provided in Scheme 3.2. Given that both $[\text{Sn}([\mathbf{15}]\text{crown-5})_2][\text{OTf}]_2$ and $[\text{Sn}([\mathbf{12}]\text{crown-4})_2][\text{OTf}]_2$ are sandwich complexes (Figure 3.3), the formation of $[\text{Sn}(\text{TEPO})_2]^{2+}$ from the addition of TEPO to $[\text{Sn}([\mathbf{15}]\text{crown-5})_2][\text{OTf}]_2$ is also expected. Identical ^{31}P chemical shifts of 76.9 ppm for the 1:1 of TEPO to either $[\text{Sn}([\mathbf{15}]\text{crown-5})_2][\text{OTf}]_2$ or $[\text{Sn}([\mathbf{12}]\text{crown-4})_2][\text{OTf}]_2$ (Table 3.1, Entries 9 & 10) corroborates this hypothesis (Table 3.1). The 2:1 addition of TEPO to $[\text{Sn}([\mathbf{15}]\text{crown-5})_2][\text{OTf}]_2$ or $[\text{Sn}([\mathbf{12}]\text{crown-4})_2][\text{OTf}]_2$ are also very similar, differing by only 1.1 ppm .



Scheme 3.2 The reaction of $[\text{Sn}([\text{12}]\text{crown-4})_2][\text{OTf}]_2$ and TEPO at room temperature and $-80\text{ }^\circ\text{C}$.

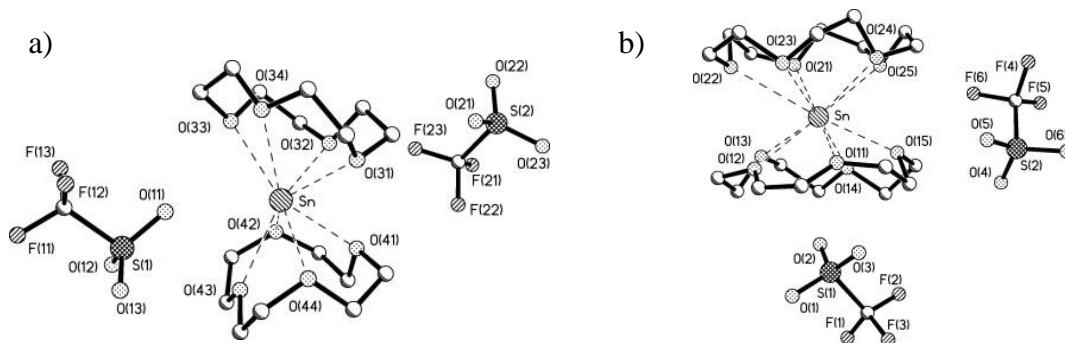


Figure 3.3 The solid-state structures of a) $[\text{Sn}([\text{12}]\text{crown-4})_2][\text{OTf}]_2$ and b) $[\text{Sn}([\text{15}]\text{crown-5})_2][\text{OTf}]_2$. Reprinted with permission from Elsevier.²⁶

3.3.2 $\text{Sn}(\text{OTf})_2$

The addition of TEPO to $\text{Sn}(\text{OTf})_2$, the precursor used in the formation of $[\text{Sn}([\text{12}]\text{crown-4})_2][\text{OTf}]_2$ was also investigated. At room temperature, the $^{119}\text{Sn}\{^1\text{H}\}$ NMR spectrum (Figure 5.4a) for the 2:1 mixture of TEPO and $\text{Sn}(\text{OTf})_2$ exhibited a single signal at -860 ppm, with a chemical shift nearly identical to that observed in the addition of TEPO to $[\text{Sn}([\text{12}]\text{crown-4})_2][\text{OTf}]_2$. The $^{31}\text{P}\{^1\text{H}\}$ NMR spectrum revealed a signal at 76.8

ppm (Figure 3.4b), similar to the ^{31}P NMR shift of 76.5 ppm observed in the addition of TEPO to $[\text{Sn}([\text{12}]\text{crown-4})_2][\text{OTf}]_2$. The nearly identical $^{119}\text{Sn}\{^1\text{H}\}$ and $^{31}\text{P}\{^1\text{H}\}$ NMR spectra are consistent with the formation of $[\text{Sn}(\text{TEPO})_2]^{2+}$ from TEPO and $\text{Sn}(\text{OTf})_2$ (Scheme 3.3). Upon cooling the solution to $-80\text{ }^\circ\text{C}$, a triplet at -854 ppm ($^2J_{\text{Sn-P}} = 232\text{ Hz}$) was observed in the $^{119}\text{Sn}\{^1\text{H}\}$ NMR spectrum, consistent the coordination of two phosphine oxides (Figure 3.4c). The magnitude of the coupling constant is similar to that of $[\text{Sn}(\text{TCPO})_2]^{2+}$ ($^2J = 251\text{ Hz}$).²⁵ In the corresponding $^{31}\text{P}\{^1\text{H}\}$ NMR spectrum, satellites consistent with tin-phosphorus coupling were observed, confirming the coordination of the phosphine oxide to the tin centre (Figure 3.4d). These results are also consistent with the formation of $[\text{Sn}(\text{TEPO})_2]^{2+}$ in the reaction of TEPO and $[\text{Sn}([\text{12}]\text{crown-4})_2][\text{OTf}]_2$ (2:1 equivalents) at room temperature.

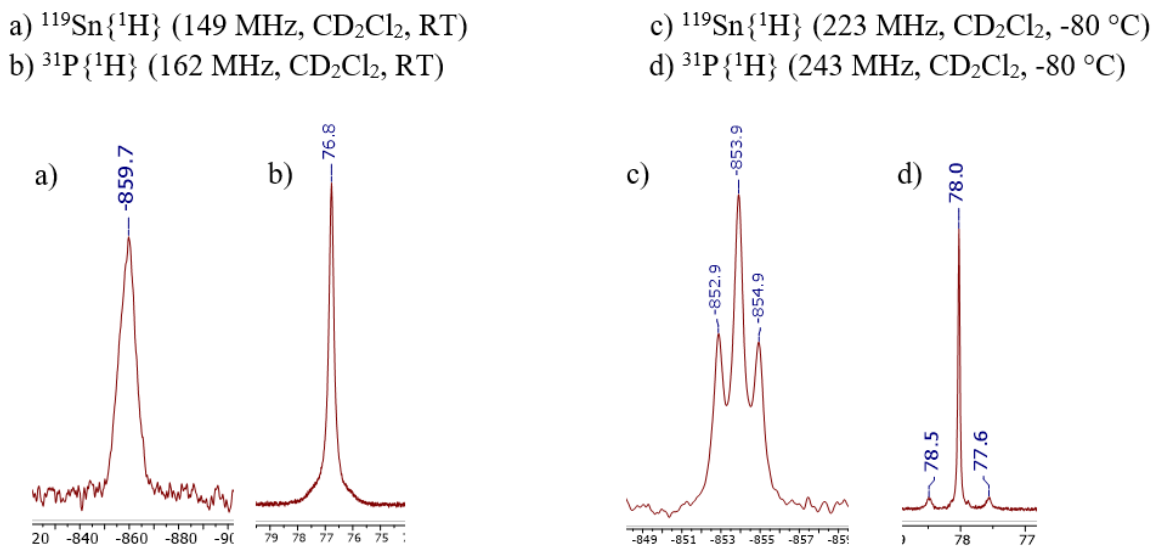
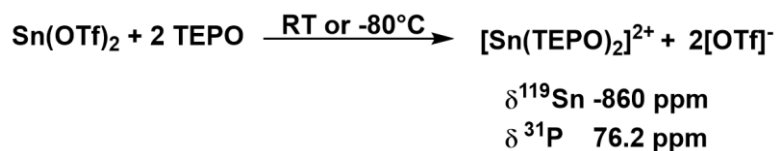


Figure 3.4 $^{119}\text{Sn}\{^1\text{H}\}$ NMR spectra and $^{31}\text{P}\{^1\text{H}\}$ NMR spectra of the addition of TEPO to $\text{Sn}(\text{OTf})_2$ at room temperature (a/b) and $-80\text{ }^\circ\text{C}$ (c/d).



Scheme 3.3 The addition of TEPO to **Sn(OTf)₂** at room temperature or -80 °C.

Surprisingly, no evidence for the formation of **[Sn(TEPO)₃]²⁺** was observed in the 2:1 addition of TEPO to **Sn(OTf)₂** at low temperature as was observed in a 2:1 TEPO and **[Sn([12]crown-4)₂][OTf]₂** mixture under the same conditions. Evidently, the presence of the [12]crown-4 ligand enables the generation of **[Sn(TEPO)₃]²⁺** presumably due to the favorable regeneration²⁷ of the **[Sn([12]crown-4)₂]²⁺** through redistribution of the TEPO and crown ether ligands compared to the less favorable regeneration of **Sn(OTf)₂** in reactions with **Sn(OTf)₂** and TEPO.

3.3.3 **[Sn([18]crown-6)][OTf]₂**

The addition of TEPO to **[Sn([18]crown-6)][OTf]₂** in a 2:1 ratio at room temperature resulted in one crown ether proton environment in the ¹H NMR spectrum and one phosphorus signal in the ³¹P{¹H} NMR spectrum at 72.8 ppm, significantly shifted from the signal assigned to **[Sn(TEPO)₂]²⁺** at 76.3 ppm or **[Sn(TEPO)₃]²⁺** at 76.0 ppm. A weak ¹¹⁹Sn{¹H} NMR signal at room temperature was observed at -820 ppm (Figure 3.5a). The chemical shift of this signal is downfield from the signal assigned to **[Sn(TEPO)₂]²⁺** (-865 ppm) but not as downfield as the chemical shift of **[Sn(TEPO)₃]²⁺** (-781 ppm). To account for a species with a ¹¹⁹Sn chemical shift between the two- and three-coordinate TEPO complexes, the signal at -820 ppm was assigned to **[Sn([18]crown-6)(TEPO)₂]²⁺**.

Accordingly $[\text{Sn}([\mathbf{18}]\text{crown-6})(\text{TEPO})_2]^{2+}$ has a higher coordination number than $[\text{Sn}(\text{TEPO})_2]^{2+}$, consistent with a downfield ^{119}Sn chemical shift; however, the weaker donor ability of [18]crown-6 compared to TEPO results in an upfield ^{119}Sn chemical shift for $[\text{Sn}([\mathbf{18}]\text{crown-6})(\text{TEPO})_2]^{2+}$ compared to $[\text{Sn}(\text{TEPO})_3]^{2+}$. The ionic radius of Sn^{2+} is 1.18 \AA ²⁸ and [18]crown-6 has a cavity size ($2.6\text{-}3.2 \text{ \AA}$),²⁹ and thus, tin(II)^{2+} can fit within the cavity of the crown ether as observed in the solid-state structure of $\text{Sn}([\mathbf{18}]\text{crown-6})[[\text{OTf}]_2]$ (Figure 3.6)²⁰ and coordinate to the two TEPO. $[\text{Sn}([\mathbf{18}]\text{crown-6})(\text{TEPO})_2]^{2+}$ is proposed to have a similar structure to $[\text{Sn}([\mathbf{18}]\text{crown-6})][[\text{OTf}]_2]$ where the trans-oriented triflate anions are replaced by the TEPO ligands.

- a) $^{119}\text{Sn}\{^1\text{H}\}$ (149 MHz, CD_2Cl_2 , RT) c) $^{119}\text{Sn}\{^1\text{H}\}$ (223 MHz, CD_2Cl_2 , $-80 \text{ }^\circ\text{C}$)
 b) $^{31}\text{P}\{^1\text{H}\}$ (162 MHz, CD_2Cl_2 , RT) d) $^{31}\text{P}\{^1\text{H}\}$ (243 MHz, CD_2Cl_2 , $-80 \text{ }^\circ\text{C}$)

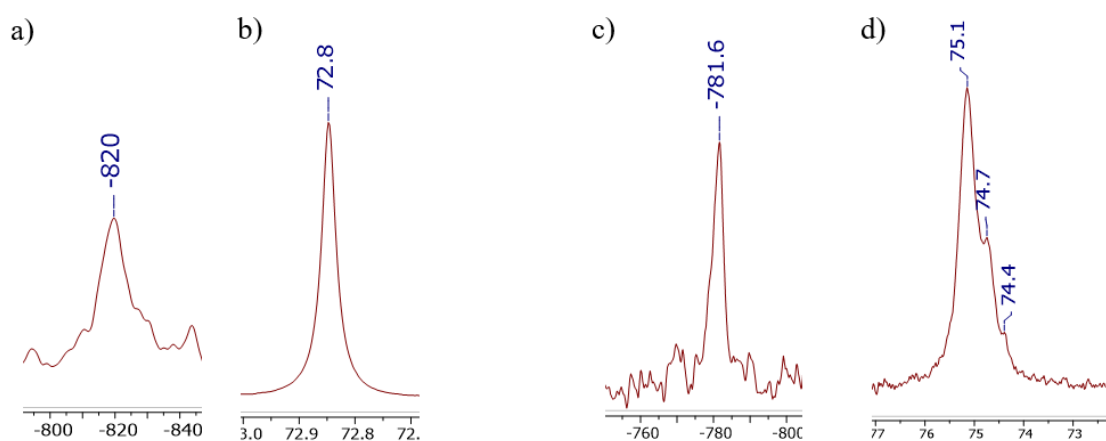
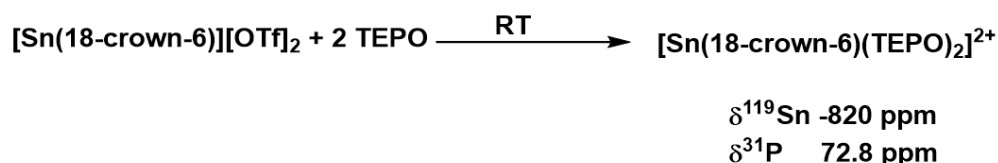


Figure 3.5 $^{119}\text{Sn}\{^1\text{H}\}$ and $^{31}\text{P}\{^1\text{H}\}$ NMR spectra of the addition of two equivalents of TEPO to $[\text{Sn}([\mathbf{18}]\text{crown-6})][[\text{OTf}]_2]$ at room temperature (a/b) and $-80 \text{ }^\circ\text{C}$ (c/d).



Scheme 3.4 The addition of TEPO to $[\text{Sn}(\text{18-crown-6})][\text{OTf}]_2$ at room temperature.

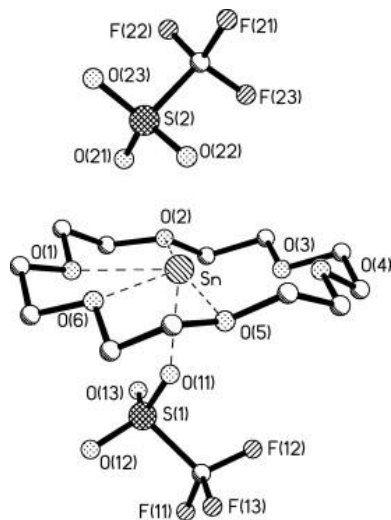
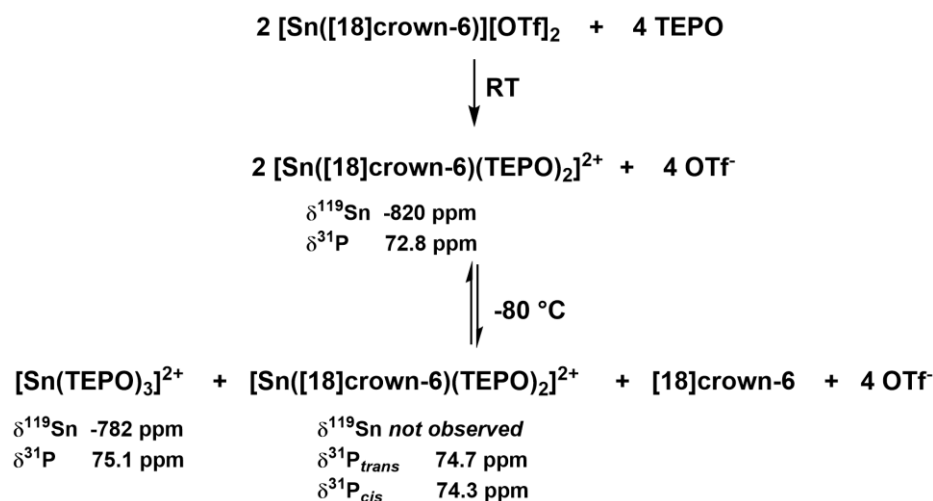


Figure 3.6 The solid state structure of $[\text{Sn}(\text{18-crown-6})][\text{OTf}]_2$. Reprinted with permission from Elsevier.²⁶

In an attempt to observe coupling between the tin and phosphorus in the 2:1 mixture of TEPO and $[\text{Sn}(\text{18-crown-6})][\text{OTf}]_2$, the solution was cooled to $-80\text{ }^\circ\text{C}$. The signal previously observed in the $^{119}\text{Sn}\{^1\text{H}\}$ NMR spectrum at room temperature disappeared and a signal at -782 ppm , consistent with the formation of $[\text{Sn}(\text{TEPO})_3]^{2+}$, was observed (Figure 3.5c). Upon cooling, three signals in the $^{31}\text{P}\{^1\text{H}\}$ NMR spectrum at $-80\text{ }^\circ\text{C}$ were present indicating a mixture of species (Figure 3.5d). The signals are 75.1 and 74.7 ppm were assigned to $[\text{Sn}(\text{TEPO})_3]^{2+}$ and $[\text{Sn}(\text{18-crown-6})(\text{TEPO})_2]^{2+}$ respectively. Although the nature of the third signal in the spectrum is not clear, the chemical shift is similar to that

of $[\text{Sn}([\text{18}]\text{crown-6})(\text{TEPO})_2]^{2+}$, which may suggest a similar structure. One possibility is where instead of the TEPO ligands being *trans* to one another, like the triflate anions in the solid-state structure of $[\text{Sn}([\text{18}]\text{crown-6})][\text{OTf}]_2$ (Figure 3.6), a *cis* orientation of the TEPO ligands could occur. Both *cis* and *trans* isomers of the TEPO adducts of bis(tetrachlorocatecholato)germane and bis(tetrabromocatecholato)germane were identified in solution, although a greater ^{31}P chemical shift difference between the two isomers was observed (4.5 and 0.8 ppm, respectively)^{3d} compared to 0.3 ppm difference observed between the proposed *trans*- $[\text{Sn}([\text{18}]\text{crown-6})(\text{TEPO})_2]^{2+}$ and *cis*- $[\text{Sn}([\text{18}]\text{crown-6})(\text{TEPO})_2]^{2+}$. Due to the mixture of compounds present and the known interconversion between $[\text{Sn}(\text{TEPO})_2]^{2+}$ and $[\text{Sn}(\text{TEPO})_3]^{2+}$, a dynamic process between the three species in solution may prevent the observation of Sn-P coupling at -80 °C. A summary of the reaction between TEPO and $[\text{Sn}([\text{18}]\text{crown-6})][\text{OTf}]_2$ is shown in Scheme 3.5.



Scheme 3.5 The reaction of $[\text{Sn}([\text{18}]\text{crown-6})][\text{OTf}]_2$ and TEPO at room temperature and -80 °C.

3.3.4 **[SnCl([18]crown-6)][SnCl₃]**

In the addition of two equivalents of TEPO to **[SnCl([18]crown-6)][SnCl₃]** at room temperature, one signal was observed in ³¹P{¹H} NMR spectrum (73.4 ppm). The ¹¹⁹Sn{¹H} NMR spectrum of the solution revealed one signal at -198 ppm (Figure 3.7a). The ¹¹⁹Sn{¹H} chemical shift of the signal is similar to that of the species generated from SnCl₂ and trimethylphosphine oxide (TMPO) [SnCl₂(TMPO)₂] (-204 ppm)³⁰ and comparable to the 1,1'-bis(phosphonyl)ferrocene coordinated SnCl₂ (-253 ppm).³¹ Thus, the species in solution was assigned to **[SnCl₂(TEPO)₂]** (Scheme 3.6). A proposed mechanism for the formation of **[SnCl₂(TEPO)₂]** is shown below (Scheme 3.7). In the first step, TEPO displaces the chloride from the [SnCl₃]⁻ anion to generate [SnCl₂(TEPO)]. The chloride then reacts with the [SnCl]⁺ fragment to generate SnCl₂ and uncoordinated [18]crown-6. Coordination of a second equivalent of TEPO to [SnCl₂(TEPO)] would then give the observed product **[SnCl₂(TEPO)₂]**. As the tin(II) complexes **[SnCl(benzo[15]crown-5)][SnCl₃]**, **[SnCl([15]crown-5)][SnCl₃]** and **[SnCl(dibenzo[18]crown-6)][SnCl₃]** also contain the reactive anion [⁻SnCl₃], similar reactivity is expected and comparable ³¹P NMR chemical shifts for these complexes are consistent with this assessment (Table 3.1, Entries 12-14).

a) $^{119}\text{Sn}\{^1\text{H}\}$ (149 MHz, CD_2Cl_2 , RT)
 b) $^{31}\text{P}\{^1\text{H}\}$ (243 MHz, CD_2Cl_2 , RT)

c) $^{119}\text{Sn}\{^1\text{H}\}$ (223 MHz, CD_2Cl_2 , -80°C)
 d) $^{31}\text{P}\{^1\text{H}\}$ (243 MHz, CD_2Cl_2 , -80°C)

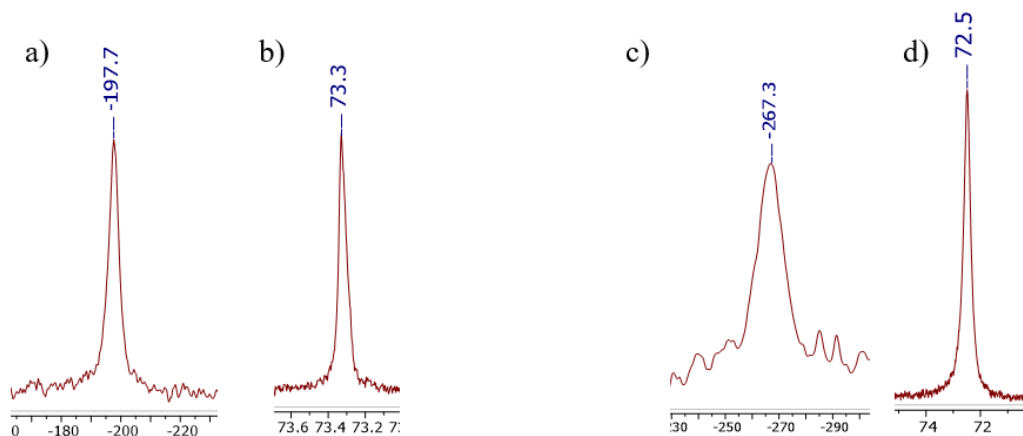
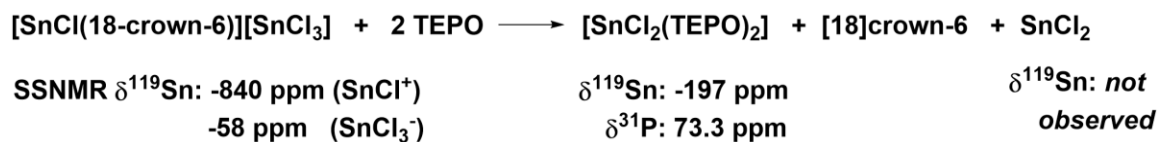
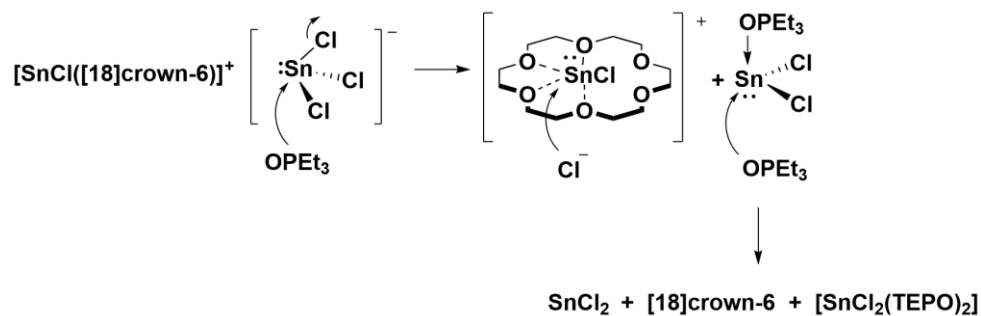


Figure 3.7 $^{119}\text{Sn}\{^1\text{H}\}$ NMR spectra of the addition of two equivalents of TEPO to $[\text{SnCl}([\text{18}]\text{crown-6})][\text{SnCl}_3]$ at room temperature (a/b) and -80°C (c/d).

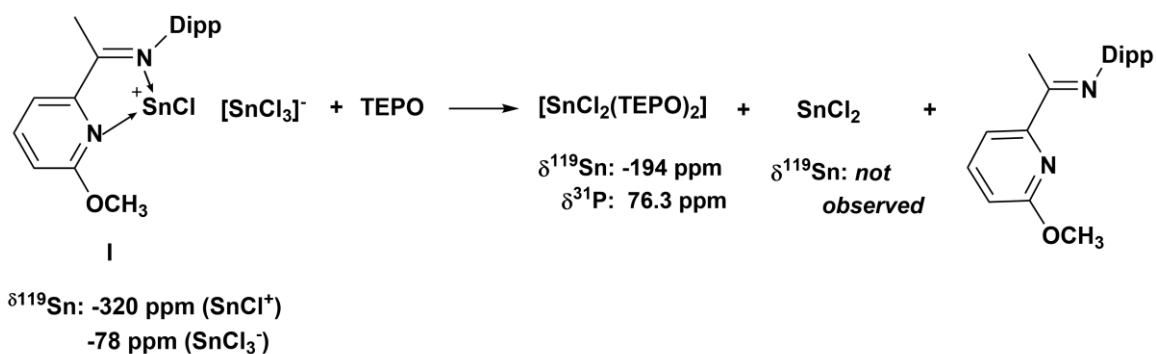


Scheme 3.6 The addition of TEPO to $[\text{SnCl}([\text{18}]\text{crown-6})][\text{SnCl}_3]$.



Scheme 3.7 Proposed mechanism for the formation of $[\text{SnCl}_2(\text{TEPO})_2]$ from two equivalents of TEPO and $[\text{SnCl}([\text{18}]\text{crown-6})][\text{SnCl}_3]$.

To further confirm that the anion, $[\text{SnCl}_3]^-$, is the cause of the undesired reactivity, another tin(II) cationic species, **I**, containing the $[\text{SnCl}_3]^-$ anion and an iminopyridine ligand was also synthesized,³² and was reacted with TEPO (Scheme 8). In the $^{119}\text{Sn}\{^1\text{H}\}$ NMR spectrum of the mixture, the loss of both the signals assigned to $[\text{SnCl}_3]^-$ (-78 ppm) and $[\text{SnCl}]^+$ (-320 ppm) was observed along with the appearance of a new signal at -195 ppm. The ^{119}Sn NMR chemical shift is consistent with the formation of $[\text{SnCl}_2(\text{TEPO})_2]$. The ^{31}P NMR chemical shift (76.3 ppm) is downfield of the signal assigned to $[\text{SnCl}_2(\text{TEPO})_2]$ derived from $[\text{SnCl}(\text{18-crown-6})][\text{SnCl}_3]^-$ which could be due in part to a difference in concentration; however, the presence of other complexes in solution are possible. As the $^{119}\text{Sn}\{^1\text{H}\}$ NMR spectroscopy is less sensitive than ^{31}P NMR spectroscopy (relative receptivity to ^1H : 6.65×10^{-2} for ^{31}P , 5.27×10^{-2} for ^{119}Sn), only one species was detected and is presumed to be the major species in solution, $[\text{SnCl}_2(\text{TEPO})_2]$. The ^{119}Sn NMR chemical shift for the addition of TEPO to **I** is consistent with reactivity at the anion.



Dipp= 2,6-diisopropylphenyl

Scheme 3.8 The addition of TEPO to **I** to form $[\text{SnCl}_2(\text{TEPO})_2]$ and relevant chemical shift data.

Independent synthesis of $[\text{SnCl}_2(\text{TEPO})_2]$ from SnCl_2 and TEPO yielded different NMR data (^{119}Sn -212 ppm; δ $^{31}\text{P}\{\text{H}\}$ 63.5 ppm) compared to the $[\text{SnCl}_2(\text{TEPO})_2]$ derived from $[\text{SnCl}(\text{18-crown-6})][\text{SnCl}_3]$ (^{119}Sn -198 ppm; δ $^{31}\text{P}\{\text{H}\}$ 73.3 ppm). As the solution of $[\text{SnCl}_2(\text{TEPO})_2]$ derived from $[\text{SnCl}(\text{18-crown-6})][\text{SnCl}_3]$ contains additional SnCl_2 (Scheme 3.7), exchange between SnCl_2 and $[\text{SnCl}_2(\text{TEPO})_2]$ could occur and influence the chemical shifts. This was probed by varying the ratio of SnCl_2 : $[\text{SnCl}_2(\text{TEPO})_2]$ and measuring the ^{31}P and ^{119}Sn NMR chemical shifts (Figure 3.8). A clear trend is observed in the ^{119}Sn NMR chemical shifts when the ratio of SnCl_2 : $[\text{SnCl}_2(\text{TEPO})_2]$ is altered. With 0.5 equivalents of SnCl_2 relative to $[\text{SnCl}_2(\text{TEPO})_2]$, the ^{119}Sn NMR signal shifts downfield relative to the spectrum with 0 equivalents of SnCl_2 . When the number of equivalents of SnCl_2 are increased to 1, the ^{119}Sn NMR signal shifts further downfield. These data account for the 14 ppm difference in ^{119}Sn NMR chemical shift between $[\text{SnCl}_2(\text{TEPO})_2]$ derived from SnCl_2 and that derived from $[\text{SnCl}(\text{18-crown-6})][\text{SnCl}_3]$. A similar trend was observed in the ^{31}P NMR chemical shifts, although the change was less linear. With 0.5 equivalents of SnCl_2 , the ^{31}P NMR chemical shift is downfield of the signal with 0 equivalents of SnCl_2 . The signal shifts downfield further when the equivalents of SnCl_2 are increased to 1; however, only slightly. The presence of the [18]crown-6 in solution may influence the proposed exchange between SnCl_2 and $[\text{SnCl}_2(\text{TEPO})_2]$ if coordination to SnCl_2 also occurs. Therefore, independent synthesis of $[\text{SnCl}_2(\text{TEPO})_2]$ from SnCl_2 corroborates the formation of $[\text{SnCl}_2(\text{TEPO})_2]$ in the reaction of TEPO and $[\text{SnCl}(\text{18-crown-6})][\text{SnCl}_3]$.

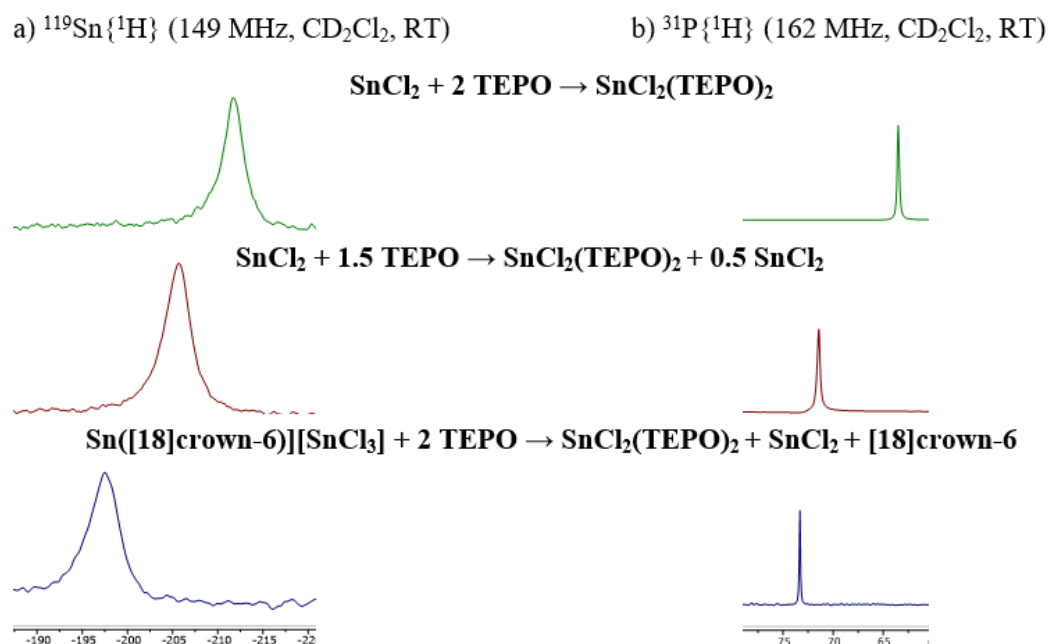


Figure 3.8 a) Stack plot of the $^{119}\text{Sn}\{^1\text{H}\}$ NMR spectra for additions in which the ratio of SnCl_2 : $[\text{SnCl}_2(\text{TEPO})_2]$ is varied. b) Stack plot of the $^{31}\text{P}\{^1\text{H}\}$ NMR spectra for additions in which the ratio of SnCl_2 : $[\text{SnCl}_2(\text{TEPO})_2]$ is varied.

At room temperature, no Sn-P coupling was evident in the NMR spectra of $[\text{SnCl}_2(\text{TEPO})_2]$. In an attempt to observe coupling in $[\text{SnCl}_2(\text{TEPO})_2]$, a solution of $[\text{SnCl}([\text{18}]\text{crown-6})][\text{SnCl}_3]$ and TEPO was cooled to $-80\text{ }^\circ\text{C}$. Broad signals were observed at -267 ppm and 72 ppm in the $^{119}\text{Sn}\{^1\text{H}\}$ and $^{31}\text{P}\{^1\text{H}\}$ NMR spectra, respectively; no ^{119}Sn - ^{31}P coupling could be discerned in either spectrum due to the breadth of the signals; however, the chemical shift of the ^{119}Sn NMR signal shifts by 60 ppm upfield. Similar spectral features were observed in the low temperature NMR analysis of $[\text{SnCl}_2(\text{TEPO})_2]$. The temperature dependence of the solution-state ^{119}Sn NMR chemical shifts of tin chlorides have been previously reported;^{31,32} however, much smaller changes in the ^{119}Sn NMR chemical shifts were observed in these tin(II) halide systems compared to a

60 ppm difference observed in this system. No change in the ^{119}Sn chemical shift was reported for $[\text{SnCl}_2(\text{TMPO})_2]$ when the solution was cooled from RT to $-90\text{ }^\circ\text{C}$ ³⁰ in clear contrast to the $[\text{SnCl}_2(\text{TEPO})_2]$ system. One possibility is the formation of a dimer, which may influence the environment about the tin(II) centre sufficiently to change the chemical shift (Figure 3.9). In the solid-state, chloride ligands preferentially occupy the axial position in phosphine oxide or phosphine complexes of SnCl_2 , as observed in the solid-state structures of $[\text{SnCl}_2(\text{TMPO})_2]$, $[\text{SnCl}_2(o\text{-C}_6\text{H}_4(\text{PPh}_2)_2)]$ and $[\text{SnCl}_2(\text{Me}_2\text{P}(\text{CH}_2)_2\text{PMe}_2)]$.³⁰ Axially-positioned chloride ligands are also anticipated for $[\text{SnCl}_2(\text{TEPO})_2]$. The structures of two possible dimer isomers include both $\mu\text{-Cl}$ and $\mu\text{-OPEt}_3$ association between the monomers (Figure 3.9); however, previous studies have shown the preferential and exclusive formation of the $\mu\text{-O}$ complexes in the solid-state in complexes containing both chloride and oxygen-based ligands, such as $\text{O}i\text{Pr}$ or OSiPh_3 .³⁴ Thus, if a solution-state dimer is formed at low temperatures, the $\mu\text{-OPEt}_3$ is the most probable isomer. However, without the ability to further probe the low temperature interaction of SnCl_2 and TEPO, the exact structure cannot be unambiguously elucidated.

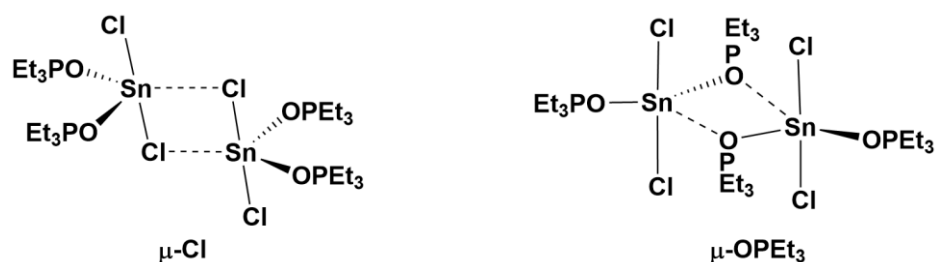


Figure 3.9 Two possible dimers of $[\text{SnCl}_2(\text{TEPO})_2]$.

The addition of 1 or 2 equivalents of TEPO to the crown ether-stabilized tin(II) complexes examined resulted in the coordination of two equivalents. In an attempt to coordinate a single equivalent of TEPO, substoichiometric equivalents of TEPO were added to **[SnCl([18]crown-6)][SnCl₃]** sequentially. With each subsequent addition of 0.2 equivalents, only one signal was observed in the ³¹P{¹H} NMR spectrum; however, the signal shifted upfield upon each addition. The gradual change in chemical shift is not consistent with the formation of a new species with only one TEPO ligand, either **[SnCl([18]crown-6)(TEPO)]²⁺** or **[SnCl₂(TEPO)]** and is instead consistent with the formation of **[SnCl₂(TEPO₂)]** based on the nearly identical shift. The gradual change in chemical shift can be attributed to the influence of concentration of the adduct formed in solution which has been reported previously to lead to ³¹P NMR chemical shift changes of up to 2 ppm.^{7a} If a new species was generated, a significantly shifted ³¹P NMR chemical would be expected for the Lewis acidic centre, such as the ~15 ppm difference between **[Si(cat^H)₂(TEPO)]** and **[Si(cat^H)₂(TEPO)₂]**.^{3b}

3.4 Analysis of the Solution-State Structures of the Germanium(II) Crown Ether-TEPO Adducts

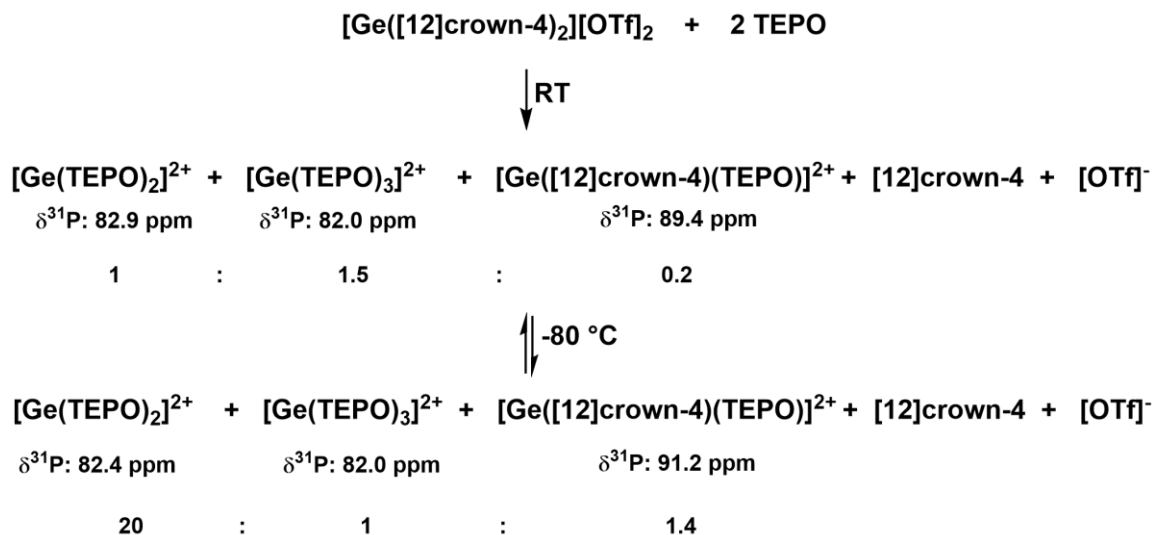
3.4.1 **[Ge([12]crown-4)₂][OTf]₂**

Without the ability to easily probe the germanium(II) centre directly due to the lack of a convenient NMR active nucleus, comparisons of the ¹H and ³¹P NMR data of the germanium(II) complexes to the NMR data for the analogous tin(II) complexes were made to provide insight into the reactivity of TEPO with the germanium(II) crown ether complexes. To evaluate the possibility of the coordination of multiple TEPO equivalents,

the NMR data from the addition of one equivalent of TEPO to $[\text{Ge}([\mathbf{12}]\text{crown-4})_2][\text{OTf}]_2$ was compared to the NMR data from the addition of two equivalents of TEPO to $[\text{Ge}([\mathbf{12}]\text{crown-4})_2][\text{OTf}]_2$. Nearly identical ^1H and $^{31}\text{P}\{^1\text{H}\}$ NMR data were observed using 1 or 2 equivalents of TEPO, consistent with the coordination of at least two equivalents of TEPO even under stoichiometric conditions. Thus, further studies were conducted on mixtures of two TEPO equivalents to one germanium(II) species.

At room temperature, the ^1H NMR spectrum of $[\text{Ge}([\mathbf{12}]\text{crown-4})_2][\text{OTf}]_2$ and two equivalents of TEPO revealed one crown ether proton environment and one set of signals for the ethyl moiety of the phosphine oxide. However, three signals were observed in the $^{31}\text{P}\{^1\text{H}\}$ NMR spectrum of the mixture at 82.0 ppm, 82.9 ppm and 89.4 ppm in a ratio of 1.5 : 1 : 0.2, respectively. The two upfield signals were assigned to $[\text{Ge}(\text{TEPO})_2]^{2+}$ (82.9 ppm) and $[\text{Ge}(\text{TEPO})_3]^{2+}$ (82.0 ppm) (Scheme 3.9) by comparison to the $^{31}\text{P}\{^1\text{H}\}$ NMR data of $[\text{Sn}(\text{TEPO})_2]^{2+}$ (76.6 ppm at $-40\text{ }^\circ\text{C}$) and $[\text{Sn}(\text{TEPO})_3]^{2+}$ (75.6 ppm at $-40\text{ }^\circ\text{C}$) derived from $[\text{Sn}([\mathbf{12}]\text{crown-4})_2][\text{OTf}]_2$ and on the basis of the relationship between $^{31}\text{P}\{^1\text{H}\}$ NMR chemical shift and the number of coordinated TEPO in which a more downfield signal is associated with a lower number of coordinated TEPO.^{3b} Despite the three phosphorus environments, only one set of signals was observed in the ^1H NMR spectrum suggesting that the environment of the ethyl hydrogens is similar in all species; the signals assigned to the methylene and methyl signals are both shifted relative to free TEPO. A similar trend was observed in the ^1H NMR spectrum of $[\text{Sn}([\mathbf{12}]\text{crown-4})_2][\text{OTf}]_2$ and TEPO, which also showed only set of signals assigned to the ethyl group

even though two signals assigned to $[\text{Sn}(\text{TEPO})_2]^{2+}$ and $[\text{Sn}(\text{TEPO})_3]^{3+}$ were observed in the $^{31}\text{P}\{^1\text{H}\}$ NMR spectrum.



Scheme 3.9 The reaction of $[\text{Ge}([\text{12}]\text{crown-4})_2][\text{OTf}]_2$ and TEPO.

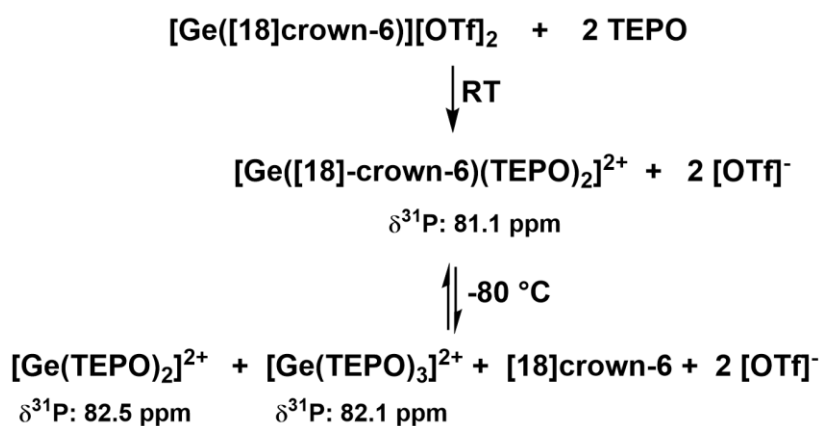
The 2:1 mixture of TEPO and $[\text{Ge}([\text{12}]\text{crown-4})_2][\text{OTf}]_2$ was cooled to $-80 \text{ }^\circ\text{C}$, revealing two signals for the P-CH₂ groups in the ^1H NMR spectrum, consistent with at least two different species. Similar to $[\text{Sn}([\text{12}]\text{crown-4})_2][\text{OTf}]_2$, the two signals assigned to $[\text{Ge}(\text{TEPO})_2]^{2+}$ (82.4 ppm at $-80 \text{ }^\circ\text{C}$) and $[\text{Ge}(\text{TEPO})_3]^{2+}$ (82.0 ppm at $-80 \text{ }^\circ\text{C}$) in the $^{31}\text{P}\{^1\text{H}\}$ NMR spectrum for the addition of TEPO to $[\text{Ge}([\text{12}]\text{crown-4})_2]^{2+}$ change in relative intensity upon cooling, from 1:1.5 at RT to 20:1 at $-80 \text{ }^\circ\text{C}$. As the solution is cooled, the doubly-coordinated phosphine oxide complex $[\text{Ge}(\text{TEPO})_2]^{2+}$ becomes the major species in solution in contrast to the behaviour of the tin system where the triply-coordinated phosphine oxide complex $[\text{Sn}(\text{TEPO})_3]^{2+}$ predominates at low temperatures. The larger size of tin relative to germanium may make the coordination of three equivalents of TEPO to tin to more favorable at low temperature. The chemical shift of the signal

furthest downfield in $^{31}\text{P}\{^1\text{H}\}$ NMR spectrum (89.5 ppm) of the addition of two equivalents of TEPO to $[\text{Ge}([\text{12}]\text{crown-4})_2][\text{OTf}]_2$ ppm indicates a species with the highest Lewis acidity in the mixture. A singly-coordinated TEPO complex, such as $[\text{Ge}([\text{12}]\text{crown-4})(\text{TEPO})]^{2+}$ could account for this signal as [12]crown-4 is a weaker donor compared to TEPO resulting in a more downfield ^{31}P chemical shift. The second set of ethyl signals visible in the ^1H NMR spectrum at $-80\text{ }^\circ\text{C}$ is, approximately, of the correct intensity to be the signals for the ethyl group of the species assigned to $[\text{Ge}([\text{12}]\text{crown-4})(\text{TEPO})]^{2+}$ and are shifted upfield compared to the chemical shift of the signal assigned to the analogous signals assigned to $[\text{Ge}(\text{TEPO})_2]^{2+}$, consistent with a stronger association of the TEPO to Ge^{2+} . A summary of the various equilibria for the addition of TEPO to $[\text{Ge}([\text{12}]\text{crown-4})_2][\text{OTf}]_2$ at room temperature and $-80\text{ }^\circ\text{C}$ is given in Scheme 3.9.

3.4.2 $[\text{Ge}([\text{18}]\text{crown-6})][\text{OTf}]_2$

The addition of two equivalents of TEPO to $[\text{Ge}([\text{18}]\text{crown-6})][\text{OTf}]_2$ revealed one set of signals assigned to the ethyl group and one crown ether environment in the ^1H NMR spectrum at room temperature. Only one signal was observed in the ^{31}P NMR spectrum at 81.1 ppm, the value of which is not consistent with the chemical shifts assigned to either $[\text{Ge}(\text{TEPO})_2]^{2+}$ (82.9 ppm) or $[\text{Ge}(\text{TEPO})_3]^{2+}$ (82 ppm) (Scheme 3.9). In the analogous tin system, $[\text{Sn}([\text{18}]\text{crown-6})][\text{OTf}]_2$, a signal with a chemical shift upfield of both $[\text{Sn}(\text{TEPO})_2]^{2+}$ and $[\text{Sn}(\text{TEPO})_3]^{2+}$ was observed. The signal was assigned to $[\text{Sn}([\text{18}]\text{crown-6})(\text{TEPO})_2]^{2+}$, and thus, given the similar features observed in the germanium system, the signal at 81.1 ppm was assigned to $[\text{Ge}([\text{18}]\text{crown-6})(\text{TEPO})_2]^{2+}$ (Scheme 3.10). When the sample was cooled to $-80\text{ }^\circ\text{C}$, only one set of signals assigned to

the ethyl moiety was observed in the ^1H NMR spectrum; however, two signals were present in the ^{31}P NMR spectrum (82.4 and 82.1 ppm) in a ratio of approximately 7:1 and are consistent with the formation of $[\text{Ge}(\text{TEPO})_2]^{2+}$ and $[\text{Ge}(\text{TEPO})_3]^{2+}$, respectively. Similar reactivity was observed for the analogous tin(II) species, $[\text{Sn}([\mathbf{18}\text{crown-6}][\text{OTf}]_2]$, at low temperatures. As the solid-state structure of $[\text{Ge}([\mathbf{15}\text{crown-5}][\text{OTf}]_2]$ is similar to $[\text{Ge}([\mathbf{18}\text{crown-6}][\text{OTf}]_2]$ (Figure 3.10), similar reactivity is expected.



Scheme 3.10 The addition of TEPO to $[\text{Ge}([\mathbf{18}\text{crown-6}][\text{OTf}]_2]$ at RT and $-80 \text{ }^\circ\text{C}$.

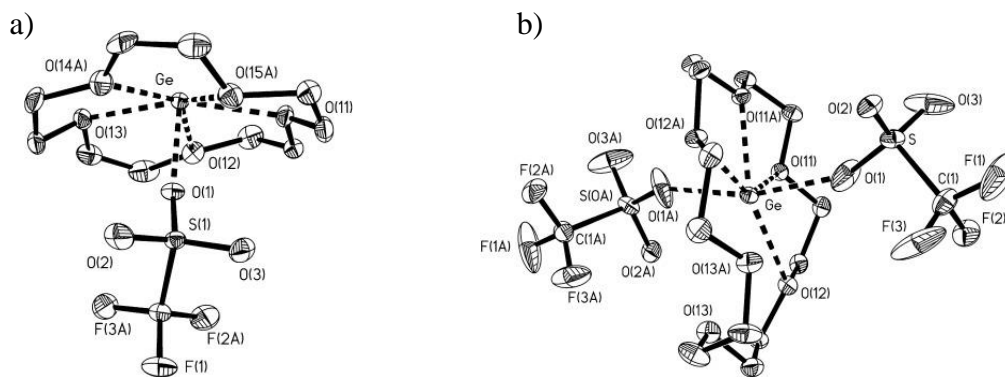
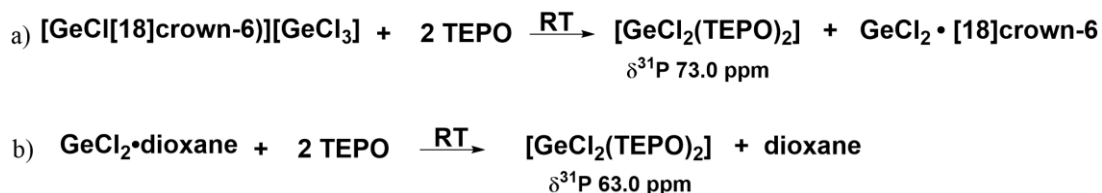


Figure 3.10 The solid state structures of a) $[\text{Ge}([\mathbf{15}\text{crown-5}][\text{OTf}]_2]$ (only 1 $[\text{OTf}]^-$ is depicted) and b) $[\text{Ge}([\mathbf{18}\text{crown-6}][\text{OTf}]_2]$. Reprinted with permission from John Wiley & Sons.³⁵

3.4.3 [GeCl([18]crown-6)][GeCl₃]

When two equivalents of TEPO were added to either GeCl₂·dioxane or [GeCl([18]crown-6)][OTf]₂, signals with similar ³¹P NMR chemical shifts were observed (Table 3.1, Entries 6 & 8). The same trend was also observed in the addition of TEPO to SnCl₂ and [SnCl([18]crown-6)][SnCl₃] to give [SnCl₂(TEPO)₂]. Thus, the formation of [GeCl₂(TEPO)₂] from TEPO and GeCl₂·dioxane or [GeCl([18]crown-6)][GeCl₃] is proposed (Scheme 3.11). Given the similar structures of [GeCl([18]crown-6)][GeCl₃] and [SnCl([18]crown-6)][SnCl₃], a similar mechanism for the formation of [GeCl₂(TEPO)₂] is anticipated (Scheme 3.7). Displacement of a chloride from the anion [GeCl([18]crown-6)][GeCl₃] by TEPO would lead to the formation of [GeCl₂(TEPO)], which could then coordinate a second equivalent of TEPO to form [GeCl₂(TEPO)₂]. The generated chloride could then react with the [GeCl]⁺ fragment to generate an equivalent of GeCl₂. Given the similar ³¹P NMR chemical shifts observed for the reaction between TEPO and [GeCl([18]crown-6)][GeCl₃], [GeCl([15]crown-5)][GeCl₃] (Table 3.1, Entry 4), GeCl(benzo[15]crown-5)][GeCl₃] (Table 3.1, Entry 5) and [GeCl₂·dibenzo[18]crown-6)] (Table 3.1, Entry 7), the formation of [GeCl₂(TEPO)₂] is believed occur in each reaction.



Scheme 3.11 The addition of TEPO to a) [GeCl([18]crown-6)][GeCl₃] and b) GeCl₂·dioxane.

The 2:1 mixture of TEPO and $[\text{GeCl}([\mathbf{18}\text{crown-6})][\text{GeCl}_3]$ was cooled to $-80\text{ }^\circ\text{C}$. The $^{31}\text{P}\{^1\text{H}\}$ NMR signal became broader and shifted 2.5 ppm upfield. These observations are similar to the $^{31}\text{P}\{^1\text{H}\}$ NMR spectral observations for $\text{SnCl}_2(\text{TEPO})_2$ at low temperatures and thus it appears that the main species at $-80\text{ }^\circ\text{C}$ is also $[\text{GeCl}_2(\text{TEPO})_2]$. The change in the ^{31}P NMR chemical shift may indicate the formation of a dimer of $[\text{GeCl}_2(\text{TEPO})_2]$ at low temperatures, as proposed previously for $[\text{SnCl}_2(\text{TEPO})_2]$ (Figure 3.9).

No additions of phosphine oxides to any germanium(II) chlorides have been reported; however, the addition of phosphine oxides to GeCl_4 has been examined. A 1:1 addition of TEPO to GeCl_4 resulted in four different ^{31}P NMR signals ranging from 74-79 ppm at $-40\text{ }^\circ\text{C}$, suggesting a complex equilibrium.³⁶ In a 2:1 addition of TEPO to GeCl_4 , the formation of $[\text{GeCl}_4(\text{TEPO})_2]$ with a ^{31}P NMR chemical shift of 60 ppm was observed.³⁷ The addition of trimethylphosphine oxide (TMPO) to GeCl_4 yielded different coordination complexes depending on the relative ratio of GeCl_4 to phosphine oxide. A 1:2 ratio GeCl_4 to TMPO resulted in the formation of $[\text{GeCl}_3(\text{TMPO})_3][\text{GeCl}_6]$ while a 1:4 ratio of GeCl_4 to TMPO yielded $[\text{GeCl}_2(\text{TMPO})_4][\text{Cl}]_2$.³⁵ No NMR evidence of additional complex equilibria in TEPO additions to $[\text{Ge}([\mathbf{18}\text{crown-6})][\text{GeCl}_3]$ or GeCl_2 -dioxane was observed. These germanium crown ether species appear to exhibit the same reactivity as their analogous tin(II) complexes and SnCl_2 towards TEPO.³⁰

3.5 Discussion of Gutmann-Beckett Results

A summary of the ANs for the germanium(II)- and tin(II)-TEPO complexes identified from the addition of TEPO to germanium(II) and tin(II) crown ethers are given in Table 3.2 and a summary of the reactivity of germanium(II) and tin(II) crown ether complexes with TEPO is given in Figure 3.11. The ANs of the germanium(II) cationic complexes are higher than any of the tin(II) cationic complexes (Table 3.2), indicating that the Ge^{2+} centre is more Lewis acidic than the Sn^{2+} centre. As TEPO is a hard donor, a stronger interaction between the Ge^{2+} than Sn^{2+} is expected due to the hardness of Ge^{2+} compared to Sn^{2+} . The singly-coordinated TEPO complex, $[\text{Ge}([\mathbf{12}]\text{crown-4})(\text{TEPO})]^{2+}$ (Table 3.2, Entry 1), has the highest AN of the identified complexes, and thus, is the most Lewis acidic. The complexes containing the [18]crown-6 ligands in addition to the TEPO ligands, $[\text{M}([\mathbf{18}]\text{crown-6})(\text{TEPO})_2]^{2+}$ ($\text{M} = \text{Ge}, \text{Sn}$) (Table 3.2, Entries 4 & 8) have lower ^{31}P NMR chemical shifts compared to the analogous doubly-coordinated complexes without a crown ether ligand, $[\text{M}(\text{TEPO})_2]^{2+}$ ($\text{M} = \text{Ge}, \text{Sn}$), although the difference in chemical shift is more significant when $\text{M} = \text{Sn}$. When comparing $[\text{GeCl}_2(\text{TEPO})_2]$ and $[\text{SnCl}_2(\text{TEPO})_2]$ derived from the direct addition of TEPO to the metal halide (as opposed to from the trichlorometallate salts) nearly identical ANs, 49 and 50 respectively, are observed. These results suggest that the presence of the chloride ligands in both complexes significantly reduces the Lewis acidity of the metal centre relative to the cationic complexes and, evidently, make the Lewis acidity of the metal centre comparable. In a computational study of the bonding of $[\text{Sn}([\mathbf{18}]\text{crown-6})(\text{OTf})]^+$ and $[\text{SnCl}([\mathbf{18}]\text{crown-6})]^+$, the covalent Sn-Cl bond was found to destabilize the tin lone pair by 1 eV relative to

the Sn-OTf complex, making the Sn-Cl complex a better electron donor.³⁸ If a similar destabilization of the lone pair on the metal centre occurs due to the presence of covalent M-Cl bonds in either $[\text{GeCl}_2(\text{TEPO})_2]$ or $[\text{SnCl}_2(\text{TEPO})_2]$, the reduced acidity could be a result of the donor ability of the chlorides making the metal centres less electrophilic, and thus less, Lewis acidic with lower ANs.

Table 3.2 The Gutmann-Beckett ANs of the germanium(II)- and tin(II)-TEPO complexes generated from the addition of TEPO to germanium(II) and tin(II) crown ether complexes.

Entry	TEPO Adduct	³¹ P NMR Chemical Shift (ppm)	AN
1	$[\text{Ge}([\text{12}]\text{crown-4})(\text{TEPO})_2]^{2+}$	89.4	107
2	$[\text{Ge}(\text{TEPO})_2]^{2+}$	82.9	92
3	$[\text{Ge}(\text{TEPO})_3]^{2+}$	82.0	91
4	$[\text{Ge}([\text{18}]\text{crown-6})(\text{TEPO})_2]^{2+}$	81.1	89
5	$[\text{GeCl}_2(\text{TEPO})_2]$	63.0	49
6	$[\text{Sn}(\text{TEPO})_2]^{2+}$	76.6 ^a	79
7	$[\text{Sn}(\text{TEPO})_3]^{2+}$	75.6 ^a	76
8	$[\text{Sn}([\text{18}]\text{crown-6})(\text{TEPO})_2]^{2+}$	72.8	70
9	$[\text{SnCl}_2(\text{TEPO})_2]$	63.5	50

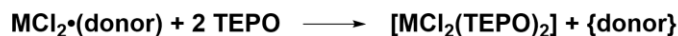
^a ³¹P NMR shifts acquired at -40 °C.

One of the key findings of this study of the Lewis acidities of germanium(II) and tin(II) crown ether complexes as assessed using the Gutmann-Beckett method is the formation of doubly- and triply-coordinated TEPO complexes. Even at substoichiometric amounts of TEPO, the formation of the doubly-coordinated species was observed. The Gutmann-Beckett method does not inherently consider the potential for the coordination of multiple TEPO equivalents due to the standard 1:1 ratio of Lewis acid to TEPO added and the assumed formation of a 1:1 adduct. However, the number of TEPO equivalents coordinated significantly influences the AN, and thus, the interpretation of the Lewis

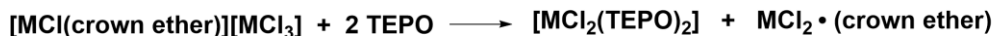
acidity of the central atom. A difference of 15 was observed between the ANs of $[\text{Ge}([\mathbf{12}]\text{crown-4})(\text{TEPO})]^{2+}$ and $[\text{Ge}(\text{TEPO})_2]^{2+}$ and a similar difference is observed for $[\text{Si}(\text{cat}^{\text{Cl}})_2(\text{TEPO})]$ and $[\text{Si}(\text{cat}^{\text{Cl}})_2(\text{TEPO})_2]^{3b}$ (Table 3.3). Furthermore, the difference between the AN of $[\text{Ge}(3,5\text{-dtbc})(\text{TEPO})]$ (dtbc = *di**tert*-butylcatecholato) and $[\text{Ge}(3,5\text{-dtbc})_2(\text{TEPO})_2]$ is 35.^{3d} If the doubly-coordinated complex had not been identified correctly in these examples, prompting further experiments to correctly identify the singly-coordinated complexes, the true Lewis acidity of the metal centre would be underestimated which would influence future studies and applications of these complexes as catalysts. Therefore, it is critical to determine the number of coordinated TEPO equivalents and make comparisons only to analogous complexes where the same number of TEPO donors are coordinated. Through the use of multinuclear NMR spectroscopy and the comparisons of the ³¹P NMR chemical shifts for the addition of 1 and 2 equivalents of TEPO, the structures of the adducts can be determined.

A second key finding of this study is the facile displacement of the crown ether ligand by TEPO for many of the germanium(II) and tin(II) crown ether complexes examined. This displacement can be understood when considering the Lewis basicities of both the crown ether and TEPO. BF_3 affinity, the change in enthalpy of the coordination of BF_3 to a Lewis base,³⁹ enables comparison of the strengths of Lewis bases. The BF_3 affinity of TEPO (119 kJ/mol) is greater than that of the crown ether ligands (74 kJ/mol) as estimated from the BF_3 affinity of 1,4-dioxane. As a result of the displacement of the crown ether ligand(s), the species assessed using the Gutmann-Beckett method were not the complexes with crown ether, rather the naked $\text{Ge}^{2+}/\text{Sn}^{2+}$ cations, with no additional

Neutral Germanium(II) and Tin(II)



Germanium(II) and Tin(II) Monocations with [MCl₃]⁻ Counterions



Germanium(II) and Tin(II) Dications with [OTf]⁻ Counterions

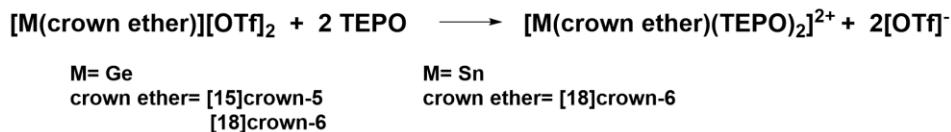
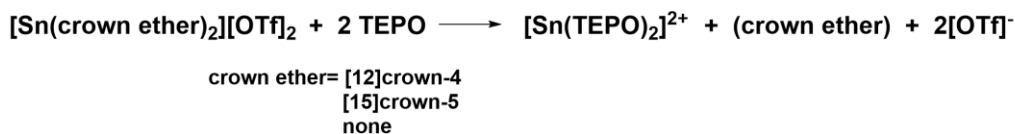
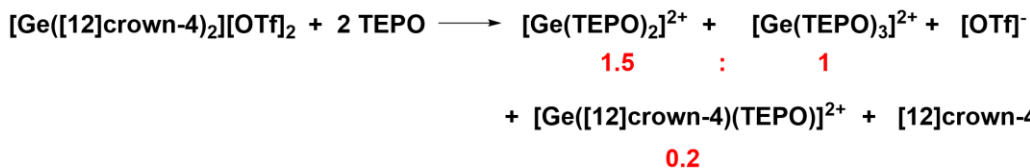


Figure 3.11 Summary of reactivity with TEPO and germanium(II) and tin(II) species at room temperature.

ligands, or GeCl₂/SnCl₂. Without an in-depth study of the structures of these complexes the identity of the generated TEPO complexes would not be known. The results of these studies have implications for Lewis acids containing ligands that are weaker donors than TEPO as displacement of these ligands by TEPO could occur during Gutmann-Beckett analysis. Considering the BF₃ affinities of some common ligands:³⁹ *N,N*-dimethylanilines

(78-112 kJ/mol), nitriles (44-78 kJ/mol), ethers (65-92 kJ/mol), amides (92-117 kJ/mol) and sulfoxides (90-108 kJ/mol), all have lower BF_3 affinities than TEPO (119 kJ/mol). Although this may be advantageous for solvent adducts of Lewis acids generated during synthesis, such as $\text{BF}_3 \cdot \text{OEt}_2$ where the ether can be displaced during assessment, the presence of the aforementioned ligands and subsequent displacement by TEPO changes the identify of the species being evaluated using the Gutmann-Beckett method. In this study, the Lewis acidity of $[\text{Sn}(\mathbf{12}\text{crown-4})_2][\text{OTf}]_2$ was not measured, instead the Lewis acidity of $\text{Sn}(\text{II})^{2+}$ was probed. For catalytic applications, in which $\text{Sn}(\text{II})^{2+}$ may not be generated from $[\text{Sn}(\mathbf{12}\text{crown-4})_2][\text{OTf}]_2$, the AN measured is not reflective of the Lewis acidity of the complex. The presence or absence of weakly coordinated ligands on a Lewis acid will change the interpretation of the AN and thus, the strong donor ability of TEPO is a limitation for complexes containing donor ligands weaker than TEPO.

Similarly, the coordination of TEPO to a Lewis acid containing a reactive fragment, such as $[\text{SnCl}_3]^-$ or $[\text{GeCl}_3]^-$, can lead to transformations that change the nature of the species being assessed. In this study, the generation of new species in solution, SnCl_2 or GeCl_2 derived from the reactive anion, occurred upon the addition of TEPO and subsequently resulted in the formation of either $[\text{SnCl}_2(\text{TEPO})_2]$ or $[\text{GeCl}_2(\text{TEPO})_2]$, respectively. These observations have implications for the Lewis acidity assessment of heavier main group halides due to the potential displacement of the halide by the phosphine oxide as observed previously in the addition of TMPO to GeCl_4 .³⁷ Thus, the results of the Gutmann-Beckett assessment for complexes containing a reactive bond or fragment should

be interpreted with caution in the absence of a thorough investigation into the coordination chemistry.

Finally, the ^{31}P NMR chemical shift was found to be dependent on the concentration of the Lewis acid-TEPO adducts. These variations were noted previously and were attributed to the different solubilities of the compounds.⁴⁰ Variations in the ^{31}P NMR chemical shifts due to concentration differences may have implications for species with similar ^{31}P NMR chemical shifts, such as $[\text{Ge}(\text{TEPO})_3]^{2+}/[\text{Ge}(\text{TEPO})_2]^{2+}$ and $[\text{Sn}(\text{TEPO})_3]^{2+}/[\text{Sn}(\text{TEPO})_2]^{2+}$, where the interpretation of the data could be compromised without careful consideration of concentration. Furthermore, the presence of other Lewis acidic species in the reaction mixture, such a second equivalent of SnCl_2 , can significantly shift the ^{31}P NMR chemical shift of the solution, due to dynamic ligand exchange or the formation of bridging species in solution. Thus, it is critical to document the specific conditions in which the data were obtained.

3.6 Comparisons of the Lewis Acidities of Ge(II) and Sn(II) Species and Literature Results

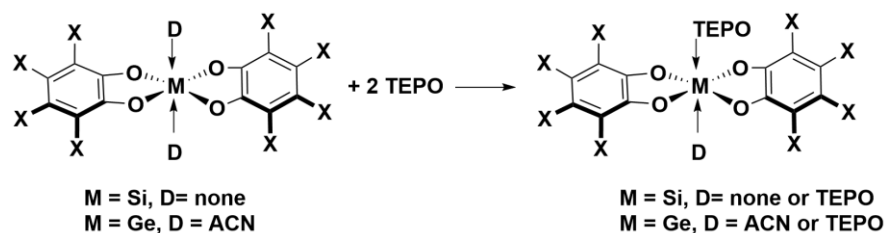
Due to the coordination of two equivalents of TEPO to the Lewis acid centre in the majority of the reactions examined, meaningful comparisons of Lewis acidity can only be made to other doubly-coordinated TEPO complexes. $[\text{GeCl}_2(\text{TEPO})_2]$ has a higher AN (49) than $[\text{GeCl}_4(\text{TEPO})_2]$ (AN = 42).³⁷ The relationship between oxidation number and Lewis acidity has been well-defined for group 15 species, in which M(III) compounds (M = P, As, Sb) are less Lewis acidic than the analogous M(V) compounds as determined using FIAs.¹⁵ The higher Lewis acidity of Ge(II) over Ge(IV) could be due to the filling of an

empty orbital of GeCl_2 upon TEPO coordination, which results in a strong interaction. In contrast, the analogous Group 15 complexes $\text{AsCl}_3/\text{AsCl}_5$ and $\text{SbCl}_3/\text{SbCl}_5$ do not have an empty orbital at the main group centre, and thus, the Lewis acidities are better understood in terms of the number of electronegative substituents (3 in M(III) or 5 in M(V)) where the greater number of electronegative substituents results in an increase in Lewis acidity of the main group centre. However, the relative acidities of $\text{GeCl}_2/\text{GeCl}_4$ are not the same for $\text{SnCl}_2/\text{SnCl}_4$. The $^{31}\text{P}\{^1\text{H}\}$ NMR chemical shift of $[\text{SnCl}_2(\text{TEPO})_2]$, at 63.5 ppm, is nearly identical to the $^{31}\text{P}\{^1\text{H}\}$ NMR chemical shift of $\text{SnCl}_4(\text{TMPO})_2$ at 63.4 ppm,³⁰ despite significantly different $^{119}\text{Sn}\{^1\text{H}\}$ NMR chemical shifts: -212 ppm for $[\text{SnCl}_2(\text{TEPO})_2]$ compared to -695 ppm for $[\text{SnCl}_4(\text{TMPO})_2]$. The difference between germanium and tin may be a consequence of the inert *s* pair effect. In SnCl_2 , the HOMO, consisting of the lone pair at tin, and LUMO, consisting of the empty *p*-orbital on tin, are lower in energy than the corresponding molecular orbitals of GeCl_2 which makes SnCl_2 less Lewis acidic in comparison to GeCl_2 . The lower Lewis acidity of SnCl_2 results in a weaker TEPO-Sn interaction such that the ^{31}P NMR chemical shifts of $[\text{SnCl}_2(\text{TEPO})_2]$ and $[\text{SnCl}_4(\text{TEPO})_2]$ are identical.

There are few examples of the coordination of two equivalents of TEPO to a Lewis acid. The coordination of both one and two equivalents of TEPO to bis(catecholato)silanes and -germanes has been reported.³ The ANs of bis(catecholato)silanes and -germanes with two coordinated TEPO have been reported fall within a range of 56-75 ppm with a clear dependence on the electronegativity of the catechol substituents (Table 3.3). The ANs of $[\text{Ge}(\text{TEPO})_2]^{2+}$ at 92 and $[\text{Sn}(\text{TEPO})_2]^{2+}$ at 79 are higher than all of the complexes shown

in Table 3.3, and thus, Sn^{2+} and Ge^{2+} are more Lewis acidic than the catechol complexes. Both $[\text{GeCl}_2(\text{TEPO})_2]$ and $[\text{SnCl}_2(\text{TEPO})_2]$ are less Lewis acidic than all the bis(catecholato)silanes and -germanes reported in Table 3.3.

Table 3.3 ANs for the the coordination of one and two equivalents of TEPO to bis(catecholato)silanes and -germanes.³



$[\text{M}(\text{cat}^{\text{X}})_2][\text{D}]_2$	AN (1 TEPO)	AN (2 TEPO)
$[\text{Si}(\text{cat}^{\text{tBu}})_2]$	90	65
$[\text{Si}(\text{cat}^{\text{Cl}})_2]$	102	71
$[\text{Si}(\text{cat}^{\text{Br}})_2]$	102	71
$[\text{Ge}(\text{cat}^{\text{tBu}})_2][\text{ACN}]_2$	92	56 ^a
$[\text{Ge}(\text{cat}^{\text{Cl}})_2][\text{ACN}]_2$	95	65
$[\text{Ge}(\text{cat}^{\text{Br}})_2][\text{ACN}]_2$	99	75

Only one species, $[\text{Ge}([\text{12}]\text{crown-4})(\text{TEPO})]^{2+}$, was found to coordinate one equivalent of TEPO, and thus, its AN can be compared to AN of other Lewis acids that coordinate a single equivalent of TEPO. The ANs of the singly-coordinated TEPO complexes of bis(catecholato)silanes and germanes (Table 3.3, Column 1), were all lower than the AN of $[\text{Ge}([\text{12}]\text{crown-4})(\text{TEPO})]^{2+}$ (107). Remarkably, with an AN of 107, $[\text{Ge}([\text{12}]\text{crown-4})(\text{TEPO})]^{2+}$ is a stronger Lewis acid than aryl silyl(IV) cations, such as $[\text{Si}(\text{C}_6\text{Me}_5)_3]^+$ and $[\text{Si}(\text{Dur})_3]^+$ (Figure 3.12) with ANs of 98 and 100, respectively.^{4c}

However, the AN of $[\text{Ge}([\text{12}]\text{crown-4})(\text{TEPO})]^{2+}$ is lower than that of the *in situ* generated catecholatorborinium ion, $[\text{B}(\text{cat})]^+$ (146).^{4c}

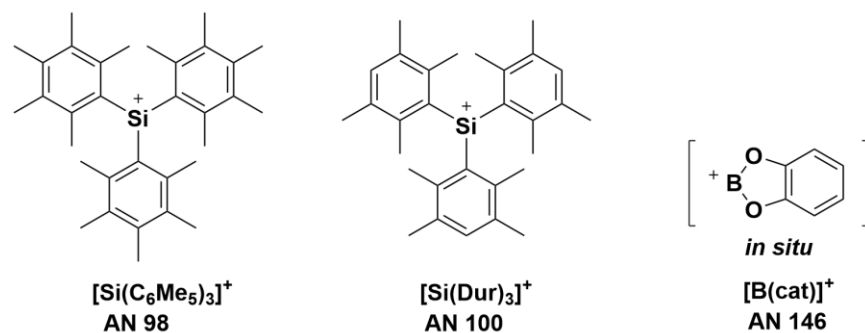
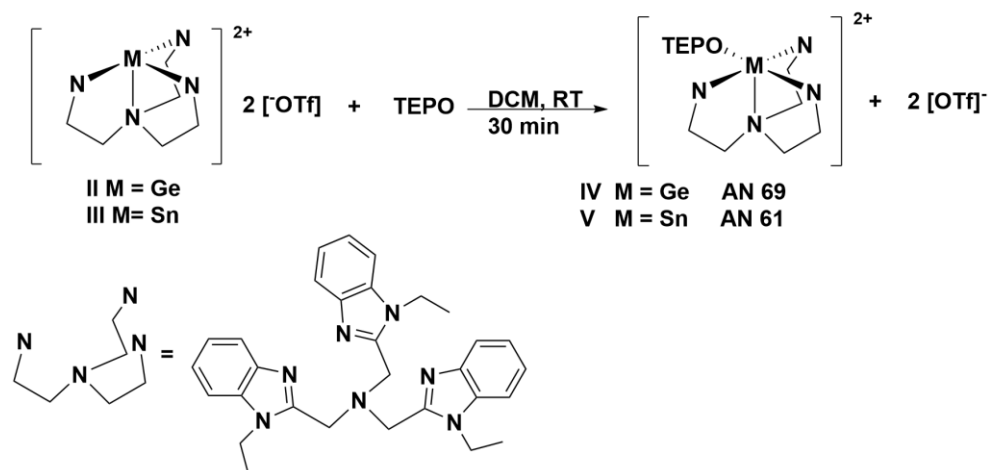


Figure 3.12 Cationic Lewis acids and their corresponding Gutmann-Beckett AN.^{4c}

The structures of the tin(II) and germanium(II) crown ether triflate complexes are similar to the structures of germanium(II) and tin(II) tris(imidazolyl)amine triflate salts, **II** and **III**, respectively (Scheme 3.12).¹⁷ The coordination of TEPO to **II** and **III** has been investigated and the structures of the 1:1 adduct between the Lewis acid and TEPO has been characterized by X-ray crystallography. Notably, the tetradentate ligand is not displaced from the germanium(II) or tin(II) centre upon coordination of TEPO. Amines are stronger Lewis bases (BF_3 affinity of triethylamine: 136 kJ/mol)³⁹ compared to crown ether, and thus, displacement of the ligands from the metal centre does not occur. Only one equivalent of TEPO coordinates to the metal centre of **II** or **III** likely because of sterics. The AN of **IV** and **V**, 69 and 61, respectively, are both lower than the AN of $[\text{Ge}([\text{12}]\text{crown-4})(\text{TEPO})]^{2+}$, and, surprisingly, lower than the ANs of $[\text{Sn}(\text{TEPO})_2]^{2+}/[\text{Ge}(\text{TEPO})_2]^{2+}$. Evidently, the strong nitrogen donor atoms of the ligand reduce the Lewis acidity of the metal centre. The relative Lewis acidities of the AN

between $[\text{Ge}(\text{[12]crown-4})(\text{TEPO})]^{2+}$ and **IV** demonstrate the significant influence of the tetradentate ligand, either crown ether or tris(imidazolyl)amine, on the Lewis acidity of the metal centre.



Scheme 3.12 The addition of one equivalent of TEPO to tris(imidazolyl)amine complexes of germanium(II) and tin(II).¹⁷

With the assessment of the Lewis acidities of germanium(II) and tin(II) crown ether complexes using the Gutmann-Beckett method, the ANs can be used to predict the catalytic potential of the complexes. A correlation between the strength of the Lewis acid and catalytic activity is well known.⁶ The silicon and germanium bis(catecholato) species (Figure 3.12) have been utilized successfully as Lewis catalysts, where the most Lewis acidic derivatives were shown to be the most efficient catalysts.³ In addition, silyl cation-facilitated Lewis acid catalysis has been extensively explored.^{4b} The AN of $[\text{Ge}(\text{[12]crown-4})(\text{TEPO})_2]^{2+}$ derived from $[\text{Ge}(\text{[12]crown-4})][\text{OTf}]_2$, is higher than the AN of the singly-coordinated TEPO complexes of bis(catecholato)silanes and -germanes and of silyl(IV) cations. The ANs of $[\text{Sn}(\text{TEPO})_2]^{2+}$ or $[\text{Sn}(\text{[18]crown-6})(\text{TEPO})_2]^{2+}$, derived

from $[\text{Sn}[\mathbf{12}\text{crown-4}]_2][\text{OTf}]_2$ and $[\text{Sn}([\mathbf{18}\text{crown-6}])][\text{OTf}]_2$ respectively, are significantly lower than the ANs of the aforementioned Group 14 Lewis acid catalysts; however, the ANs are comparable to other effective Lewis acid catalysts, such as $\text{B}(\text{C}_6\text{F}_5)_3$ (AN= 82).²⁴

In summary, the Lewis acidities of a series of cationic and neutral crown-ether complexes of germanium(II) and tin(II) have been assessed using the Gutmann-Beckett method, identifying $\text{Ge}([\mathbf{12}\text{crown-4}]_2)[\text{OTf}]_2$ to be the strongest Lewis acid, and thus, the most promising Lewis acid catalyst. Notably, NMR analysis of the additions of TEPO to Group 14 crown ether complexes revealed the formation of multiple species in solution including the formation of multiply-coordinated TEPO complexes as well as dynamic equilibria. The complex nature of the systems reported herein have highlighted the importance of performing a careful analysis of all species in solution as well as in the interpretation of the ^{31}P NMR chemical shift, particularly for Lewis acids with large central atoms and/or weakly associated ligands when reporting Gutmann-Beckett ANs.

3.7 Litchenberg-Modified Gutmann-Beckett Method

In the Gutmann-Beckett method, displacement of the crown ether in germanium(II) and tin(II) crown ether complexes by TEPO was observed. TEPO is a hard donor and is expected to form strong interactions with hard metal centres such as germanium. The Litchenberg-Modified Gutmann-Beckett method (LMGB)¹⁰ utilizes a softer donor, trimethylphosphine sulfide (TMPS) which may be more suitable for the tin, a softer metal centre. This method was developed for bismuth(III) cations which showed strong

interactions with both trimethylphosphine sulfide (TMPS) and trimethylphosphine selenide in solution and also in the solid-state. The BF_3 affinity of TEPO (119 kJ/mol) is significantly higher than the BF_3 affinity of TMPS (66-67 kJ/mol) as estimated from the BF_3 affinity of thionophosphates ($\text{S}=\text{P}(\text{OR}_3)$).³⁹ In addition, the BF_3 affinity of TMPS is lower than that of a crown ether (74 kJ/mol), and thus, may not displace the crown ether during analysis.

Table 3.4 The Litchenberg-Modified Gutmann-Beckett Acceptor Number (AN^{LM}) and ^{31}P NMR chemical shifts for the addition of TMPS to main group Lewis acids in DCM.

Entry	Compound	AN^{LM}	1 Equivalent TMPS (ppm)
1	$[\text{Ge}([\text{12}]\text{crown-4})_2][\text{OTf}]_2$	85	42.5
2	$[\text{Ge}([\text{15}]\text{crown-5})][\text{OTf}]_2$	76	41.0
3	$[\text{Ge}([\text{18}]\text{crown-6})][\text{OTf}]_2$	21	32.3
4	$[\text{Sn}([\text{12}]\text{crown-4})_2][\text{OTf}]_2$	15	31.5
5	$[\text{Sn}([\text{15}]\text{crown-5})_2][\text{OTf}]_2$	0	30.9
6	$[\text{Sn}([\text{18}]\text{crown-6})][\text{OTf}]_2$	0	30.9
7	$[\text{Ge}([\text{18}]\text{crown-6})][\text{GeCl}_3]$	55	37.7
8	$[\text{SnCl}([\text{18}]\text{crown-6})][\text{SnCl}_3]$	0	30.9
9	SnOTf_2	83	42.1
10	$\text{GeCl}_2 \cdot \text{dioxane}$	75	40.9
11	TMPS	-	30.9
12	Me_3SiOTf	1	29.3
13	$\text{B}(\text{C}_6\text{F}_5)_3$	42	35.8

The results of the LMGB method for the addition of TMPS to one equivalent of Lewis acid are shown in Table 3.4. For all crown ether complexes examined, only one signal was observed in the $^{31}\text{P}\{^1\text{H}\}$ NMR spectra, suggesting that at room temperature, only one compound is present in solution: either free TMPS (when $\text{AN}^{\text{LM}} = 0$) or a Lewis acid-TMPS complex ($\text{AN}^{\text{LM}} \neq 0$). In general, higher Lewis acidities were observed for the germanium(II) complexes (Table 3.4, Entries 1-3, 7 & 10) than the tin(II) complexes

(Table 3.4, Entries 4-6, & 8), which was also observed using the Gutmann-Beckett method. These results, in addition to the results of the Gutmann-Beckett study, indicate that germanium(II) is a both a better soft and hard Lewis acid than tin(II).

Surprisingly, no evidence of coordination was observed for several of the tin(II) crown ether complexes as determined by the absence of change in the ^{31}P NMR chemical shift of TMPS in the presence of Lewis acid resulting an AN^{LM} of 0 (Table 3.4, Entry 5,6 & 8). The ionic radius of tin(II) (1.18 Å) is larger than the ionic radius of Bi(III) (1.03 Å),⁴¹ and thus, the softness of the atoms should be fairly comparable. However, the stronger interaction of the crown ether to the tin(II) based on the BF_3 affinities (74 kJ/mol for crown ether; 66 kJ/mol for TMPS)³⁹ may prevent association of the TMPS. The chelating effect of the crown ether may also favor the coordination of the crown ether over TMPS. In $[\text{Sn}([\text{15}]\text{crown-5})_2]$, the tin(II) centre is encapsulated in a sandwich complex between the two [15]crown-5 ligands and does not strongly associate with the triflate anions in the solid state (Figure 3.3). This indicates that coordination of a weak donor, such as triflate, is not favorable as the [15]crown-5 ligands stabilize the tin(II) centre sufficiently. Evidently, the coordination of the weak donor TMPS is also not favorable ($\text{AN}^{\text{LM}}=0$ Table 3.4, Entry 5). In $[\text{Sn}([\text{12}]\text{crown-4})_2][\text{OTf}]_2$, which did result in coordination as evidenced by a non-zero AN^{LM} (Table 3.4, Entry 4), the smaller ligands encapsulate the metal in a tilted sandwich complex in the solid-state which may provide an accessible coordination site for TMPS. Attempts to acquire $^{119}\text{Sn}\{^1\text{H}\}$ NMR spectra on any of the TMPS and tin(II) crown ether complexes at room temperature were unsuccessful. A relatively large acceptor number (AN^{LM} 82) was observed when TMPS was added to $\text{Sn}(\text{OTf})_2$ (Table 3.4, Entry 9)

indicating a strong association of the two species in solution. The AN^{LM} of **Sn(OTf)₂** in comparison to the AN^{LM} of the crown ether complexes of tin(II) highlight the decrease in Lewis acidity upon the coordination of crown ether ligands to an Sn^{2+} centre. Although a clear association of TMPS and both **Sn(OTf)₂** and **[Sn([12]crown-4)₂][OTf]₂** is observed based on the AN^{LM} , the number of coordinated TMPS or crown ether ligands in the case of **Sn([12]crown-4)₂][OTf]₂** is unclear.

The highest AN^{LM} was observed in the reaction of TMPS with **[Ge([12]crown-4)₂][OTf]₂** (AN^{LM} 85) and a high AN was observed for **[Ge([15]crown-5)][OTf]₂** (AN 76) (Table 3.4, Entries 1 & 2). The AN^{LM} of **[Ge([18]crown-6)][OTf]₂** was significantly lower than the other germanium(II) crown ether triflate salts (AN^{LM} 21) (Table 3.4, Entry 3). The solid state structure of **[Ge([15]crown-5)][OTf]₂** and **[Ge([18]crown-6)][OTf]₂** are very similar (Figure 3.10), but a stark difference in their solution behavior is evident as **[Ge([18]crown-6)][OTf]₂** is significantly less Lewis acidic based on AN^{LM} . The reason for this significant difference is unclear from the room temperature data. The reaction of **GeCl₂·dioxane** and TMPS resulted in a comparable AN^{LM} to **[Ge([15]crown-5)][OTf]₂**.

In summary, the germanium(II) crown ether complexes were shown to be soft Lewis acids and highly Lewis acidic based on AN^{LM} . Despite the single signal in the ³¹P NMR spectra, the number of coordinated TMPS equivalents remains unclear for all species with an $AN^{LM} \neq 0$. Additional NMR experiments, including the addition of 2 equivalents of TMPS, is required to understand the structures of the TMPS adducts formed.

3.8 Fluoride Ion Affinity Method

3.8.1 Computational Results

The Lewis acidities of the germanium(II) and tin(II) crown ether complexes were assessed using Fluoride Ion Affinity (FIA). The FIAs were calculated for a series of cationic complexes that are representative of the different solid-state structures of the germanium(II) and tin(II) crown ether complexes assessed using the Gutmann-Beckett method (Table 3.5). To prevent inflation of the FIA due to charge neutralization of the fluoride and cationic centre (M = Ge, Sn), which has been previously shown to increase the FIA by over 200 kJ/mol,^{4c} the values were calculated using solvation in the form of the conductor-like polarization model (CPCM). The FIAs of the cationic germanium(II) and tin(II) species are all greater than 500 kJ/mol (Table 3.5), and thus are designated as Lewis superacids, defined as a Lewis acid with a FIA higher than that of SbF₅.⁴³

Table 3.5 The FIAs of various germanium(II) and tin(II) crown ether species calculated at B3LYP D3(BJ)/def2-TZVPP level of theory.⁴²

Entry	Compound	FIA _{Solv} (kJ/mol)
1	[Ge([18]crown-6)] ²⁺	840
2	[Ge([18]crown-6)(OTf)] ⁺	765
3	[Sn([18]crown-6)] ²⁺	764
4	[Sn([18]crown-6)(OTf)] ⁺	740
5	[Sn([12]crown-4) ₂] ²⁺	737
6	[Ge([12]crown-4) ₂] ²⁺	729
7	[GeCl([18]crown-6)] ⁺	669
8	[SnCl([18]crown-6)] ⁺	662
9	Sn(OTf) ₂	523
10	GeCl ₂	438
11	SnCl ₂	435
12	SiCl ₄ ¹⁵	328
13	GeCl ₄ ¹⁵	323
14	SnCl ₄ ¹⁵	360
15	B(C ₆ F ₅) ₃ ¹⁵	448
16	[Si(cat ^F) ₂] ^{3b}	490
17	[Si(cat ^{Cl}) ₂] ^{3b}	507
18	[Ge(cat ^{Cl}) ₂] ^{3d}	504
19	[Si(Dur) ₃] ^{+ 4}	397
20	[Si(Mes) ₃] ^{+ 4}	407
21	[Bcat] ^{+ 4}	770
22	[Si(CH ₂) ₃ (terpy)] ^{2+ 44}	296
23	[Si(Ph) ₂ (terpy)] ^{2+ 44}	263
24	SiPh ₂ ^{2+ 44}	673
25	Si(CH ₂) ₃ ^{2+ 44}	691

The triflate ion was also included in calculations of the [18]crown-6 complexes of tin(II) and germanium(II) due to the potential association of the ion to the metal centre in these complexes and to assess influence of this counterion on the FIA (Table 3.5, Entries 2 and 4). The FIA of [Ge([18]crown-6)(OTf)]²⁺ decreases by 75 kJ/mol in comparison to

that of $[\text{Ge}(\text{[18]crown-6})]^{2+}$; however, the FIA of $[\text{Ge}(\text{[18]crown-6})(\text{OTf})]^{2+}$ is still higher than any of the other germanium(II) or tin(II) species examined, and thus, inclusion of the counterion does not change the interpretation of the relative Lewis acidities. In contrast, a difference of over 170 kJ/mol is observed between the FIAs of $[\text{Ge}(\text{[18]crown-6})]^{2+}$ and $[\text{GeCl}(\text{[18]crown-6})]^+$ (Table 5.5, Entries 1 & 7), demonstrating the significant decrease in Lewis acidity of the germanium(II) with a covalently-attached chloride. The same trend was also observed in the Gutmann-Beckett experiments. A smaller difference (24 kJ/mol) in FIA between $[\text{Sn}(\text{[18]crown-6})]^{2+}$ and $[\text{Sn}(\text{[18]crown-6})(\text{OTf})]^{2+}$ compared to the FIA difference between $[\text{Ge}(\text{[18]crown-6})]^{2+}$ and $[\text{GeCl}(\text{[18]crown-6})]^+$ was observed. Computational analysis on the bonding in $[\text{Sn}(\text{[18]crown-6})(\text{OTf})]^+$ revealed that the interaction between $[\text{OTf}]^-$ and Sn^{2+} is an electrostatic interaction between the oppositely-charged fragments which is in contrast to the covalent bonding of the Sn-Cl moiety in $[\text{SnCl}(\text{[18]crown-6})]^+$,³⁸ accounting for the small influence of the triflate ion on the FIA value of $[\text{Sn}(\text{[18]crown-6})(\text{OTf})]^+$ in comparison to the large influence of the chloride ligand. Although a similar analysis of the bonding of $[\text{GeCl}(\text{[18]crown-6})]$ and $[\text{Ge}(\text{[18]crown-6})(\text{OTf})]^+$ has not been conducted, given the similarities in the influence of the ligands on the FIA and in the solid-state structures, the difference between the FIA values of the triflate and chloride derivatives of germanium(II) [18]crown-6 complexes (Table 3.5, Entries 2 & 7) can also be attributed to a difference in electrostatic versus covalent bonding. $[\text{Ge}(\text{[18]crown-6})]^{2+}$ has the highest FIA of the cationic complexes (Table 3.5, Entry 1), and based on this observation $[\text{Ge}(\text{[18]crown-6})][\text{OTf}]_2$ is anticipated to be the most catalytically active complex. As is evident from the solid-state

structure, $[\text{Ge}([\mathbf{18}]\text{crown-6})][\text{OTf}]_2$ (Figure 5.6b)¹⁸ has a fewer number of oxygen contacts compared germanium(II) centre in $[\text{Ge}([\mathbf{12}]\text{crown-4})_2][\text{OTf}]_2$. The lower number of oxygen contacts evidently results in a higher FIA. The FIAs of the neutral species GeCl_2 , SnCl_2 , and $\text{Sn}(\text{OTf})_2$ were all lower than the cationic complexes (Table 3.5, Entries 9-11) reflecting strong covalent interactions with the Cl or OTf ligands. Higher FIAs were observed for GeCl_2 and SnCl_2 (Table 3.5, Entries 10 & 11) in comparison to GeCl_4 and SnCl_4 (Table 3.5, Entries 13 & 14).¹⁵ These results are in contrast to the trend observed in group 15 where compounds which have a higher oxidation number have a higher FIA.¹⁵

The FIAs of the bis(catecholato)silanes and -germanes (FIA range 390-538 kJ/mol, Table 3.5, Entries 16-18) are significantly lower than that of $[\text{Ge}([\mathbf{18}]\text{crown-6})]^{2+}$, the most Lewis acidic species, and over 100 kJ/mol lower than the crown ether complex with the lowest FIA, $[\text{SnCl}([\mathbf{18}]\text{crown-6})]^+$ (FIA 662 kJ/mol, Table 3.5, Entry 8). In comparison to aryl silyl(IV) cations (FIAs of ~ 400 kJ/mol, Table 3.5, Entries 19 & 20),^{4c} the FIAs of all the tin(II) and germanium(II) cations are higher (Table 3.5, Entries 1-8). This trend in FIA is in agreement with the Gutmann-Beckett AN of $[\text{Ge}([\mathbf{12}]\text{crown-4})(\text{TEPO})]^{2+}$ which was found to be more Lewis acidic than the aryl silyl cations. The FIAs of the germanium(II) and tin(II) species are comparable to a $[\text{B}(\text{cat})]^+$ (Figure 3.12) with an FIA of 770 kJ/mol (Table 3.5, Entry 21).^{4c}

In general, the resulting compounds assessed using the FIA method are anionic or neutral, as this method has been primarily used for the assessment of neutral or monocationic complexes, respectively. However, many crown ether complexes examined

in this study (Table 3.5, Entries 1, 3, 5 & 6) remain cationic upon fluoride coordination due to the dicationic metal centre. Few examples of FIA calculations of dicationic species are known; however, the FIAs of a series of silicon(IV) dications were recently reported (Figure 3.13).⁴⁴ The FIA for two terpyridine-stabilized silicon(IV) dications, $[\text{Si}(\text{CH}_2)_3(\text{terpy})]^{2+}$ and $[\text{Si}(\text{Ph})_2(\text{terpy})]^{2+}$, ranged between 934-1000 kJ/mol (Table 4, Entries 15 & 16) and are comparable to the unsolvated FIA values for $[\text{Ge}([\mathbf{12}]\text{crown-4})_2]^{2+}$ and $[\text{Sn}([\mathbf{12}]\text{crown-4})_2]^{2+}$ of 956 kJ/mol and 1113 kJ/mol, respectively. However, the FIA_{solv} for the terpyridine-stabilized silicon(IV) dications significantly decreased by more than 700 kJ/mol to a range of 263-306 kJ/mol. In contrast, a decrease in FIA of only 200-400 kJ/mol was observed for the germanium(II) and tin(II) dications with FIA_{solv} values for $[\text{Ge}([\mathbf{12}]\text{crown-4})_2]^{2+}$ and $[\text{Sn}([\mathbf{12}]\text{crown-4})_2]^{2+}$ of 728 kJ/mol and 737 kJ/mol (Table 4, Entries 5 & 6). Evidently, the crown ether ligands are better at stabilizing the dicationic centre, as the solvent effects on the FIA are negligible. Although both the terpyridine complexes and the crown ether complexes are dicationic, the difference between the Group 14 element as well as oxidation number also influence the magnitude of the solvent effect on the FIA.

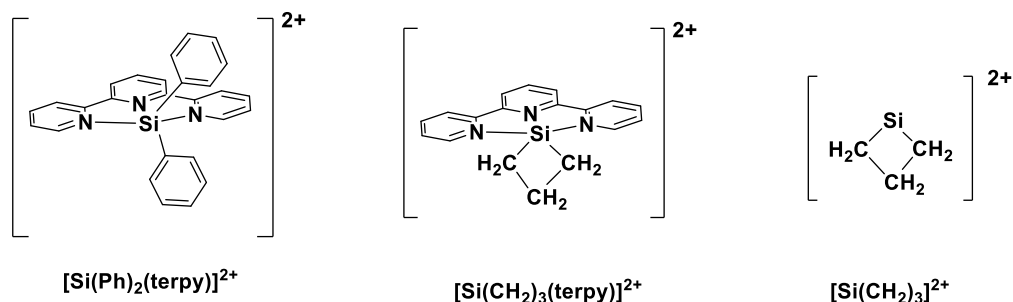


Figure 3.13 Silicon dications assessed using the FIA method.⁴⁴

3.8.2 Comparison of FIA and Gutmann-Beckett Results

In general, the Gutmann-Beckett ANs correlate well to the calculated FIAs of main group Lewis acids, noted previously with aryl silyl(IV) cations.^{4c} However, a much weaker correlation is observed in the crown ether derivatives (Figure 3.14) ($R^2 = 0.46$) compared to the silyl cation correlation ($R^2 = 0.99$) and is attributed to the significant structural differences between the structures of the species that were assessed in the FIA calculations (with crown ether ligands) and those assessed by the Gutmann-Beckett method (with TEPO ligands). The FIA and the Gutmann-Beckett method ANs of the silyl cations are measuring the Lewis acidity of a species with a single Lewis base coordinated, and while this is true for the FIA of the germanium(II) and tin(II) crown ether complexes examined in this work, the Gutmann-Beckett ANs are primarily for doubly-coordinated TEPO complexes. The difference in the presence/absence of the crown ether ligand and the number of coordinated Lewis bases evidently leads to a weaker correlation between the two methods. However, both the Gutmann-Beckett and FIA results clearly demonstrate the higher Lewis acidity for germanium(II) crown ether triflate salts in comparison to the analogous tin(II) crown ether triflate salts. Both Lewis acidity assessment methods revealed the lower Lewis acidity for the monocationic crown ether complexes in which a chloride ligand is present on either the germanium(II) or tin(II) centre, demonstrating that a ligand on the metal centre decreases the Lewis acidity of the metal centre.

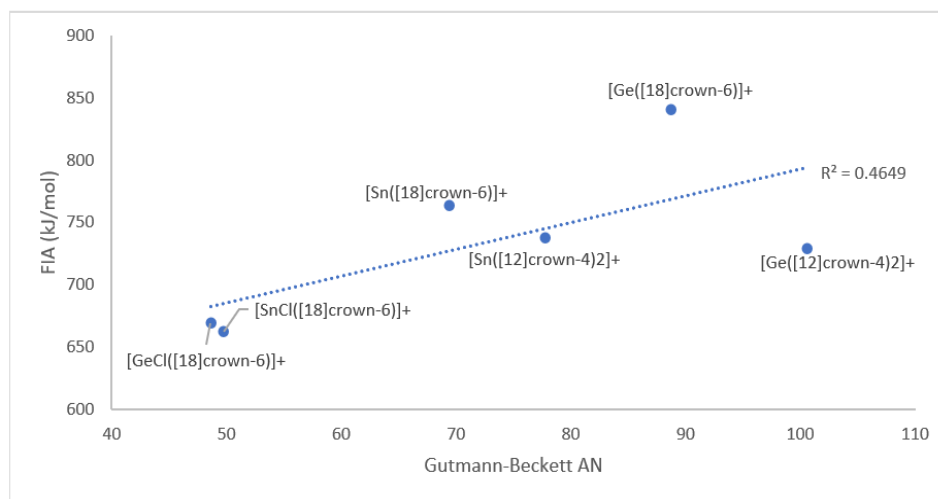


Figure 3.14 Plot of the Gutmann-Beckett Method AN and FIAs for the cationic germanium(II) and tin(II) crown ether complexes.

3.9 Other Lewis Acidity Assessments

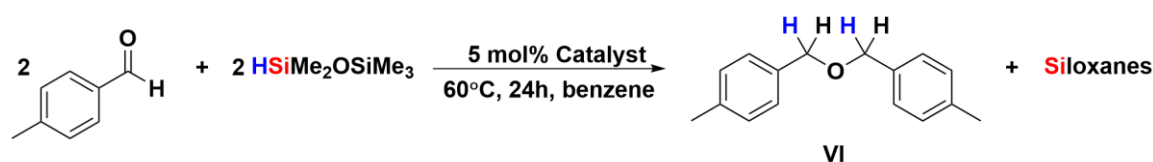
Two additional experimental methods for the assessment of Lewis acidity were employed in an effort to assess the Lewis acidity of the germanium(II) and tin(II) complexes: the fluorobenzonitrile method^{7d} and Child's method.^{7c} Both of these methods rely on a change in an NMR chemical shift; however, no change in the NMR chemical shift was observed upon the addition of the reagents to the four Lewis acids examined: [Ge([12]crown-4)₂][OTf]₂, [Ge([18]crown-6)][OTf]₂, [Sn([12]crown-4)₂][OTf]₂ and [SnCl([18]crown-6)][SnCl₃]. Thus, these methods were not suitable for Lewis acidity assessments of the cationic tin(II) and germanium(II) complexes in this work.

3.10 Preliminary Studies of Lewis Acid Catalysis of the Ge(II) and Sn(II) Crown Ether Triflate Salts

Both the Gutmann-Beckett and the FIA affinities indicate that the germanium(II) crown ether triflate salts are more Lewis acidic than the tin(II) crown ether triflate salts

highlighting that the germanium species are promising Lewis acid catalysts. To probe this, the Lewis acid catalyzed hydrosilylation of 4-methylbenzaldehyde was investigated using pentamethyldisiloxane (PMDS) as the reducing agent and the crown ether complexes. All three germanium(II) complexes showed excellent conversion to exclusively **VI**, while the tin(II) species showed little or no conversion to any reduced species (Table 3.6). Conversion to the symmetric ether rather than the silyl ether has been observed previously.^{4d} These results are consistent with both the FIA and Gutmann-Beckett assessments of Lewis acidity where higher Lewis acidity was observed for the germanium(II) complexes in comparison to the tin(II) complexes and indicate that quantitative Lewis acidity assessments can be utilized to predict catalytic activity for these complexes. Further investigations into the catalytic activity of these complexes will be explored in Chapter 4.

Table 3.6 Reduction of 4-methylbenzaldehyde with pentamethyldisiloxane catalyzed by germanium(II) and tin(II) crown ether complexes.



Catalyst ^a	Yield of VI ^b (%)
[Ge([12]crown-4) ₂][OTf] ₂	95
[Ge([15]crown-5)][OTf] ₂	90
[Ge([18]crown-6)][OTf] ₂	88
[Sn([12]crown-4) ₂][OTf] ₂	<5
[Sn([15]crown-5) ₂][OTf] ₂	trace
[Sn([18]crown-6)][OTf] ₂	no conversion
No catalyst	no conversion

^a[Silane],[4-methylbenzaldehyde]= 0.150 M ^b Yield determined by ¹H NMR spectroscopy using mesitylene as an internal standard.

3.11 Summary and Conclusions

The Lewis acidities of several germanium(II) and tin(II) crown ether complexes have been assessed using three different quantitative methods. The Gutmann-Beckett method revealed the coordination of two or three equivalents of TEPO to the complexes in comparison to the single equivalent observed for many reported Lewis acid-TEPO complexes. Higher ANs for the germanium(II) complexes indicated that these species are more Lewis acidic than the tin(II) species and may be suitable for Lewis acid catalysis utilizing reagents containing hard donors. In the Lichtenberg-Modified Gutmann-Beckett method, coordination of TMPS to the germanium(II) crown ether complexes was observed, but no evidence of coordination was observed for most of the tin(II) crown ether complexes, indicating that the germanium(II) centre is also a better soft Lewis acid in comparison to tin(II) and may also be useful in Lewis acid catalysis utilizing substrates containing soft donor atoms. The FIAs of the germanium(II) and tin(II) crown ether complexes also indicated higher Lewis acidity for the germanium(II) crown ether complexes. The etherification of 4-methylbenzaldehyde catalyzed by the crown ether triflate salts showed excellent conversion by the germanium(II) derivatives, consistent with the quantitative Lewis acidity assessments.

The results herein have highlighted a number of critical considerations for the interpretation of the results of the assessment of Lewis acidity using the Gutmann-Beckett method for complexes containing weak donor atoms. Notably, the coordination of multiple TEPO equivalents even at substoichiometric equivalents of TEPO and the displacement of ligands from the Lewis acid during analysis. The identification of these potential issues

should help promote the careful identification of the TEPO-Lewis acid adducts through a multitude of NMR analyses. Further the assessment of the Lewis acidities of the germanium(II) and tin(II) complexes is the first report on the Lewis acidities of dicationic Group 14 Lewis acids. The higher Lewis acidities exhibited by the Ge^{2+} cation in comparison to the cationic and neutral germanium(IV) complexes may promote future studies into the development of dicationic Group 14 Lewis acids.

3.12 Experimental

3.12.1 General Experimental

All manipulations were performed under an inert atmosphere of argon using Schlenk techniques or under an atmosphere of nitrogen in an MBraun glovebox. Solvents were purified using an Innovative Technologies 400-5 Solvent Purification System and were stored over activated 4 Å molecular sieves. All NMR solvents were dried over activated 4 Å molecular sieves. Chemicals purchased from commercial sources were used without further purification. $\text{GeCl}_2 \cdot \text{dioxane}$,⁴⁵ germanium(II) crown ether complexes,¹⁸ tin(II) crown ether complexes¹⁹ and trimethylphosphine sulfide⁴⁶ were synthesized according to literature procedures.

NMR spectra were recorded on an Inova 600 MHz NMR spectrometer or Bruker Avance III 400 MHz NMR spectrometer. The NMR standards used are as follows: ^1H NMR spectra were referenced to residual CH_2Cl_2 (5.32 ppm); $^{31}\text{P}\{^1\text{H}\}$ NMR spectra in CH_2Cl_2 were externally referenced to 85% H_3PO_4 in aqueous solution. ^1H NMR chemical shifts are relative to SiMe_4 , ^{119}Sn chemical shifts are relative to SnMe_4 (0 ppm) and ^{31}P chemical shifts are relative to 85% H_3PO_4 in aqueous solution (0 ppm). For some ^{119}Sn

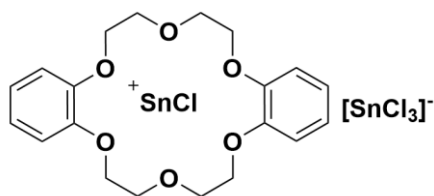
NMR spectra, $\text{Cr}(\text{acac})_3$ was used as a relaxation agent. NMR spectra for new compounds, stacked plot of VT-NMR spectra and stacked plot of comparative NMR spectra can be found in Appendix B. Electrospray ionization mass spectra were collected using a Bruker micrOTOF II spectrometer. Mass spectral data are reported in mass-to-charge units (m/z). Sodium iodide was used as an ionizing agent resulting in anion exchange with the metal halides.

3.12.2 Synthesis of New Complexes



[GeCl₂•dibenzo[18]crown-6]

Dibenzo[18]crown-6 (155 mg, 0.430 mmol) was added to THF (~ 1 mL) which was added to a solution of $\text{GeCl}_2 \cdot \text{dioxane}$ (100 mg, 0.430 mmol) in THF (~ 5 mL). The crown ether did not completely dissolve. The pale-brown mixture was left to stir for 24 hours and then the solvent was removed under reduced pressure. The product was washed with pentane (5 mL \times 3) and then THF (5 mL \times 3) to yield a pale beige solid (190 mg, 87%). Attempts to crystallize the resulting product or obtain ^{13}C NMR data were unsuccessful. ^1H NMR (400 MHz, CD_3Cl) 7.05-6.96 (m, 8H, Ar-H), 4.40 (br s, 16H, CH_2). High resolution ESI-MS positive ion m/z for $[\text{C}_{20}\text{H}_{24}\text{O}_6\text{ClGe}]^+$ calc. 469.0473, found 469.0462. Negative ion ESI: no signal.^{47,48}



[SnCl(dibenzo[18]crown-6)][SnCl₃]

Dibenzo[18]crown-6 (190 mg, 0.5 mmol) was added to DCM (~1 mL) which was added to a

solution of SnCl₂ (200 mg, 1.0 mmol) in DCM (~ 5 mL). The crown ether did not completely dissolve. The pale-brown mixture was left to stir for 24 hours after which the colour of the undissolved solid faded to white. The solvent was removed under reduced pressure and the product was washed with pentane (5 mL × 3) to provide a pale beige solid (380 mg, 98%). Attempts to crystallize the resulting product or obtain ¹³C data were unsuccessful. ¹H NMR (400 MHz, ACN-*d*₃) 7.13-7.07 (m, 8H, Ar-H), 4.35-4.37 (multiplet, 8H, ³J_{HH} = 4 Hz, CH₂), 4.23 (br s, 8H, CH₂). High resolution positive ion ESI-MS *m/z* for [C₂₀H₂₄O₆ClSn]⁺ calc. 515.02834, found 515.0287. Negative ion ESI-MS *m/z*: 224.8 [SnCl₃]⁻, 316.7 [SnCl₂I]⁻ and 408.7 [SnClI₂]⁻.



[SnCl(benzo[15]crown-5)][SnCl₃]

A solution of benzo[15]crown-5 (70 mg, 0.26 mmol) in DCM (~ 1 mL) was added to a solution of SnCl₂ (100 mg, 0.52 mmol) in DCM (~ 5 mL). The opaque white solution was left to stir for 24 hours and then the solvent was removed under reduced pressure. The product was washed with pentane (5 mL × 3) to yield a white solid (381 g, 98%). Attempts to crystallize the product or obtain ¹³C data were unsuccessful. ¹H NMR spectrum (400 MHz, ACN-*d*₃) 6.97-6.90 (br m, 4H, Ar-H), 4.11-4.13 (multiplet, 4H, CH₂),⁴⁷ 3.94-3.96 (multiplet, 4H, CH₂), 3.81 (br s, 8H, CH₂). High resolution positive ion ESI-MS *m/z* for [C₁₄H₂₀O₅ClSn]⁺ calc. 423.0021, found 423.0017. Negative ion ESI-MS *m/z*: 224.8 [SnCl₃]⁻, 408.7 [SnClI₂]⁻.⁴⁹

[Ge(TEPO)₂]²⁺ ³¹P{¹H} (243 MHz, CD₂Cl₂, 0 °C) 82.9 ppm.

$[\text{Ge}(\text{TEPO})_3]^{2+}$ $^{31}\text{P}\{^1\text{H}\}$ (243 MHz, CD_2Cl_2 , 0 °C) 82.0 ppm.

$[\text{Ge}([\text{12}]\text{crown-4})(\text{TEPO})]^{2+}$ $^{31}\text{P}\{^1\text{H}\}$ (243 MHz, CD_2Cl_2 , 0 °C) 89.5 ppm.

$[\text{GeCl}_2(\text{TEPO})_2]$ ^1H NMR (400 MHz, CD_2Cl_2 , 25 °C) 1.84 (dq, 6H, $^2J_{\text{H-P}} = 12$ Hz, $^3J_{\text{H-H}} = 8$ Hz, CH_2), 1.16 (dt, 6H, $^{33}J_{\text{H-P}} = 17$ Hz, $^3J_{\text{H-H}} = 8$ Hz, CH_3); $^{31}\text{P}\{^1\text{H}\}$ (202 MHz, CD_2Cl_2 , 25 °C) 63.0 ppm.

$[\text{Sn}(\text{TEPO})_2]^{2+}$ $^{31}\text{P}\{^1\text{H}\}$ (202 MHz, CD_2Cl_2 , -80 °C) 78.0 ppm; $^{119}\text{Sn}\{^1\text{H}\}$ (224 MHz, CD_2Cl_2 , -80 °C) -854 ppm (t, $^2J_{\text{Sn-P}} = 323$ Hz).

$^{31}\text{P}\{^1\text{H}\}$ (202 MHz, CD_2Cl_2 , 25 °C) 76.5 ppm; $^{119}\text{Sn}\{^1\text{H}\}$ (149 MHz, CD_2Cl_2 , 25 °C) -864 ppm (br s).

$[\text{Sn}(\text{TEPO})_3]^{2+}$ $^{31}\text{P}\{^1\text{H}\}$ (243 MHz, CD_2Cl_2 , -80 °C) 75.8 ppm; $^{119}\text{Sn}\{^1\text{H}\}$ (224 MHz, CD_2Cl_2 , -80 °C) -781 ppm (q, $^2J_{\text{Sn-P}} = 172$ Hz).

$[\text{SnCl}_2(\text{TEPO})_2]$ ^1H NMR (400 MHz, CD_2Cl_2 , 25 °C) 1.84 (dq, 6H, $^2J_{\text{H-P}} = 12$ Hz, $^3J_{\text{H-H}} = 8$ Hz, CH_2), 1.16 (dt, 6H, $^{33}J_{\text{H-P}} = 17$ Hz, $^3J_{\text{H-H}} = 8$ Hz, CH_3); $^{31}\text{P}\{^1\text{H}\}$ (202 MHz, CD_2Cl_2 , 25 °C) 63.5 ppm; $^{119}\text{Sn}\{^1\text{H}\}$ (149 MHz, CD_2Cl_2 , 25 °C) -212 ppm (br s).

3.12.3 Lewis Acidity Assessment of Ge (II) and Sn(II) Crown Ether Complexes using the Gutmann-Beckett Method (Table 3.1)

TEPO (10 mg, 0.074 mmol or 20 mg, 0.15 mmol) was dissolved in DCM (~0.3 mL) and was added to the Lewis acid (0.074 mmol) also dissolved in DCM (~2 mL). The solution was further diluted to give a total volume of 2.5 mL. Complete dissolution of the

Lewis acid was not observed for $[\text{GeCl}([\text{15crown-5})][\text{GeCl}_3]$, $[\text{GeCl}([\text{18crown-6})][\text{GeCl}_3]$, $[\text{SnCl}(\text{benzo}[15]\text{-crown-5})][\text{SnCl}_3]$, SnCl_2 and $\text{Sn}(\text{OTf})_2$.

3.12.4 The 2:1 Additions of TEPO to Ge(II) and Sn(II) Crown Ether Complexes for VT-NMR

TEPO (20 mg, 0.15 mmol) was dissolved in $\text{DCM-}d_2$ (1000 μL) and was added to the Lewis acid (0.074 mmol) dissolved in $\text{DCM-}d_2$ (1000 μL). Complete dissolution of the Lewis acid was observed for all samples except $\text{Sn}(\text{OTf})_2$ and SnCl_2 .

3.12.5 Titration of $[\text{SnCl}([\text{18crown-6})][\text{OTf}]_2$

$[\text{SnCl}([\text{18crown-6})][\text{SnCl}_3]$ (48 mg, 0.07 mmol) was dissolved in $\text{DCM-}d_2$ (1000 μL) in an NMR tube and 0.2 equivalents of TEPO (0.2 mL of a 0.074 M solution in $\text{DCM-}d_2$) was added sequentially and the $^{31}\text{P}\{^1\text{H}\}$ NMR spectrum was recorded until 1 equivalent of TEPO was added.

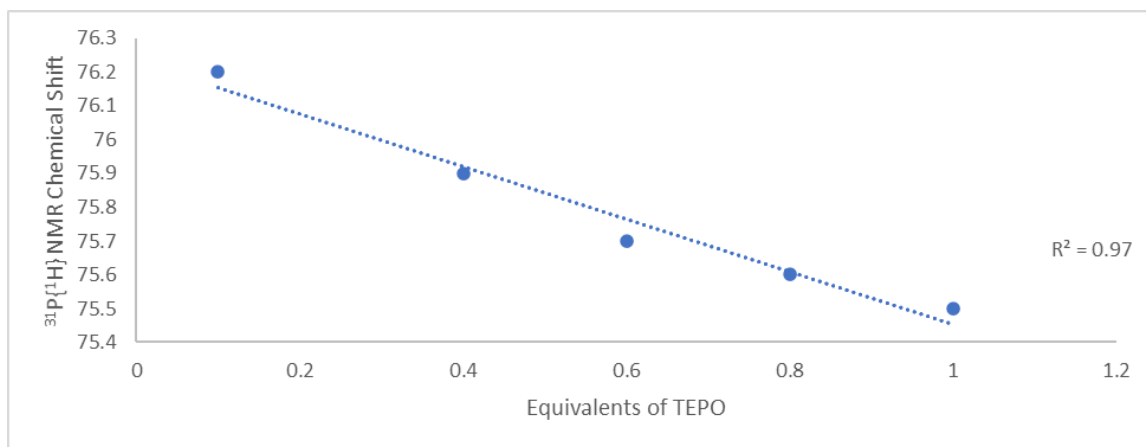


Figure 3.15 The change in ^{31}P NMR chemical shift when TEPO is added to $[\text{SnCl}([\text{18crown-6})][\text{SnCl}_3]$.

3.12.6 Lewis Acidity Assessment of Ge(II) and Sn(II) Crown Ether Complexes using Litchenberg-Modified Gutmann-Beckett (Table 3.4)

Trimethylphosphine sulfide (10 mg, 0.033 mmol) was dissolved in DCM (~ 0.3 mL) was added to the Lewis acid (0.033 mmol) and dissolved DCM (2 mL). The solution was further diluted to give a total volume of 2.5 mL. Complete dissolution of the Lewis acid was not observed for **[GeCl([18]-crown-6)][GeCl₃]**, and Sn(OTf)₂.

3.12.7 Lewis Acidity Assessment of Ge(II) and Sn(II) Crown Ether Complexes using Child's Method

Crotonaldehyde (8.4 μL, 0.14 mmol) was added to a solution of Lewis acid (0.14 mmol) DCM-*d*₂ (2 mL). The ¹H NMR spectra of the resulting solutions were recorded. No change in the ¹H NMR chemical shift of the hydrogens assigned to the aldehyde was observed in the presence of **[Ge([12]crown-4)₂][OTf]₂**, **[Ge([18]crown-6)][OTf]₂**, **[Sn([12]crown-4)₂][OTf]₂** or **[SnCl([18]crown-6)][SnCl₃]**.

3.12.8 Lewis Acidity Assessment of Germanium(II) and Tin(II) crown ether complexes using the Fluorobenzonitrile Method

4-Fluorobenzonitrile (10 mg, 0.08 mmol) dissolved in ACN (~0.3 mL). The solution was added to the Lewis acid (0.08 mmol) dissolved in ACN (1 mL). The ¹⁹F{¹H} NMR spectrum was acquired. No change in the ¹⁹F NMR chemical shift was observed in the presence of **[Ge([12]crown-4)₂][OTf]₂**, **[Sn([12]crown-4)₂][OTf]₂**, **[Ge([18]crown-6)][OTf]₂** or **[SnCl([18]crown-6)][SnCl₃]**.

3.12.9 Computational Details

All computations were performed in collaboration with Andrew T. Henry. All calculations (except G3/G4) were performed with ORCA 4.1.2 and ORCA 4.2. Except in cases where a crystal structure was found, starting geometries were generated using Avogadro and preliminary optimizations. Geometry optimizations were performed with PBEh-3c/def2-mSVP as implemented in ORCA, using grid5 settings. All calculated geometries were confirmed as energetic minima on the potential energy surface by analytical calculation of harmonic frequencies at the PBEh-3c level. In case of negative frequencies $>10\text{ cm}^{-1}$, the geometries were reoptimized with grid6, TightOPT and VeryTightSCF settings. The optimized geometries were then used to calculate the single point energies at B3LYP D3(BJ)/def2-TZVPP level of theory using the RIJCOSX approximation and def2/J as the auxiliary basis set. Solvation calculations were performed using the conductor-like polarization model (CPCM). The calculations of the chlorinated tetrylenes (ECI_2) were performed treating the compounds as singlet tetrylenes.

Table 3.7 Calculated data for the determination of the FIA values of the germanium(II) and tin(II) crown ether complexes.

LA ^{a,b}	E DSD-BLYP		Thermal Correction PBEh-3c/def2-SVP		Electronic + Thermal	LA + Me ₃ SiY	Me ₃ Si ⁺ + LA-F-	Reaction 1	FIA
	Hartree	kJ	Hartree	kJ					
[Ge(12c4) ₂] ²⁺	-3307.2172	-8683099	0.5392	1415.5513	-8681683	-10018134	-10017910	223.7201	728.7799
[Ge(12c4) ₂ F] ⁺	-3407.2598	-8945761	0.5422	1423.6367	-8944337				
[Ge(18c6)] ²⁺	-2999.5517	-7875323	0.4045	1061.9880	-7874261	-9210712	-9210600	112.2883	840.2117
[Ge(18c6)F] ⁺	-3099.6372	-8138098	0.4080	1071.2113	-8137026				
[GeCl(18c6)] ⁺	-3459.9508	-9084101	0.4077	1070.3261	-9083030	-10419481	-10419198	283.0074	669.4926
[GeCl(18c6)F]	-3559.9690	-9346698	0.4089	1073.5132	-9345625				
[GeOTf(18c6)] ⁺	-3961.2696	-10400313	0.4439	1165.4235	-10399148	-11735599	-11735411	187.8569	764.6431
[GeOTf(18c6)F]	-4061.3255	-10663010	0.4466	1172.4702	-10661838				
[Sn(12c4) ₂] ²⁺	-1444.6325	-3792883	0.5391	1415.2847	-3791467	-5127918	-5127703	215.0591	737.4409
[Sn(12c4) ₂ F] ⁺	-1544.6782	-4055553	0.5419	1422.6533	-4054130				
[Sn(18c6)] ²⁺	-1136.9734	-2985124	0.4045	1062.0729	-2984062	-4320512	-4320324	188.5693	763.9307
[Sn(18c6)F] ⁺	-1237.0291	-3247820	0.4072	1069.2027	-3246751				
[SnCl(18c6)] ⁺	-1597.3736	-4193904	0.4075	1069.8709	-4192834	-5529285	-5528995	290.0025	662.4975
[SnCl(18c6)F]	-1697.3897	-4456497	0.4093	1074.5724	-4455422				
[SnOTf(18c6)] ⁺	-2098.6938	-5510121	0.4439	1165.4125	-5508955	-6845406	-6845194	211.7804	740.7196
[SnOTf(18c6)F]	-2198.7401	-5772792	0.4461	1171.1845	-5771621				
GeCl ₂	-2997.3452	-7869530	0.0063	16.5427	-7869513	-9205237	-9204723	514.4962	438.0038
GeCl ₂ F ⁻	-3097.3321	-8132045	0.0097	25.4402	-8132020				
SnCl ₂	-1134.7444	-2979271	0.0062	16.1779	-2979255	-4314979	-4314462	516.9401	435.5599
SnCl ₂ F ⁻	-1234.7302	-3241784	0.0094	24.8032	-3241759				
Sn(OTf) ₂	-2137.3765	-5611682	0.0776	203.7165	-5611478	-6947202	-6946773	429.5033	522.9967
Sn(OTf) ₂ F ⁻	-2237.3948	-5874280	0.0801	210.2731	-5874070				

Table 3.8 The anchor point data used in the determination of FIA values.

Species	kJ	Reaction 2
Me ₃ Si ⁺	-1071911.3	
Me ₃ SiF	-1334866.1	952.5
F ⁻	-262002.2	

3.13 References

- [1] Recent reviews on Main Group catalysts: a) Dagorne, S.; Bellemin-Laponnaz, S. In *The group 13 metals aluminium, gallium, indium and thallium: Chemical patterns and peculiarities*; Wiley: Chichester, 2011; pp 654–692. b) Woodward, S.; Blümke T.; Dagorne, S. *Modern organoaluminum reagents preparation, structure, reactivity and use*; Topics in Organometallic Chemistry; Springer: Berlin, 2013; Vol. 41. c) Hadlington, T. J.; Driess, M.; Jones, C. *Chem. Rev.*, **2018**, *47*, 4176-4197. d) Lipshultz, J. M.; Li, G.; Radosevich, A. T. *J. Am. Chem. Soc.*, **2021**, *143*, 1699–1721.
- [2] a) Ould, D. M. C.; Carden, J. L.; Page, R.; Melen, R. L. *Inorg. Chem.*, **2020**, *59*, 14891–14898. b) Parks, D. J.; Piers, W. E. *J. Am. Chem. Soc.*, **1996**, *118*, 9440-9441. c) Carden, J. L.; Gierlich, L. J.; Wass, D. F.; Browne, D. L.; Melen, R. L. *Chem. Commun.*, **2019**, *55*, 318-321. d) Maotong, X.; Possart, J.; Waked, A. E.; Roy J.; Werner, U.; Stephan, D. W. *Phil. Trans. R. Soc. A*, **2017**, *375*, 37520170014.
- [3] a) Liberman-Martin, A. L.; Bergman, R. G.; Tilley, T. D. *J. Am. Chem. Soc.*, **2015**, *137*, 5328-5331. b) Hartman, D.; Schädler, M.; Grev, L. *Chem. Sci.*, **2019**, *10*, 7379-7388. c) Roth, D.; Wadepohl, H.; Greb, L. *Angew. Chem. Int. Ed.*, **2020**, *59*, 20930-20934. d) Henry, A. T.; Cosby, T. P. L.; Boyle, P. D.; Baines, K. M. *Dalton Trans.*, **2021**, *50*, 15906–15913.
- [4] a) Stefkova, K.; Gierlich, L.; Willcox, D.; Melen, R. L. *Borocations in Catalysis. Encyclopedia of Inorganic and Bioinorganic Chemistry*, 2020, 1–37. b) Walker, J. C.; Klare, H. F.; Oestreich, M., *Nat. Rev. Chem.*, **2019**, *4*, 54–62. c) Großekappenberg, H.;

- Reißmann, M.; Schmidtman, M.; Müller, T. *Organometallics*, **2015**, *34*, 4952-4958. d) Fritz-Langhals, E.; Werge, S.; Kneissl, S.; Piroutek, P. *Org. Process Res. Dev.*, **2020**, *24*, 1484–1495. e) Fritz-Langhals, E. *Org. Process Res. Dev.*, **2019**, *23*, 2369-2377.
- [5] a) Hadlington, T. J.; Hermann, M.; Frenking, G.; Jones, C. *J. Am. Chem. Soc.*, **2014**, *136*, 3028-3031. b) Bayne, J. W.; Stephan, D. W. *Chem. Rev.*, **2016**, *45*, 765-774. c) Li, Z.; Thiery, G.; Lichtenthaler, M. R.; Guillot, R.; Krossing, I.; Gandon, V.; Bour, C. *Adv. Synth. Cat.*, **2018**, *360*, 544-549.
- [6] Corma, A.; Garcia, H. *Chem. Rev.*, **2003**, *103*, 4307-4336.
- [7] a) Mayer, U.; Gutmann, V.; Gerger, W. *Montash. Chem.*, **1973**, *106*, 1235-1257. b) Beckett, M. A.; Strickland, G. C.; Holland, J. R.; Varma, K. S. *Polymer*, **1996**, *37* 4629-4631. c) Childs, R. F.; Mulholland, D. L.; Nixon, A. *Can. J. Chem.*, **1982**, *60* , 801-808. d) Künzler, S.; Rathjen, S.; Merk, A.; Schmidtman, Müller, T. *Chem. Eur. J.*, **2019**, *25*, 15123-15130.
- [8] Haartz, J. C.; McDaniel, D. H. *J. Am. Chem. Soc.*, **1973**, *95*, 8562-8565.
- [9] Pearson, R. G. *J. Chem. Ed.*, **1968**, *45*, 581-587.
- [10] Ramler, J.; Litchenberg, C. *Chem, Eur. J.*, **2020**, *26*, 10250-10258.
- [11] a) Gaffen, J. R.; Bentley, J. N.; Torres, L. C.; Chu, C.; Baumgartner, T.; Caputo, C. B. *Chem*, **2019**, *5*, 1567–1583. b) Bentley, J. N.; Elgadi, S. A.; Gaffen, J. R.; Demay-Drouhard, P.; Baumgartner, T.; Caputo, C. B. *Organometallics*, **2020**, *39*, 3645-3655.

- [12] a) Parr, R. G.; Szentpály, L. v.; Liu, S. *J. Am. Chem. Soc.* **1999**, *121*, 1922-1924. b) Maynard, A. T.; Huang, M.; Rice, W. G.; Covell, D. G. *Proc. Natl. Acad. Sci.*, **1998**, *95*, 11578-11583. c) Jupp, A. R.; Johnstone, T. C.; Stephan, D. W. *Dalton Trans.*, **2018**, *47*, 7029-7035.
- [13] a) Mukaiyama, T.; Ueki, M.; Izawa, T.; Kuwahara, M. *Chem. Lett.*, **1972**, *1*, 443-444. b) Tang, Z.; Chen, W.; Zhu, Z.; Liu, H. *Synthetic Commun.*, **2008**, *42*, 1372-1383. c) Denmark, S. E.; Beutner, G. L.; Wynn, T.; Eastgate, M. D. *J. Am. Chem. Soc.*, **2005**, *127*, 3774-3789. d) Matsuo, J.; Sasaki, S.; Hoshikawa, T.; Ishibashi, H. *Org. Lett.*, **2009**, *11*, 3822-3825.
- [14] a) Davydova, E. I.; Timoshkin, A. Y.; Sevastianova, T. N.; Suvorov, A. V.; Frenking, G. *J. Mol. Struct-Theochem*, **2006**, *767*, 103-111. b) Feshin, V. P.; Feshina, E. V. *Rus. J. Gen Chem+*, **2008**, *78*, 210-215.
- [15] Erdmann, P.; Leitner, J.; Schwarz, J.; Greb, L. *ChemPhysChem*, **2020**, *21*, 987 – 994.
- [16] Jennings, J. J.; Wigman, B. W.; Armstrong, B. M.; Franz, A. K. *J. Org. Chem.*, **2019**, *84*, 15845-15853.
- [17] Suter, R.; Swidan, A.; Macdonald, C. L. B.; Burford, N.; Ferguson, M. J. *Inorg. Chem.*, **2019**, *58*, 6238-6245.
- [18] Rugar, P. A.; Bandyopadhyay, R.; Cooper, B. F. T.; Stinchombe, M. R.; Ragona, P. J.; Macdonald, C. L. B.; Baines, K. M. *Angew. Chem. Int. Ed.*, **2009**, *48*, 5155-5158.

- [19] Secara, A. M.; Binder, J. F.; Swidan, A.; Macdonald, C. L. B. *Can. J. Chem.*, **2018**, *96*, 570-577.
- [20] Bandyopadhyay, R.; Cooper, B. F. T.; Rossini, A. J.; Schurko, R. W.; Macdonald, C. L. B. *J. Organomet. Chem.*, **2010**, *695*, 1012-1018.
- [21] Wolff, M.; Harmening, T.; Pöttgen, R.; Feldmann, C. *Inorg. Chem.*, **2009**, *48*, 3153-3156.
- [22] For a review see: Swidan, A.; Macdonald, C. L. B. *Chem. Soc. Rev.*, **2016**, *45*, 3883-3915.
- [23] Bandyopadhyay, R.; Nguyen, J. H.; Swidan, A.; Macdonald, C. L. B. *Angew. Chem. Int. Ed.*, **2013**, *52*, 3469-3472.
- [24] Beckett, M. A.; Brassington, D. S.; Coles, S. J.; Hursthouse, M. B. *Inorg. Chem. Commun.*, **2000**, *3*, 530-533
- [25] Dean, P. W. *Can. J. Chem.*, **1982**, *60*, 2921-2926.
- [26] Copyright permission for the reprinting of the figures from Elsevier are given in Appendix E.
- [27] Complete conversion from $\text{Sn}(\text{OTf})_2$ to $[\text{Sn}(\text{12crown-4})_2][\text{OTf}]_2$ in the presence of 12crown-4 indicates that $[\text{Sn}(\text{12crown-4})_2][\text{OTf}]_2$ is favored in the equilibrium.
- [28] Persson, I.; D'Angelo, P.; Lundberg, D. *Chem. Eur. J.*, **2016**, *22*, 18583-18592.
- [29] Christensen, J. J.; Hill, J. O.; Izatt, R. M. *Science*, **1971**, *174*, 469-467.

- [30] Gurnani, C.; Hector, A. L.; Jager, E.; Levason, W.; Pugh, D.; Reid, G. *Dalton Trans.*, **2013**, *42*, 8364-8373.
- [31] Gawron, M.; Dietz, C.; Lutter, M.; Duthie, A.; Jouikov, V.; Jurkschat, K. *Chem. Eur. J.*, **2015**, *21*, 16609-16622.
- [32] Bouška, M.; Dostál, L.; Růžička, A.; Jambor, R. *Organometallics*, **2013**, *32*, 1995-1999.
- [33] a) Taylor, M. J.; Coddington, J. M. *J. Chem. Soc. Dalton Trans.*, **1989**, *11*, 2223-2227. b) Coddington, J. M.; Taylor, M. J. *Polyhedron*, **1992**, *11*, 1531-1544.
- [34] Wang, L.; Kefalidis, C. E.; Roisnell, T.; Sinbandhit, S.; Maron, L.; Carpentier, J.-F.; Sarazin, Y. *Organometallics*, **2015**, *34*, 2139-2150.
- [35] Copyright permission for the reprinting of the figures from John Wiley & Sons are given in Appendix E.
- [36] Yoder, C. H.; Agee, T. M.; Schaeffer, C. D.; Carroll, M. J.; Fleisher, A. J.; DeToma, A. S. *Inorg. Chem.*, **2008**, *47*, 10765-10770.
- [37] Cheng, F.; Davis, M. F.; Hector, A. L.; Levason, W.; Reid, G.; Webster, M.; Zhang, W. *Eur. J. Inorg. Chem.*, **2007**, *17*, 2488-2495.
- [38] Macdonald, C. L.B.; Bandyopadhyay, R.; Cooper, B. F. T.; Friedl, W. W.; Rossini, A. J.; Schruko, R. W.; Eichhorn, S. H.; Herber, R. H. *J. Am. Chem. Soc.*, **2012**, *134*, 4332-4345.

- [39] Laurence, C.; Gal Jean-François. *Lewis basicity and Affinity Scales: Data and measurement*; John Wiley & Sons: Chichester, West Sussex, 2010.
- [40] Complete dissolution of several $[MCl_3]^-$ (M= Ge, Sn) salts was not observed.
- [41] Näslund, J.; Persson, I.; Sandström, M. *Inorg. Chem.*, **2009**, *39*, 4012-4021.
- [42] a) Becke, A. D. *J. Chem. Phys.*, **1993**, *98*, 5648-5652. b) Grimme, S.; Antony, J.; Ehrlich, S.; Krieg, H. *J. Chem. Phys.*, **2010**, *132*, 154104. c) Grime, S.; Antony, J.; Ehrlich, S.; Krieg, H. *J. Chem. Phys.* **2010**, *132*, 154104-1. d) Grimm, S.; Ehrlich, S.; Goerigk, L. *J. Comput. Chem.*, **2011**, *32*, 1456-1465. e) Johnson, E. R.; Becke, A. D. *J. Chem. Phys.*, **2005**, *123*, 024101. f) Becke, A. D.; Johnson, E. R. *J. Chem. Phys.*, **2005**, *122*, 154101. g) Schafer, A.; Huber, C.; Ahlrichs, R. *J. Chem. Phys.*, **1994**, *100*, 5829-5835. h) Grimme, S.; Brandenburg, J. G.; Bannwarth, C.; Hansen, A. *J. Chem. Phys.*, **2015**, *143*, 054107. i) Cavin, A. T.; Hillisch, A.; Uellendahl, F.; Schneckener, S.; Göller, A. H. *J. Chem. Inf. Model.*, **2018**, *58*, 1005–1020. j) Klamt, A.; Schüürmann, G. *J. Chem. Soc., Perkin Trans. 2*, **1993**, 799. k) Andzelm, J.; Kölmel, C.; Klamt, A. *J. Chem. Phys.*, **1995**, *103*, 9312-9320. l) Barone, V.; Cossi, M. *J. Phys. Chem. A*, **1998**, *102*, 1995-2001. m) Cossi, M.; Rega, N.; Scalmani, G.; Barone, V. *J. Comput. Chem.*, **2003**, *24*, 669-681.
- [43] Greb, L. *Chem. Eur. J.*, **2018**, *24*, 17881-17896.
- [44] Hermannsdorfer, A.; Dreiss, M. *Angew. Chem. Int. Ed.*, **2020**, *59*, 23132-23136.
- [45] Kouvetakis, J.; Haaland, A.; Shorokhov, D. J.; Volden, H. V.; Girichev, G. V.; Sokolov, V. I.; Matsunaga, P. *J. Am. Chem. Soc.*, **1998**, *120*, 6738-6744.

[46] Morgan, M. T.; Yang, B.; Harankhedkar, S.; Nabatilan, A.; Bourassa, D.; McCallium, A. M.; Sun, F.; Wu, R.; Forest, C. R.; Fahrni, C. J. *Angew. Chem. Int. Ed.*, **2018**, *130*, 9859-9863.

[47] The syntheses of these novel crown ether complexes are not reliable. In many attempts, residual GeCl_2 or SnCl_2 were evident in the acquired mass spectra. Unreacted crown ether or GeCl_2 -dioxane was also visible on several occasions in the ^1H NMR spectra.

[48] Nefedov, O. M.; Kolesnikov, S. P.; Rogozhin, I. S. *Izv. Akad. Nauk SSSR, Ser. Khim.*, **1980**, 170–173

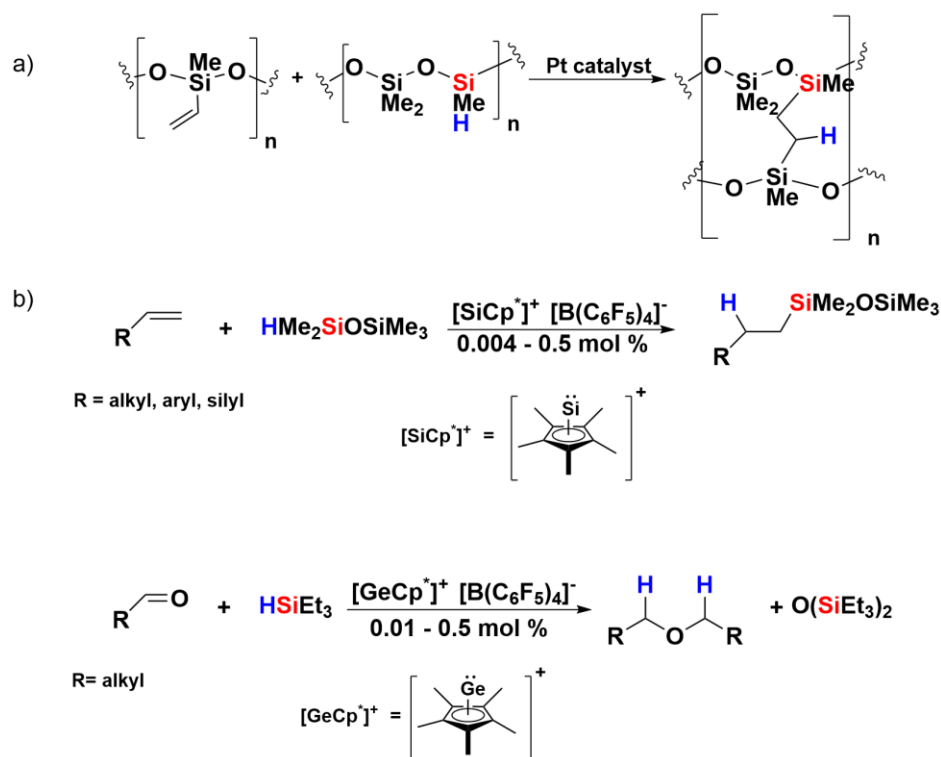
[49] The peak pattern is consistent with an AA'BB'' spin system. See also: Buchana, G. W.; Moghimi, A.; Ratcliffe, C. I. *Can. J. Chem.*, **1996**, *74*, 1437-1446.

Chapter 4

4 Carbonyl Reduction by Group 14 Crown Ether Complexes

4.1 Introduction

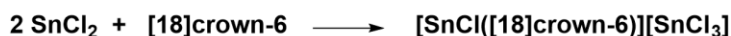
In the last two decades, main group Lewis acids have been shown to catalyze a number of chemical transformations,¹ and have achieved comparable catalytic performance as transition metal catalysts.² The reduction of unsaturated species through hydrosilylation is one area of current interest due to the potential industrial applications, such as the cross-linking of polysiloxane chains (Scheme 4.1).³ The development of $[\text{SiCp}^*][\text{B}(\text{C}_6\text{F}_5)_4]$ as a catalyst has enabled alkene hydrosilylation at the parts-per-million catalyst loading level,⁴ demonstrating the efficacy of a group 14 cationic catalyst. The analogous germanium(II) catalyst, $[\text{GeCp}^*][\text{B}(\text{C}_6\text{F}_5)_4]$ was also recently shown to facilitate the hydrosilylation of carbonyl compounds to give symmetric ethers and disiloxanes⁵ at comparable catalyst loadings to $[\text{SiCp}^*][\text{B}(\text{C}_6\text{F}_5)_4]$. Apart from these examples, only one other example of a cationic, divalent group 14 catalyst has been reported,⁶ although there has been several examples of catalysis by neutral, divalent Group 14 species.⁷



Scheme 4.1 a) The crosslinking of polysiloxane chains using a platinum catalyst and b) hydrosilylation of alkenes by $[\text{SiCp}^*][\text{B}(\text{C}_6\text{F}_5)_4]^-$ and c) hydrosilylation of aldehydes by $[\text{GeCp}^*][\text{B}(\text{C}_6\text{F}_5)_4]^-$.⁵

Inspired by the success achieved with the $[\text{MCp}^*][\text{B}(\text{C}_6\text{F}_5)_4]$ (M= Si, Ge) as catalysts, we have investigated the use of germanium(II) and tin(II) cations, notably those stabilized by crown ether ligands, as potential catalysts for hydrosilylation. Many of the crown ether complexes shown in Figure 4.1 are cationic and may exhibit similar reactivity. In contrast to the syntheses of many other low valent cationic Group 14 complexes, including $[\text{MCp}^*][\text{B}(\text{C}_6\text{F}_5)_4]$ (M= Si, Ge),^{4,5} the crown ether complexes of germanium(II) and tin(II) can be synthesized in a one-step reaction from commercially available materials with the generation of only volatile by-products (Scheme 4.2). The yields of the complexes are high (>90%) and no separation or purification steps are required to obtain the reaction

product in reasonable purity. The simple syntheses of these complexes provide a distinct advantage over other cationic germanium(II) catalyst.



Scheme 4.2 Representative synthesis of the germanium(II) and tin(II) crown ether complexes.⁸

The only reaction examined to date of any germanium(II) or tin(II) cationic crown ether complex is the coordination of water and ammonia to $[\text{Ge}(\text{[15-crown-5})][\text{OTf}]_2$, highlighting the Lewis acidic nature of the complex.⁹ Quantitative Lewis acidity studies of the crown ether complexes illustrated in Figure 4.1 revealed that the germanium(II) cationic crown ether complexes $[\text{Ge}(\text{[12]crown-4})_2][\text{OTf}]_2$, $[\text{Ge}(\text{[15]crown-5})][\text{OTf}]_2$ and $[\text{Ge}(\text{[18]crown-6})][\text{OTf}]_2$ are highly Lewis acidic, with high fluoride ion affinities (FIA) and Gutmann-Beckett Acceptors Numbers (AN).¹⁰ The Lewis acidity of the aforementioned germanium(II) species as revealed by the Gutmann-Beckett method (³¹P NMR δ 82-89.4 ppm) is higher than that of $\text{B}(\text{C}_6\text{F}_5)_3$ (³¹P NMR δ 78.0 ppm), a known hydrosilylation catalyst.¹¹ Herein, the reactivity of cationic and neutral crown ether-stabilized germanium(II) and tin(II) complexes as catalysts in the hydrosilylation reactions of carbonyl compounds will be explored.

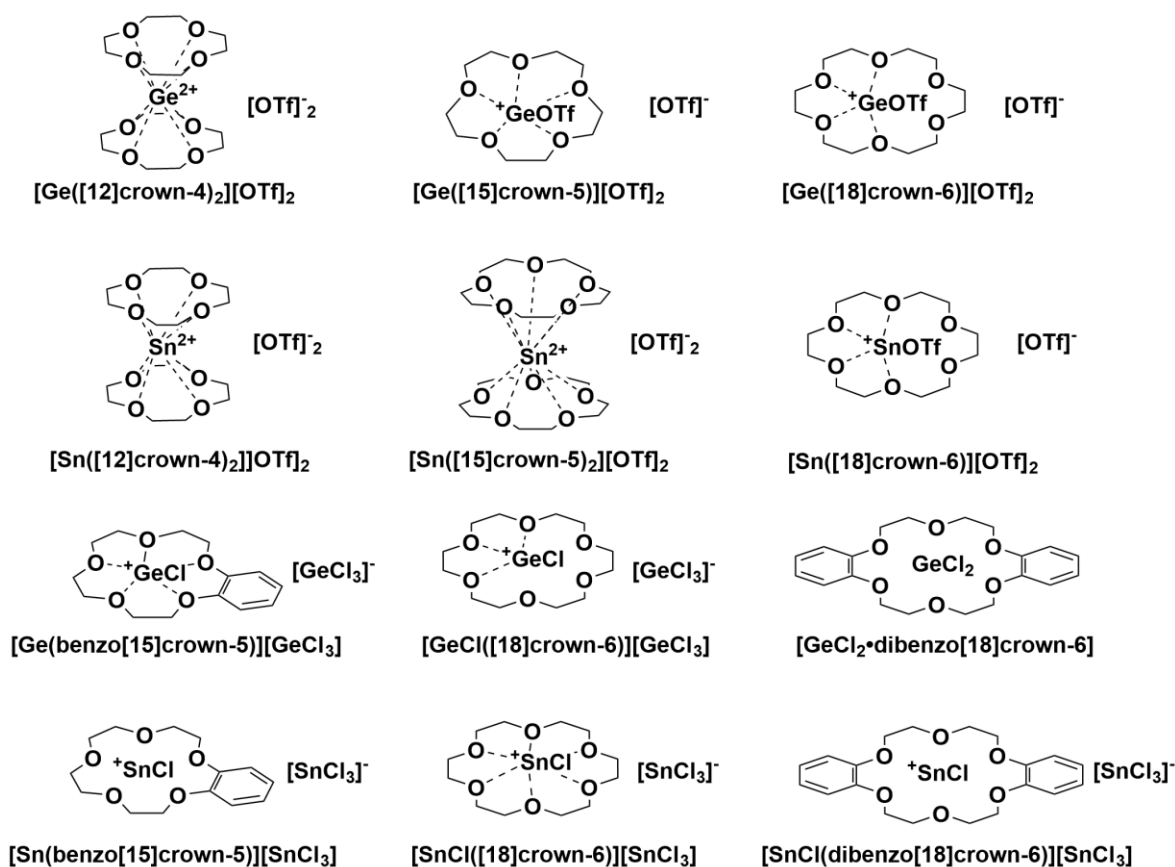


Figure 4.1 Germanium(II) and tin(II) crown ether-stabilized complexes studied in this work. Oxygen contacts are depicted with dashed lines for compounds with published solid-state X-ray diffraction data.⁸

4.2 Aldehyde Reduction Results

4.2.1 Aldehyde Reduction by Group 14 Crown Ether Triflate Salts

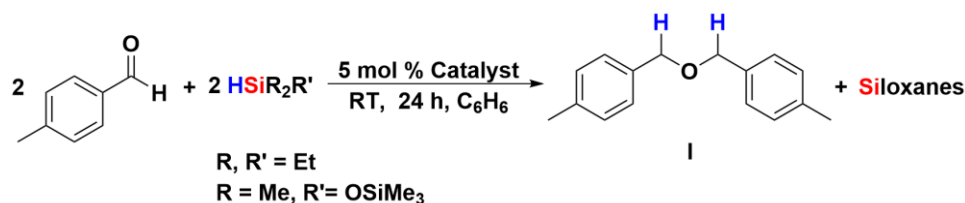
To probe the catalytic activity of selected germanium(II) and tin(II) crown ether complexes, the hydrosilylation of 4-methylbenzaldehyde was chosen as a benchmark reaction due its diagnostic NMR signals in both the aryl and alkyl regions of the ¹H NMR spectrum. In reactions with the germanium(II) triflate salts, conversion to 1,1'-[oxybis(methylene)]bis[4-methyl-benzene], **I**, was observed (Table 4.1). Siloxanes¹² were

generated as the silicon by-product in reactions with both triethylsilane (TES) and pentamethyldisiloxane (PMDS) (Table 4.1, Entries 1-6). Although the formation of the silyl ether was anticipated, conversion to symmetric ethers was observed and has been previously reported under similar conditions including in a recent report where $[\text{GeCp}^*][\text{B}(\text{C}_6\text{F}_5)_4]$ was utilized as a catalyst.⁵ Without a detailed understanding of the mechanism of reaction, it cannot be concluded whether the hydrosilylated product, for example 1-methyl-4-[[triethylsiloxy]methyl]benzene, **IIb**, in the reaction with triethylsilane, is formed, and thus, the reactions will be referred to as a *reduction* or *etherification* as opposed to hydrosilylation.

Despite different coordination environments about the germanium centres between the two germanium(II) triflate salts, $[\text{Ge}([\text{12crown-4}]_2)[\text{OTf}]_2]$, and $[\text{Ge}([\text{15crown-5}]_2)[\text{OTf}]_2]$, in the solid-state as evidenced by X-ray diffraction,^{8b} virtually identical conversions were observed (both >95%, Table 4.1 Entries 1-4) suggesting that, under these conditions, the coordination environment of the catalyst in the solid-state is not a significant indicator of reactivity. On addition of TEPO to $\text{Ge}([\text{12crown-4}]_2)[\text{OTf}]_2$ or $[\text{Ge}([\text{15crown-5}]_2)[\text{OTf}]_2]$ displacement of the crown ether ligand by TEPO occurred in solution leading to the same solution-state species, $[\text{Ge}(\text{TEPO})_2]^{2+}$.¹⁰ Similarly, displacement of the crown ether ligands, presumably by the aldehyde, may give the same intermediate and account for the identical reaction outcomes. For $[\text{Ge}([\text{18crown-6}]_2)[\text{OTf}]_2]$, significantly lower conversions to ether **I** were observed in comparison to [12]crown-4 and [15]crown-5 complexes (Table 4.1, Entries 5 & 6). The addition of TEPO to $[\text{Ge}([\text{18crown-6}]_2)[\text{OTf}]_2]$ yielded $[\text{Ge}([\text{18crown-6}](\text{TEPO})_2)]^{2+}$; displacement of the

crown ether did not occur. The lack of crown ether displacement in reactions with $[\text{Ge}([\text{18}]\text{crown-6})][\text{OTf}]_2$ may account for the decrease in conversion compared to $\text{Ge}([\text{12}]\text{crown-4})_2][\text{OTf}]_2$ and $[\text{Ge}([\text{15}]\text{crown-5})][\text{OTf}]_2$.

Table 4.1 Etherification of 4-methylbenzaldehyde by germanium(II) or tin(II) triflate salts in the presence of silane.



Entry	Catalyst	Silane	Conversion to I (%) ^a
1	[Ge([12]crown-4) ₂][OTf] ₂	PMDS	>98
2		TES	95
3	[Ge([15]crown-5)][OTf] ₂	PMDS	>98
4		TES	>98
5	[Ge([18]crown-6)][OTf] ₂	PMDS	23
6		TES	Trace
7	[Sn([12]crown-4) ₂][OTf] ₂	PMDS	>5
8		TES	Trace ^b
9	[Sn([15]crown-5) ₂][OTf] ₂	PMDS	Trace
10		TES	Trace
11	[Sn([18]crown-6)][OTf] ₂	PMDS	Trace
12		TES	No conversion
13	-	PMDS	No conversion
14		TES	No conversion

^aThe [aldehyde] and [silane] were 0.150 M. Yields were determined by ¹H NMR spectroscopy using mesitylene as an internal standard. PMDS= pentamethyldisiloxane TES= triethylsilane. Reactions were run in duplicate and conversion values were within ± 2%. ^b Trace refers to the presence of visible signals in the ¹H NMR spectrum consistent with **I** but which integrate to less than 0.05 compared to mesitylene.

Minimal conversion to any product was observed for the analogous tin(II) triflate salts were utilized as catalysts (Table 4.1, Entries 7-12), even at elevated temperatures. The differences in conversion achieved using the germanium(II) compared to the tin(II) complexes are consistent with the relative strengths of the germanium(II) and tin(II) Lewis

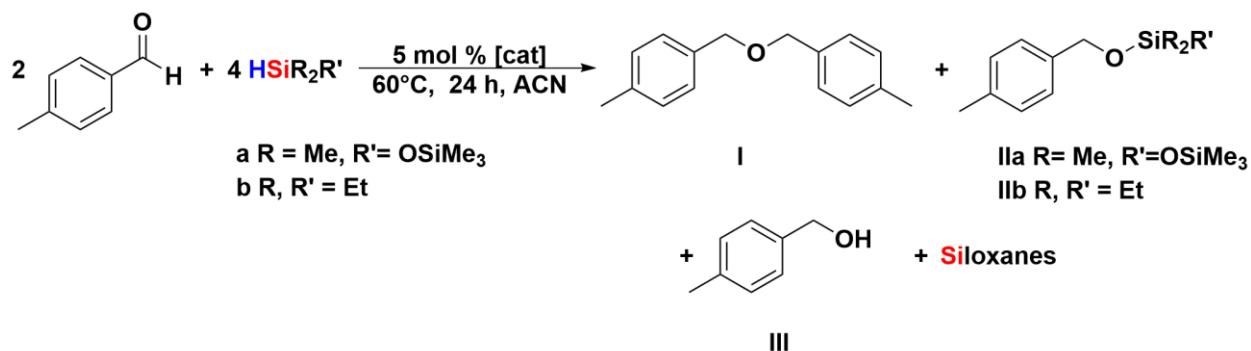
acids, where the more Lewis acidic germanium complexes are better Lewis acid catalysts.¹⁰ The identity of the silane, either PMDS or TES, does not influence the extent of the conversion to **I** (Table 4.1). In the reduction of 4-methylbenzaldehyde catalyzed by $[\text{Sn}([\mathbf{15}]\text{crown-5})_2][\text{OTf}]_2$ in presence of triethylsilane, trace signals consistent with silyl ether **IIb**¹³ were observed in the ¹H NMR spectrum which suggests that silyl ether **IIb** may be formed during the course of the reaction enroute to the 1,1'-[oxybis(methylene)]bis[4-methyl-benzene], **I** (Table 4.1, Entry 10).

4.2.2 Aldehyde Reduction by Group 14 Crown Ether Trichlorometallate Salts

Under the same conditions for the reduction of 4-methylbenzaldehyde (room temperature, 5 mol% catalyst, 1 equivalent of silane) little to no conversion to any reduced product was observed using the trichlorometallate salts of either the tin(II) or the germanium(II) crown ether complexes as catalysts. Through optimization, at a temperature of 60 °C using acetonitrile as the solvent and with two equivalents of silane, higher conversions to three reduction products were observed (Table 4.2). In addition to **I**, conversion to the silyl ether **IIa** or **IIb**, as well as the 4-methylbenzyl alcohol, **III**, was observed. Excellent conversion (91 %) and selectivity (100 %) for the formation of **IIa** was achieved using $[\text{SnCl}([\mathbf{18}]\text{crown-6})][\text{SnCl}_3]$ as the catalyst in reactions with PMDS; however, significantly lower conversions and selectivity was achieved with TES and the same catalyst (Table 4.2, Entries 11 & 12). High selectivity for **I** was observed in reactions using $[\text{GeCl}([\mathbf{18}]\text{crown-6})][\text{GeCl}_3]$ as a catalyst and PMDS (83% **I**), while much lower selectivity was observed in the reduction with TES using the same catalyst (41% **I**) (Table

4.2, Entries 5 & 6). In reactions catalyzed by $[\text{SnCl}(\text{dibenzo}[18]\text{crown-6})][\text{SnCl}_3]$, high selectivity for the symmetric ether was observed with TES (83 % **I**), while slightly lower conversion was observed with PMDS but the selectivity was instead for silyl ether **IIa** (100 %) (Table 4.2, Entries 13 & 14). These results suggest that the nature of the silane significantly influences the conversion to and selectivity of the products in contrast to the results obtained using the germanium(II) and tin(II) crown ether triflate salts. All reaction solutions containing the germanium(II) and tin(II) crown ether triflate salts as catalysts were colourless; however, in reactions with $[\text{SnCl}(\text{benzo}[15]\text{crown-5})][\text{SnCl}_3]$ as a catalyst, a yellow solution was observed suggesting the catalyst may have decomposed during the reaction. No clear trends were evident in the result obtained utilizing different germanium(II) or tin(II) trichlorometallate complexes.

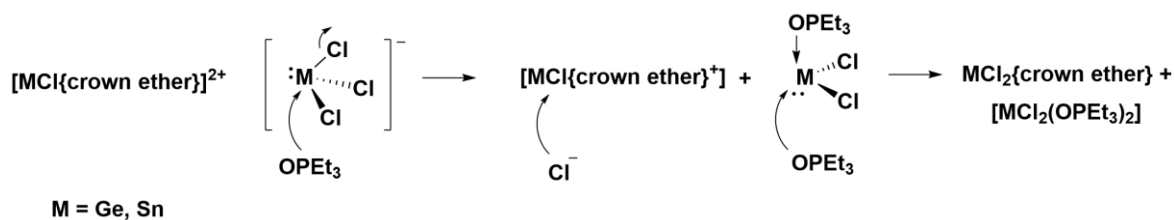
Table 4.2 Etherification of 4-methylbenzaldehyde in the presence of silane catalyzed by tin(II) or germanium(II) trichlorogermanate salts.



Entry	Catalyst	Silane	Conversion to Reduced Products (%)	Product Distribution (%) ^a		
				I	II	III
1	[GeCl([15]crown-5)][GeCl ₃]	PMDS	23	83	17	-
2		TES	23	66	29	5
3	[GeCl(benzo[15]crown-5)][GeCl ₃]	PMDS	52	75	-	25
4		TES	53	6	61	33
5	[GeCl([18]crown-6)][GeCl ₃]	PMDS	54	83	-	16
6		TES	21	41	18	41
7	[GeCl ₂ ·dibenzo[18]crown-6]	PMDS	52	75	-	24
8		TES	33	3	73	24
9	[SnCl(benzo[15]crown-5)][SnCl ₃] ^b	PMDS	No conversion	-	-	-
10		TES	No conversion	-	-	-
11	[SnCl([18]crown-6)][SnCl ₃]	PMDS	91	Trace ^c	>98	Trace
12		TES	43	7	63	30
13	[SnCl(dibenzo[18]crown-6)][SnCl ₃]	PMDS	54	83	-	16
14		TES	34	-	100	-
15	-	PMDS	No conversion	-	-	-
16		TES	No conversion	-	-	-

^aThe [aldehyde] was 0.150 M and [silane]. Yields were determined by ¹H NMR spectroscopy using mesitylene as an internal standard. Reactions were run in duplicate and conversion values were within $\pm 2\%$. The distribution of products varied by $\pm 5\%$ ^b Decomposition of catalyst occurred. ^c Trace refers to the presence of signals in the ¹H NMR spectrum consistent with **I**, **II** or **III** but which integrate to a value of less than 0.05 relative to mesitylene.

In reactions between the germanium(II) and tin(II) crown ether trichlorometallate salts and TEPO, the formation of $[\text{SnCl}_2(\text{TEPO})_2]$ or $[\text{GeCl}_2(\text{TEPO})_2]$ was observed, presumably by displacement of a chloride in the $[\text{MCl}_3]^-$ anion by TEPO and subsequent coordination of a second equivalent of TEPO (Scheme 4.3).¹⁰ Compared to TEPO, 4-methylbenzaldehyde is a weaker donor (BF_3 affinity of benzaldehyde 79 kJ/mol compared to 119 kJ/mol for TEPO),¹⁴ and thus, displacement of the chloride may not be favored. However, GC-MS analysis of the reaction mixtures revealed trace amounts of chlorinated species consistent with the loss of chloride from the complexes. The formation of triethylsilyl chloride in reductions with TES may account for the need to utilize more than one equivalent of silane in the reduction. The conditions and product selectivity observed in reactions with the germanium(II) and tin(II) chloride-containing complexes are not consistent with the germanium(II) and tin(II) triflate catalysts. If the chloride was lost or abstracted from $[\text{SnCl}([\mathbf{18}\text{-crown-6})]^+$, for example, similar activity to $[\text{Sn}([\mathbf{18}\text{crown-6})][\text{OTf}]_2$, or lack thereof, would be anticipated as tin(II) centre, $[\text{Sn}([\mathbf{18}\text{crown-6})]^{2+}$, should have identical Lewis acidities. However, significantly higher conversions were observed for $[\text{SnCl}([\mathbf{18}\text{-crown-6})][\text{SnCl}_3]$ compared to $[\text{Sn}([\mathbf{18}\text{crown-6})][\text{OTf}]_2$, (91% at 60 °C and no conversion at 60 °C respectively) which is not consistent with the same Lewis acidic framework. Thus, there must be at least one chloride ligand still on the metal centre. Attempts to further optimize the reaction conditions to improve selectivity or increase the conversion were not successful, and thus, further studies were conducted exclusively on the germanium(II) triflate salt catalysts which showed greater selectivity.



Scheme 4.3 The formation of $[\text{MCl}_2(\text{TEPO})_2]$ ($M = \text{Ge, Sn}$) through chloride displacement.

4.2.3 Optimization of Aldehyde Etherification by $[\text{Ge}([\text{12}]\text{crown-4})_2][\text{OTf}]_2$

Although both $[\text{Ge}([\text{12}]\text{crown-4})_2][\text{OTf}]_2$ and $[\text{Ge}([\text{15}]\text{crown-5})][\text{OTf}]_2$ enabled excellent conversion of 4-methylbenzaldehyde to the symmetric ether **I**, the synthesis of $[\text{Ge}([\text{12}]\text{crown-4})_2][\text{OTf}]_2$ is more reliable and thus was selected for further analyses. Optimization of the reaction conditions for the etherification of 4-methylbenzaldehyde with PMDS catalyzed by $[\text{Ge}([\text{12}]\text{crown-4})_2][\text{OTf}]_2$ revealed that the catalyst loading and reaction time could be lowered to 2.5 mol% and 6 hours, respectively without significant loss in conversion to the symmetric ether (Table 4.3, Entries 1-3). When the reaction was run in an NMR tube in C_6D_6 , the reaction time was similar to the reaction time required for reactions conducted in a vial; however, in an NMR tube with $\text{DCM-}d_2$ as the solvent, the reaction time could be lowered to one hour (Table 4.3, Entry 4). Evidently, the solvent enabled for a faster reaction time, presumably due to increased solubility in the more polar $\text{DCM-}d_2$. For $[\text{Ge}([\text{15}]\text{crown-5})][\text{OTf}]_2$, a decrease in reaction time to six hours gave excellent conversion to **I** (Table 4.3, Entry 6). Due to the more reliable synthesis of $[\text{Ge}([\text{12}]\text{crown-4})_2][\text{OTf}]_2$, this species was selected as the catalyst for further analyses.

Table 4.3 The influence of catalyst loading and time on the etherification of 4-methylbenzaldehyde in the presence of silane catalyzed by germanium(II) triflate complexes.



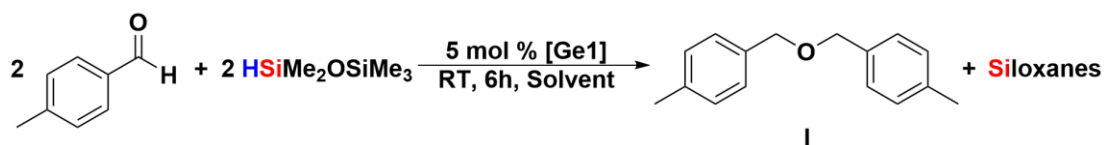
Entry ^a	Catalyst Loading (mol %)	Time (h)	Conversion of I (%)
1	5	24	>98
2	5	6	>98
4	5	1	94
5	1	1	96
6	0.5	1	93
7	0.1	1	17
8	0.01	1	0

^a The [aldehyde] and [silane] was 0.137 M in DCM-*d*₂. Yields were determined by ¹H NMR spectroscopy using mesitylene as an internal standard. Reactions were run in duplicate and conversion values were within ± 2%.

The influence of solvent on the etherification of 4-methylbenzaldehyde with PMDS was then probed using [Ge([12]crown-4)₂][OTf]₂ as the catalyst (Table 4.4). Benzene was initially selected as the solvent due to its similar boiling point to PMDS and low reactivity; however, similar conversion to the symmetric ether **I** was also observed in toluene and DCM (Table 4, Entries 3 & 4). Conversion to the symmetric ether was more than 20% lower when the reaction was performed in hexanes (Table 4.4, Entry 1), presumably due to the decreased solubility of the catalyst. In donating solvents, such as ACN and diethyl ether, a 10-15% decrease in conversion to **I** (Table 4.4, Entries 5 & 6) was observed. The donor numbers (DN)¹⁵ of ACN and ether are higher than those of benzene, toluene and DCM (Table 4.4). Given the high Lewis acidity of the germanium complexes, coordination

of the donor solvents may compete effectively with the aldehyde substrate (DN = 16)¹⁵ or the donor solvent may coordinate to a reaction intermediate along the reaction pathway, evidently decreasing the yield of the reaction.

Table 4.4 The influence of solvent on the yield of **I** in the etherification of 4-methylbenzaldehyde in the presence of silane catalyzed by [Ge([12]crown-4)₂][OTf]₂.



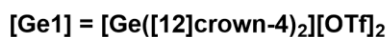
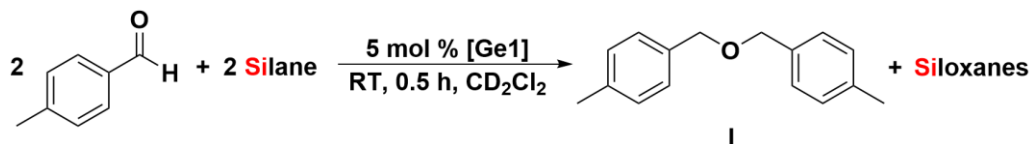
Entry	Solvent	Conversion of I (%)	Donor Number of Solvent (DN) ¹¹
1	Hexanes	77	0
2	Benzene	>98	0.1
3	Toluene	>98	0.1
4	DCM	>98	1.0
5	Diethyl ether	89	19.2
6	ACN	76	14.1

^aThe [aldehyde] and [silane] were 0.150 M. Yields were determined using ¹H NMR spectroscopy using mesitylene as an internal standard. Reactions were run in duplicate and conversion values were within ± 2%.

Although no dependence on the identity of the silane was observed in the reduction of 4-methylbenzaldehyde at RT with 5 mol% [Ge([12]crown-4)₂][OTf]₂ for 24 hours, reducing the time frame of the reaction to 0.5 hours, revealed some differences (Table 4.5). For PMDS, triethylsilane and dimethylphenylsilane, high conversion to the ether **I** was observed after just 0.5 hours. Interestingly, there was no correlation between bond dissociation energies (BDEs) of the Si-H bond of silanes and the degree of conversion. For example, TES and HSi(*i*Pr)₃ are both alkyl silanes and are estimated to have a comparable BDE of approximately 396 kJ/mol;¹⁶ however, at 0.5 hours only 3% conversion to **I** was observed with HSi(*i*Pr)₃ in comparison to a 77% conversion with TES (Table 4.5, Entries 1

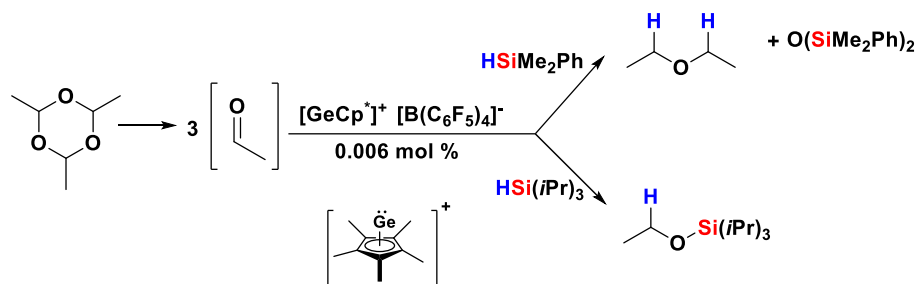
& 5). The BDEs of HSiMe₂Ph and HSiMePh₂ are 377 kJ/mol and 361 kJ/mol (Table 4.5, Entries 3 & 4) respectively, and conversions to **I** using these silanes as reducing agents were 90% and 49%, respectively. The silane with the weakest Si-H bond, HSi(SiMe₃)₃, showed no significant conversion to **I** (Table 4.5, Entry 6). Rather than BDE, increasing the steric bulk about the silicon of the silane appears to correlate more strongly with lower conversions. Between TES and HSi(*i*Pr)₃, HSi(*i*Pr)₃ has more steric bulk around the silicon, making the Si-H less accessible and leading to a decrease in the conversion to **I**. Similarly, with two phenyl substituents in HSiMePh₂, a 50% decrease in conversion to **I** is observed compared to HSiMe₂Ph with only one phenyl group. The steric bulk of the silane was previously shown to influence the identity of the products in the hydrosilylation of paraldehyde using [GeCp*][B(C₆F₄)₄] as a catalyst (Scheme 4.4).⁵ When HSiMe₂Ph was used as the silane source, conversion to the symmetric ether, diethyl ether, was observed. However, when triisopropylsilane was used as the silane, only trace amounts of symmetric ether were formed; the major product was the silyl ether, H₃CH₂COSi(*i*Pr)₃. In the etherification of 4-methylbenzaldehyde using [Ge([12]crown-4)₂][OTf]₂ as a catalyst, bulky silanes give lower conversions as opposed to changing product selectivity.

Table 4.5 The influence of silane on the yield of I in the etherification of 4-methylbenzaldehyde catalyzed by $[\text{Ge}([\text{12}]\text{crown-4})_2][\text{OTf}]_2$.



Entry	Silane ^a	Conversion of I (%)	BDE of Si-H (kJ/mol) ¹⁶
1	$\text{HSiMe}_2\text{OSiMe}_3$	69	391 ^b
2	HSiEt_3	77	396
3	HSiMe_2Ph	90	377
4	HSiMePh_2	49	361
5	$\text{HSi}(i\text{Pr})_3$	3	396 ^c
6	$\text{HSi}(\text{SiMe}_3)_3$	trace	350

^aThe [aldehyde] and [silane] were 0.137 M in 1 mL of $\text{DCM-}d_2$. Conversions were determined by ^1H NMR spectroscopy using mesitylene as an internal standard. ^b BDE for MeOSiH_3 . ^c BDE for HSiEt_3 , another trialkyl silane.



Scheme 4.4 The hydrosilylation of paraldehyde using $[\text{GeCp}^*][\text{B}(\text{C}_6\text{F}_5)_4]$ as a catalyst and either dimethylphenylsilane or triisopropylsilane as the silane source.⁵

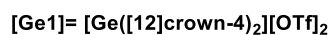
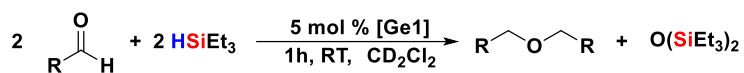
4.2.4 Substrate Scope for Aldehyde Etherification Catalyzed by $[\text{Ge}([\text{12}]\text{crown-4})_2][\text{OTf}]_2$

The scope of aldehyde etherification was probed to evaluate if the catalytic activity of $[\text{Ge}([\text{12}]\text{crown-4})_2][\text{OTf}]_2$ was compatible with aldehydes containing a variety of functional groups (Figure 4.2). The silane source selected for the substrate scope was TES

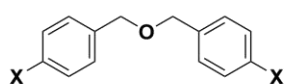
as the ^1H NMR signals associated with the product hexaethyldisiloxane do not overlap with the NMR signals associated with the products. Furthermore, multiple siloxane by-products were observed when PMDS is used as the reducing agent compared to the single product observed with TES.

For the substituted benzaldehydes, electron-withdrawing groups at the *para* position were compatible with the reaction, although lower conversions were observed with the two benzaldehydes substituted with strongly electron-withdrawing substituents, 4-nitrobenzaldehyde (77%) and 4-cyanobenzaldehyde (54%) (Figure 4.2) compared to benzaldehyde (>98%). Notably, significant conversion to the silyl ether was observed with these substrates (~25%), but no silyl ether was present in any other etherifications. No evidence of reduction of either the $-\text{NO}_2$ group or the $-\text{CN}$ group was observed by ^1H NMR spectroscopy. Under the conditions outlined in Figure 4.2, benzaldehydes containing strongly-donating groups with oxygen or nitrogen donor atoms, such as 4-methoxy- or 4-diphenylaminobenzaldehyde, were not tolerated, potentially due to strong coordination to the catalyst through the aldehyde oxygen or coordination to the catalyst through the second donor atom. Surprisingly, reactions of these aldehydes with PMDS under similar conditions proceeded with a low conversion (<30%) to the corresponding symmetric ether. However, with either PMDS or TES, no etherification was observed with 4-dimethylaminobenzaldehyde. These results show that, for some aldehydes, the nature of the silane significantly influences the reaction. Aldehydes containing weak electron-donating groups, such as 4-methylbenzaldehyde, 4-isopropylbenzaldehyde and 4-*tert*-butylbenzaldehyde, gave high conversions to the symmetric ether with TES. For saturated

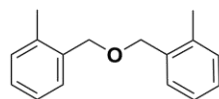
aldehydes, excellent conversions to the symmetric ether were observed. With a bulky substituent direct attached to the aldehyde, such as 1-naphthaldehyde, a lower conversion to the symmetric ether was observed (65%). However,



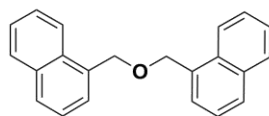
Aromatic Aldehydes



X= H	>98%
Me	94%
Cl	94%
F	97%
iPr	90%
CF ₃	94%
Br	89%
CO ₂ Me	>98%
t-Bu	86%

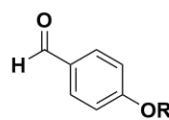


>98 %

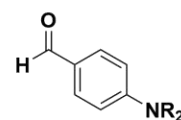


65 %

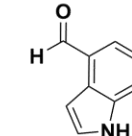
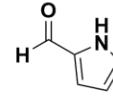
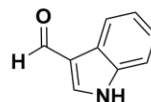
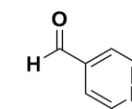
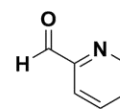
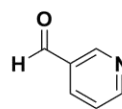
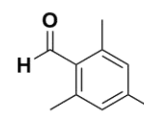
No reaction with



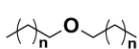
R = Me, Et



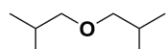
R = Me, Ph



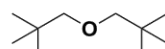
Aliphatic Aldehydes



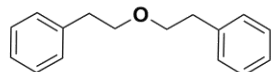
n = 1, 2, 3
all >98 %



>98 %

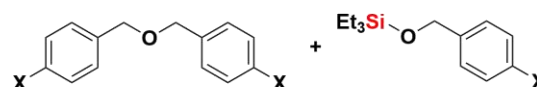


>98 %



90 %

Strong EWG-Substituted Benzaldehydes



X	OR ₂	SiOR	Total Conv.
CN	24%	30%	54%
NO ₂	26%	41%	77%

Figure 4.2 Substrate scope for the etherification of aldehydes with TES catalyzed by [Ge([12]crown-4)₂][OTf]₂. Conversions determined by ¹H NMR spectroscopy. Reactions were run in duplicate and conversion values were within ± 3%

2-methylbenzaldehyde was well tolerated in this reaction despite the methyl substituent *ortho* to the aldehyde. No conversion to any reduced product was observed with 2,4,6-trimethylbenzaldehyde indicating that two methyl substituents *ortho* to the carbonyl significantly hinder reactivity. Similar to the nitrogen-substituted benzaldehydes, the presence of nitrogen-containing heterocycles halted all catalytic activity, again consistent with coordination of the aldehyde to the catalyst, although it is unclear whether the coordination is through the oxygen or nitrogen.

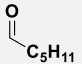
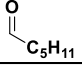
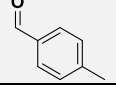
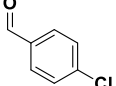
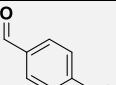
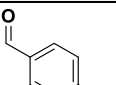
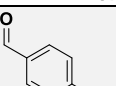
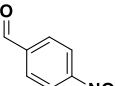
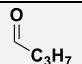
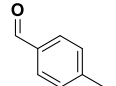
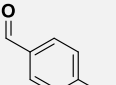
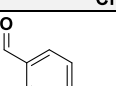
In summary, germanium(II) crown ether triflate salts were found to be highly effective catalysts for the etherification of aldehydes on the basis of conversion and selectivity. $[\text{Ge}([\mathbf{12}]\text{crown-4})_2][\text{OTf}]_2$ was found to be the most effective catalyst and found to be compatible with a number of different functional groups, such as halides and esters, on the aldehyde. However, the reaction was not compatible with functional groups containing strongly electron-donating substituents and nitrogen-containing heterocycles. Etherification by $[\text{Ge}([\mathbf{12}]\text{crown-4})_2][\text{OTf}]_2$ was found to proceed in a number of different solvents, although lower yields in donating solvents suggests coordination of the donor solvent to the catalyst or competition with a substrate or intermediate along the reaction pathway. Lower conversions to ether **I** were observed when sterically bulky silanes, such as tris(trimethylsilyl)silane were used as the reducing agent in comparison to PMDS and TES. The presence of silylated products in reactions catalyzed by the germanium(II) and tin(II) trichlorometallate salts suggests that the silyl ether may be an intermediate in the reaction pathway.

4.2.5 Comparisons of the Performances of Other Main Group Catalysts in Hydrosilylation/Etherification Reactions

One of the challenges in the field of main group catalysis is the large variation in reaction conditions and substrates employed making it difficult to compare the performances of main group catalysts. In general, studies of main group catalysts examine single examples of several different reactions, such as hydrosilylation. The focus is to demonstrate catalytic ability rather than to examine the scope and limitations of any given reaction. Recognizing these limitations, a summary of the reaction conditions, aldehydes and products for a few relevant reactions is provided in Table 4.6 and a comparison to the analogous reactions catalyzed by **[Ge[12]crown-4)₂][OTf)₂** is made.

The preferential formation of the ether over the silyl alcohol may be attributed to the difference in the oxidation number of the central atom: typically M(IV) (M= Si, Ge) complexes, such as silyl(IV) cations or the bis(catecholato)silane and -germane complexes (Si(IV) and Ge(IV) respectively), yield the silyl ether,¹⁸⁻²⁰ while the M(II) complexes favor the formation of the symmetric ether. The hydrosilylation of hexanal by the silicon(II) and germanium(II) complexes **[MCp^{*}][B(C₆F₅)₄]**,⁵ resulted in excellent conversions to the symmetric ether (>95 %) at catalyst loadings of 0.005 and 0.006 mol % in less than an hour, respectively (Table 4.6, Entries 1 & 2). Similar conversion to the symmetric ether in the etherification of butanal was achieved by **[Ge([12]crown-4)₂][OTf)₂** (>98 %); however, a higher catalyst loading (5 mol %) and a slightly longer reaction time (1 hour) are required (Table 4.6, Entry 9). The mechanism of reaction for the hydrosilylation of aldehyde catalyzed by **[GeCp^{*}][B(C₆F₅)₄]** or **[SiCp^{*}][B(C₆F₅)₄]** was proposed to occur through a

Table 4.6 Summary of aldehyde reduction using silanes as the reducing agent catalyzed by main group catalysts.

Entry	Catalyst	Aldehyde	Silane	Time (h)	Catalyst Loading (mol %)	Aldehyde-Derived Product	Conversion (%)
1	[SiCp*][B(C ₆ F ₅) ₄] ^a		TES	0.3	0.005	Symmetric Ether	96 ⁵
2	[GeCp*][B(C ₆ F ₅) ₄] ^a		TES	0.5	0.06	Symmetric Ether	>95 ⁵
3	B(C ₆ F ₅) ₃ ^b		HSiPh ₃	~10 ^c	2	Silyl Ether	82 ¹¹
4	B(C ₆ F ₅) ₃		HSiPh ₃	~3.5 ^c	2	Silyl Ether	81 ¹¹
5	B(C ₆ F ₅) ₃		HSiPh ₃	~0.2 ^c	2	Silyl Ether	96 ¹¹
6	[Si(cat ^F) ₂] ^b		TES	0.5	5	Silyl Ether	92 ^{18a}
7	[Si(cat ^F) ₂]		HSi <i>i</i> Pr ₃	0.5	5	Silyl Ether	>95 ^{18a}
8	[Ge(cat ^{Cl}) ₂][ACN] ₂ ^d		TES	24	5	Silyl Ether	>97 ¹⁹
9	[Ge1] ^e		TES	1	5	Symmetric Ether	>98
10	[Ge1]		TES	1	0.5	Symmetric Ether	93
11	[Ge1]		TES	1	5	Symmetric Ether	94
12	[Ge1]		TES	1	5	Symmetric Ether	53

^a No aromatic aldehydes investigated. ^b No alkyl aldehydes investigated. ^c Time estimated from TOF provided. ^d No linear alkyl aldehydes investigated. ^e [Ge1] = [Ge([12]crown-4)₂][OTf]₂.

carbonyl-activated pathway;⁵ however, no direct evidence of carbonyl-coordination was provided. The coordination of dimethoxyethane to $[\text{SiCp}^*][\text{B}(\text{C}_6\text{F}_5)_4]$ has been previously documented.¹⁷

$\text{B}(\text{C}_6\text{F}_5)_3$ is a well-known, effective Lewis acid catalyst and is often used as a comparator for new main group catalysts. In the hydrosilylation of 4-methylbenzaldehyde, $\text{B}(\text{C}_6\text{F}_5)_3$ required 10 hours to achieve an 82 % conversion to the silyl ether using HSiPh_3 at a catalyst loading of 2 mol% (Table 4.6, Entry 3).¹¹ In comparison to $[\text{Ge}([\mathbf{12}]\text{crown-4})_2][\text{OTf}]_2$, a significantly lower reaction time (1 hour) was required to achieve 94% conversion to the symmetric ether at a lower catalysts loading of 0.5 mol% (Table 4.6, Entry 10). $\text{B}(\text{C}_6\text{F}_5)_3$ was shown to proceed through a silane-activated hydrosilylation pathway and a decrease in reaction rate was observed with benzaldehydes containing electron-donating groups, such as methyl. The rate of silyl ether formation catalyzed by $\text{B}(\text{C}_6\text{F}_5)_3$ increased significantly with benzaldehydes with electron-withdrawing substituents as seen with a decrease in reaction time to achieve the same conversion percentage. The hydrosilylation of 4-nitrobenzaldehyde by $\text{B}(\text{C}_6\text{F}_5)_3$ was extremely efficient, requiring less than 10 minutes to achieve 96% conversion to the silyl ether (Table 4.6, Entries 5). The reduction of 4-nitrobenzaldehyde by $[\text{Ge}([\mathbf{12}]\text{crown-4})_2][\text{OTf}]_2$ achieved only a 53% conversion requiring a longer reaction time (Table 4.6, Entry 12), significantly worse than catalysis by $\text{B}(\text{C}_6\text{F}_5)_3$. However, $[\text{Ge}([\mathbf{12}]\text{crown-4})_2][\text{OTf}]_2$ was more effective in the reduction of 4-chlorobenzaldehyde compared to $\text{B}(\text{C}_6\text{F}_5)_3$ (Table 4.6, Entries 4 and 11).

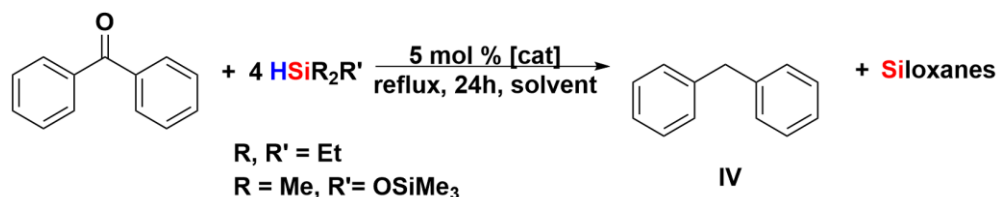
Bis(catecholato)silanes^{18,19} and -germanes,²⁰ neutral Group 14 complexes, have also been shown to efficiently catalyze the hydrosilylation of benzaldehydes containing electron-withdrawing substituents. Bis(tetrafluorocatecholato)silane achieved >95% conversion to the silyl ether in the catalytic hydrosilylation of 4-chlorobenzaldehyde in under an hour at 5 mol% catalyst (Table 4.6, Entry 6),^{18a} comparable to the results with **[Ge([12]crown-4)₂][OTf]₂** (Table 4.6, Entry 11). However, the hydrosilylation reaction using **[Si(cat^F)₂]** was not compatible with benzaldehydes containing electron-donating substituents and saturated aldehydes were not investigated. When the bulk of the silane was changed in reactions using **[Si(cat^F)₂]**, no influence on conversion to the silyl ether was observed; even with triisopropylsilane >95% conversion was achieved (Table 4.6, Entry 7). Negligible conversion to any reduced products were observed when HSi(*i*Pr)₃ was used as the silane and **[Ge([12]crown-4)₂][OTf]₂** was used as a catalyst in the etherification of 4-methylbenzaldehyde (Table 4.5, Entry 5). The hydrosilylation of benzaldehydes containing electron-withdrawing substituents was also observed using bis(tetrachlorocatecholato)-germane as a catalyst; however, the reactions took 24 hours at 5 mol % (Table 4.6, Entry 8).²⁰

4.3 Ketone Reduction

4.3.1 Ketone Reduction Catalyzed by Group 14 Crown Ether Triflate Salts

With the success of the reduction of aldehydes using the germanium(II) crown ether triflates salts, the hydrosilylation of ketones was then attempted. The hydrosilylation of benzophenone was selected as the benchmark reaction to screen the catalysts using both

TES and PMDS as the reducing agents (Table 4.7). Surprisingly, rather than the formation of the symmetric ether, the formation of diphenylmethane was observed, even with 1 equivalent or substoichiometric amounts of silane. Conversion to the fully-reduced product has been previously observed in ketone hydrosilylation with catalysts such as bis(pertrifluoromethylcatecholato)silane^{18b} and $[P(C_6F_5)_3(OC_6F_5)][B(C_6F_5)_3]$.²¹ On occasion, trace amounts of the symmetric ether were also observed in the reactions catalyzed by germanium(II) triflate salts, which suggests that this species may be an intermediate along the reaction path to form diphenylmethane. Significantly lower conversion to reduced species was observed with benzophenone (Table 4.7, Entries 1-6) compared to reductions to the symmetric ether with 4-methylbenzaldehyde using the same germanium(II) complexes (Table 4.1, Entries 1-6). The decrease in conversion for 1-naphthaldehyde (65%) and mesitylaldehyde (0%) compared to 4-methylbenzaldehyde (94%) highlights the influence of the steric bulk of the substituents in the reduction of aldehydes, and thus, it is probable that the additional phenyl group in benzophenone prevents facile reduction.

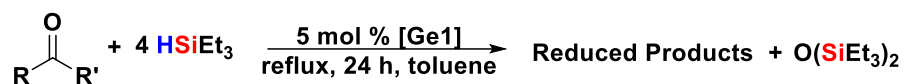
Table 4.7 Aldehyde reduction catalyzed by germanium(II) and tin(II) triflate salts.

Entry ^a	Catalyst	Silane	Yield of IV (%) ^b
1	[Ge([12]-crown-4) ₂][OTf] ₂	PMDS	14
2		TES	5
3	[Ge([15]-crown-5)][OTf] ₂	PMDS	22
4		TES	38
5	[Ge([18]-crown-6)][OTf] ₂	PMDS	22
6		TES	22
7	[Sn([12]-crown-4) ₂][OTf] ₂	PMDS	No conversion
8		TES	No conversion
9	[Sn([15]-crown-5) ₂][OTf] ₂	PMDS	No conversion
10		TES	No conversion
11	[Sn([18]-crown-6)][OTf] ₂	PMDS	No conversion
12		TES	No conversion
13	-	PMDS	No conversion
14		TES	No conversion

^a Reactions with PMDS were conducted in benzene and reactions with TES were conducted in toluene. ^bThe [ketone] and [silane] was 0.150 M. Yields were determined by ¹H NMR spectroscopy using mesitylene as an internal standard.

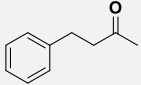
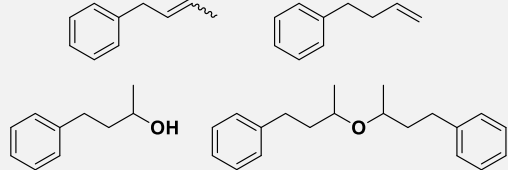
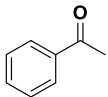
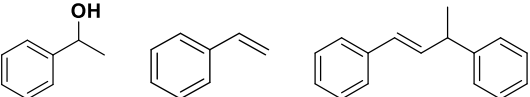
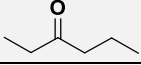
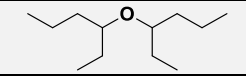
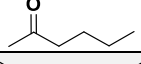
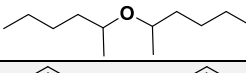
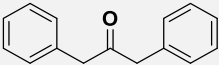
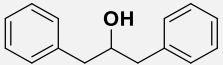
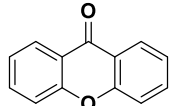
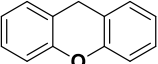
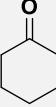
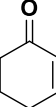
A limited number of substrates for the reduction of ketones was examined; low conversions were observed for all reactions (<30%). Depending on the substituents on the ketone, different reduction products were observed (Table 4.8). For 4-phenyl-2-butanone (Table 4.8, Entry 1), both the alcohol and symmetric ether were observed as well as three alkenes. The alkenes were identified by GC-MS and appear to be products of deoxygenation of the ether or alcohol; dehydration of alcohols has been previously documented for some Lewis acids, such as B(C₆F₅)₃²² and Ga(OTf)₃.²³ Reduction of acetophenone resulted in the formation of two unsaturated species, styrene and one dimer of styrene as well as the alcohol (Table 4.8, Entry 2). No unsaturated products were

Table 4.8 Ketone reduction catalyzed by [Ge([12]crown-4)₂][OTf]₂.



[Ge1] = [Ge([12]crown-4)₂][OTf]₂

Conversions to reduced products are <30%

Entry	Ketone	Product Mixture
1		
2		
3		
4		
5		
6		
7		No reduced product
8		No reduced product

^a Reactions with TES were conducted in benzene and reactions with TES were conducted in toluene. ^bThe [ketone] and [silane] was 0.150 M.

observed in reductions of 2-pentanone or 3-pentanone (Table 4.8, Entries 3 & 4) which only formed the ether; it is unclear why a mixture of products was observed for 4-phenyl-2-butanone and acetophenone. Perhaps the presence of both a methyl ketone and an aromatic ring in the molecule enables dehydration. Reduction of 1,3-diphenyl-2-propanone resulted

in the exclusive formation of the alcohol (Table 4.8, Entry 5). As the alcohol can be converted to the ether through dehydrative coupling, perhaps a longer reaction time would have favored the ether. Xanthone was reduced to the 1H-xanthene similar to the reduction of benzophenone to diphenylmethane suggesting the adjacent phenyl ring may make the reduction from the alcohol/ether to the alkane more favorable (Table 4.8, Entry 6). Surprisingly, no evidence of reduction was observed for either cyclohexanone or 2-cyclohexenone. The justification for the absence of reactivity with these substrates is not immediately clear. Given the mixtures of products and low conversions, further studies into the reductions of ketones were not performed.

The hydrosilylation of ketones has been achieved using a variety of main group catalysts. For the hydrosilylation of acetophenones by $B(C_6F_5)_3$ using $HSiPh_3$ as the reducing agent, higher conversion was observed for 4'-methyl-acetophenone compared to 4-methylbenzaldehyde.¹¹ The opposite is observed in the analogous reactions using $[Ge([12]crown-4)_2][OTf]_2$ as a catalyst where high conversions for aldehydes was observed compared to ketones. The hydrosilylation of cyclobutanone catalyzed by $[GeCp^*][B(C_6F_5)_4]$ using TES gave >90% conversion to the symmetric ether; however, an elevated temperature (45 °C) and longer reaction time (15 hours) was required for the reduction of cyclobutanone to achieve comparable yields to the reduction of aldehydes (Table 4.6, Entry 2).⁵ Furthermore, the hydrosilylation of 2-butanone with TES catalyzed by $[SiCp^*][B(C_6F_5)_4]$, yielded 79% of the symmetric ether in contrast to the 96-98% conversions achieved for saturated aldehydes. These two examples illustrate that ketone activation is more challenging for the M(II) catalysts in comparison to the aldehydes,

consistent with the results observed for $[\text{Ge}([\mathbf{12}]\text{crown-4})_2][\text{OTf}]_2$. Carbonyl deoxygenation in the hydrosilylation of acetophenone was facilitated by bis(pertrifluoromethylcatecholato)silane achieving 80% conversion after 3 days at 100 °C.^{18b} When the substrate was benzophenone, the reaction yielded diphenylmethane in a 99% yield at room temperature and after only 0.5 hours illustrating the difference in the reactivity of benzophenone in comparison to acetophenone using the bis(catecholato)silanes as catalysts. The formation of cyclohexene was observed in the catalytic deoxygenative hydrosilylation of cyclohexanone catalyzed by bis(pertrifluoromethylcatecholato)silane;^{18b} the formation of alkene is similar to the reduction of 4-phenyl-2-butanone which gave alkene products as well.

In summary, the reduction of ketones was achieved by the germanium(II) crown ether triflate complexes; however, the reaction was not very efficient, achieving less than 30% conversion for any ketone tested. Trace formation of the symmetric ether during the hydrosilylation of benzophenone may indicate a stepwise reduction from the ketone to first form the symmetric ether, followed by another reduction to yield diphenylmethane. As the conditions could not be optimized to give good yields of any reduced product, no further studies into ketone reduction were conducted.

4.4 Preliminary Mechanistic Studies into Aldehyde Hydrosilylation by $[\text{Ge}([\mathbf{12}]\text{crown-4})_2][\text{OTf}]_2$

4.4.1 Etherification of Silyl Ether **IIb**

The reduction of aldehydes is catalyzed by cationic germanium(II) crown ether triflate salts, however, there are a number of unanswered questions regarding the

mechanism of the reaction and whether a hydrosilylation reaction occurs. Although trace amounts of the silyl ether **IIb** were observed in the reduction of 4-methylbenzaldehyde by tin(II) triflates, exclusive formation of the symmetric ether **I** was observed with the analogous germanium(II) complexes. To provide evidence for the intermediacy of silyl ether **II** in reactions catalyzed by $[\text{Ge}([\text{12}]\text{crown-4})_2][\text{OTf}]_2$, **IIb** was synthesized independently and added to a catalytic amount of $[\text{Ge}([\text{12}]\text{crown-4})_2][\text{OTf}]_2$. Complete conversion to **I** was observed (Scheme 4.5). As $[\text{Ge}([\text{12}]\text{crown-4})_2][\text{OTf}]_2$ can facilitate the transformation from a silyl ether to a symmetric ether, the silyl ether is a reasonable intermediate along the reaction pathway. From this evidence, it can be concluded that the mechanism of reaction is consistent with an initial hydrosilylation step.

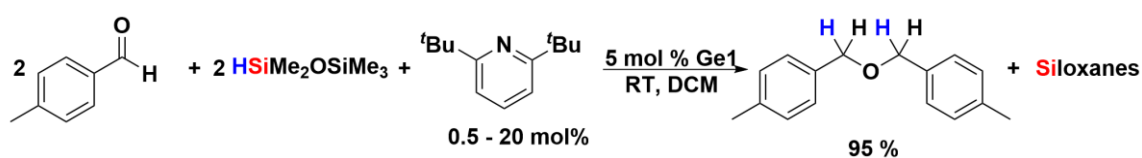


Scheme 4.5 Conversion of 4-methylbenzyl triethylsilyl ether to 1,1'-[oxybis(methylene)]bis[4-methylbenzene] in the presence of $[\text{Ge}([\text{12}]\text{crown-4})_2][\text{OTf}]_2$.

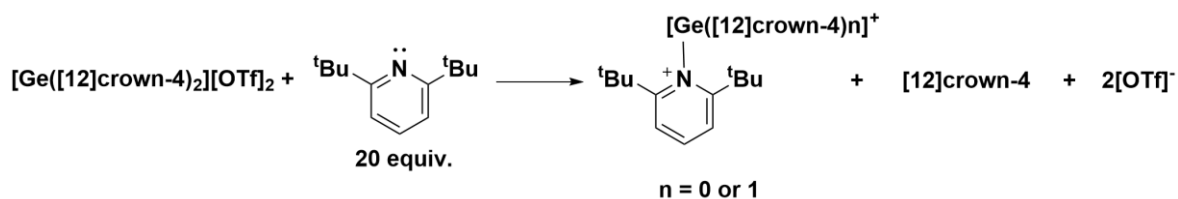
4.4.2 Ruling out Brønsted Acid Catalysis in the Etherification of Aldehydes by $[\text{Ge}([\text{12}]\text{crown-4})_2][\text{OTf}]_2$

Brønsted acid catalysis is analogous to Lewis acid catalysis and produces similar products. Thus, it is critical to rule out Brønsted acid catalysis in the etherification of aldehydes using germanium(II) catalysts. One method to rule out Brønsted acid catalysis involves the sequestering of protons in solution with a bulky base preventing Brønsted acid catalysis. When 2,6-di-tert-butylpyridine was added (0.1-4 equivalents relative to

$[\text{Ge}([\text{12}]\text{crown-4})_2][\text{OTf}]_2$ to a mixture of 4-methylbenzaldehyde, PMDS and a catalytic amount of $[\text{Ge}([\text{12}]\text{crown-4})_2][\text{OTf}]_2$, the yield and selectivity of the product was unchanged (Scheme 4.5), consistent with catalysis derived from $[\text{Ge}([\text{12}]\text{crown-4})_2][\text{OTf}]_2$ and not Brønsted acid catalysis. When the concentration of 2,6-di-*tert*-butylpyridine was increased to the same concentration as 4-methylbenzaldehyde, no ether formation was observed. As the crown ether in $[\text{Ge}([\text{12}]\text{crown-4})_2][\text{OTf}]_2$ can be displaced by a Lewis base, as seen previously with TEPO,⁵ coordination of 2,6-di-*tert*-butylpyridine may have occurred at high concentrations of pyridine, quenching the reactivity of the catalyst (Scheme 4.7).



Scheme 4.6 Etherification of 4-methylbenzaldehyde with PMDS in the presence of 2,6-di-*tert*-butylpyridine. Mole percent is relative to the aldehyde concentration.



Scheme 4.7 Proposed coordination of 2,6-di-*tert*-butylpyridine to $[\text{Ge}([\text{12}]\text{crown-4})_2][\text{OTf}]_2$.

4.4.3 Ruling out Silyl Cation Catalysis in the Etherification of Aldehydes by **[Ge([12]crown-4)₂][OTf]₂**

Another potential catalytic agent in the hydrosilylation reactions is a silyl cation. If a silyl(IV) cation, such as SiEt_3^+ is generated during hydrosilylation reactions with TES, the silyl cation could compete with **[Ge([12]crown-4)₂][OTf]₂** to catalyze the reaction. No direct evidence of a silyl cation was found in the reaction of 4-methylbenzaldehyde and TES or PMDS by ^1H NMR or ^{29}Si NMR spectroscopy. Furthermore, a comparison of the reactivity of SiEt_3^+ to the observed reactivity when **[Ge([12]crown-4)₂][OTf]₂** is used as a catalyst provides indirect evidence in support of a germanium-catalyzed reaction. When Me_3SiOTf (10 mol%) is used as the hydrosilylation catalyst and TES as the reducing agent, aldehydes and ketones are converted into the corresponding symmetric ether within minutes.²⁴ In contrast, when using **[Ge([12]crown-4)₂][OTf]₂** in a catalytic amount, low conversions were obtained when ketones were used as the carbonyl substrate (Table 4.7 Entries 1-5). Most notably, when Me_3SiOTf is used as a catalyst, quantitative conversion to the corresponding symmetric ether is observed with cyclohexanone as a substrate and a mixture of products with cyclohexenone was observed when the unsaturated ketone was used as a substrate.²⁴ In analogous reactions using **[Ge([12]crown-4)₂][OTf]₂** as a catalyst, no conversion to any reduced products was observed for these two ketones (Table 4.8, Entries 6 & 7), even at elevated temperatures and longer reaction times. If SiEt_3^+ was generated throughout the course in the reductions using **[Ge([12]crown-4)₂][OTf]₂** as a catalyst and cyclohexanone or cyclohexenone and able to compete with **[Ge([12]crown-4)₂][OTf]₂** catalytically, then the formation of some reduced product would be expected. Furthermore, aryl aldimine reduction has been reported using $[\text{SiMe}_3]^+$

*t*Bu(ferrocenyl)][B(C₆F₅)₄] as the catalyst, achieving 40-90% conversion to the corresponding amine.²⁵ In similar reactions using [Ge(**12**crown-**4**)₂][OTf]₂ as a catalyst, no imine reduction was observed, even at elevated temperatures and longer reaction times.

4.5 Summary and Conclusions

In summary, the reduction of aldehydes and ketones was probed using a series of germanium(II) and tin(II) complexes as catalysts in the presence of silane. The crown ether-stabilized germanium(II) triflate salts were found to be efficient in the reduction of aldehydes to symmetric ethers, while the tin(II) triflate salts were not effective. The trichlorometallate salts of germanium(II) and tin(II) were also found to facilitate the reduction of aldehydes; however, under different reaction conditions and a mixture of reduced products was formed. Low conversions were observed for ketones, with only the germanium(II) triflate complexes showing any reactivity towards these substrates. With the success of the germanium(II) triflate complexes as catalysts in the reduction of aldehydes, the mechanism of this reaction will be explored. Preliminary mechanistic studies demonstrated that etherification of aldehyde proceeds through an initial hydrosilylation step. Catalytic activity was found to be exclusively derived from [Ge(**12**crown-**4**)₂][OTf]₂ and not a Brønsted acid or a silyl cation. With the success of the cationic germanium(II) complexes as Lewis acid catalysts demonstrated in this study, the potential for cationic germanium complexes in the field of Lewis acid catalysis has been highlighted and will hopefully inspire future work in the area of cationic Group 14 complexes.

4.6 Experimental

4.6.1 General Experimental

All manipulations were performed under an inert atmosphere of argon using Schlenk techniques or under an atmosphere of nitrogen in an MBraun glovebox. Solvents were purified using an Innovative Technologies 400-5 Solvent Purification System and were stored over activated 4 Å molecular sieves or 3 Å molecular sieves for ACN. All NMR solvents were dried over activated 4 Å molecular sieves. Chemicals purchased from commercial sources were used without further purification.

GeCl_2 ·dioxane,²⁶ germanium(II) crown ether complexes^{8b} and tin(II) crown ether complexes^{8c} were synthesized according to literature procedures. The procedures for the synthesis of **[GeCl₂·dibenzo[18]crown-6]**, **[SnCl(dibenzo[18]crown-6)][SnCl₃]** and **[SnCl(benzo[15]crown-5)][SnCl₃]** are described in Chapter 2.

NMR spectra were recorded on an Inova 600 MHz NMR spectrometer or Bruker Avance III 400 MHz NMR spectrometer. The NMR standards used were as follows: ¹H NMR spectra were referenced to residual CH_2Cl_2 (5.32 ppm), CHCl_3 (7.27 ppm), $\text{C}_6\text{D}_5\text{H}$ (7.16 ppm) or CD_2HCN (1.94 ppm). A relaxation time of 10 seconds was used for all ¹H NMR spectra acquired. Gas chromatography– mass spectra were obtained on a Shimadzu GCMS-QP2010 instrument with a GC-2010 gas chromatograph at an ionizing voltage of 70 eV (EI), with a quadrupole mass filter, and a DB-5MS 30 m x 0.25 μm column from J & W Scientific and used to confirm the identity of some products.

Liquid reagents were dispensed using a micropipette. Calibration of the pipette was attempted; however, many reagents were found to be highly viscous and delivered

inconsistent amounts upon repeat measurements. Mesitylene was used as the internal standard and was found to pipette a consistent volume (with less than 5% deviation by mass), and thus, was used as an absolute reference of molar quantity in all experiments.

Conversion was determined using a known amount of mesitylene which was added to the NMR tube prior to the acquisition of the ^1H NMR spectrum for all reactions. From the ^1H NMR spectrum, the relative integrations of the residual aldehyde/ketone, symmetric ether, silyl ether or alcohol were used to calculate the total molar amount of aldehyde/ketone at the beginning of the reaction (t_0). The quotient of the molar amount of the reduced species (symmetric ether, silyl ether and alcohol) and the total molar amount of aldehyde/ketone at t_0 was taken and multiplied by 100 to get the percent conversion. Reactions were conducted in duplicate and the average conversion is reported.

4.6.2 General Catalytic Methods for the Etherification of Aldehydes

4.6.2.1 Method 1 (Tables 4.1 - 4.4)

To a 20 mL screw-cap vial with a magnetic stir bar, catalyst (0, 0.013 mmol or 0.022 mmol), 4-methylbenzaldehyde (1000 μL from a 0.450 M stock solution) and silane (1000 μL from either a 0.450 M or 0.900 M solution) were added. Solvent (1000 μL), as specified in the Tables, was added to vial and the vial was sealed with electrical tape. The solution was stirred and heated at the temperature specified in the Tables for 24 hours. The solution was then exposed to air and the solvent was removed under vacuum. CDCl_3 (~0.5 mL) was added directly to oily residue and the resulting solution was added to an NMR tube. Mesitylene (10.0 μL 0.0719 mmol) was directly to the NMR tube and the ^1H NMR

spectrum was acquired. In reactions utilizing **[Sn(benzo[15]crown-5)][SnCl₃]**, **[Sn(dibenzo[18]crown-6)][SnCl₃]**, and **[GeCl₂·dibenzo[18]crown-6]**, complete dissolution of the catalyst was not observed.

4.6.2.2 Method 2 (Table 4.5 and Figure 2)

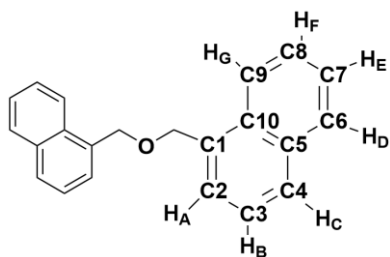
To an NMR tube, **[Ge([12]crown-4)₂][OTf]₂** (200 μ L of a 0.0345 M stock solution in DCM-*d*₂), aldehyde (0.136 μ L), mesitylene (10.0 μ L 0.0719 mmol) and silane (0.137 mmol) were added. DCM-*d*₂ was added to the NMR tube such that the total volume was 1 mL. The NMR tube was sealed with a cap and Teflon tape. The ¹H NMR spectrum was acquired after 30 minutes or 1 hour, as indicated in the Table or Figure.

4.6.3 General Catalytic Method for the Reduction of Ketones (Tables 4.7 & 4.8)

To a 20 mL screw-cap vial with a magnetic stir bar, catalyst (0 or 0.022 mmol), ketone (0.45 mmol) and triethylsilane (1000 μ L from a 0.900 M solution in toluene) were added. Toluene (1000 μ L) was added to the vial and the vial was then sealed with electrical tape. The solution was heated to 90 °C for 24 hours. For ketones with aryl substituents, the solvent was removed and CDCl₃ (~0.5 mL) was added directly to oily residue. Mesitylene (10.0 μ L 0.0719 mmol) was added directly to the NMR tube and the ¹H NMR spectrum was acquired. For alkyl ketones, the solvent could not be removed due to the volatility of the ketone and products, and thus, the solutions were analyzed by GC-MS to elucidate the products. From the GC-MS traces, it was estimated that less than 30% of the ketone was converted to reduced products.

4.6.4 NMR Data for Synthesized Compounds

^1H and/or $^{13}\text{C}\{^1\text{H}\}$ NMR data has been previously reported for a number of products synthesized and are in agreement with the ^1H NMR data obtained in the experiments described in this Chapter: bis(diphenylmethyl) ether,²⁷ 1'-[oxybis(methylene)]bis[4-methoxy-benzene],²⁷ 1,1'-[oxybis(methylene)]bis[4-methyl-benzene],²⁸ 1,1'-[oxybis(methylene)]bis[4-chloro-benzene],²⁹ 1,1'-[oxybis(methylene)]bis[4-nitro-benzene],³⁰ 1,1'-[oxybis(methylene)]bis[4-fluoro-benzene],³¹ 1,1'-[oxybis(methylene)]bis[4-cyano-benzene],³⁰ 1,1'-[oxybis(methylene)]bis[4-isopropyl-benzene],³² 1,1'-[oxybis(methylene)]bis[4-trifluoromethyl-benzene],³³ 1,1'-[oxybis(methylene)]bis[4-bromo-benzene],³⁴ 1,1'-[oxybis(methylene)]bis[4-*tert*-butyl-benzene],³⁴ 1,1'-dimethyl 4,4'-[oxybis(methylene)]bis[benzoate],³⁴ dipropyl ether,³⁵ dibutyl ether,³⁴ bis(2-phenylethyl) ether,³⁴ 1,1'-[oxybis(methylene)]bis[2-methyl-benzene],³⁴ 2,2'-difurfuryl ether,³⁶ triethyl((4-methylbenzyl)oxy)silane,¹³ 4-methylbenzyl alcohol,³⁷ 1,1,1,3,3-pentamethyl-4-[(4-methylphenyl)methyl]-disiloxane,³⁸ diphenylmethane,³⁹ xanthene⁴⁰ 1,1'-[oxybis(3-methyl-3,1-propanediyl)]bis-benzene,⁴¹ 1,3-diphenyl-2-propanol,⁴² bis(2-hexyl) ether,⁴³ triethyl((4-nitrobenzyl)oxy)silane,³⁴ E/Z-2-butenylbenzene,⁴⁴ 3-butenylbenzene,⁴⁵ 4-phenyl-2-butanol,⁴⁶ diisobutyl ether,⁴⁷ dineopentyl ether⁴⁸ and dipentyl ether.⁴⁹



^1H NMR (400 MHz, CDCl_3) 8.09-8.11 (m, 2H, H_G), 7.88 (dd, 2H, $^3J = 7$ Hz, $^3J = 8$ Hz, H_D), 7.83 (d, 2H, $^3J = 8$ Hz, H_C), 7.54 (d, 2H, $^3J = 7$ Hz, H_A), 7.43-7.52 (m, 6H, H_B , H_E , H_F), 5.07 (s, 4H, OCH_2); $^{13}\text{C}\{^1\text{H}\}$ (101 MHz, CDCl_3)

133.94 (C₅), 133.82 (C₁₀), 131.99 (C₁), 128.85 (C₄), 128.64 (C₆), 126.91 (C₂), 126.29 (C₇), 125.93 , 125.34, 124.36 (C₉).

4.6.5 Conversion of Silyl Ether **IIb** to Symmetric Ether **I**

4.6.5.1 Conversion in the Presence of **[Ge([12]crown-4)₂][OTf]₂**

B(C₆F₅)₃ (11 mg, 0.0225 mmol) was added to a 20 mL vial with a magnetic stir bar and dissolved in DCM (1000 μL). 4-methylbenzaldehyde (1000 μL from a 0.450 M stock solution in DCM) and triethylsilane (1000 μL from a 0.450 M stock solution in DCM) were added to the vial and the solution was allowed to stir for 6 hours. An aliquot of the reaction mixture was dried under vacuum and a ¹H NMR spectrum was acquired, confirming the quantitative formation of silyl ether **IIb**.⁹ **[Ge([12]crown-4)₂][OTf]₂** (16 mg, 0.0225 mmol) was then added to the reaction mixture in the vial and the reaction was stirred for 12 hours. After 12 hours, the solvent was removed under vacuum. The NMR tube was sealed with a cap and Teflon tape. The ¹H NMR spectrum was acquired immediately, and then again after 1 hour.

4.6.5.2 Conversion in the Absence of **[Ge([12]crown-4)₂][OTf]₂**

The silyl ether was generated according to the above procedure. The mixture was allowed to stir for an additional 3 days without the addition of **[Ge([12]crown-4)₂][OTf]₂**, after which the solvent was removed under vacuum and C₆D₆ was added. No conversion to the symmetric ether was noted by ¹H NMR spectroscopy.

4.6.6 Test for Brønsted Acid Catalysis

4.6.6.1 Test for the Presence of Brønsted Acid in **[Ge([12]crown-4)₂][OTf]₂**

[Ge([12]crown-4)₂][OTf]₂ (34 mg, 0.0463 mmol) and 2,6-di-*tert*-butylpyridine (10 μL, 0.0463 mmol) were added to an NMR tube. DCM-*d*₂ (~0.5 mL) was added and the NMR tube which was then sealed with a cap and Teflon tape. The ¹H NMR spectrum was acquired immediately, and then again after 1 hour.

4.6.6.2 Test for the Presence of Brønsted Acid in 4-methylbenzaldehyde or Triethylsilane

4-methylbenzaldehyde (10 μL, 0.0848 mmol) or triethylsilane (10 μL, 0.0624 mmol) was added to DCM-*d*₂ (~0.5 mL). 2,6-di-*tert*-butylpyridine (0.0848 mmol or 0.0624 mmol) was added to the solution. The NMR tube was sealed with a cap and Teflon tape. The ¹H NMR spectrum was acquired immediately, and then again after 1 hour.

4.6.6.3 Test for Brønsted Acid Catalysis

To an NMR tube, **[Ge([12]crown-4)₂][OTf]₂** (200 μL of a 0.0345 M stock solution in DCM-*d*₂), mesitylene (10 μL, 0.072 mmol), 4-methylbenzaldehyde (0.136 mmol) and triethylsilane (0.137 mmol) were added. In 4 different experiments, 0.1, 0.5, 1, 2 and 4 equivalents of 2,6-di-*tert*-butylpyridine (0.00069 mmol- 0.0276 mmol) was added to the mixture. DCM-*d*₂ was then added such that the total volume of solution was 1 mL. The NMR tube was then sealed with a cap and Teflon tape. The ¹H NMR spectrum was acquired after 1 hour.

4.7 References

- [1] Corma, A.; Garcia, H. *Chem. Rev.*, **2003**, *103*, 4307-4366.
- [2] Power, P. P. *Nature*, **2010**, *463*, 171-177.
- [3] Lewis, L. N.; Stein, J.; Gao, Y.; Colborn, R. E.; Hutchins, G. *Platinum Metals Rev.*, **1997**, *41*, 66-75.
- [4] Fritz-Langhals, E. *Org. Process Res. Dev.*, **2019**, *23*, 2369–2377.
- [5] Fritz-Langhals, E. ; Werge, S.; Kneissl, S.; Piroutek, P. *Org. Process Res. Dev.*, **2020**, *24*, 1484–1495.
- [6] Sinhababu, S.; Singh, D.; Sharma, M. K.; Siwatch, R. K.; Mahawar, P.; Nagendran, S. *Dalton Trans.*, **2019**, *48*, 4094-4100.
- [7] a) Hadlington, T. J.; Hermann, M.; Frenking, G.; Jones, C. *J. Am. Chem. Soc.*, **2014**, *136*, 3028-3031. b) Hadlington, T. J.; Kefadlidis, C. E.; Maron, L.; Jones, C. *ACS Catal.*, **2017**, *7*, 1853–1859. c) Barman, M. K.; Baishya, A.; Peddaraao, T.; Nembenna, S. *J. Organomet. Chem.*, **2014**, *772*, 265-270. d) Dasgupta, R.; Das, S.; Hiwase, S.; Pati, S. K.; Khan, S. *Organometallics*, **2019**, *38*, 1429–1435. e) Arsenyeva, K. V.; Pashanova, K. I.; Trofimova, O. Y.; Ershova, I. V.; Chegerev, M. G.; Starikova, A. A.; Cherkasov, A. V.; Syroeshkin, M. A.; Kozmenkova, A. Y.; Piskunov, A. V. *New J. Chem.*, **2021**, *45*, 11758-11767.
- [8] a) Drew, M. G. B.; Nicholson, D. G. *J. Chem. Soc., Dalton Trans.*, **1986**, 1543-1549. b) Rupa, P. A.; Bandyopadhyay, R.; Cooper, B. F. T.; Stinchombe, M. R.; Ragogna, P. J.; Macdonald, C. L. B.; Baines, K. M. *Angew. Chem. Int. Ed.*, **2009**, *48*, 5155-5158. c)

- Bandyopadhyay, R.; Cooper, B. F. T.; Rossini, A. J.; Schurko, R. W.; Macdonald, C. L. B. *J. Organomet. Chem.*, **2010**, *695*, 1012-1018.
- [9] Macdonald, C. L. B.; Bandyopadhyay, R.; Cooper, B. F. T.; Friedl, W.; Rossini, A. J.; Schurko, R. W.; Eichhorn, S. H.; Herber, R. H. *J. Am. Chem. Soc.*, **2012**, *134*, 4332-4345.
- [10] The Lewis acidities of the germanium(II) and tin(II) crown ether complexes were investigated in Chapter 2 of this thesis as well as the structures of the TEPO adducts of these complexes.
- [11] Parks, D. J.; Piers, W. E. *J. Am. Chem. Soc.*, **1996**, *118*, 9440-9441.
- [12] A number of linear and cyclic siloxanes were generated through redistribution in reactions with PMDS.
- [13] Rawat, S.; Bhandari, M.; Porwal, V. K. ; Singh, S. *Inorg. Chem.* **2020**, *59*, 7195–7203.
- [14] Laurence, C.; Gal Jean-François. *Lewis basicity and Affinity Scales: Data and measurement*; John Wiley & Sons: Chichester, West Sussex, 2010.
- [15] Gutmann, V. *Donor-acceptor approach to molecular interactions*; Springer: New York, NY, 1978.
- [16] Luo, Y.-R. *Handbook of bond dissociation energies in organic compounds*; CRC Press: Boca Raton, FL, 2003.
- [17] Leszczyńska, K.; Mix, A.; Berger, R. J. F.; Rummel, B.; Neumann, B.; Stammer, H.-G.; Jutzi, P. *Angew. Chem. Int. Ed.*, **2011**, *50*, 6843 –6846.

- [18] a) Liberman-Martin, A. L.; Bergman, R. G.; Tilley, T. D. *J. Am. Chem. Soc.*, **2015**, *137*, 5328-5331. b) Thorwart, T.; Roth, D.; Greb, L. *Chem. Eur. J.*, **2021**, *27*, 10422-10427.
- [19] Hartmann, D.; Schadler, M.; Greb, L. *Chem. Sci.*, **2010**, *10*, 7379-7388. c) Tschernuth, F. S.; Thorwart, T.; Greb, L.; Hanusch, F.; Inoue, S. *Angew. Chem. Int. Ed.*, **2021**, *60*, 25799-25803.
- [20] Roth, D.; Wadepohl, H.; Greb, L. *Angew. Chem. Int. Ed.*, **2020**, *59*, 20930-20934.
- [21] LaFortune, J. H. W.; Johnstone, T. C.; Pérez, M.; Winkelhaus, D.; Podgorny, V.; Stephan, D. W. *Dalton Trans.*, **2016**, *45*, 18156-18162.
- [22] Fang, H. ; Oestreich, M. *Chem. Sci.*, **2020**, *11*, 12604-12615.
- [23] Bach, P.; Albright, A.; Laali, K. K. *Eur. J. Chem.*, **2009**, *12*, 1961-1966.
- [24] Sassaman, M. B.; Kotian, K. D.; Prakash, K. S.; Olah, G. A. *J. Org. Chem.*, **1987**, *52*, 4314-4319.
- [25] Müther, K.; Mohr, J.; Oestreich, M. *Organometallics*, **2013**, *22*, 6643-6646.
- [26] Kouvetakis, J.; Haaland, A.; Shorokhov, D. J.; Volden, H. V.; Girichev, G. V.; Sokolov, V. I.; Matsunaga, P. *J. Am. Chem. Soc.*, **1998**, *120*, 6738-6744.
- [27] Molander, G. A.; Canturk, B. *Org. Lett.*, **2008**, *10*, 2135-2138.
- [28] Barbero, M.; Bazzi, S.; Cadamuro, S.; Dughere, S. *Eur. J. Org. Chem.*, **2009**, *3*, 430-436.
- [29] Torii, S.; Takagishi, S.; Inokuchi, T.; Orumoto, H. *Bull. Chem. Soc. Jpn.*, **197**, *60*, 775-776.
- [30] Takadate, A.; Tahara, T.; Goya, S. *Synthesis*, **1983**, *10*, 806-807.

- [31] Funke, U.; Jia, H.; Fischer, S.; Scheunemann, M.; Steinbach, J. *J. Labelled Comp. Rad.*, **2006**, *49*, 745-755.
- [32] Chun, S.; Chung, Y. K. *Org. Lett.* **2018**, *20*, 5583–5586.
- [33] Kaithal, A.; Kalsi, D.; Krishnakumar, V.; Pattanaik, S.; Bordet, A.; Leitner, W.; Gunanathan, C. *ACS Catal.* **2020**, *10*, 14390–14397.
- [34] Monsigny, L.; Thuery, P.; Berthet, J. C.; Cantat, T. *ACS Catal.*, **2019**, *9*, 9025-9033.
- [35] Cavanaugh, J. R.; Dailey, B. P. *J. Chem. Phys.*, **1961**, *34*, 1094-1098.
- [36] Khusnutdinov, R. I.; Baiguzina, A. R.; Smirnov, A. A.; Mukminov, R. R.; Dzhemilev, U. M. *Russ. J. Appl. Chem+*, **2007**, *80*, 1687-1690.
- [37] Koren-Selfridge, L.; Londino, H. N.; Vellucci, J. K.; Simmons, B. J.; Casey, C. P.; Clark, T. B. *Organometallics*, **2009**, *28*, 2085–2090.
- [38] Vasilikogiannaki, E.; Titilas, I.; Gryparis, C.; Louka, A.; Lykakis, I. N.; *Tetrahedron*, **2014**, *70*, 6106–6113.
- [39] Peña-López, M.; Ayán-Varela, M.; Sarandeses, L. A.; Pérez Sestelo, J. *Chem. Eur. J.*, **2010**, *16*, 9905-9909.
- [40] Okuma, K.; Nojima, A.; Matsunaga, N.; Shioji, K. *Org. Lett.*, **2009**, *11*, 169–171.
- [41] Gellert, B. A.; Kahlcke, N.; Feurer, M.; Roth, S. *Chem. Eur. J.*, **2011**, *17*, 122203-12209.
- [42] Misal Castro, L. C.; Bézier, D.; Sortais, J.-B.; Darcel, C. *Adv. Synth. Catal.*, **2011**, *353*, 1279-1284.

- [43] Liu, S.; Li, T.; Jurca, T.; Stair, P. C.; Lohr, T. L.; Marks, T. J. *Catal. Sci. Technol.*, **2017**, *7*, 2165-2169.
- [44] Yang, C.-G.; He, C. *J. Am. Chem. Soc.*, **2005**, *127*, 6966–6967.
- [45] Lebel, H.; Ladjel, C. *Organometallics*, **2008**, *27*, 2676-2678.
- [46] Maytum, H. C.; Francos, J.; Whatrup, D. J.; Williams, J. M. J. *Chem. Asian J.*, **2010**, *5*, 538-542.
- [47] Huang, L.; Bismuto, A.; Rath, S. A.; Trapp, N.; Morandi, B. *Angew. Chem. Int. Ed.*, **2021**, *60*, 7290-7296.
- [48] Gash, V. W. *J. Org. Chem.*, **1972**, *37*, 3197-2201.
- [49] Chambers, R. D. *J. Fluorine Chem.*, **2010**, *131*, 933-936.

Chapter 5

5 Mechanistic Study on the Etherification of Aldehydes by **[Ge([12]crown-4)₂][OTf]₂**

5.1 Introduction

Understanding the mechanisms of chemical reactions has enabled significant improvements in the selectivity, efficiency and yield of chemical transformations.¹ These improvements have been critical in a number of industries, including the multi billion-dollar pharmaceutical and petrochemical industries, for reducing waste, maximizing output, reducing impurities and lowering costs.^{1,2} Of particular interest are catalytic reactions and their associated mechanisms, where the elementary steps in these reactions are often not obvious. A thorough understanding of the mechanism of catalysis can enable more effective substrate selection, the ability to alter product selectivity and even the potential to alter the structure of the catalyst to improve its activity.

With the growing interest in Lewis acid and low valent main group catalysis, the identification and elucidation of their mechanisms of catalysis is a developing area of research. One of the most common reactions catalyzed by main group Lewis acids is the hydrosilylation of carbonyl compounds. For this reaction, two common reaction pathways have been proposed. The first is carbonyl-activated hydrosilylation (Figure 5.1a), where the first step in the mechanism is the coordination of the carbonyl to the Lewis acid centre. In the second step, hydride transfer from the silane occurs, followed by the transfer of the silyl cation, releasing the silyl ether product. Although the mechanism is shown as stepwise in Figure 5.1a, an asynchronous concerted addition of silane is also possible. The second

pathway begins with the activation of the Si-H bond where a hydride is abstracted by the catalyst and the silyl group is transferred to the carbonyl. Hydride transfer from the catalyst to the carbonyl carbon then occurs releasing the silyl ether product. With two possible reaction pathways in the Lewis acid catalyzed hydrosilylation of carbonyl compounds, it is necessary to identify the mechanism of operation for a specific Lewis acid.

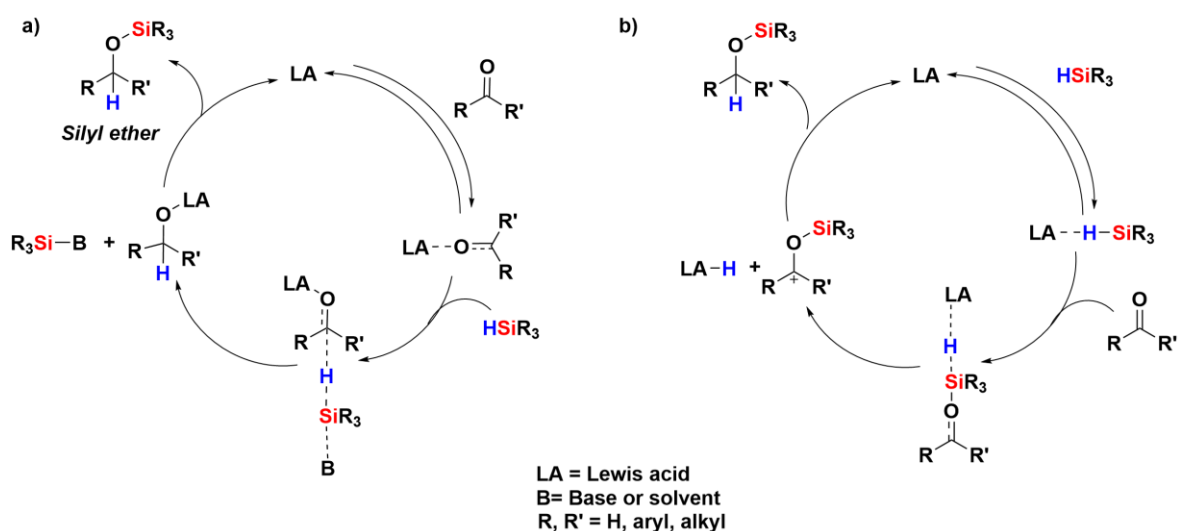
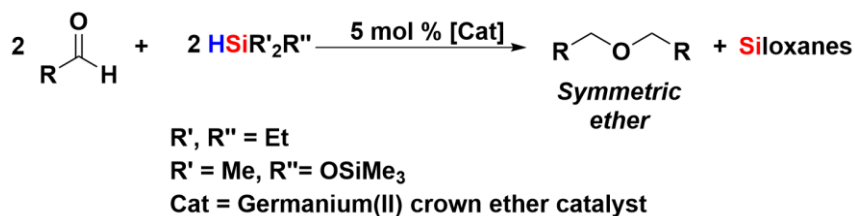


Figure 5.1 The Lewis acid-catalyzed hydrosilylation of carbonyl compounds through a) a carbonyl-activated pathway and b) through a silane-activated pathway.

The catalytic activity of germanium(II) and tin(II) crown ether compounds in the hydrosilylation of aldehydes (Scheme 5.2) has been investigated.³ High conversions to the symmetric ether under mild conditions were achieved using $[Ge([12]crown-4)_2][OTf]_2$, $[Ge([15]crown-5)][OTf]_2$ or $[Ge([18]crown-6)][OTf]_2$ as a catalyst. Conversion of the silyl ether, which was synthesized independently, revealed conversion to the symmetric ether in the presence of $[Ge([12]crown-4)_2][OTf]_2$ is consistent with initial hydrosilylation of the substrate. In order to understand the hydrosilylation pathway as well as the

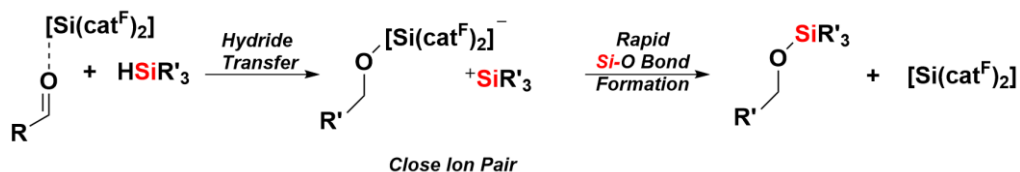
conversion to the symmetric ether, mechanistic studies were conducted. [Ge([12]crown-4)₂][OTf]₂ was selected as a representative catalyst for mechanistic investigations, as the mechanisms for [Ge([15]crown-5)][OTf]₂ and [Ge([18]crown-6)][OTf]₂ are anticipated to be analogous.



Scheme 5.1 Etherification of an aldehyde by a germanium(II) crown ether catalyst.

There have only been a few studies carried out to elucidate the mechanisms of hydrosilylation by Group 14 complexes. Within Group 14, both bis(catecholato)silanes⁴ and -germanes⁵ as have been proposed to facilitate hydrosilylation through carbonyl-activated hydrosilylation pathways; however, minimal evidence was provided in each system. The carbonyl moiety of *N,N'*-bis(diisopropyl)benzamide was shown to coordinate to [Si(cat^F)₂] by ¹H NMR spectroscopy and X-ray crystallography.^{4a} When the chiral silane R-(+)-methyl-(1-naphthyl)phenylsilane was implemented in the hydrosilylation of 4-nitrobenzaldehyde using [Si(cat^F)] as a catalyst, retention of the stereochemistry of the silane was observed (70% ee). On the basis of these observations, hydrosilylation was proposed to occur through the formation of a silylium alkoxy[Si(cat^F)] close ion pair which rapidly combine, displacing the catalyst and forming the Si-O bond. This occurs quickly before tumbling of the silylium in solution can occur preserving the stereochemistry at the

silicon centre (Scheme 5.3). No comment on the reaction pathway of hydrosilylation catalyzed by $[\text{Ge}(\text{cat}^{\text{Cl}})_2][\text{ACN}]$ was provided.^{5a}



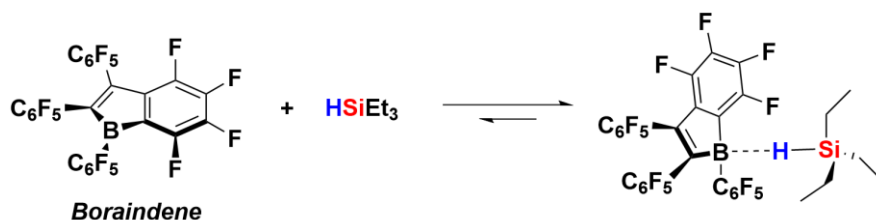
Scheme 5.2 Proposed pathway for the formation of silyl ethers from aldehydes and silanes catalyzed by $[\text{Si}(\text{cat}^{\text{F}})_2]$.^{4a}

Hydrosilylation catalyzed by divalent Group 14 complexes $[\text{MCp}^*][\text{B}(\text{C}_6\text{F}_5)_4]$ (M= Si, Ge) was also proposed to proceed through carbonyl-activated hydrosilylation. No experiments were conducted to determine the reaction pathway, instead carbonyl-activated hydrosilylation was assumed to be operative.⁶ Formation of the symmetric ether in reactions catalyzed by $[\text{MCp}^*][\text{B}(\text{C}_6\text{F}_5)_4]$ (M= Si, Ge) was proposed to occur through initial hydrosilylation to generate two equivalents of silyl ether coordinated to the $\text{M}(\text{II})^{2+}$ centre and coupling to give the disiloxane and the symmetric ether (Scheme 5.4). The only evidence provided in support of the proposed reaction pathway was the observation that only the silyl ether in hydrosilylation reactions using triisopropylsilane, which was attributed to steric interactions with the bulky silyl substituents preventing the coordination of two equivalents of silyl ether and subsequent coupling.



Scheme 5.3 Proposed pathway for the formation of symmetric ethers from aldehydes and silanes catalyzed by $[\text{MCp}^*][\text{B}(\text{C}_6\text{F}_5)_4]$.⁵

Several main group species, including $\text{Ga}(\text{OTf})_3$ and $\text{Bi}(\text{OTf})_3$ ⁷ as well as $\text{B}(\text{C}_6\text{F}_5)_3$,⁸ have been proposed to catalyze hydrosilylation through a silane-activated Lewis acid pathway. The coordination of triethylsilane to a boraindene was observed by X-ray crystallography providing evidence of Si-H activation (Scheme 5.5).⁹ The loss of Si-H coupling in the ¹H NMR spectrum of the boraindene-TES adduct further demonstrated the activation of the Si-H bond. These data provided support for a silane-activated hydrosilylation pathway of aldehydes and ketones by $\text{B}(\text{C}_6\text{F}_5)_3$. This proposed mechanism accounted for some inconsistencies in the assignment of a carbonyl-activated pathway, most notably, an increase in reaction rate in the hydrosilylation when benzaldehydes with electron-withdrawing substituents were utilized as substrates compared to benzaldehyde.



Scheme 5.4 The coordination of triethylsilane to a boraindene.⁹

Several experimental techniques were used to elucidate the nature of the mechanism of aldehyde hydrosilylation using $[\text{Ge}(\text{12crown-4})_2][\text{OTf}]_2$ as a catalyst.

These experiments include stoichiometric additions, a Hammett study, Kinetic Isotope Experiments (KIE) and Variable Time Normalization Analysis (VTNA), a form of Visual Kinetic Analysis to determine the rate law. The data acquired from these experiments allowed for the proposal of a mechanism for the etherification of aldehydes using silanes catalyzed by $[\text{Ge}([\text{12}]\text{crown-4})_2][\text{OTf}]_2$.

5.2 Results and Discussion

5.2.1 Stoichiometric Additions to $[\text{Ge}([\text{12}]\text{crown-4})_2][\text{OTf}]_2$

$[\text{Ge}([\text{12}]\text{crown-4})_2][\text{OTf}]_2$ was added stoichiometrically to triethylsilane and PMDS; however, upon analysis of the solution by ^1H NMR spectroscopy, no changes in the ^1H NMR chemical shifts of the signals assigned to the catalyst or silane or the ^{29}Si NMR chemical shift of the silane were observed.

In a 1:1 addition of 4-methylbenzaldehyde to $[\text{Ge}([\text{12}]\text{crown-4})_2][\text{OTf}]_2$, no changes in the ^1H NMR chemical shifts 4-methylbenzaldehyde or $[\text{Ge}([\text{12}]\text{crown-4})_2][\text{OTf}]_2$ were observed, indicating no coordination. Notably, no coordination complex was formed between crotonaldehyde and $[\text{Si}(\text{cat}^{\text{F}})_2]$; however, a coordination complex was formed between an amide, *N,N'*-bis(diisopropyl)benzamide, and $[\text{Si}(\text{cat}^{\text{F}})_2]$.^{4a} Thus, an aldehyde with a strongly-donating substituent may coordinate to $[\text{Ge}([\text{12}]\text{crown-4})_2][\text{OTf}]_2$ and so 4-dimethylaminobenzaldehyde was added stoichiometrically to the germanium(II) complex (Figure 5.2). Upon addition of aldehyde, the colourless solution of $[\text{Ge}([\text{12}]\text{crown-4})_2][\text{OTf}]_2$ became bright yellow in colour and the signals assigned to the aldehyde broadened in the ^1H NMR spectrum of the mixture (Figure 5.2b). A 0.1 ppm shift

downfield was observed for the signal assigned to the crown ether hydrogens. In an attempt to identify the product formed in the addition, a low temperature ^1H NMR spectrum of the solution was recorded; however, only further broadening of the signals assigned to the aromatic hydrogens of the aldehyde was observed. When 4-dimethylaminobenzaldehyde was added to the analogous tin(II) complex, $[\text{Sn}([\mathbf{12}]\text{crown-4})_2][\text{OTf}]_2$, no colour change or significant change in the chemical shifts in the ^1H NMR spectrum of the mixture was observed although the signals assigned to the aromatic hydrogens of the aldehyde broadened (Figure 5.2c). Attempts to isolate the aldehyde-M(II) adducts were unsuccessful.

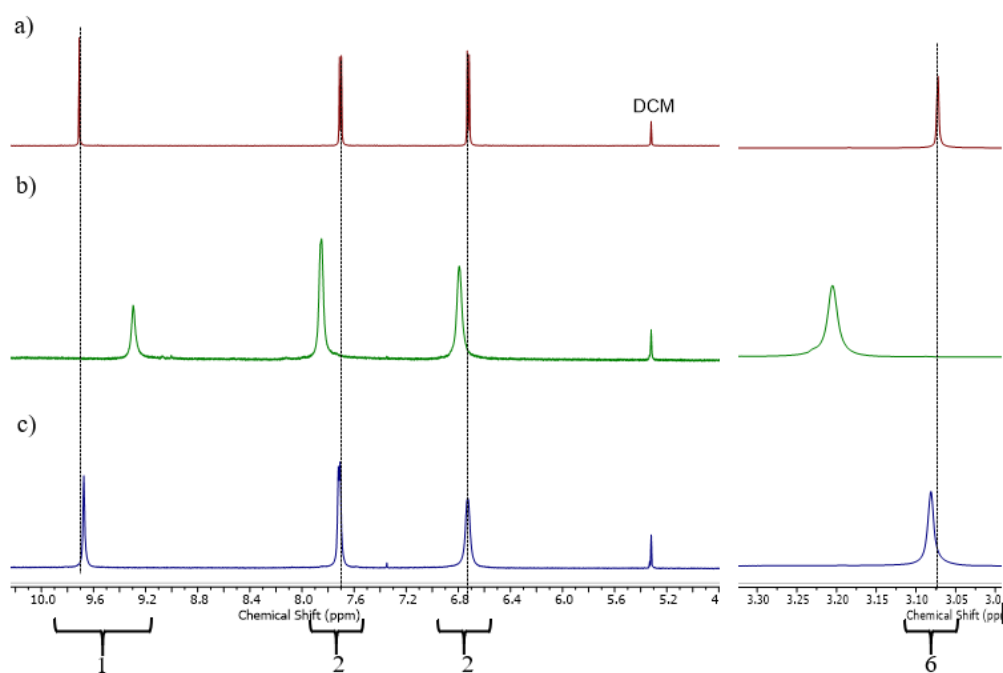


Figure 5.2 ^1H NMR spectra (600 MHz, CD_2Cl_2) for a) 4-dimethylaminobenzaldehyde, b) the addition of 4-dimethylaminobenzaldehyde to $[\text{Ge}([\mathbf{12}]\text{crown-4})_2][\text{OTf}]_2$, c) the addition of 4-dimethylaminobenzaldehyde to $[\text{Sn}([\mathbf{12}]\text{crown-4})_2][\text{OTf}]_2$.

Although the change in the chemical shifts of the signals in the ^1H NMR spectrum provided some evidence for the coordination of the aldehyde to $[\text{Ge}(\text{[12]crown-4})_2][\text{OTf}]_2$, the structure of the Lewis-acid base adduct is uncertain due to the presence of two potential donor sites. To investigate the site of coordination, the addition of 4-dimethylaminobenzaldehyde to $\text{B}(\text{C}_6\text{F}_5)_3$ was selected for comparison. Stoichiometric addition of 4-dimethylaminobenzaldehyde to $\text{B}(\text{C}_6\text{F}_5)_3$ resulted in a yellow solution similar in colour to that of the solution observed in the reaction of $[\text{Ge}(\text{[12]crown-4})_2][\text{OTf}]_2$ and 4-dimethylaminobenzaldehyde. Analysis of the solution by ^1H NMR spectroscopy revealed a distinct loss of symmetry in the signals assigned to the aromatic hydrogens of the aldehyde suggesting the formation of the zwitterionic species, **5.1** (Figure 5.3). Coordination through the oxygen of 4-dimethylaminobenzaldehyde is proposed as the loss of symmetry in the NMR spectrum would not be expected for a nitrogen-coordinated adduct. For comparison, *N,N*-dimethylaniline was also added to $\text{B}(\text{C}_6\text{F}_5)_3$ (Figure 5.4). A downfield shift and broadening in the ^1H NMR chemical shifts of the signals assigned to the *ortho* and *para* hydrogens of the aniline was observed upon coordination to $\text{B}(\text{C}_6\text{F}_5)_3$. The signal assigned to the *N*-methyl substituents also shifted downfield compared to the free aniline. Notably, there was no loss of symmetry for the aromatic signals providing further evidence for coordination of oxygen of 4-dimethylaminobenzaldehyde to $\text{B}(\text{C}_6\text{F}_5)_3$.

The addition of *N,N*-dimethylaniline to $[\text{Ge}(\text{[12]crown-4})_2][\text{OTf}]_2$ was also investigated; all ^1H signals shifted downfield compared to free aniline. Notably, the direction of the change in the chemical shift of the ^1H NMR signals in the additions of *N,N*-dimethylaniline or 4-dimethylaminobenzaldehyde to $[\text{Ge}(\text{[12]crown-4})_2][\text{OTf}]_2$ are the

same and thus these data do not provide direct evidence for nitrogen-coordination in the addition of *N,N*-dimethylbenzaldehyde to $[\text{Ge}([\text{12}]\text{crown-4})_2][\text{OTf}]_2$. Although this experiment does not appear to assist in the assignment of either N- or O-coordination of 4-dimethylaminobenzaldehyde, it does demonstrate that the dimethylamino group is capable of coordinating to $[\text{Ge}([\text{12}]\text{crown-4})_2][\text{OTf}]_2$. Due to the presence of the electron-withdrawing substituent in the *para* position aldehyde, the lone pair of the nitrogen would be less nucleophilic, and thus, the coordination to the oxygen of 4-dimethylaminobenzaldehyde by $[\text{Ge}([\text{12}]\text{crown-4})_2][\text{OTf}]_2$ is the most probable. Given the structure of the 4-dimethylaminobenzaldehyde- $\text{B}(\text{C}_6\text{F}_5)_3$ adduct and the fact that both

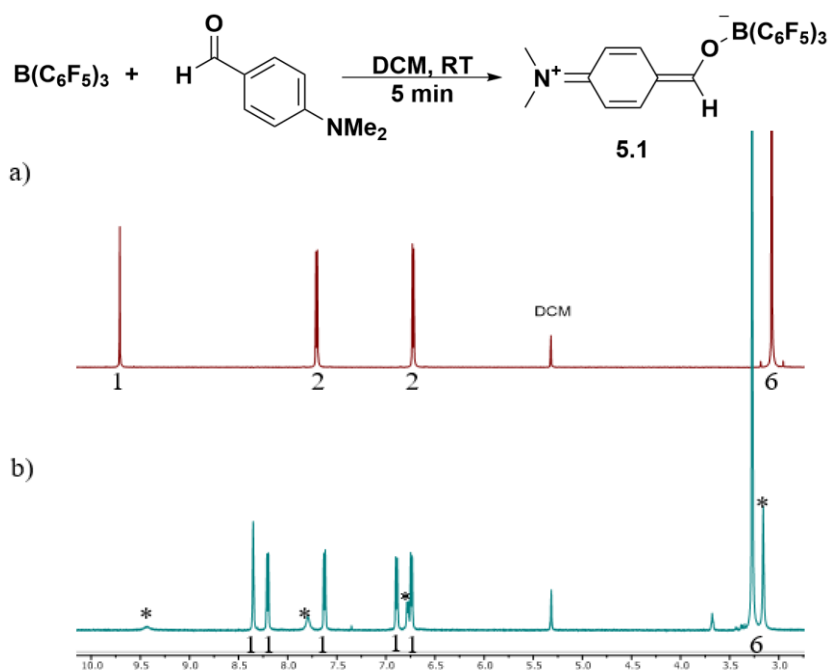


Figure 5.3 a) The ^1H NMR (400 MHz, CD_2Cl_2) spectrum 4-dimethylaminobenzaldehyde and b) the ^1H NMR (400 MHz, CD_2Cl_2) spectrum for the addition of 4-dimethylaminobenzaldehyde to $\text{B}(\text{C}_6\text{F}_5)_3$. Signals from trace amounts of protonated 4-dimethylaminebenzaldehyde are denoted with *.

solutions are yellow, consistent with extended conjugation of the aldehyde and the Lewis acid, the aldehyde is believed to coordinate to $[\text{Ge}([\text{12}]\text{crown-4})_2][\text{OTf}]_2$ through the oxygen.

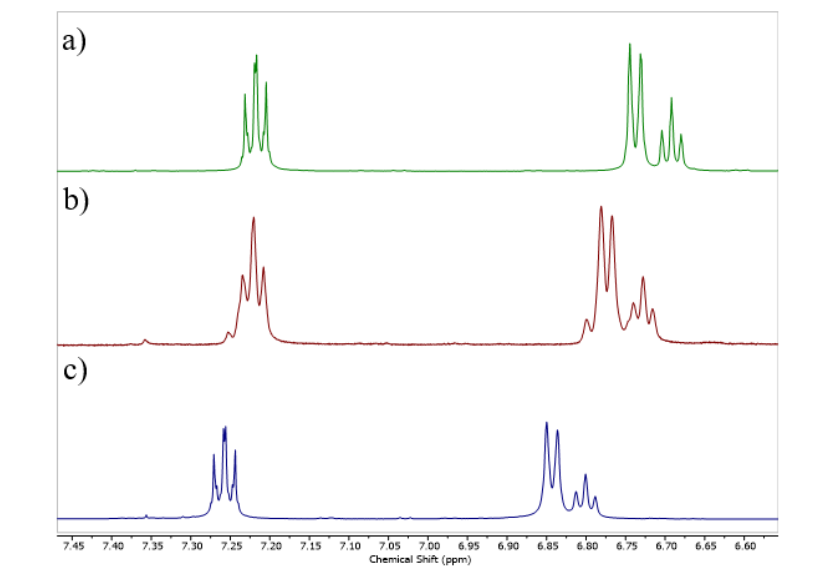


Figure 5.4 a) The ^1H NMR (400 MHz, CD_2Cl_2) spectrum of *N,N*-dimethylaniline, b) the ^1H NMR (400 MHz, CD_2Cl_2) spectrum for the addition of *N,N*-dimethylaniline to $\text{B}(\text{C}_6\text{F}_5)_3$ and c) the ^1H NMR (400 MHz, CD_2Cl_2) spectrum for the addition of *N,N*-dimethylaniline to $[\text{Ge}([\text{12}]\text{crown-4})_2][\text{OTf}]_2$.

5.3 Crown Ether Coordination in the Active Catalyst

Although two equivalents of the crown ether are present in the solid-state of $[\text{Ge}([\text{12}]\text{crown-4})_2][\text{OTf}]_2$, the number of coordinated crown ether equivalents may vary over the course of the etherification pathway. Displacement of the crown ether by TEPO in $[\text{Ge}([\text{12}]\text{crown-4})_2][\text{OTf}]_2$ has been observed. To evaluate the potential for the loss of crown ether from $[\text{Ge}([\text{12}]\text{crown-4})_2][\text{OTf}]_2$ during catalysis, the ^1H NMR chemical shift of the signal assigned to the crown ether hydrogens of $[\text{Ge}([\text{12}]\text{crown-4})_2][\text{OTf}]_2$ was

analyzed during the etherification of 4-methylbenzaldehyde with PMDS catalyzed by $[\text{Ge}([\text{12}]\text{crown-4})_2][\text{OTf}]_2$: a gradual shift upfield by 0.05 ppm was observed (Figure 5.5a). The change in the chemical shift is significantly greater in magnitude than the chemical shift drift observed over time (less than 0.01 ppm) as evidenced by the drift of the signal assigned to the methylene hydrogens of 1,1'-[oxybis(methylene)]bis[4-methylbenzene] (Figure 5.5b). Furthermore, VT ^1H NMR spectra of a solution of $[\text{Ge}([\text{12}]\text{crown-4})_2][\text{OTf}]_2$ revealed that the chemical shift of the crown ether hydrogens is an average between that of the uncoordinated crown ether (3.60 ppm) and that of the germanium(II) complex (4.00 ppm). When additional [12]crown-4 was added to $[\text{Ge}([\text{12}]\text{crown-4})_2][\text{OTf}]_2$, the chemical shift of the signals assigned to the crown ether shifts upfield closer to the chemical shift of free [12]crown-4. Finally, a change in the chemical shift of the signal assigned to the crown ether hydrogens was also observed in the addition of 2 equivalents of TEPO to $[\text{Ge}([\text{12}]\text{crown-4})_2][\text{OTf}]_2$ where an upfield shift of 0.04 ppm was observed upon the formation of $[\text{Ge}(\text{TEPO})_2]^{2+}$ and $[\text{Ge}(\text{TEPO})_3]^{2+}$.¹⁰ Taken together, the evidence suggests that throughout the course of the reaction, [12]crown-4 is displaced by another species in solution, such as 4-methylbenzaldehyde or PMDS. As the chemical shift of the signal assigned to the crown ether hydrogens is not 3.60 ppm (the chemical shift of uncoordinated [12]crown-4) after 6 hours, some [12]crown-4 remains complexed which is consistent with dissociation of only one equivalent of [12]crown-4 from $[\text{Ge}([\text{12}]\text{crown-4})_2][\text{OTf}]_2$ to generate an active catalyst.

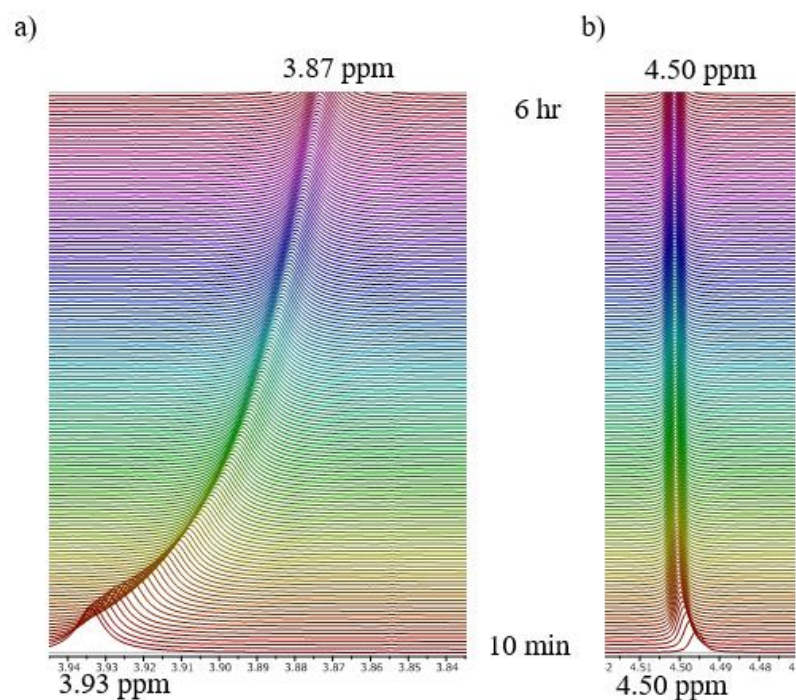
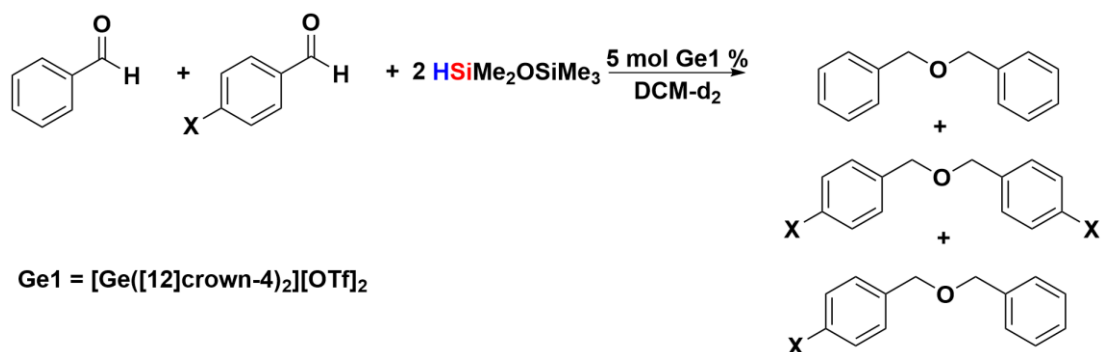


Figure 5.5 The change in the ¹H NMR chemical shift of a) the signals assigned to the crown ether hydrogens in [Ge([12]crown-4)₂][OTf]₂ over time and b) the signals assigned to the methylene hydrogens of 1,1'-[oxybis(methylene)]bis[4-methyl-benzene].

5.4 Hammett Analysis and Proposed Mechanism

The generation and interpretation of a Hammett plot can provide insight into the mechanism of a reaction depending on both the magnitude and sign of the slope of the plot.¹¹ The Hammett plot for the hydrosilylation of benzaldehydes using [Ge([12]crown-4)₂][OTf]₂ was obtained through a series of experiments (Scheme 5.5), where the rate of the loss of aldehyde, either a substituted benzaldehyde or benzaldehyde, was measured by ¹H NMR spectroscopy. The results of the Hammett study are shown in Figure 5.6. Rather than a negative or positive linear correlation for the substituents examined; a concave

downward plot was observed. This is consistent with a change in the rate-limiting step of a reaction depending on the nature of the substituent.¹¹



Scheme 5.5 Competition experiment in the hydrosilylation of benzaldehyde and substituted benzaldehydes.

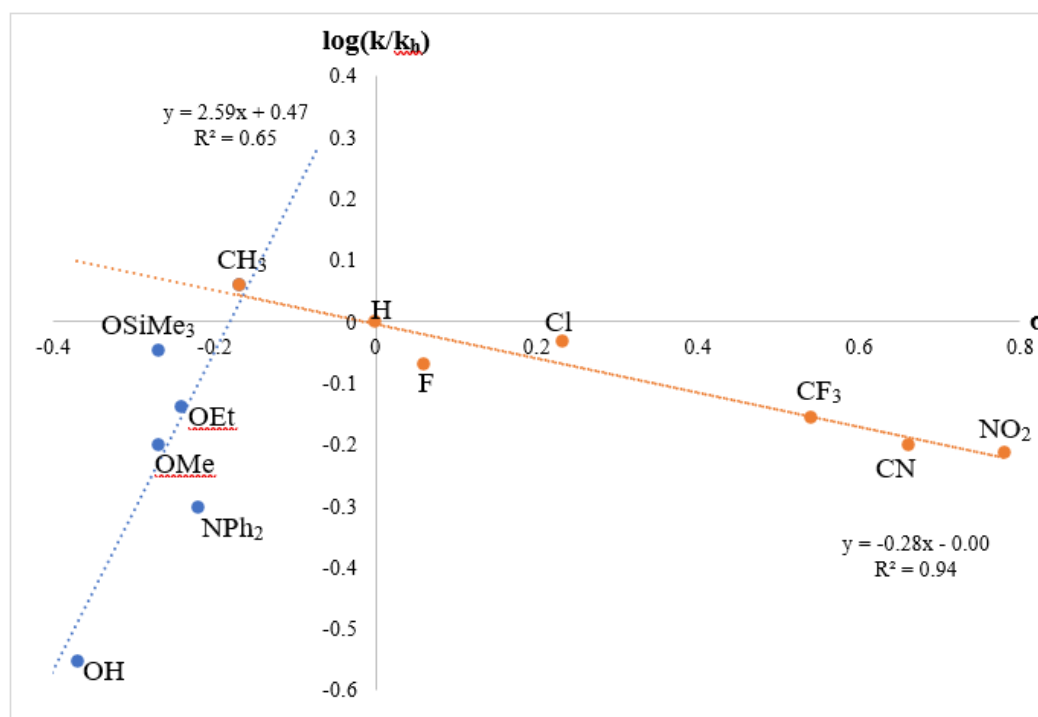
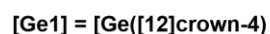
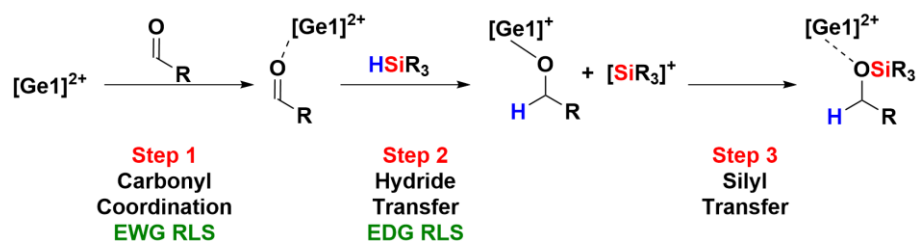


Figure 5.6 Hammett plot for the hydrosilylation of benzaldehydes catalyzed by [Ge([12]crown-4)₂][OTf]₂.

A strong linear correlation ($R^2 = 0.94$) and a small, negative slope of -0.28 was observed for electron-withdrawing groups (EWG) (Figure 5.6). A negative slope is consistent with the build up of positive charge in the transition state of the rate-limiting step. The small slope for the reaction indicates that the reaction is less sensitive to the substituents than those utilized in the ionization of benzoic acid.¹² A weak, linear correlation ($R^2 = 0.52$) and a positive slope of 2.6, consistent with a build up of negative charge in the transition state of the rate-limiting step, was observed for benzaldehydes with electron-donating groups (EDG). The slope is greater than 1, indicating that for EDGs, the reaction is more sensitive to the substituent than in the ionization of benzoic acid. The weak correlation observed for electron-donating substituents may be attributed to off-cycle coordination of the second donor atom (O, N) for aldehydes containing two donor sites.

Using the data from the Hammett study, a mechanism for carbonyl hydrosilylation can be proposed. The negative slope observed with the EWGs is consistent with a build up of positive charge in the transition state of the rate-limiting step, and thus, for EWGs, carbonyl coordination, which would result in a build up of positive charge at the carbonyl carbon, is believed to be the rate-limiting step (RLS) of the reaction (Scheme 5.6, Step 1). Aromatic aldehydes with EWGs are weak donors, due to polarization of electron density away from the carbonyl oxygen, which makes coordination to the Lewis acid centre less favorable. The second step is hydride transfer from the silane to the activated carbonyl (Scheme 5.6, Step 2). As the hydride is transferred, a build up of negative charge occurs during the transition state, consistent with the positive slope observed in the Hammett plot for benzaldehydes containing EDGs, and thus, is believed to be the rate limiting step for

benzaldehydes with EDGs. Aromatic aldehydes with EDGs will reduce the electrophilicity of the carbonyl carbon by donating electron density to the carbon making hydride transfer less favorable. The third step in the pathway is silyl transfer to generate the silyl ether intermediate. As catalysis by silylium ions was ruled out, the intermediate silyl cation is not anticipated to persist in solution for an extended period of time, much like the proposal made in the hydrosilylation of aldehydes by $[\text{Si}(\text{cat}^{\text{F}})_2]$.^{4a}



Scheme 5.6 The three elementary steps in carbonyl-activated hydrosilylation.

Although the hydrosilylation is depicted stepwise (Scheme 5.6, Steps 2 and 3), the concerted, asynchronous transfer of the silane is also a possibility. If a concerted, asynchronous transfer of the silane were to occur, the primitive process in which the hydride begins to form would be the rate-limiting step for benzaldehydes substituted with EDGs as a build up electron density near the aldehyde occurs, still in agreement with the slope of the Hammett plot. The experimental conditions of the etherification reaction catalyzed by $[\text{Ge}(\text{[12]crown-4})_2][\text{OTf}]_2$, notably the weakly donating solvent DCM, the absence of strong Lewis bases for stabilization in solution and the small alkyl substituents on the silane, may make the generation of a silyl cation challenging. Therefore, if the silane were to add in one step, the generation of the high energy silylium intermediate would be

avoided. Computational studies would be required to evaluate both the stepwise and concerted, asynchronous hydrosilylation step(s) and to determine the pathway with the lowest energy. For the purpose of clarity in this thesis, a stepwise mechanism has been shown.

The final step in the mechanism is etherification. Once the carbonyl is silylated, the saturated carbon adjacent to the substituted aromatic ring will reduce the influence of the substituents on the rate of the reaction. As a significant influence of the substituents was observed, this step was ruled out as a possible rate-limiting step. In order to achieve etherification, two equivalents of silyl ether are required to be in close proximity to couple both the silyl groups and the alkoxy groups. As the coordination of multiple TEPO equivalents was observed in the reaction of TEPO and $[\text{Ge}(\text{[12]crown-4})_2][\text{OTf}]_2$,¹⁰ the coordination of two equivalents of aldehydes is reasonable. Furthermore, the silyl ether is not detected in solution by ^1H NMR spectroscopy using aldehydes containing weak EWGs or EDGs suggesting that the silyl ether is quickly converted to the symmetric ether.

From the results of the Hammett plot and the understanding of the coordination of multiple aldehyde equivalents, a mechanism for aldehyde etherification by $[\text{Ge}(\text{[12]crown-4})_2][\text{OTf}]_2$ is proposed (Figure 5.7). In the etherification step, one silyl group is transferred to the second equivalent of silyl ether followed by elimination, to generate the disiloxane, and coupling of the alkoxy and alkyl groups to generate the symmetric ether.

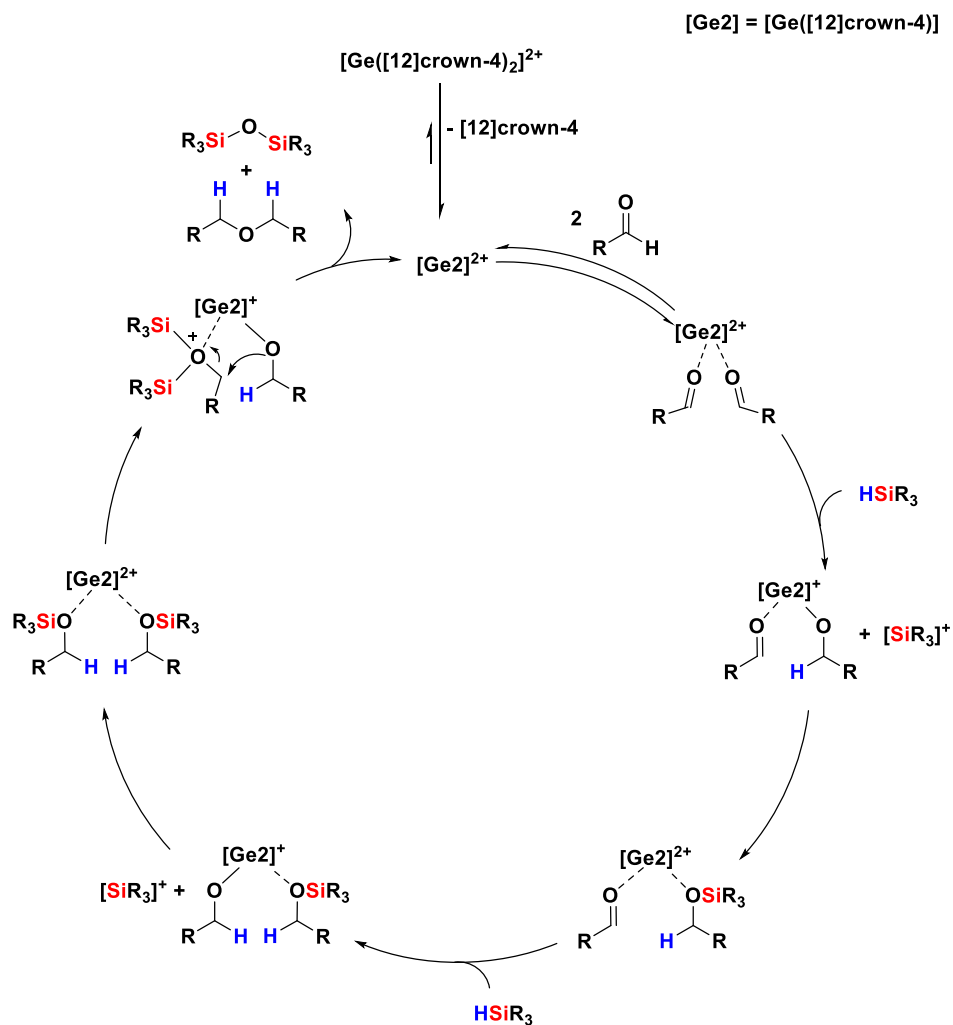


Figure 5.7 Proposed mechanism for the hydrosilylation of aldehyde catalyzed by $[\text{Ge}([12]\text{crown-4})_2][\text{OTf}]_2$.

The formation of the silyl ether in reactions with 4-cyanobenzaldehyde and 4-nitrobenzaldehyde can be understood in terms of the proposed mechanism (Figure 5.7). Both 4-cyano- and 4-nitrobenzaldehyde contain EWGs which make carbonyl coordination less favorable. A decrease in Lewis acidity of the germanium(II) centre occurs after the coordination of one equivalent of aldehyde and the less nucleophilic C=O of 4-cyanobenzaldehyde and 4-nitrobenzaldehyde makes coordination of a second equivalent

less favorable. Therefore, upon hydrosilylation, dissociation of the silyl ether occurs in the absence of a second equivalent to enable the coupling reaction.

The proposed mechanism for the etherification of aldehydes by **[Ge([12]crown-4)₂][OTf]₂** is similar to that proposed for the etherification of aldehydes and ketones using **[MCp^{*}][B(C₆F₅)₄]** (M = Si, Ge). In the etherification of aldehydes by **[Ge([12]crown-4)₂][OTf]₂**, the coordination of two aldehydes is proposed as the first step in the mechanism and requires two accessible orbitals on the germanium(II) centre. An orbital analysis of **[Ge([12]crown-4)₂]²⁺** revealed that the LUMO (-6.797 eV) and LUMO+1 (-6.330 eV) (Figure 5.9) are located on the germanium(II) centre and are presumably utilized in the coordination of the two equivalents of aldehyde. For **[MCp^{*}][B(C₆F₅)₄]** (M = Si, Ge), two doubly degenerate LUMO orbitals are present (-14.107 eV),¹³ capable of coordinating two equivalents of aldehyde and accounting for the observance of the symmetric ether in the hydrosilylation of paraformaldehyde by **MCp^{*}][B(C₆F₅)₄]** (M = Si, Ge). Silyl(IV) cations and Group 13 catalysts are anticipated to coordinate a single equivalent of aldehyde in hydrosilylation reactions,⁶ and therefore, are unable to undergo the direct coupling to form the symmetric ether accounting for the formation of the silyl ether in these reactions.

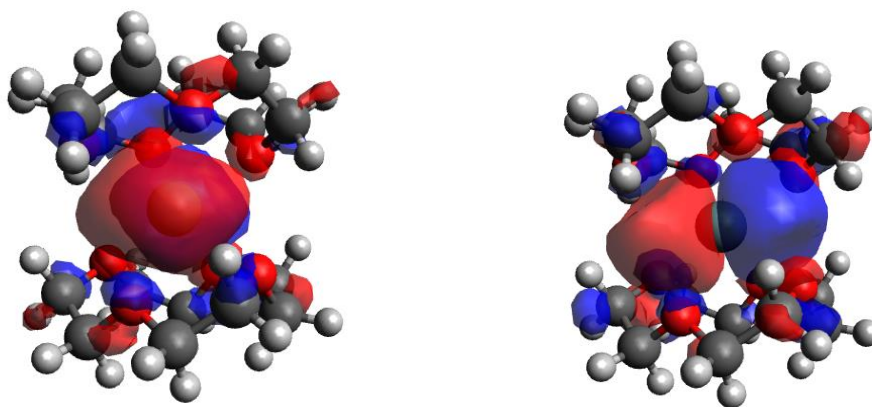


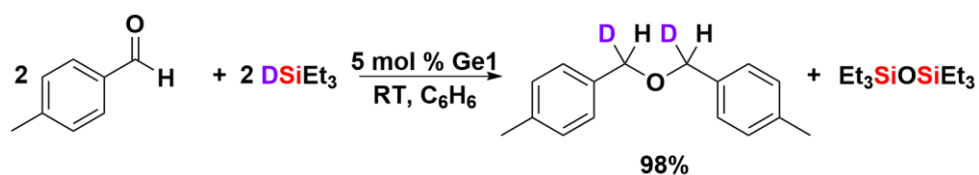
Figure 5.8 a) LUMO of $[\text{Ge}([\text{12}]\text{crown-4})_2]^{2+}$ and b) LUMO+1 of $[\text{Ge}([\text{12}]\text{crown-4})_2]^{2+}$. Geometries were optimized using PBEh-3c/def2-mSVP.

On the basis of the similarities in structure and bonding¹⁴ in the other germanium(II) and tin(II) triflate salts, $[\text{Ge}([\text{15}]\text{crown-5})][\text{OTf}]_2$, $[\text{Ge}([\text{18}]\text{crown-6})][\text{OTf}]_2$, $[\text{Sn}([\text{12}]\text{crown-4})_2][\text{OTf}]_2$, $[\text{Sn}([\text{15}]\text{crown-5})_2][\text{OTf}]_2$ and $[\text{Sn}([\text{18}]\text{crown-6})][\text{OTf}]_2$ the mechanism for the etherification of aldehydes is expected to be the same as that for the $[\text{Ge}([\text{12}]\text{crown-4})_2][\text{OTf}]_2$ catalyst. The mechanism for the hydrosilylation and etherification of aldehydes by the germanium(II) and tin(II) crown ether trichlorometallate salts is less clear due to the significant structural differences between these complexes and $[\text{Ge}([\text{12}]\text{crown-4})_2][\text{OTf}]_2$. Further studies are required to understand the mechanism of aldehyde etherification by the germanium(II) and tin(II) crown ether trichlorometallate salts.

5.5 Deuterium Labelling and Kinetic Isotope Effect

The Kinetic Isotope Effect (KIE) can be used to evaluate the rate-limiting step of a reaction and also can confirm that the hydride source is derived from the silane. The ^1H

NMR spectra of the product from the reduction of 4-methylbenzaldehyde using triethylsilane-*d* and catalyzed by $[\text{Ge}([\text{12crown-4}]_2)[\text{OTf}]_2]$ revealed the presence of one deuterium at each benzylic position (Scheme 5.6). Incorporation of deuterium into 1,1'-[oxybis(methylene)]bis[4-methyl-benzene] was also observed in the ^2H NMR spectrum as well as in the $^{13}\text{C}\{^1\text{H}\}$ NMR spectrum. The evidence strong suggests that the hydride source is indeed the silane. Comparable yields of the deuterated and protiated ethers were obtained (>98%).



$[\text{Ge1}] = [\text{Ge}([\text{12crown-4}]_2)[\text{OTf}]_2]$

Scheme 5.7 Incorporation of deuterium into 1,1'-[oxybis(methylene)]bis[4-methyl-benzene].

Kinetic isotope experiments were conducted to evaluate whether the rate-limiting step involves the breaking the Si-H bond. The reaction of 4-methylbenzaldehyde was attempted using HSiEt_3 and DSiEt_3 and $[\text{Ge}([\text{12crown-4}]_2)[\text{OTf}]_2]$ as a catalyst and the initial rates of the reactions were compared. Typically, the quotient of the rate constants of the heavy and light element is evaluated; however, the rate of the reaction is proportional to the rate constant and can be used an alternative when the order of the reaction is not known. The value of the KIE was determined to be 1.00 ± 0.05 , assuming standard error,¹⁴ and is consistent with no primary or secondary kinetic isotope effect indicating that rate-limiting step does not involve Si-H cleavage or bond cleavage adjacent to the Si-H bond.

This result is agreement with the Hammett plot, where 4-methylbenzaldehyde, a weakly EDG, is at the apex of the concave downward plot and, evidently, behaves like an EWG, where the rate-limiting step is carbonyl-coordination, not Si-H bond cleavage.

5.6 Reaction Order Determination Using Visual Kinetic Analysis

Visual kinetic analysis is an emerging field enabling the assessment of kinetic data through the visual comparison of processed data sets. One method is Variable Time Normalization Analysis (VTNA),¹⁵ where the visual similarity between a series of plots normalized by the order and reagent concentration is used to indicate the order of the reaction, decided by the most closely overlapped plots. The VTNA plots for the etherification of 4-methylbenzaldehyde using triethylsilane and $[\text{Ge}([\text{12}]\text{crown-4})_2][\text{OTf}]_2$ as the catalyst are shown (Figure 5.8). A series of reactions orders, 0-3, were considered for all reagents as well as inverse or negative orders; however, these data are not consistent with either inverse or negative orders. When the influence of silane on the reaction rate was probed in the etherification reaction (Figure 5.8a), the order in silane was found to be 1. For 4-methylbenzaldehyde, the order in aldehyde was found to be 2 (Figure 5.8b). A fractional order of 0.5 was observed for $[\text{Ge}([\text{12}]\text{crown-4})_2][\text{OTf}]_2$ (Figure 9c). This gives an overall rate law for the etherification of aldehydes by $[\text{Ge}([\text{12}]\text{crown-4})_2][\text{OTf}]_2$:

$$\text{rate} = k[\text{Aldehyde}]^2 [\text{Silane}] [\text{Ge}([\text{12}]\text{crown-4})_2][\text{OTf}]_2]^{0.5}$$

Fractional orders of reagents are often observed for catalysts in catalytic reactions indicating that the reaction involves a series of steps and/or is complex.¹⁶ As a result, the

order of reagents in the rate law determined from the VTNA cannot be used to interpret the number of species involved in the rate-limiting step.¹⁶ Nonetheless, the results of the VTNA are consistent with a complex mechanism involving catalysis by **[Ge([12]crown-4)₂][OTf)₂]** and the involvement of all reagents in throughout the course of the reaction and is consistent with the proposed mechanism of reaction (Figure 5.9).

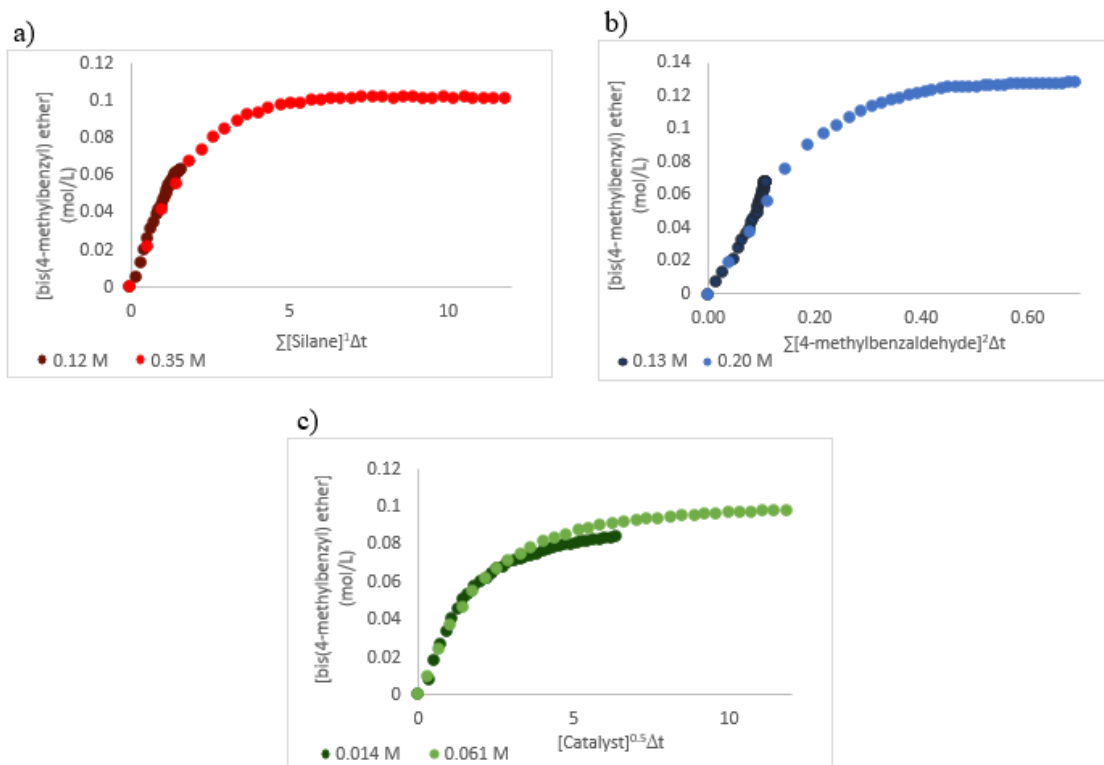
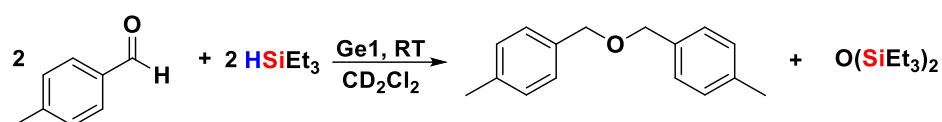


Figure 5.9 The VTNA plots for aldehyde etherification with the best visual correlations for a) triethylsilane, b) 4-methylbenzaldehyde and c) **[Ge([12]crown-4)₂][OTf)₂]**.

5.7 Comparison to Silane-Activated Mechanism by Group 13 Catalysts

An alternate mechanism to account for the formation of symmetric ethers in the hydrosilylation of ketones or aldehydes catalyzed by $\text{Ga}(\text{OTf})_3$ has been proposed (Figure 5.10).⁷ The first step involves the activation of the Si-H bond to generate the silylcarboxonium cation, **IV** (Figure 5.10) Reaction of cation **IV** with an equivalent of silyl ether generates intermediate **V**. Transfer of the silyl group from one oxygen to another generates intermediate **VI**, which eliminates $\text{O}(\text{SiEt}_3)_2$ leaving the symmetric ether as the other product. As the hydrosilylation of aldehydes results in the formation of symmetric ethers when catalyzed by $\text{Ga}(\text{OTf})_3$, evidently, k_2 , the rate of symmetric ether formation, is faster than k_1 , the rate of silyl ether formation.

$\text{B}(\text{C}_6\text{F}_5)_3$ also activates the silane in a similar fashion to $\text{Ga}(\text{OTf})_3$ but exclusive formation of the silyl ether in DCM indicates that for $\text{B}(\text{C}_6\text{F}_5)_3$, k_1 , hydride transfer from $[\text{HB}(\text{C}_6\text{F}_5)_3]^-$ to **IV**, is faster than k_2 (Figure 5.10). Changing the solvent for hydrosilylation reactions catalyzed by $\text{B}(\text{C}_6\text{F}_5)_3$ from DCM to ACN resulted in a change in selectivity from the silyl ether to the symmetric ether⁷ due to the generation of a silylnitrilium ion, $[\text{MeCN-SiEt}_3]^+$, which extends the lifetime of the silylcarbonium ion and making k_2 competitive with k_1 . The difference in the rates of hydride transfer versus etherification accounts for the different product selectivities observed for silane-activated Lewis acid catalysts. The selectivity can be altered using the polarity of the solvent.

Although the silyl ether can be formed using the pathway proposed in Figure 5.10, the key difference between this pathway and the pathway proposed for **[Ge([12]crown-**

$4)_2][\text{OTf}]_2$ is the coupling step. For $\text{Ga}(\text{OTf})_3$, an intermolecular pathway is proposed where a silyl ether couples with the silylcarboxonium cation, **IV**, in solution with no association of the $\text{Ga}(\text{OTf})_3$ catalyst, while for $[\text{Ge}([\mathbf{12}\text{crown-4}]_2)[\text{OTf}]_2]$, the coupling is proposed to occur while the two equivalents of silyl ether remain coordinated to the catalyst and primed for coupling due to their close proximity.

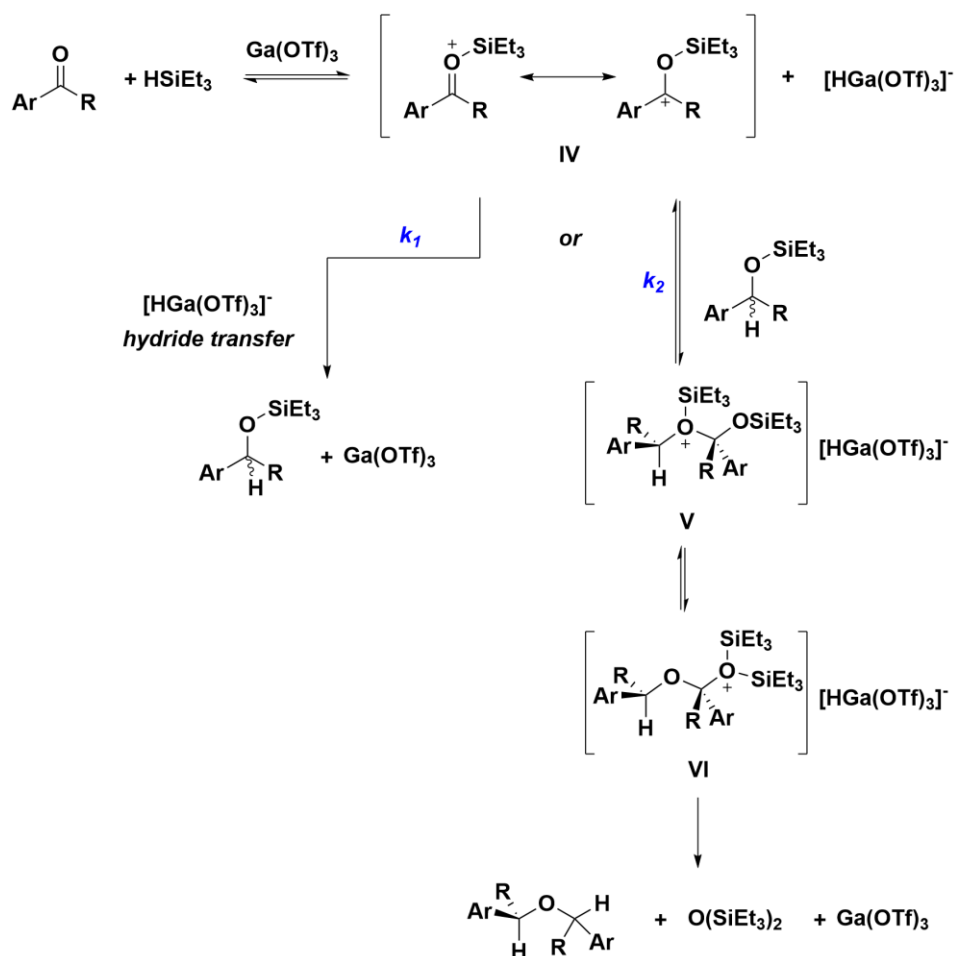


Figure 5.10 Proposed mechanism for the formation of the silyl ether and symmetric ether using $\text{Ga}(\text{OTf})_3$.

5.8 Summary and Conclusions

In summary, the available data have allowed for a mechanism to be proposed for the etherification of aldehydes by $[\text{Ge}([\mathbf{12}]\text{crown-4})_2][\text{OTf}]_2$. The reaction pathway begins coordination of two carbonyl moieties to the catalyst followed by transfer of the hydride to generate the activated alcohols and finally silyl transfer to form the silyl ethers. Coupling of the two silyl ethers coordinated to the catalysts gives the symmetric ether and disiloxane products. The shape of the Hammett plot revealed a change in the rate-limiting step between benzaldehydes containing EWGs and EDGs. For aldehydes containing electron-withdrawing groups, the rate-determining step is proposed to be carbonyl-coordination. For aldehydes containing electron-donating groups, the rate-determining step is proposed to be hydride transfer. No kinetic isotope effect was observed for the etherification of 4-methylbenzaldehyde catalyzed by $[\text{Ge}([\mathbf{12}]\text{crown-4})_2][\text{OTf}]_2$ which is consistent with the position of this point on the Hammett plot. The final step in the reaction pathway is the coupling of the silyl ethers to give the symmetric ether and disiloxane. VTNA analysis revealed a complex mechanism, involving the catalyst, silane and aldehyde and is also consistent with the proposed mechanism.

From this study, for the first time, substantial evidence in support of the carbonyl-activated mechanism as well as the nature of the active catalyst was examined using multiple experimental techniques. The active catalyst was found to be $[\text{Ge}([\mathbf{12}]\text{crown-4})]^{2+}$. This work will hopefully inspire further and more detailed studies into the mechanism of hydrosilylation and/or etherification by Group 14 cationic catalysts.

5.9 Experimental

5.9.1 General Experimental

All manipulations were performed under an inert atmosphere of argon using Schlenk techniques or under an atmosphere of nitrogen in an MBraun glovebox. Solvents were purified using an Innovative Technologies 400-5 Solvent Purification System and were stored over activated 4 Å molecular sieves. All NMR solvents and liquid reagents were dried over activated 4 Å molecular sieves. Chemicals purchased from commercial sources were used without further purification. $[\text{Ge}([\mathbf{12}]\text{crown-4})_2][\text{OTf}]_2^{14a}$ and $[\text{Sn}([\mathbf{12}]\text{crown-4})_2][\text{OTf}]_2^{14b}$ were synthesized according to literature procedures.

NMR spectra were recorded on a Varian Inova 600 MHz NMR spectrometer or a Bruker Avance III 400 MHz NMR spectrometer. The NMR standards used are as follows: ^1H NMR spectra were referenced to residual CH_2Cl_2 (5.32 ppm) or $\text{C}_6\text{D}_5\text{H}$ (7.16 ppm). A 10 second relaxation delay was utilized for all ^1H NMR spectra. The ^2H NMR spectra were referenced externally to a sample of C_6D_6 (7.16 ppm).

Liquid reagents were dispensed using a micropipette. Mesitylene was used as the internal standard and was found to pipette a consistent volume (with less than 5% deviation by mass), and thus was used as an absolute reference of molar quantity in all experiments. *In situ* monitoring of the integration of mesitylene throughout the course of etherification revealed no significant change in the concentration of mesitylene throughout the reaction (less than 2%) based on the absolute integrations. Therefore, the relative integrations and

subsequent concentrations derived from the mesitylene should be highly accurate and the error associated with this value is encompassed by the standard error of 5%.^{14b}

5.9.2 Stoichiometric Additions to **[Ge([12]crown-4)₂][OTf]₂**

The reagent (10 μ L *vide infra*) was added to an NMR tube along with **[M([12]crown-4)₂][OTf]₂** where M= Ge, Sn (1 equivalent) and the mixture was dissolved in C₆D₆ or CD₂Cl₂ (~0.5 mL). The ¹H NMR spectrum was acquired immediately and then again after 24 hours. Reactions were performed with pentamethyldisiloxane, triethylsilane, 4-methylbenzaldehyde, 4-dimethylaminobenzaldehyde (10 mg) and *N,N*-dimethylaniline. A yellow solution was observed in the addition of **[Ge([12]crown-4)₂][OTf]₂** to 4-dimethylaminobenzaldehyde. No change in the ¹H NMR chemical shifts were observed in the additions of pentamethyldisiloxane, triethylsilane or 4-methylbenzaldehyde to either 12-crown-4 complex.

4-dimethylaminobenzaldehyde: ¹H NMR (400 MHz, CD₂Cl₂) 9.71 (br s, 1H, CHO), 7.71 (d, 2H, ³J = 9 Hz, Ar-H), 6.79 (d, 2H, ³J = 9 Hz Ar-H), 3.07 (s, 6H, NCH₃).

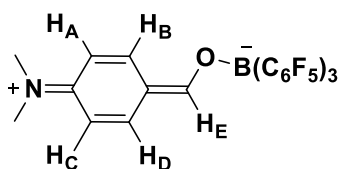
[Ge([12]crown-4)₂][OTf]₂·(4-dimethylaminobenzaldehyde): ¹H NMR (600 MHz, CD₂Cl₂) 9.29 (br s, 1H, CHO), 7.85 (br s, 2H, Ar-H), 6.79 (br s, 2H, Ar-H), 3.85 (br s, 32H, OCH₂), 3.20 (br s, 9H, NCH₃).

***N,N*-dimethylaniline:** ¹H NMR (400 MHz, CD₂Cl₂) 7.20-7.24 (m, 2H, *m*-H), 6.73-6.75 (m, 2H, *o*-H), 6.68-6.71 (m, 1H, *p*-H), 2.94 (s, 6H, NCH₃).

[Ge([12]crown-4)₂][OTf]₂·*N,N*-dimethylaniline: ¹H NMR (600 MHz, CD₂Cl₂) 7.27-7.24 (m, 2H, *m*-H), 6.73-6.75 (br d, 2H, ³*J* = 8 Hz, *o*-H), 6.68-6.71 (br t, 1H, ³*J* = 7 Hz, *p*-H), 2.94 (s, 6H, NCH₃).

5.9.3 Stoichiometric Additions to B(C₆F₅)₃

4-dimethylaminobenzaldehyde (10 mg, 0.067 mmol) or *N,N*-dimethylaniline (10 mg, 0.082 mmol) was added to B(C₆F₅)₃ (0.067 mmol or 0.082 mmol) and dissolved in CD₂Cl₂ (~0.5 mL) to give a bright yellow solution. The ¹H NMR spectrum was acquired immediately. Trace amounts of protonated aldehyde were also observed along with the **5.1**.



5.1

¹H NMR (400 MHz, CD₂Cl₂) 8.35 (br s, 1H, H_E), 8.21 (dd, ³*J*_{HH} = 9 Hz, ⁴*J*_{HH} = 2 Hz, 1H, H_B), 7.63 (dd, ³*J* = 9 Hz, ⁴*J* = 2 Hz, 1H, H_D), 6.90 (ddd, ³*J* = 9 Hz, ⁴*J* = 2 Hz, ⁴*J* = 0.9 Hz, 1H, H_A), 6.74 (dd, ³*J* = 9 Hz, ⁴*J* = 2 Hz, 1H, H_C), 3.27 (s, 6H, NCH₃); ¹³C{¹H} (121 MHz, CD₂Cl₂) 185.03 (C-O), 159.62 (C=N), 142.54 (C-H_D), 134.88 (C-H_B), 119.49 (C=CO), 114.71 (C-H_C), 112.32 (C-H_A), 41.33 (NCH₃); ¹⁹F{¹H} (565 MHz, CD₂Cl₂) -134.3 (dd, ³*J* = 24 Hz, ⁴*J* = 9 Hz, 2H, *o*-F), -158.5 (t, ³*J* = 20 Hz, 1H, *p*-F), -164.8-165.0 (m, 1H, *m*-F); ¹¹B (192 MHz, CD₂Cl₂) 0.91 (br s).

B(C₆F₅)₃·*N,N*-dimethylaniline: ¹H NMR (400 MHz, CD₂Cl₂) 7.25-7.19 (m, 2H, *m*-H), 6.79-6.76 (m, 2H, *o*-H), 6.75-6.71 (m, 1H, *p*-H), 2.94 (s, 6H, NCH₃).

5.9.4 Hammett Study

5.9.4.1 Experimental Set-Up

[Ge([12]crown-4)₂][OTf]₂ (5 mg, 0.0069 mmol) was dissolved in CD₂Cl₂ (~0.5 mL) and added to an NMR tube. Mesitylene (10 μL, 0.072 mmol), benzaldehyde (0.068 mmol), substituted benzaldehyde (0.068 mmol) and pentamethyldisiloxane (27 μL, 0.14 mmol) were added to the NMR tube and CD₂Cl₂ was added such that the total volume of solution was 1 mL. The NMR tube was sealed with Teflon tape and the ¹H NMR spectrum of the mixture was recorded every 5 minutes.

Reactions were run in at least duplicate resulting in a similar trend in the k_X/k_H value; however, only the values where the [benzaldehyde] and [substituted aldehyde], determined from the integrations of the aldehyde protons, were within 10% of one another *at the time of NMR acquisition* were included in the plot to avoid concentration effects. To achieve comparable concentrations for 4-hydroxybenzaldehyde, 4-methoxybenzaldehyde, 4-ethoxybenzaldehyde, 4-cyanobenzaldehyde and 4-nitrobenzaldehyde and benzaldehyde at the time of acquisition in the experiments, a greater proportion of benzaldehyde was added in initially in reactions with these substituted aldehydes, the amount of which was determined through a series of trial experiments.

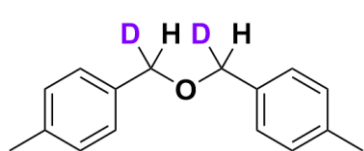
5.9.4.2 Plotting the Data

The integrations of the signal assigned to the aldehydic hydrogen of benzaldehyde and the analogous signal for the substituted benzaldehyde were measured over time and converted to concentrations. A plot of time vs [aldehyde] was plotted for both aldehydes;

the linear portion of the plot was isolated and the slope of the line for the benzaldehyde plot and substituted benzaldehyde plot were determined. The quotient of the slopes ($k_{\text{Substituted}}/k_{\text{Benzaldehyde}}$) was taken and plotted against the Hammett parameter¹² for each aldehyde.

5.9.5 Deuterium Labelling Experiments

An NMR tube was loaded with $[\text{Ge}([\mathbf{12}]\text{crown-4})_2][\text{OTf}]_2$ (200 μL of a 0.0345 M stock solution in C_6H_6), mesitylene (10 μL , 0.072 mmol), 4-methylbenzaldehyde (16 μL , 0.14 mmol) and triethylsilane-*d* (22 μL , 0.14 mmol). C_6H_6 was added such that the total volume of solution was 1 mL. The NMR tube was sealed with Teflon tape and the ^2H NMR spectrum was acquired after 24 hours. The experiment was repeated in C_6D_6 to acquire other chemical shift data.



^2H (92 MHz, C_6H_6) 4.36 ppm

^1H (400 MHz, C_6D_6) 7.25 (d, 4H, $^3J_{\text{HH}} = 8$ Hz Ar-H), 7.01 (d, 4H, $^3J_{\text{HH}} = 8$ Hz Ar-H), 4.38 (br s, 2H, CHD), 2.13 (s, 6H, CH_3); $^{13}\text{C}\{^1\text{H}\}$ (101 MHz, C_6D_6) 137.08 (*p*-C), 136.21 (*i*-C), 129.30 (*o*-C), 127.38 (*m*-C), 71.60 (t, $^1J_{\text{CD}} = 21$ Hz, CHD), 21.16 (CH_3).

5.9.6 Visual Kinetic Analysis

For each experiment, the desired mass of $\text{Ge}([\mathbf{12}]\text{crown-4})_2[\text{OTf}]_2$ was dissolved in CD_2Cl_2 (~0.5 mL) and added to an NMR tube. Mesitylene (10 μL , 0.072 mmol) and the desired amounts of 4-methylbenzaldehyde and triethylsilane were added to the NMR tube

and CD₂Cl₂ was added such that the total volume was 1 mL. The NMR tube was sealed with Teflon tape and the ¹H NMR spectrum was recorded every 5 minutes. The following amounts of reagents were used in the 6 experiments:

VTNA Reagent Examined	[Ge([12]crown-4)₂][OTf]₂ (mg)	Triethylsilane (μL)	4-methylbenzaldehyde (μL)
Triethylsilane	2	19	30
	2	55	30
[Ge([12]crown-4)₂][OTf]₂	2	40	24
	2	40	15
4-methylbenzaldehyde	10	40	30
	44	40	30

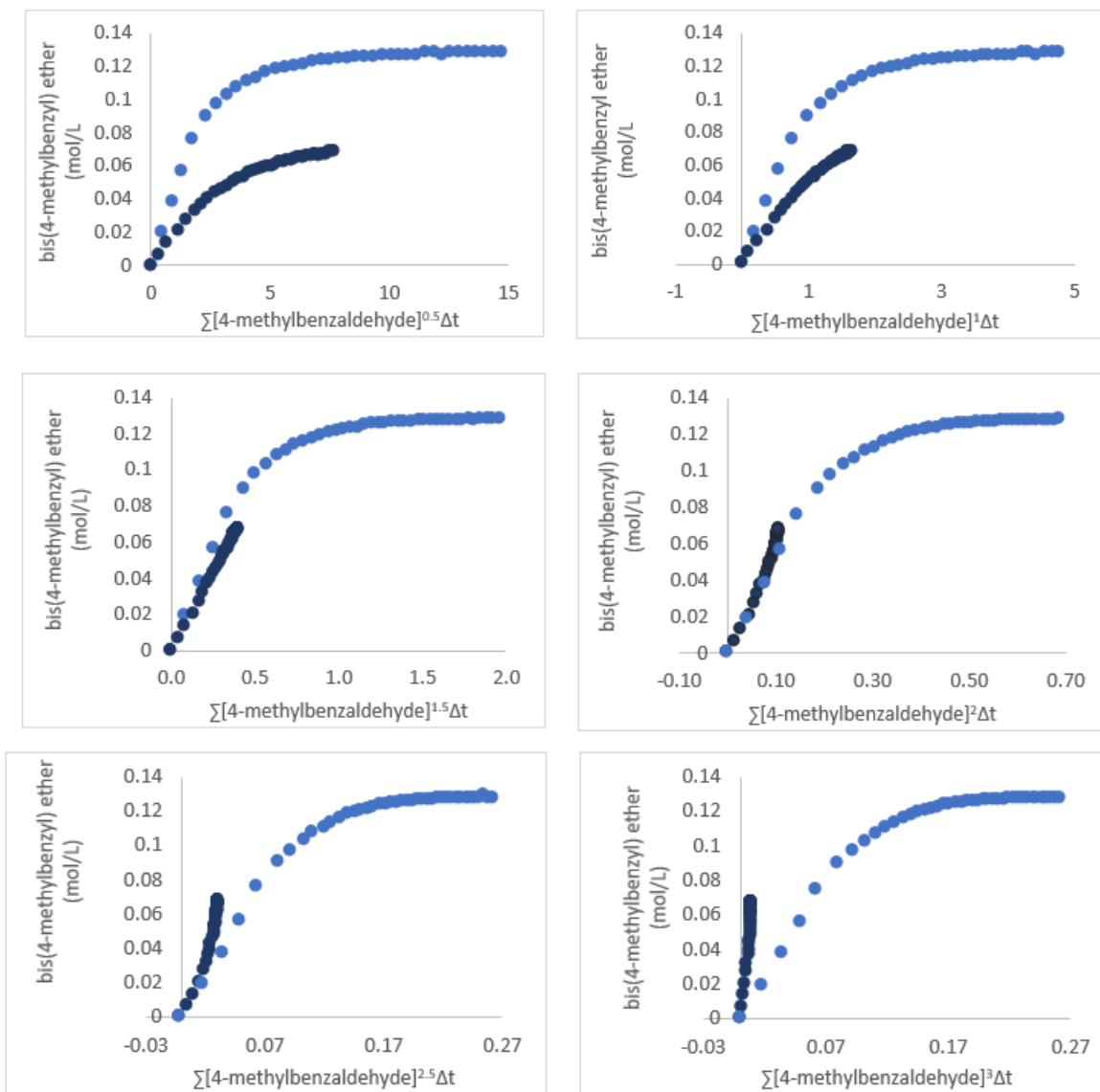


Figure 5.11 The VTNA plots for aldehyde etherification for 4-methylbenzaldehyde.

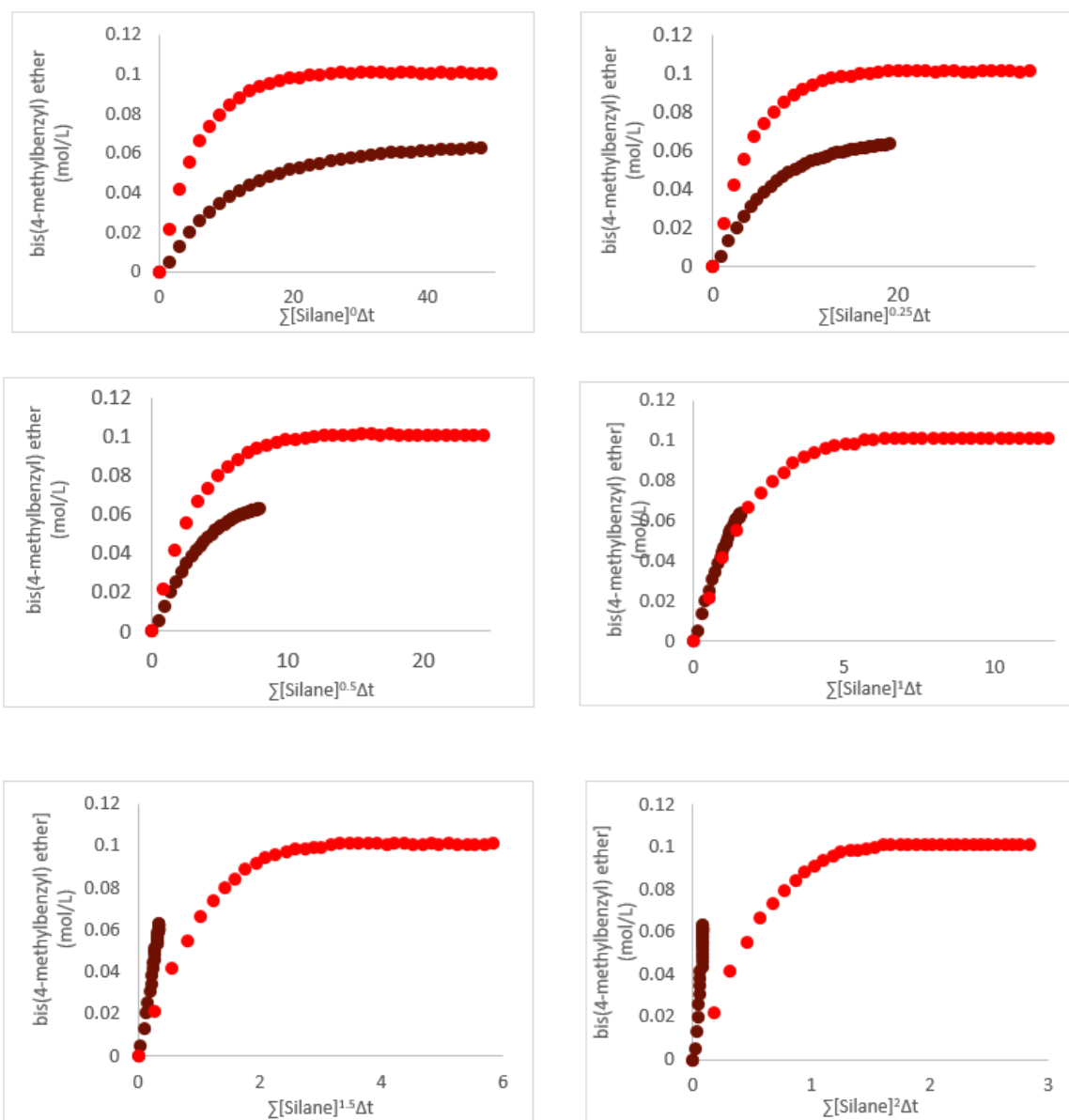


Figure 5.12 The VTNA plots for aldehyde etherification for triethylsilane.

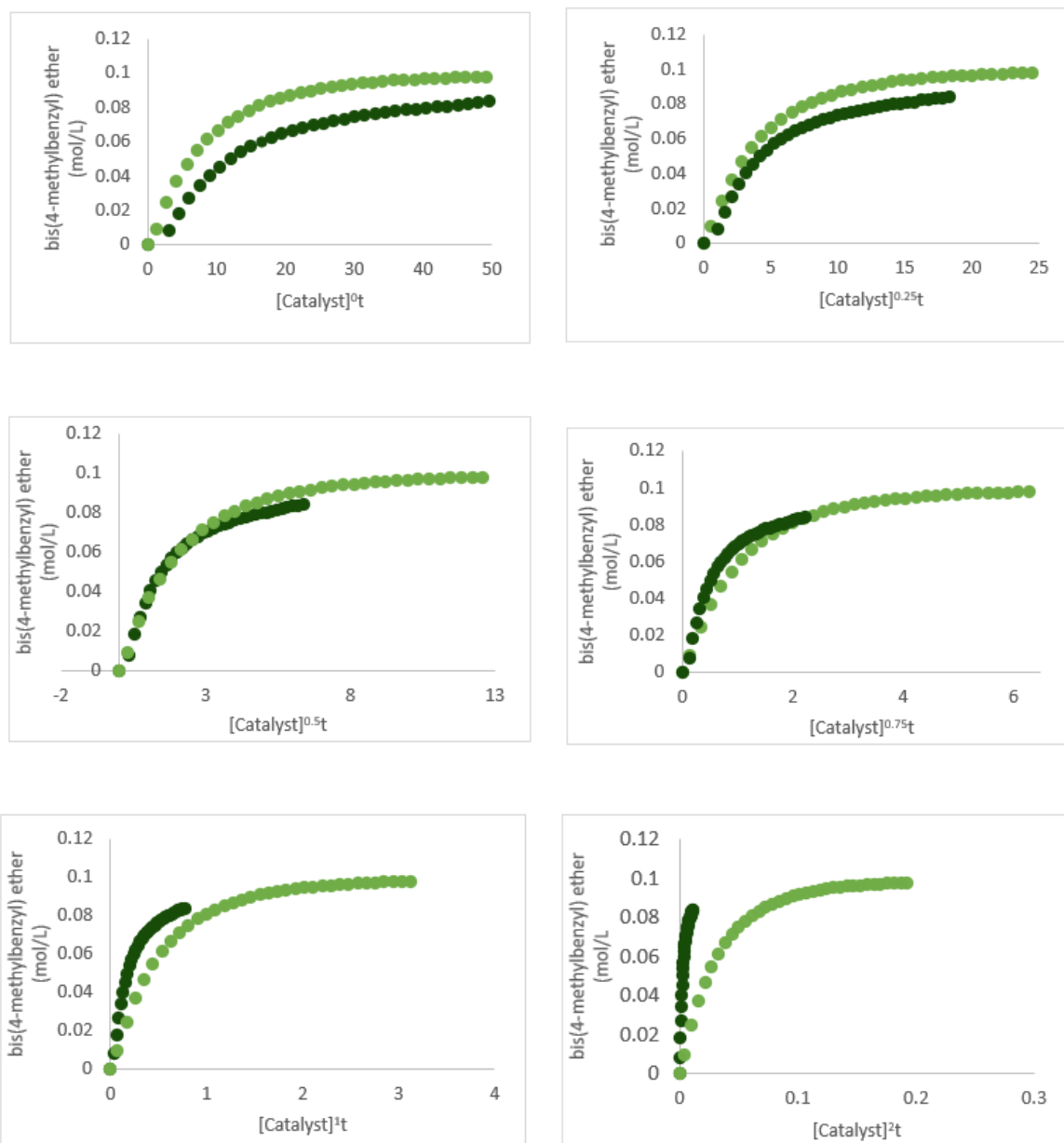


Figure 5.13 The VTNA plots for aldehyde etherification for $[\text{Ge}([\text{12}]\text{crown-4})_2][\text{OTf}]_2$.

5.10 References

- [1] Howard, P.; Morris, G.; Sunley, G. In *Metal-catalysis in Industrial Organic Processes*; Chiusoli, G. P., Maitlis, P. M., Eds.; RSC Publishing: Cambridge, 2019; pp 1–21.
- [2] Bhaduri, S.; Mukesh, D. In *Homogeneous catalysis: Mechanisms and industrial applications, 2nd edition*; John Wiley & Sons: Hoboken, NJ, 2014; pp 1–95.
- [3] The catalytic activity of the germanium(II) and tin(II) crown ether complexes is presented in Chapter 4 of this thesis.
- [4] a) Libermann-Martin, A. L.; Bergman, R. G.; Tilley, T. D. *J. Am. Chem. Soc.*, **2015**, *137*, 5328-5331. b) Thorwart, T.; Roth, D.; Greb, L. *Chem. Eur. J.*, **2021**, *27*, 10422-10427.
- [5] Roth, D.; Wadepohl, H.; Greb, L. *Angew. Chem. Int. Ed.*, **2020**, *132*, 21116-21120.
- [6] Fritz-Langhals, E.; Werge, S.; Kneissl, S.; Piroutek, P. *Org. Process Res. Dev.*, **2020**, *8*, 1484-1495.
- [7] Bach, P.; Albright, A.; Laali, K. K. *Eur. J. Chem.*, **2009**, *12*, 1961-1966.
- [8] Parks, D. J.; Piers, W. E. *J. Am. Chem. Soc.*, **1996**, *118*, 9440-9441.
- [9] Houghton, A. Y.; Hurmalainen, J.; Mansikkamäki, A.; Piers, W. E.; Tuononen, H. *M. Nat. Chem.*, **2014**, *6*, 983-988.
- [10] The addition of TEPO to germanium(II) and tin(II) crown ether complexes is presented in Chapter 3 of this thesis.
- [11] Schreck, J. O. *J. Chem. Educ.*, **1971**, *48*, 103-107.

- [12] Hansch, C.; Leo, A.; Taft, R. W. *Chem. Rev.*, **1991**, *91*, 165-195.
- [13] Jutzi, P. *Chem. Eur. J.*, **2014**, *20*, 9191-9207.
- [14] a) Rugar, P. A.; Bandyopadhyay, R.; Cooper, B. F. T.; Stinchcombe, M. R.; Ragogna, R. J.; Macdonald, C. L. B.; Baines, K. M. *Angew. Chem. Int. Ed.*, **2009**, *48*, 5155-5158. b) Bandyopadhyay, R.; Cooper, B. F. T.; Rossini, A. J.; Schurko, R. W.; Macdonald, C. L. B. *J. Organomet. Chem.*, **2010**, *695*, 1012-1028. c) Macdonald, C. L. B.; Bandyopadhyay, R.; Cooper, B. F. T.; Friedl, W. W.; Rossini, A. J.; Schruko, R. W.; Eichhorn, S. H.; Herber, R. H. *J. Am. Chem. Soc.*, **2012**, *134*, 4332-4345.
- [14] a) Yau, H. M.; Croft, A. K.; Harper, J. B. *Chem. Commun.*, **2012**, *48*, 8937-8939. b) Monsigny, L.; Thuéry, P.; Berthet, J.-C.; Cantat, T. *ACS Catal.*, **2019**, *9*, 9025-9033.
- [15] a) Nielsen, C. D.-T.; Burés, J. *Chem. Sci.*, **2018**, *10*, 348-353. b) Burés, J. *Angew. Chem. Int. Ed.*, **2016**, *55*, 16084-16087.
- [16] Atkins, P.; Julio, P. D. *Atkins' physical chemistry*; W.H. Freeman: New York, 2006; pp 830–834.

Chapter 6

6 Summary, Conclusions and Future Work

6.1 Summary and Conclusions

The work presented in this thesis has addressed three goals of this thesis: 1) to explore the activation and functionalization of small molecules by ditetrelenes 2) to investigate the Lewis acidity of low valent Group 14 complexes and 3) to evaluate the catalytic activity of low valent main group compounds and understand the mechanism of catalysis.

The activation of ammonia and organoamines can be achieved using a simple, tetraaryldisilene with no unusual structural features. The addition of ammonia and primary amines to tetramesityldisilene resulted in excellent conversion to disilylamines, the N-H activated products. Computational studies revealed the lowest energy reaction pathway involved three distinct steps: *anti*-donor adduct formation, inversion at the silicon bearing the lone pair and *syn* proton transfer. Attempts to utilize the disilylamines for further amine functionalization through the silylamination of electron deficient alkynes was not successful due to the steric limitations of the system. With the end goal being the functionalization of small molecules, such as ammonia, the steric limitations of the systems currently being used to activate small molecules are often not considered; the results herein have highlighted this as an issue within the field of ditetrelene catalysis. Reinvestigations into the silylamination of electron-deficient alkynes revealed low stereoselectivity and high sensitivity to moisture.

The quantitative assessment of the Lewis acidity of a series of low valent Group 14 crown ether complexes was conducted using three methods. The Gutmann-Beckett method indicated that the germanium(II) centre in the crown ether complexes was more Lewis acidic than the tin(II) centre and that the presence of a chloride ligand on the metal centre significantly decreases the Lewis acidity. A number of disadvantages of the Gutmann-Beckett method were realized, notably the ability of TEPO to displace the crown ether ligands changing the nature of the entity being assessed. The soft Lewis acidity of the crown ether complexes was investigated using a modified Gutmann-Beckett method employing TMPS as the Lewis base. Once again the germanium(II) derivatives were more Lewis acidic in comparison to the tin(II) complexes. FIA calculations also highlighted the greater Lewis acidity of germanium in comparison to tin. The catalytic activity of the germanium(II) and tin(II) crown ether triflate salts was investigated. In the reduction of 4-methylbenzaldehyde, high conversion to the symmetric ether was observed when the germanium complexes were used as catalysts while negligible conversion was observed using the analogous tin catalyst, in agreement with the results of the Lewis acidity assessment.

Investigations into and optimization of the etherification of 4-methylbenzaldehyde catalyzed by germanium(II) and tin(II) crown ether complexes revealed that the most selective and efficient catalyst is $[\text{Ge}(\text{[12]crown-4})_2][\text{OTf}]_2$ which was used to probe the scope of aldehyde hydrosilylation. The reaction was shown to tolerate a number of functional groups; however, low yields were observed for benzaldehydes with electron-

donating substituents in the *para*-position or aldehydes containing nitrogen donor atoms. Ketone hydrosilylation showed low conversion to any reduced product.

The mechanism of aldehyde hydrosilylation by $[\text{Ge}([\mathbf{12}\text{crown-4}]_2)[\text{OTf}]_2$ was probed using a variety of experimental techniques. The shape of the Hammett plot for the hydrosilylation of *para*-substituted aldehydes was concave, indicating a change the rate-limiting step between benzaldehydes with EWGs and those with EDGs. A negative slope for EWGs is consistent with a carbonyl-activated mechanism. No KIE was observed for the hydrosilylation of 4-methylbenzaldehyde with triethylsilane in agreement with the Hammett plot.

The work reported herein describes detailed investigations into the reactivity and catalytic activity of low valent Group 14 compounds. From the studies utilizing the Gutmann-Beckett method, it was revealed that weakly coordinated ligands could be easily displaced by the strong Lewis base changing the species being assessed. Furthermore, the coordination of multiple TEPO even at substoichiometric equivalents relative to the Lewis acid revealed that caution must be exercised in the assignment of the structures of TEPO-coordinated species to ensure accurate interpretation of the ANs. These results will help to ensure that, in future studies, the nature of the complexes in solution are correctly identified. In addition, this quantitative study has demonstrated the higher Lewis acidity of a germanium(II) complex in comparison to germanium(IV) complexes which may inspire further investigations into the development of germanium(II) Lewis acids. The study on the mechanism of hydrosilylation and subsequent etherification of aldehydes catalyzed by a

germanium(II) cation has provided direct evidence for a carbonyl-activated mechanism in contrast to the current proposed mechanisms in the field of cationic Group 14 catalysis.

6.2 Future Work

6.2.1 Experimental Determination of *Anti* or *Syn* Ammonia Addition to a Disilene

Wendel *et. al*¹ have previously reported the formation of an *anti* adduct of ammonia to a *Z* isomer of a disilene and is the only example of a stereochemical study of the addition of ammonia to a disilene. Thus, to expand the scope of amine additions and to further understand stereochemistry of the addition, the addition of ammonia to disilenes, such as **I-III**,² with known stereochemistry should be investigated (Figure 6.1). The *syn/anti* stereochemistry of the resulting adducts can be assigned using X-ray crystallography. The results of these experiments may further support the proposed general mechanism reported herein and also provide another example of an experimentally-determined stereochemical study of the reaction.

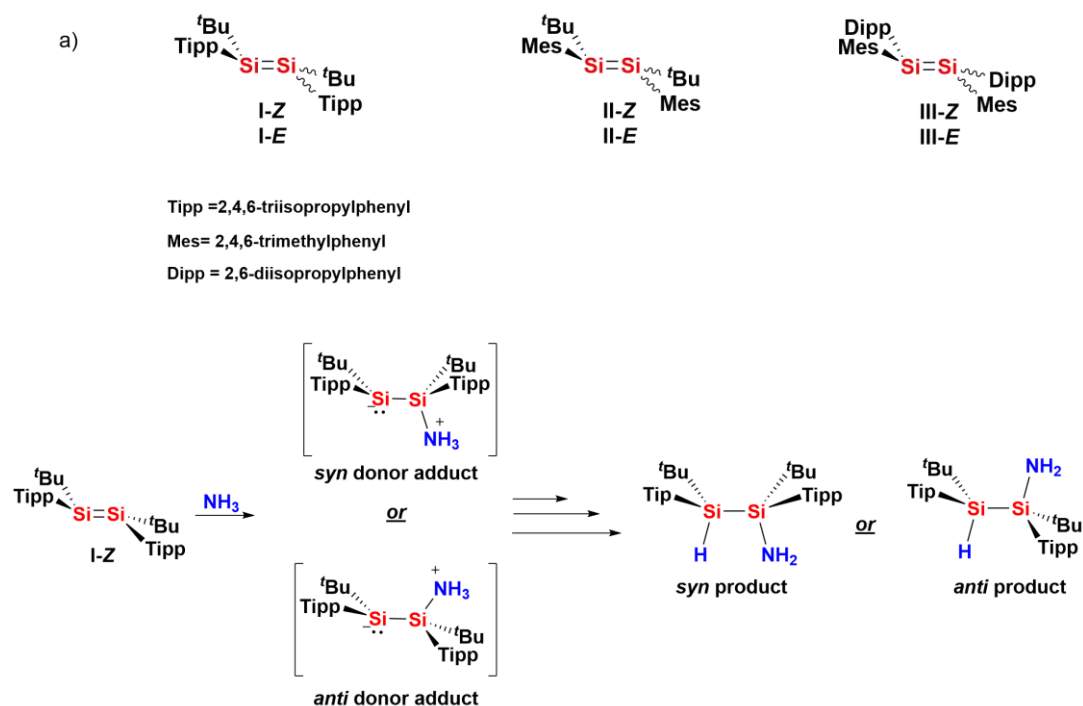


Figure 6.1 a) The structures of some disilenes with known stereochemistry. b) Possible reaction pathway for the addition of ammonia to a disilenes **I-Z** showing both possible donor adducts and the two possible reaction products.

6.3 Lewis Acidity Assessments

By definition, to measure the FIA of a Lewis acid, a single fluoride ion is added to the Lewis acid and the enthalpy of formation of the Lewis acid-base adduct is measured.³ This method inherently assumes that the most probable Lewis-acid base adduct formed will be a 1:1 adduct between a Lewis acid and fluoride ion; however, as observed in reactions with the germanium(II) and tin(II) crown ether complexes and TEPO, the coordination of two equivalents of Lewis base was observed with the displacement of the crown ether ligand. Given this information, FIA for the addition of two equivalents of fluoride the germanium(II) and tin(II) crown ether complexes (Figure 6.2) should be calculated as the

FIA's determined will be a better representation of the experimental reactivity of the complexes. In addition, calculations with and without the crown ether ligands should be conducted and may also provide further understanding of the Lewis acidity of the metal centre. These calculations may correlate better to the experimental results observed with the Gutmann-Beckett analysis as the Lewis-acid base adducts analyzed would better resemble the solution-state species.

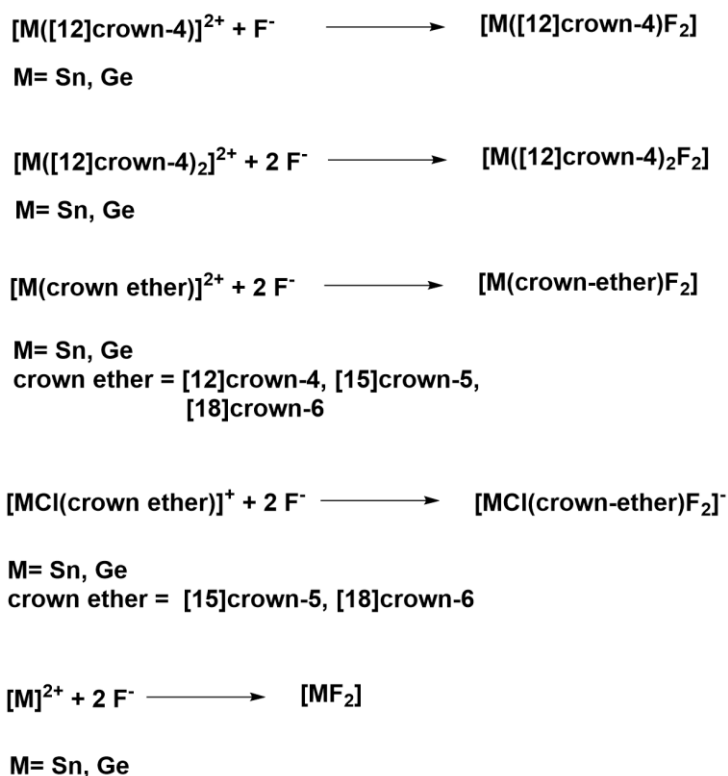
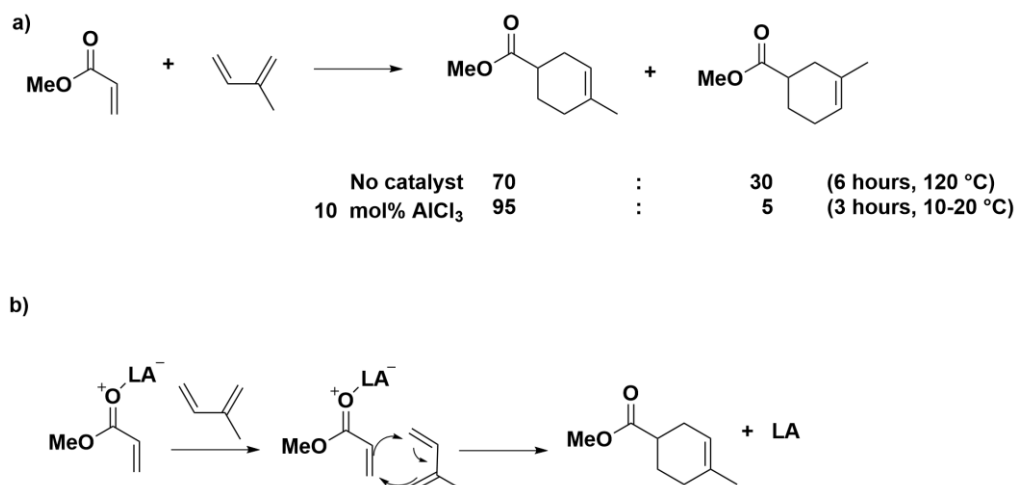


Figure 6.2 Proposed FIA calculations with the germanium(II) and tin(II) crown ether complexes.

6.4 Other Lewis Acid Catalysis

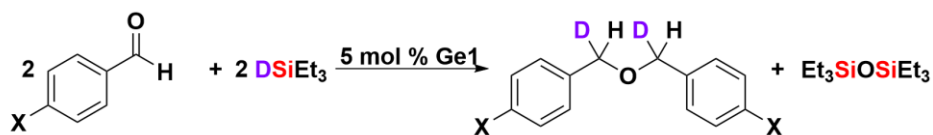
Lewis acid catalysis is a broad field encompassing a number of reactions. As activity towards aldehyde etherification using $[\text{Ge}([\text{12crown-4})_2][\text{OTf}]_2$ as a catalyst was observed through a carbonyl-activated mechanism, this catalyst may be suitable for other Lewis acid-catalyzed reactions. The selectivity of Diels-Alder reaction has been well-documented to be influenced by Lewis acids (Scheme 6.1a).⁴ When the dienophile contains a carbonyl group, the Lewis acid can coordinate (Scheme 6.1b), polarizing the double bond increasing reactivity towards the diene. The steric bulk of the Lewis acid can favor one transition state (*exo* with bulky substituents) leading to higher selectivity for one product over the other.⁵ The Diels-Alder reaction between methyl acrylate and 2-methyl-1,3-butadiene catalyzed by $[\text{Ge}([\text{12crown-4})_2][\text{OTf}]_2$ could be investigated as another example of Lewis acid catalysis to expand the applications of this catalyst.



Scheme 6.1 a) The influence of AlCl_3 on the Diels alder reaction between 2-methyl-1,3-butadiene and methyl acrylate and b) the mechanism of Lewis acid Diels alder catalysis.

6.5 Kinetic Isotope Effect Studies

No kinetic isotope effect was found in the etherification of 4-methylbenzaldehyde using $\text{HSiEt}_3/\text{DSiEt}_3$. The concave shape of the Hammett plot indicated that benzaldehydes with electron-withdrawing groups have a different rate-determining step than aldehydes with electron-donating groups. 4-Methylbenzaldehyde was found to lie on the intersection of the two linear relationships between $k_{\text{H}}/k_{\text{X}}$ in the Hammett plot, and thus, the absence of a KIE is not surprising. However, to further understand the mechanism, the KIE of other *para*-substituted benzaldehydes should be determined, notably those with EWGs and EDGs to see if the interpretation of the slopes of the Hammett plot are in agreement with the measured KIEs.



X = H, CN, F, OSiMe₃
Ge1 = [Ge([12]crown-4)₂][OTf]₂

Scheme 6.2 The reaction of *para*-substituted benzaldehydes and triethylsilane-*d*.

6.6 Mechanistic Study on the Hydrosilylation and Etherification of Aldehydes by Group 14 Crown Ether Trichlorometallate Salts

The reactivity of the germanium(II) and tin(II) crown ether trichlorometallate salts in the reduction of aldehydes was significantly different than the analogous triflate complexes, as evidenced by a mixture of products observed and different reaction conditions required.⁶ The different reactivity as well as the structural difference observed

between the triflate and trichlorometallate crown ether salts are such that the established mechanism of aldehyde etherification by $[\text{Ge}([\text{12}]\text{crown-4})_2][\text{OTf}]_2$ cannot be extended to the trichlorometallate crown ether. Instead, a separate mechanistic study on the reduction of aldehydes by $[\text{GeCl}([\text{18}]\text{crown-6})][\text{GeCl}_3]$ and $[\text{SnCl}([\text{18}]\text{crown-6})][\text{SnCl}_3]$, the most effective germanium and tin trichlorometallate complexes, respectively. In this study, determination of the activate catalyst, a Hammett analysis, VTNA studies and KIE experiments could be used to propose a mechanism for reduction in reactions using these catalysts.

The catalysis reported herein is one of four examples of catalysis by a cationic germanium(II) centre and the only example in which linear free energy relationships were implemented to understand the reaction mechanism. The ability of the germanium(II) crown ether complexes to coordinate Lewis bases and hydrosilylation/etherification catalysis will hopefully inspire the development of more cationic germanium(II) complexes and further investigation of germanium(II) crown ether complexes as catalysts.

6.7 References

- [1] Wendel, D.; Szilvási, T.; Henschel, D.; Altmann, P. J.; Jandl, C.; Inoue, S.; Rieger, B. *Angew. Chem. Int. Ed.*, **2018**, *57*, 14575-14579.
- [2] a) Fink, M. J.; Mchalczyk, M. J.; Haller, K. J.; West, R. *Organometallics*, **1994**, *3*, 793-800. b) Archibald, R. S.; van den Winkel, Y.; Millevolte, A. J.; Desper, J M.; West, R. *Organometallics*, **1992**, *11*, 3276-3281. c) Batcheller, S. A.; Tsumuraya, T.; Tempkin, O.; Davis, W. M.; Masamune, S. *J. Am. Chem. Soc.*, **1990**, *112*, 9394-9395.

- [3] Erdmann, P.; Leitner, J.; Schwarz, J.; Greb, L. *ChemPhysChem*, **2020**, *21*, 987 – 994.
- [4] Inukai, T.; Kojima, T. *J. Org. Chem.*, **1966**, *31*, 1121-1123.
- [5] Yepes, D.; Pérez, P.; Jaque, P.; Fernández, I. *Org. Chem. Front.*, **2017**, *4*, 1390-1399.
- [6] The mechanism of aldehyde etherification catalyzed by [Ge([12]crown-4)][OTf]₂ is presented in Chapter 5 of this thesis.

Appendices

Appendix A : Supplementary Materials for Chapter 2

AA Table 1 Summary of crystal data for **2.3**.

Formula	C ₃₉ H ₅₃ NSi ₂
CCDC #	2025827
Formula Weight (g/mol)	592.00
Crystal Dimensions (mm)	0.243 × 0.057 × 0.055
Crystal Color and Habit	colourless prism
Crystal System	Triclinic
Space Group	P -1
Temperature, K	110
a, Å	11.803(6)
b, Å	12.244(7)
c, Å	12.493(6)
α, °	86.15(3)
β, °	88.39(3)
γ, °	70.61(2)
V, Å ³	1699.2(16)
Number of reflections to determine final unit cell	2497
Min and Max 2θ for cell determination, °	4.9, 44.0
Z	2
F(000)	644
ρ (g/cm)	1.157
λ, Å, (MoKα)	0.71073
μ, (cm ⁻¹)	0.132
Diffractometer Type	Bruker Kappa Axis Apex2
Scan Type(s)	phi and omega scans
Max 2θ for data collection, °	48.84
Measured fraction of data	0.995
Number of reflections measured	24512
Unique reflections measured	5581
R _{merge}	0.0857
Number of reflections included in refinement	5581
Cut off Threshold Expression	I > 2sigma(I)
Structure refined using	full matrix least-squares using F ²
Weighting Scheme	w=1/[sigma ² (Fo ²)+(0.0783P) ² +0.8302P] where P=(Fo ² +2Fc ²)/3
Number of parameters in least-squares	399
R ₁	0.0606
wR ₂	0.1424
R ₁ (all data)	0.1094
wR ₂ (all data)	0.1655
GOF	1.020

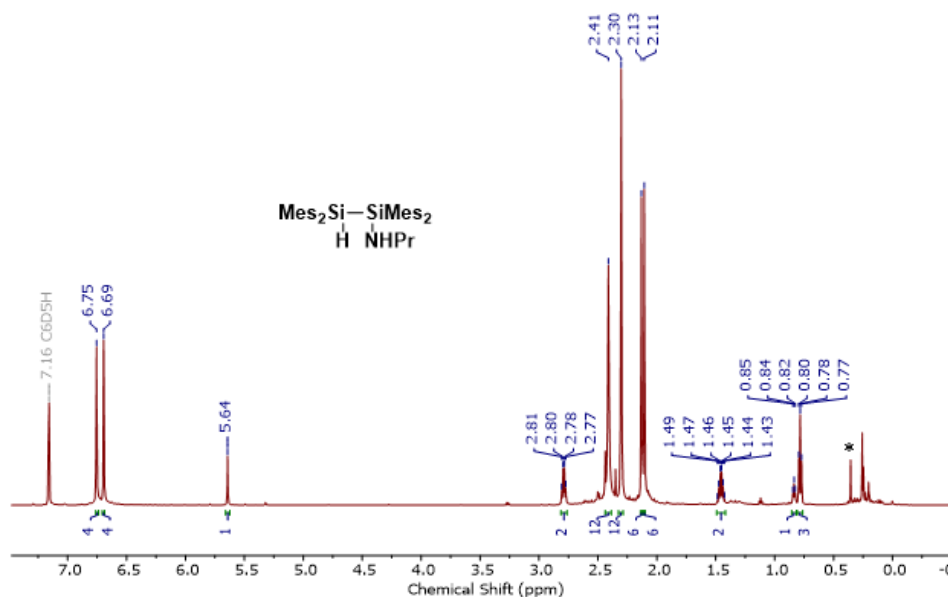
Maximum shift/error	0.000
Min & Max peak heights on final ΔF Map ($e^-/\text{\AA}$)	-0.365, 0.567

Where:

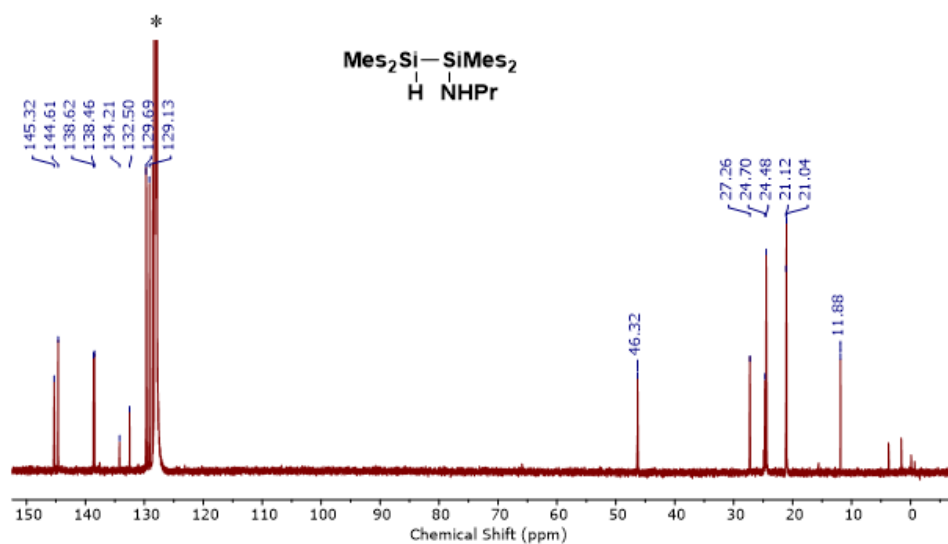
$$R_1 = \Sigma (|F_o| - |F_c|) / \Sigma F_o$$

$$wR_2 = [\Sigma (w (F_o^2 - F_c^2)^2) / \Sigma (w F_o^4)]^{1/2}$$

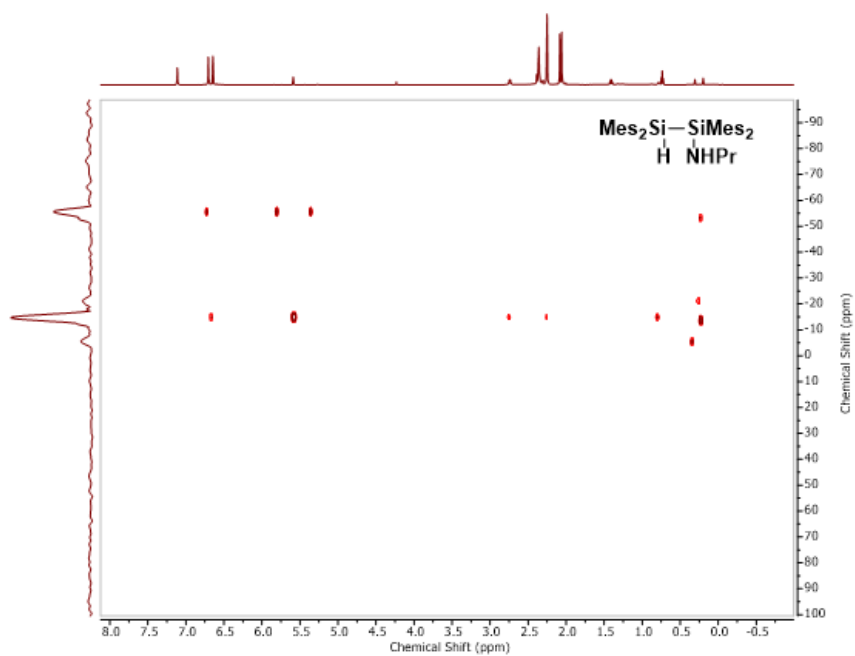
$$\text{GOF} = [\Sigma (w (F_o^2 - F_c^2)^2) / (\text{No. of reflns.} - \text{No. of params.})]^{1/2}$$



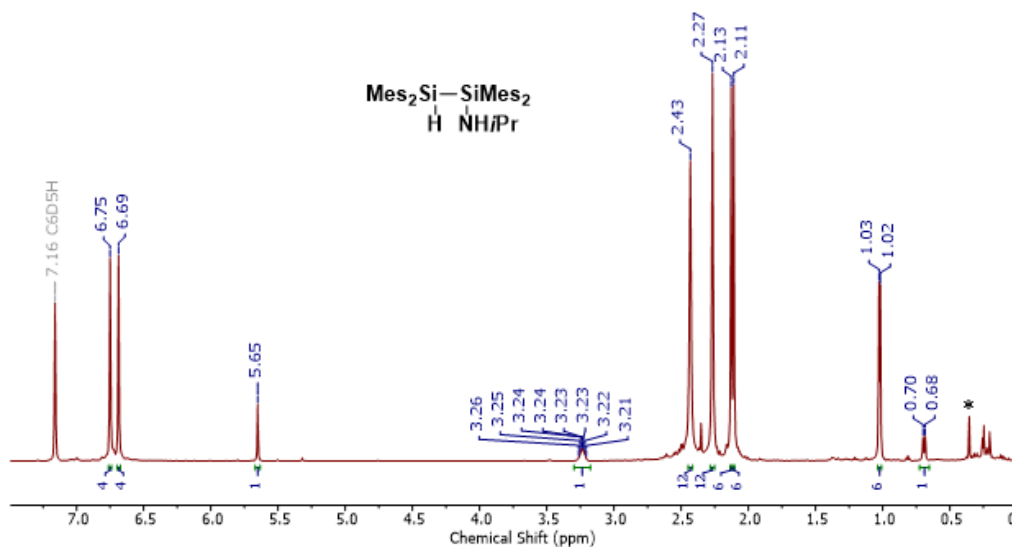
AA Figure 1 ^1H NMR spectrum (600 MHz, C_6D_6) of **2.3**. The signal denoted by * is trace water. Upfield signals in the spectrum are attributed to trace impurities from the synthesis of **2.1**.



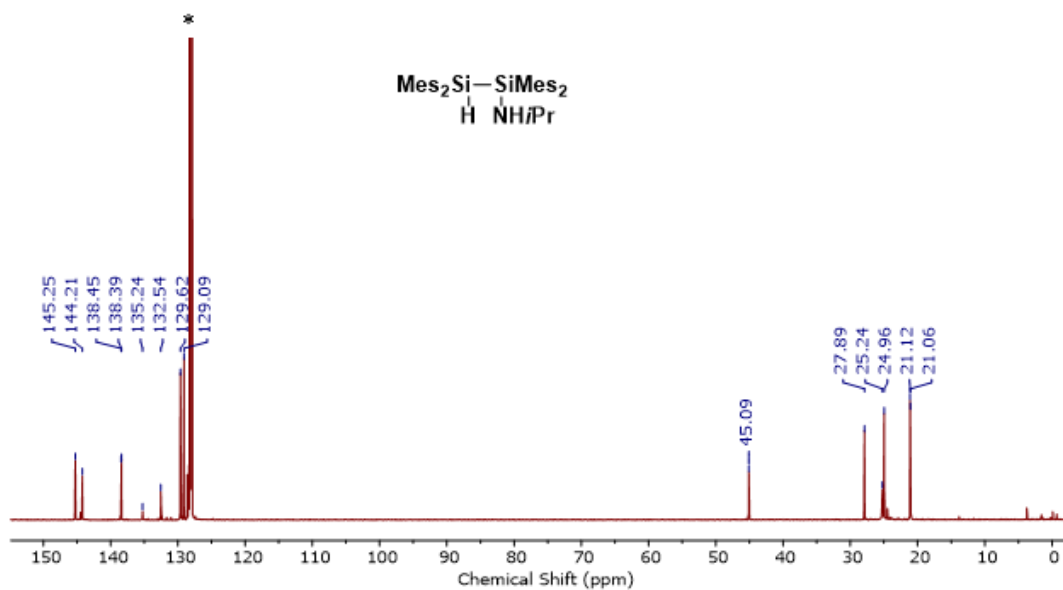
AA Figure 2 $^{13}\text{C}\{^1\text{H}\}$ NMR spectrum (151 MHz, C_6D_6) of **2.3**. The signal denoted with * is the solvent C_6D_6 . The unlabeled upfield peaks are trace impurities from the synthesis of **2.1**.



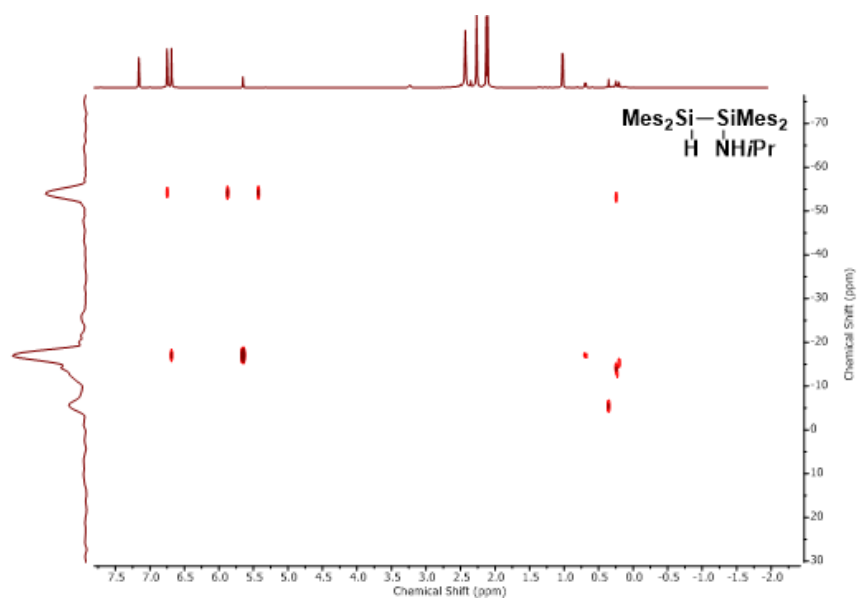
AA Figure 3 $^1\text{H}-^{29}\text{Si}$ gHMBC spectrum (C_6D_6) of **2.3**.



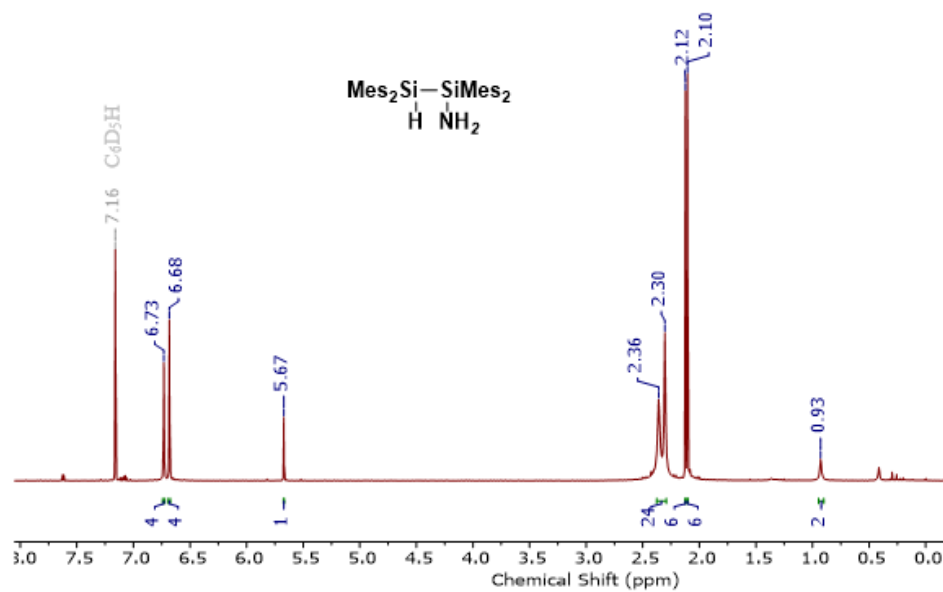
AA Figure 4 ^1H NMR spectrum (600 MHz, C_6D_6) of **2.4**. The signal denoted with * is trace water. Upfield signals in the spectrum are attributed to trace impurities from the synthesis of **2.1**.



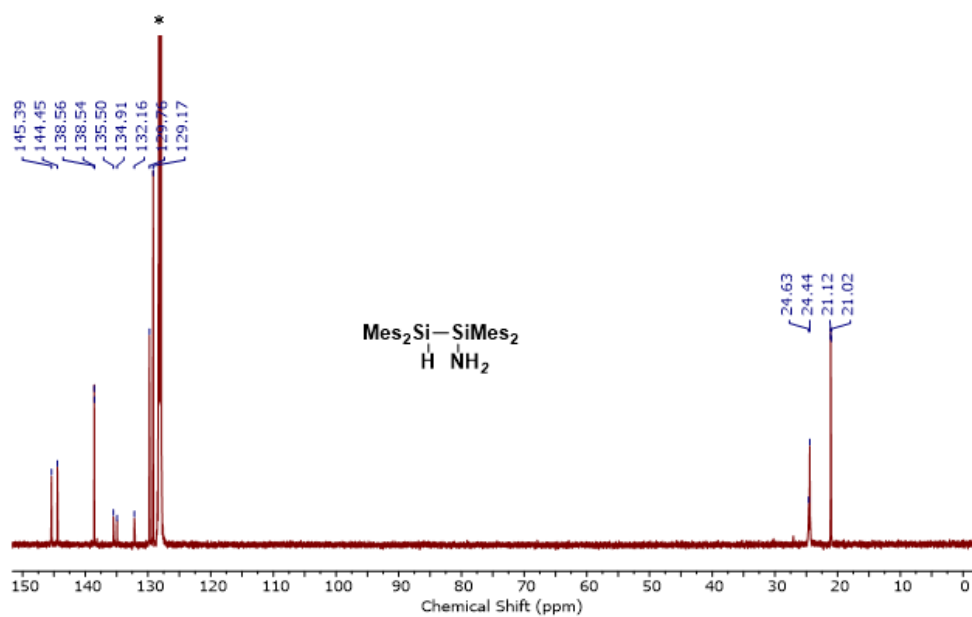
AA Figure 5 $^{13}\text{C}\{^1\text{H}\}$ NMR spectrum (151 MHz, C_6D_6) of **2.4**. The signal denoted with * is the solvent C_6D_6 .



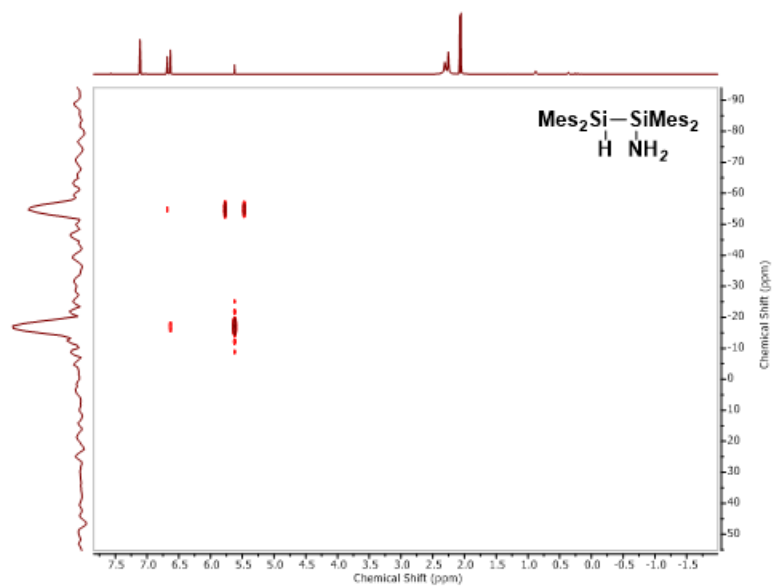
AA Figure 6 ^1H - ^{29}Si gHMBC spectrum (C_6D_6) of **2.4**.



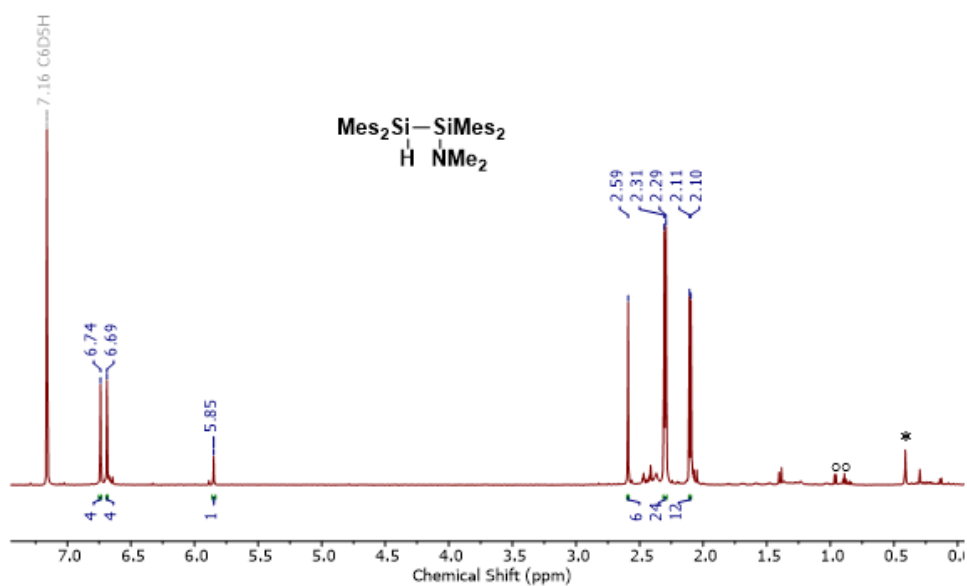
AA Figure 7 ^1H NMR spectrum (600 MHz, C_6D_6) of **2.5**.



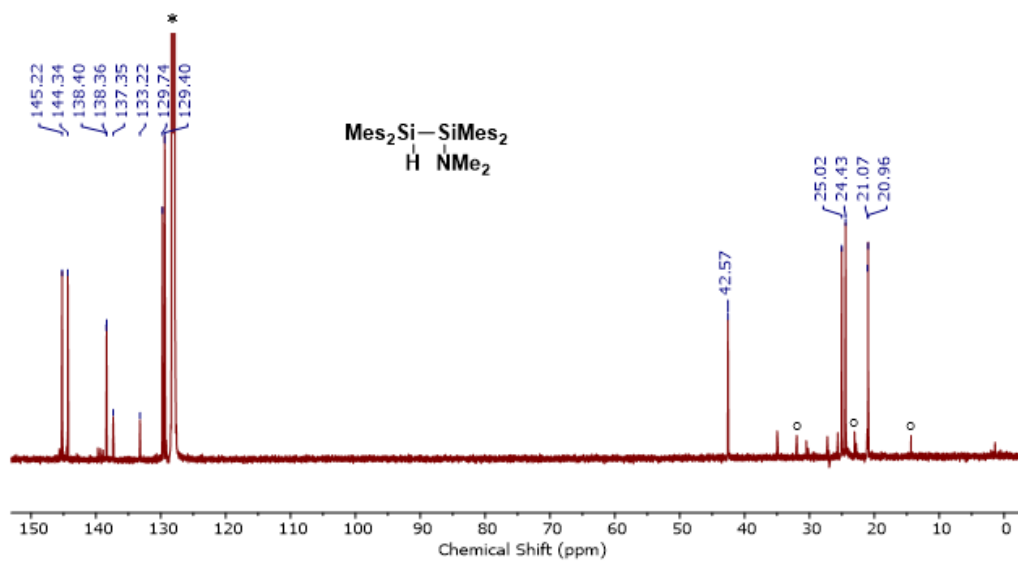
AA Figure 8 $^{13}\text{C}\{^1\text{H}\}$ NMR spectrum (151 MHz, C_6D_6) of **2.5**. The signal denoted with * is the solvent C_6D_6 .



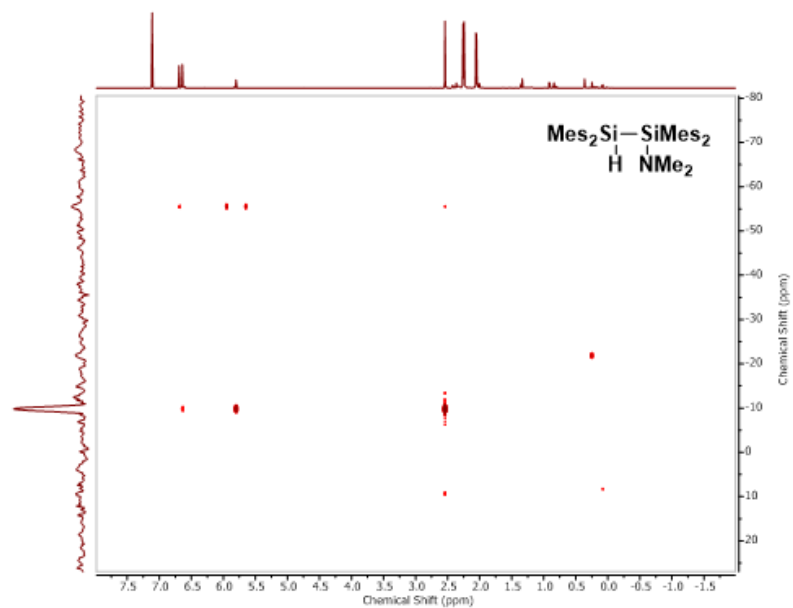
AA Figure 9 $^1\text{H}-^{29}\text{Si}$ gHMBC spectrum (C_6D_6) of **2.5**.



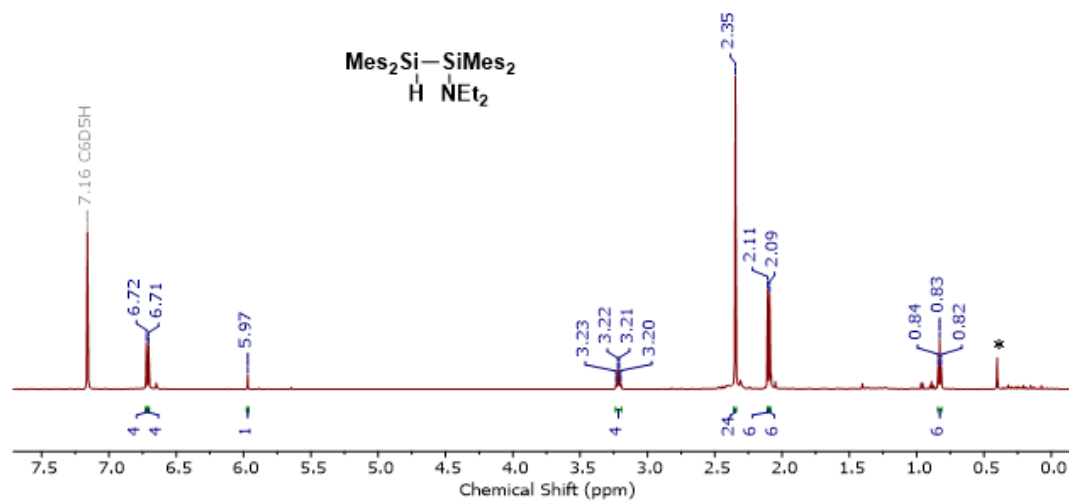
AA **Figure 10** ^1H NMR spectrum (600 MHz, C_6D_6) of **2.6**. The signal denoted with * is trace water. The signal denoted with $^\circ$ are residual hexanes.



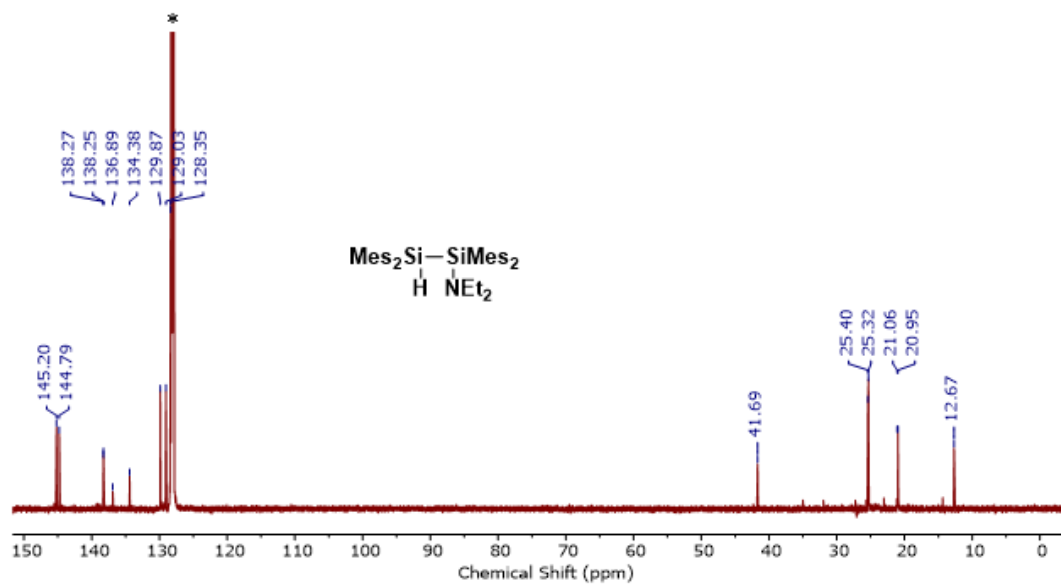
AA **Figure 11** $^{13}\text{C}\{^1\text{H}\}$ NMR spectrum (151 MHz, C_6D_6) of **2.6**. The signal denoted with * is the solvent C_6D_6 . The signals denoted with $^\circ$ are residual hexanes.



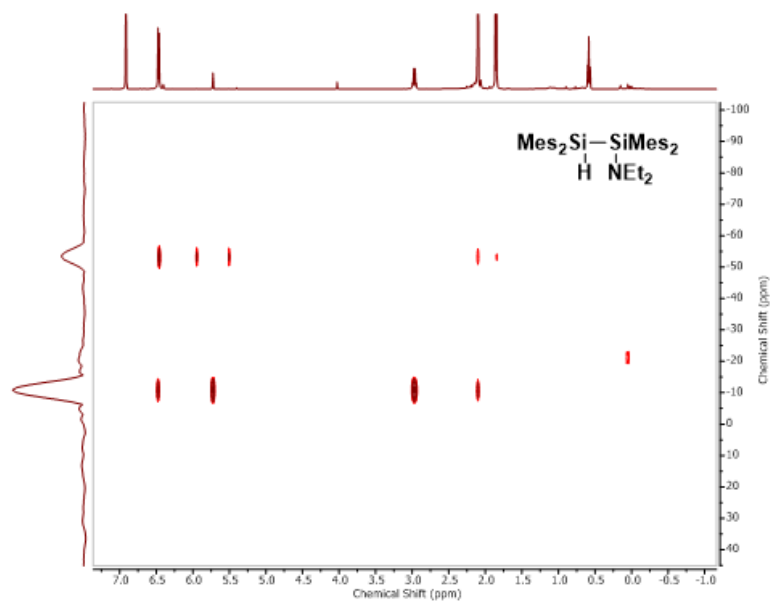
AA Figure 12 $^1\text{H}-^{29}\text{Si}$ gHMBC spectrum (C_6D_6) of **2.6**.



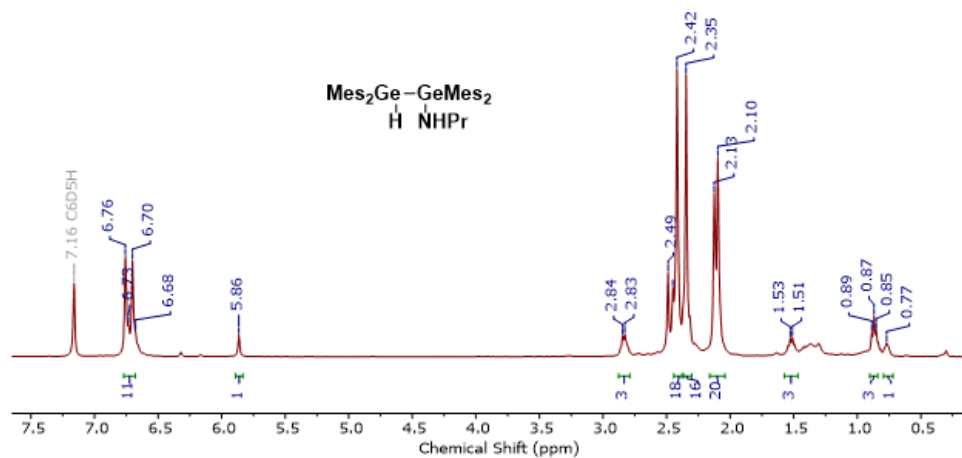
AA Figure 13 ^1H NMR spectrum (600 MHz, C_6D_6) of **2.7**. The signal denoted with * is trace water.



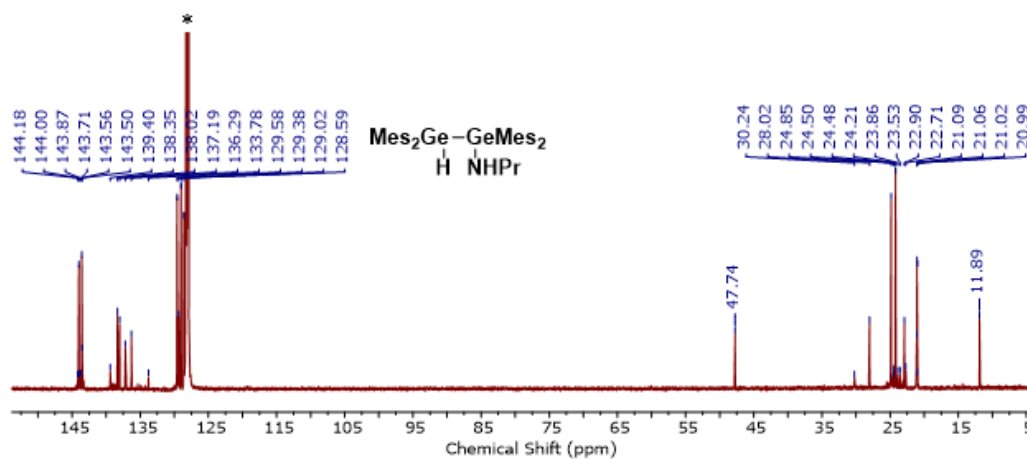
AA Figure 14 $^{13}\text{C}\{^1\text{H}\}$ NMR spectrum (151 MHz, C_6D_6) of **2.7**. The signal denoted with * is the solvent C_6D_6 .



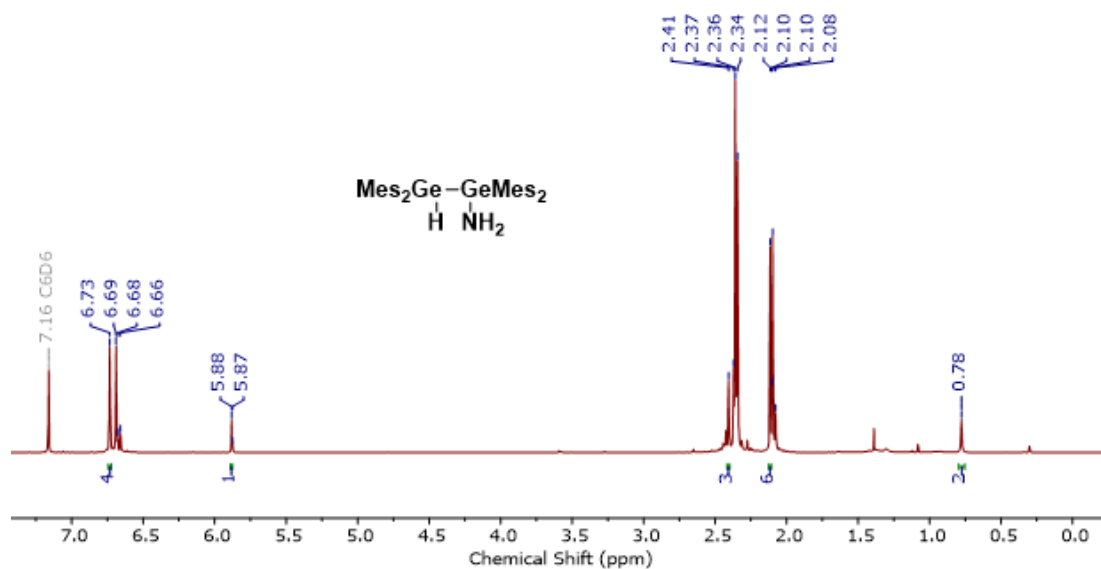
AA Figure 15 $^1\text{H}-^{29}\text{Si}$ gHMBC spectrum (C_6D_6) of **2.7**.



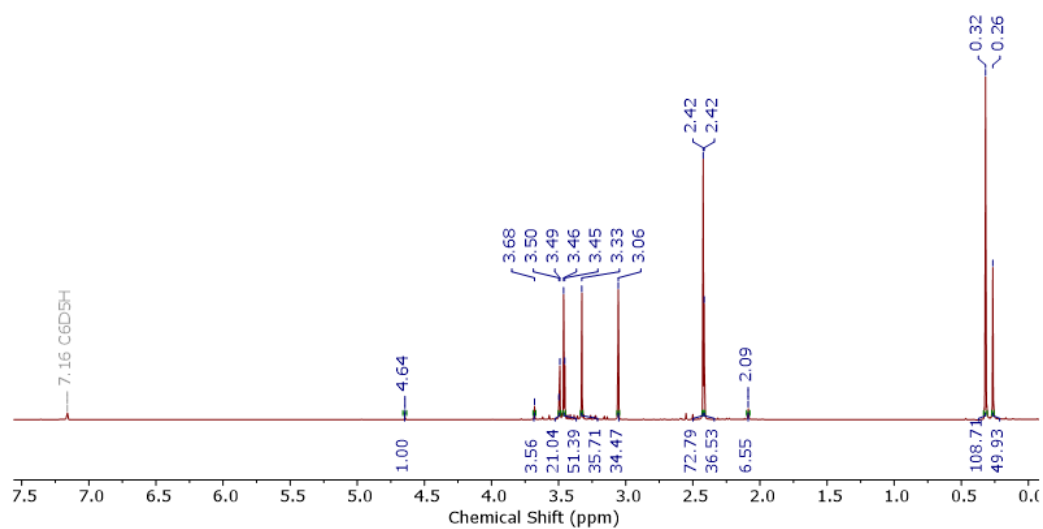
AA Figure 16 ^1H NMR spectrum (600 MHz, C_6D_6) of crude **2.8**. The second set of signals are consistent with 1,1,2,2-tetramesityldigermanol.



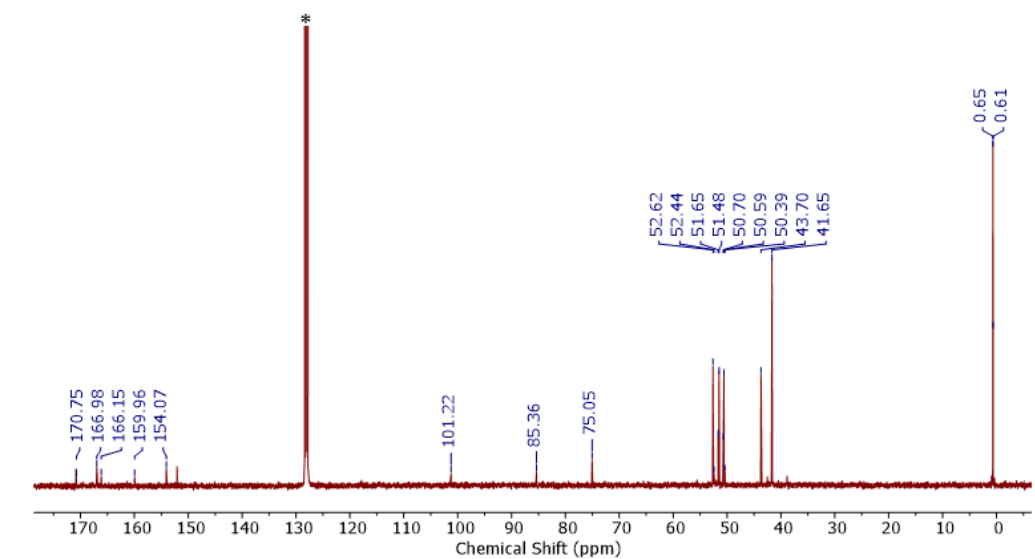
AA Figure 17 $^{13}\text{C}\{^1\text{H}\}$ NMR spectrum (151 MHz, C_6D_6) of crude **2.8**. The signal denoted with * is the solvent C_6D_6 .



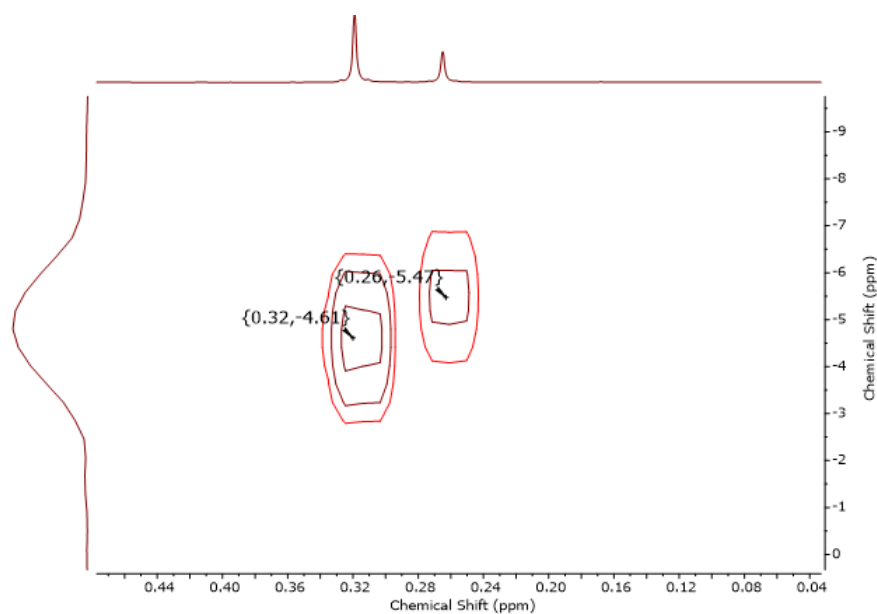
AA Figure 18 ^1H NMR spectrum (600 MHz, C_6D_6) of crude **2.9**. 1,1,2,2-tetramesityldigermanol can also be observed in the spectrum.



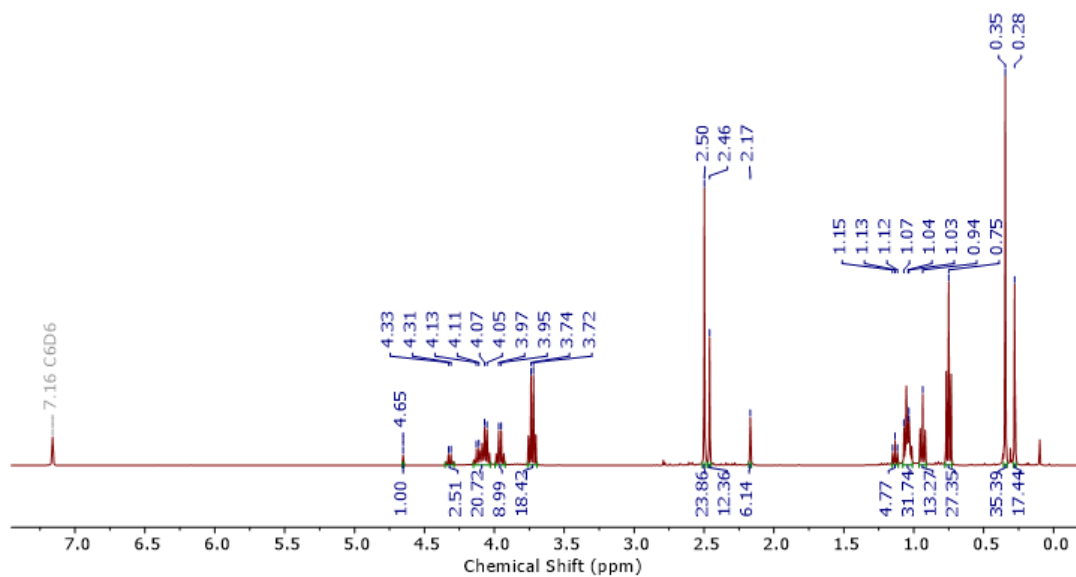
AA Figure 19 ^1H NMR spectrum of the reaction of N, N-dimethyl(trimethylsilyl)amine and dimethyl acetylenedicarboxylate (Table 2.1, Entry 1).



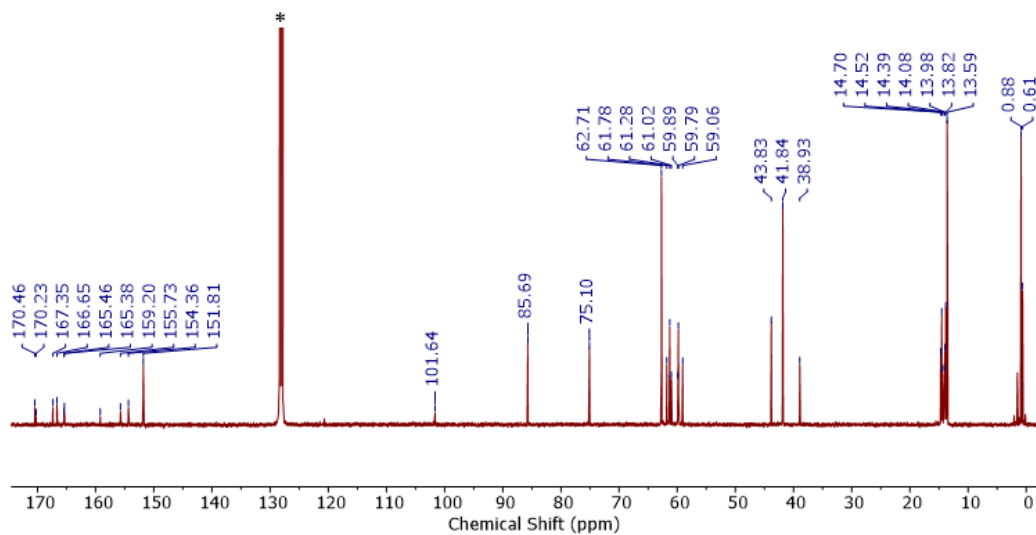
AA Figure 20 $^{13}\text{C}\{^1\text{H}\}$ NMR spectrum for the reaction of N, N-dimethyl(trimethylsilylamine) and dimethyl acetylenedicarboxylate (Table 2.1, Entry 1). The signal denoted with * is the solvent C_6D_6 .



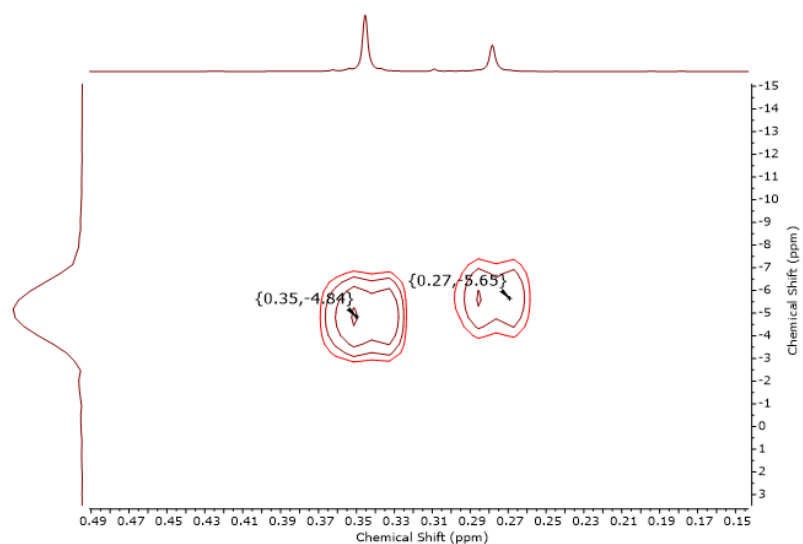
AA Figure 21 $^1\text{H}\text{-}^{29}\text{Si}$ HMBC NMR spectrum of the reaction of N, N-dimethyl(trimethylsilylamine) and dimethyl acetylenedicarboxylate (Table 2.1, Entry 1).



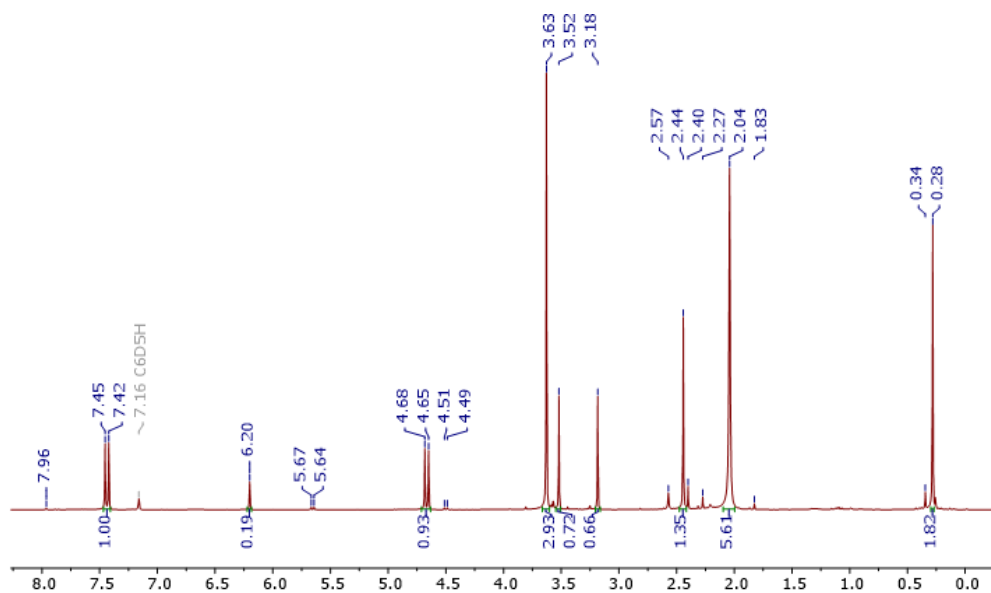
AA Figure 22 ^1H NMR spectrum of the reaction of N, N-dimethyl(trimethylsilylamine) and diethyl acetylenedicarboxylate (Table 2.1, Entry 2).



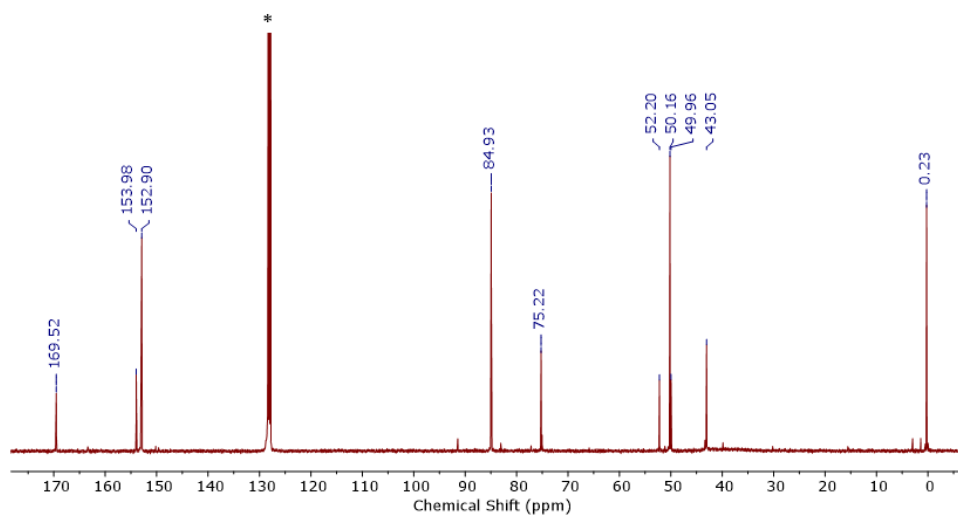
AA Figure 23 $^{13}\text{C}\{^1\text{H}\}$ NMR spectrum for the reaction of N, N-dimethyl(trimethylsilylamine) and diethyl acetylenedicarboxylate (Table 2.1, Entry 2). The signal denoted with * is the solvent C_6D_6 .



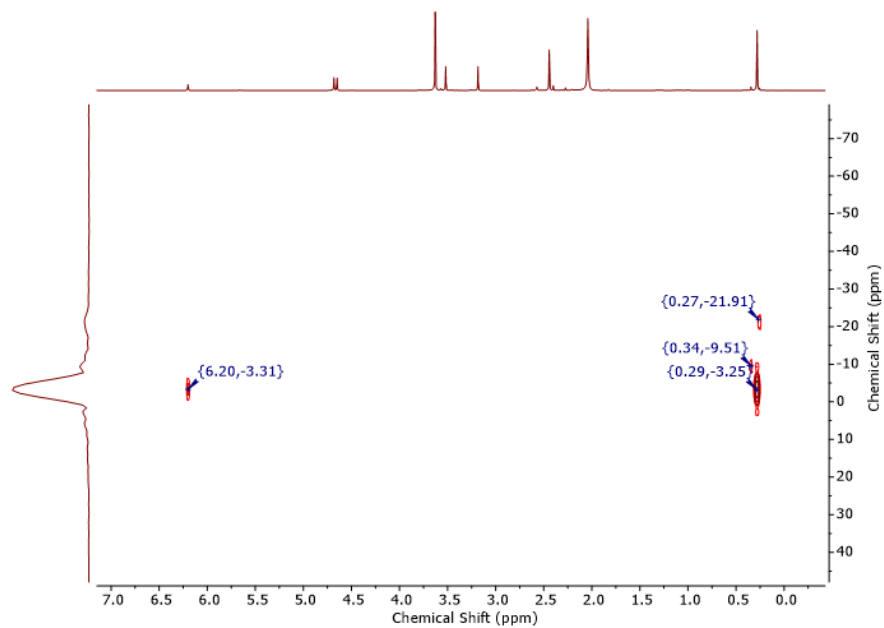
AA Figure 24 ¹H-²⁹Si HMBC NMR spectrum of the reaction of N, N-dimethyl(trimethylsilylamine) and diethyl acetylenedicarboxylate (Table 2.1, Entry 2).



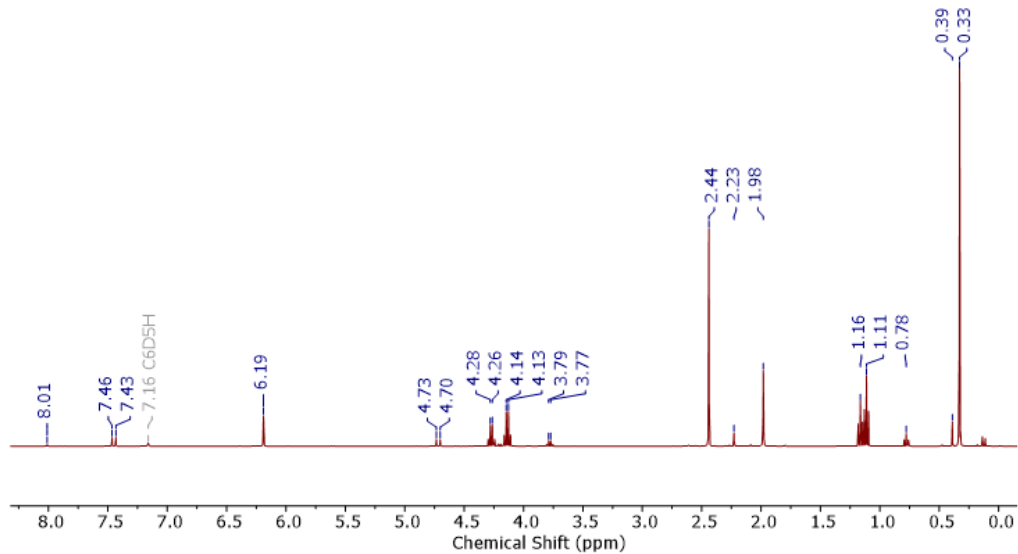
AA Figure 25 ¹H NMR spectrum of the reaction of N, N-dimethyl(trimethylsilylamine) and methyl propiolate (Table 2.1, Entry 3).



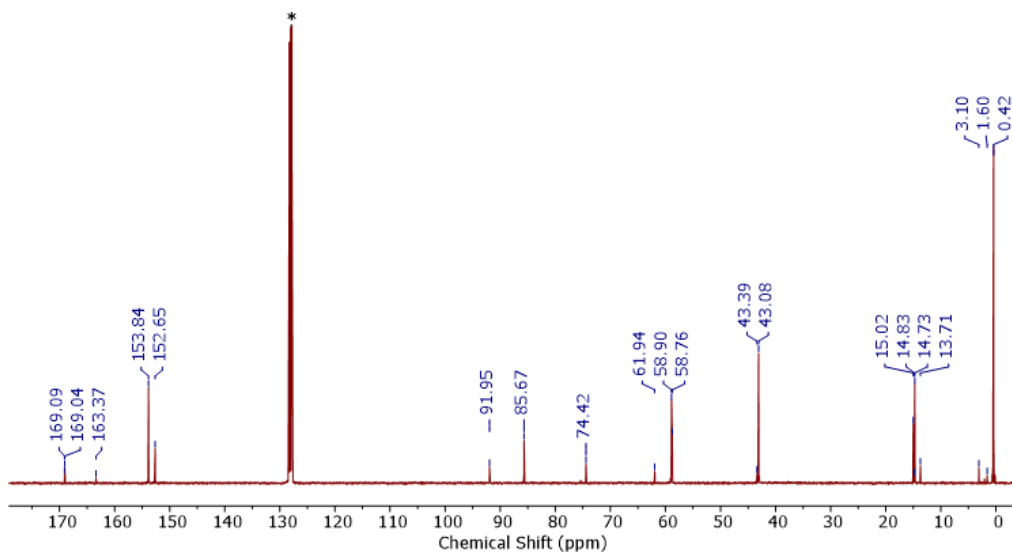
AA Figure 26 $^{13}\text{C}\{^1\text{H}\}$ NMR spectrum for the reaction of N, N-dimethyl(trimethylsilylamine) and methyl propiolate (Table 2.1, Entry 3). The signal denoted with * is the solvent C_6D_6 .



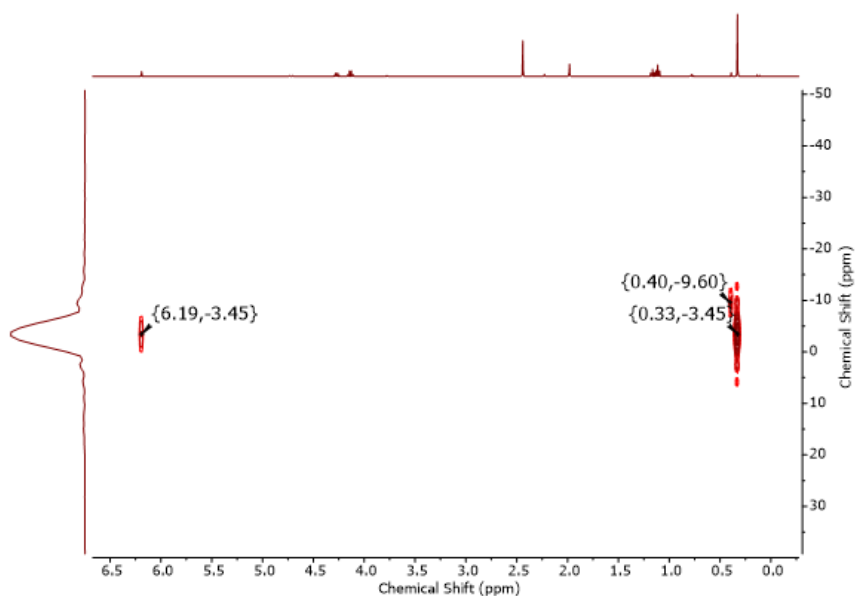
AA Figure 27 ^1H - ^{29}Si HMBC NMR spectrum of the reaction of N, N-dimethyl(trimethylsilyl-amine) and methyl propiolate (Table 2.1, Entry 3).



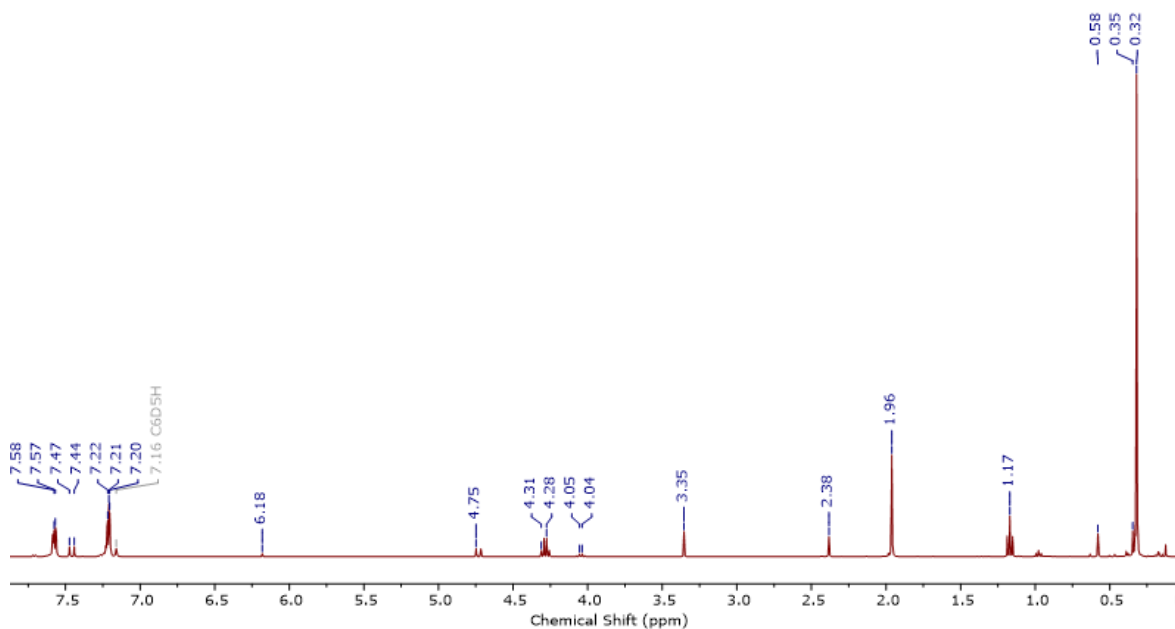
AA Figure 28 ^1H NMR spectrum of the reaction of N, N-dimethyl(trimethylsilylamine) and ethyl propiolate (Table 2.1, Entry 4).



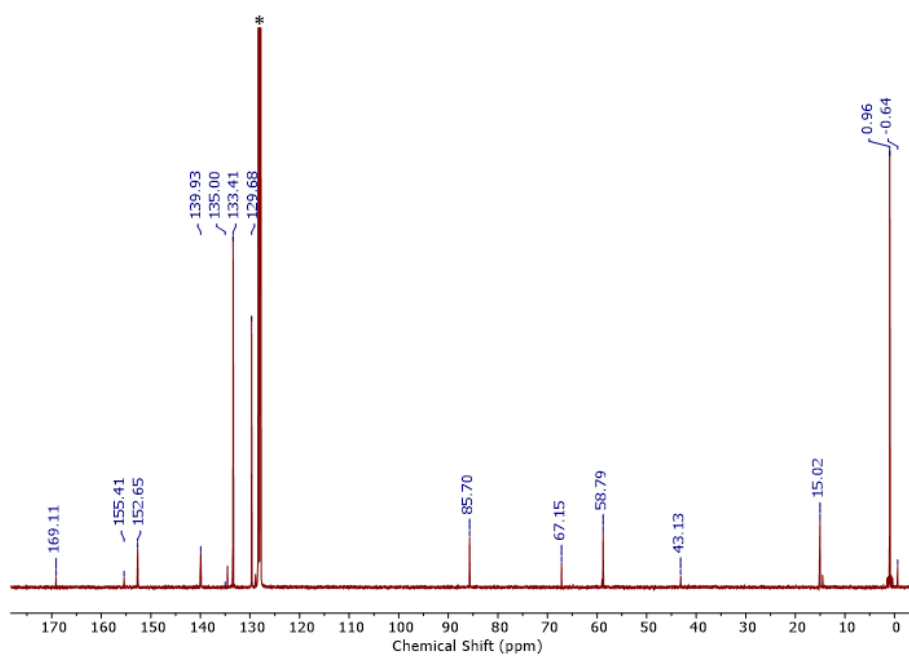
AA Figure 29 $^{13}\text{C}\{^1\text{H}\}$ NMR spectrum for the reaction of N, N-dimethyl(trimethylsilylamine) and ethyl propiolate (Table 2.1, Entry 4). The signal denoted with * is the solvent C_6D_6 .



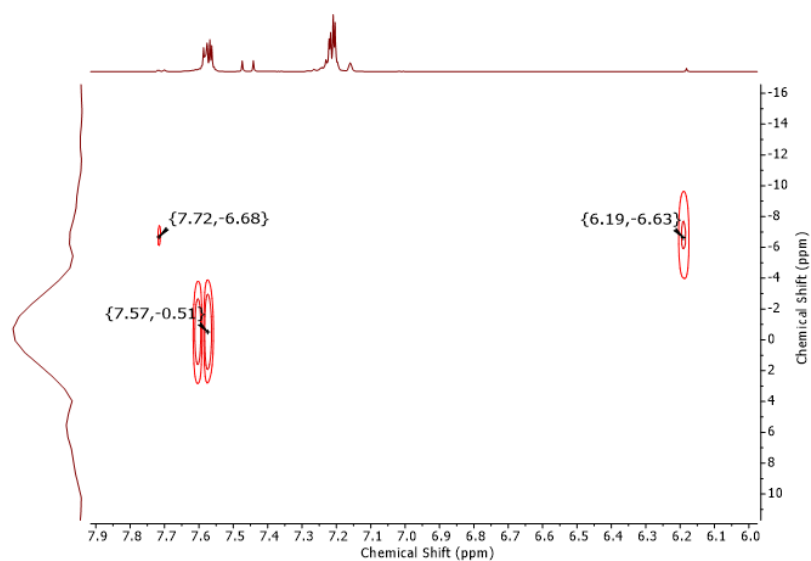
AA Figure 30 ^1H - ^{29}Si HMBC NMR spectrum of the reaction of N, N-dimethyl(trimethylsilyl-amine) and ethyl propiolate (Table 2.1, Entry 4).



AA Figure 31 ^1H NMR spectrum of the reaction of N, N-dimethyl((dimethylphenylsilyl)amine) and ethyl propiolate (Table 2.1, Entry 12).

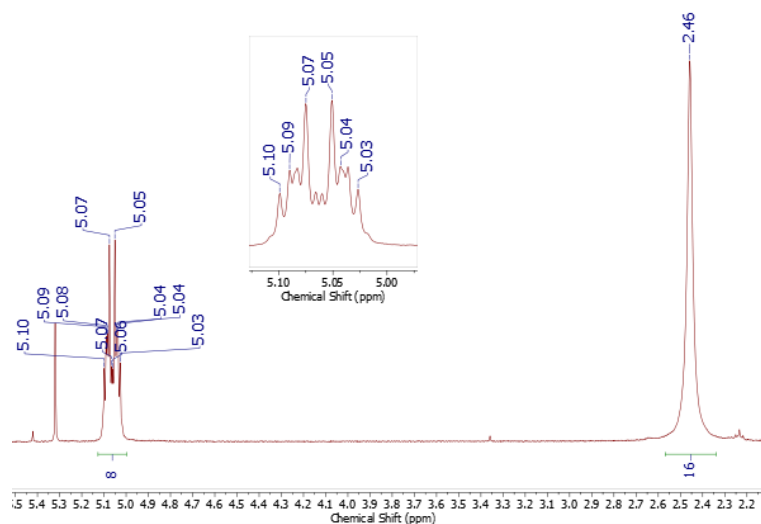


AA Figure 32 $^{13}\text{C}\{^1\text{H}\}$ NMR spectrum for the reaction of N, N-dimethyl((dimethylphenylsilyl)amine) and ethyl propiolate (Table 2.1, Entry 12). The signal denoted with * is the solvent C_6D_6 .

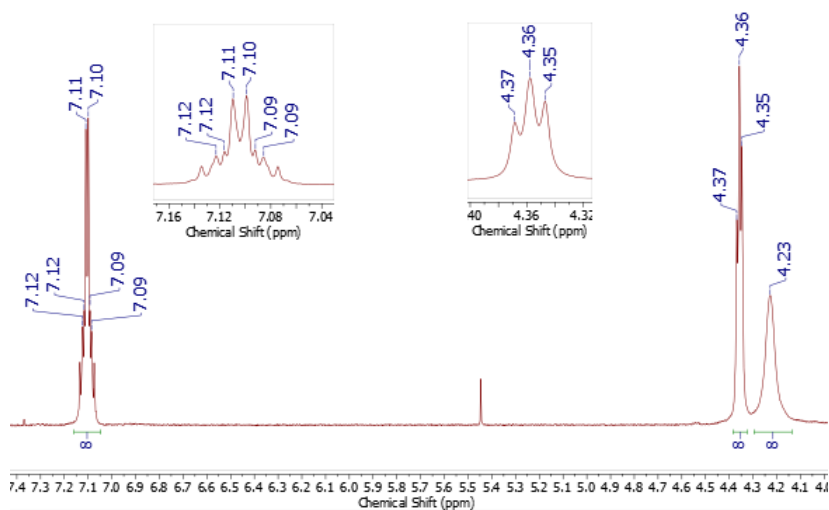


AA Figure 33 Upfield portion of the ^1H - ^{29}Si HMBC NMR spectrum of the reaction of N, N-dimethyl((dimethylphenylsilyl)amine) and ethyl propiolate (Table 2.1, Entry 12).

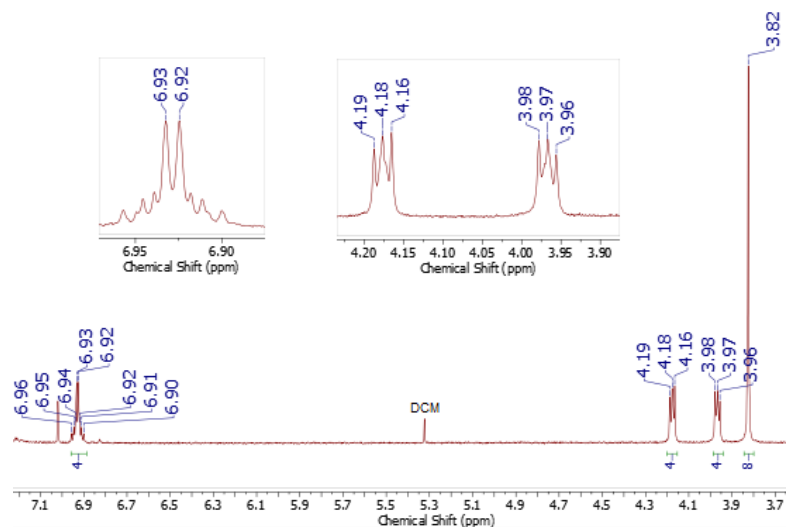
Appendix B: Supplementary Material for Chapter 3



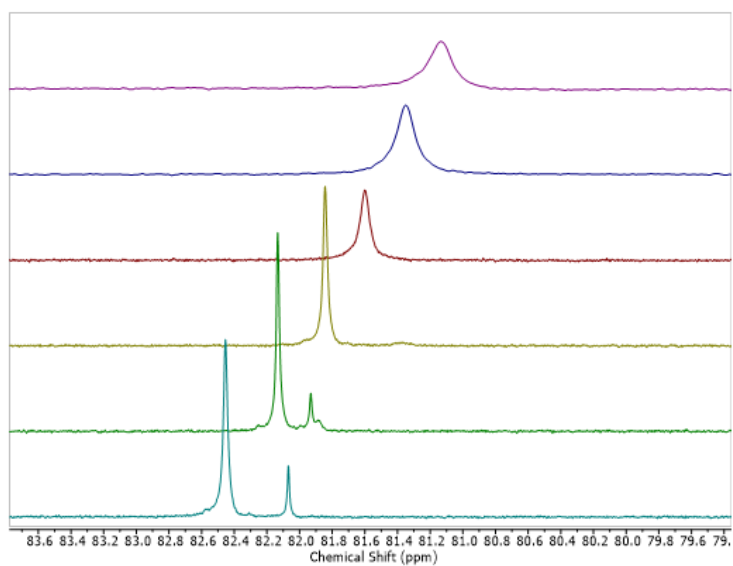
AB Figure 1 ^1H NMR spectrum (400 MHz, CDCl_3) of $[\text{GeCl}_2(\text{dibenzo}[18]\text{crown-6})]$.



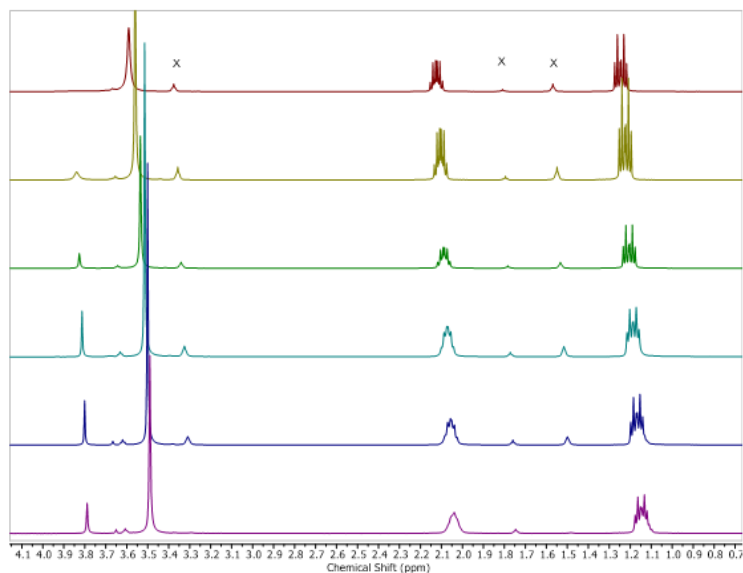
AB Figure 2 ^1H NMR spectrum (400 MHz, $\text{ACN-}d_3$) of $[\text{SnCl}(\text{dibenzo}[18]\text{crown-6})][\text{SnCl}_3]$.



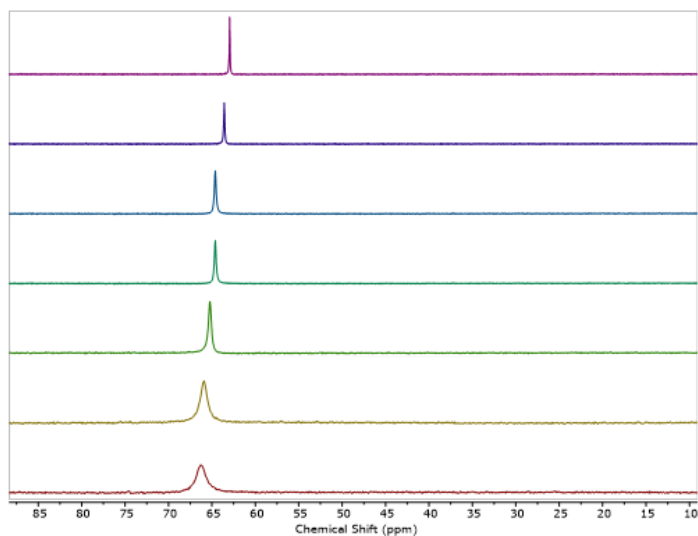
AB Figure 3 ^1H NMR spectrum (400 MHz, CDCl_3) of $[\text{SnCl}(\text{benzo}[15]\text{crown-5})][\text{SnCl}_3]$.



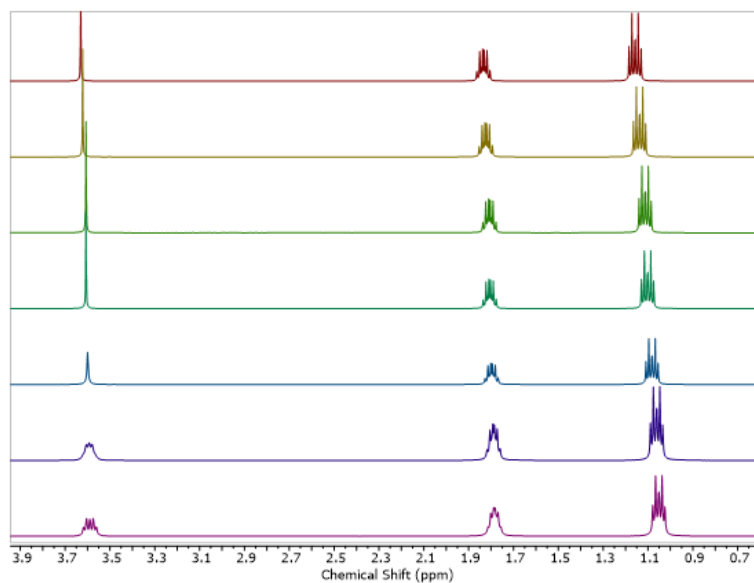
AB Figure 4 Stacked plot of the $^{31}\text{P}\{^1\text{H}\}$ NMR spectra (243 MHz, CD_2Cl_2 , 25 to -80°C) of the addition of TEPO to $[\text{Ge}(18\text{-crown-6})][\text{OTf}]_2$ at different temperatures.



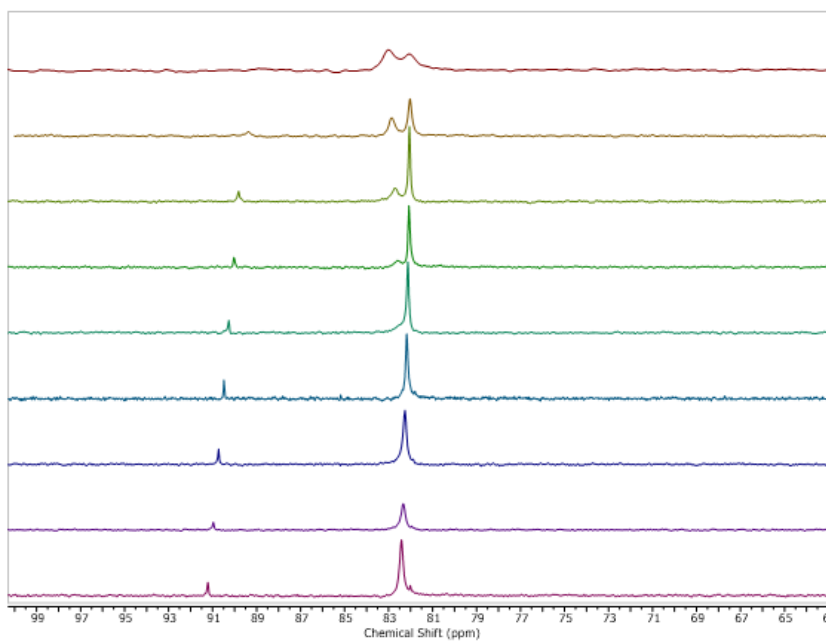
AB Figure 5 Stacked plot of the ^1H NMR spectra (600 MHz, CD_2Cl_2 , 25 to $-80\text{ }^\circ\text{C}$) for the addition of two equivalents of TEPO to $[\text{Ge}(18\text{-crown-}6)][\text{OTf}]_2$. Trace amounts of THF and polymerized THF denoted with X are present from the synthesis of $[\text{Ge}(18\text{-crown-}6)][\text{OTf}]_2$.



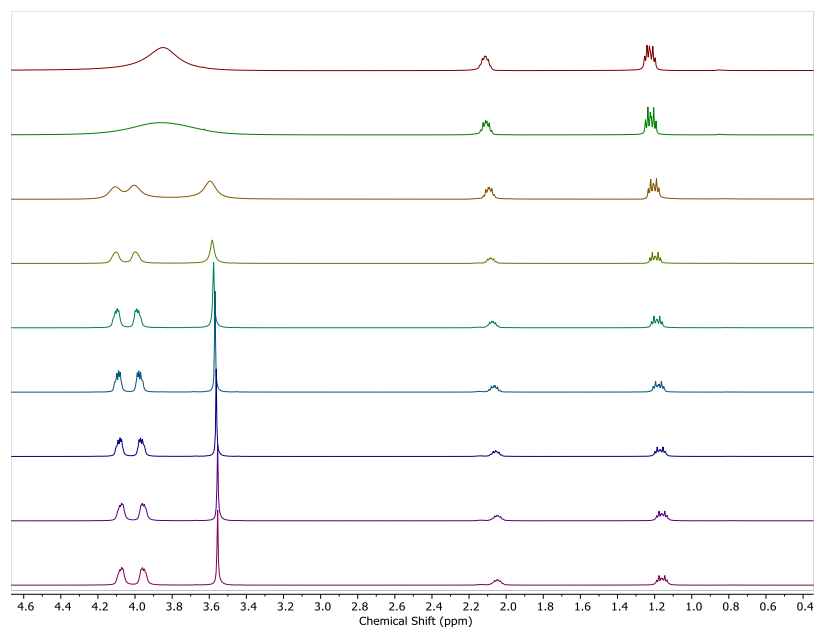
AB Figure 6 Stacked plot of the $^{31}\text{P}\{^1\text{H}\}$ NMR spectrum (243 MHz, CD_2Cl_2 , 25 to $-90\text{ }^\circ\text{C}$) for the addition of TEPO to $\text{GeCl}_2\cdot\text{dioxane}$.



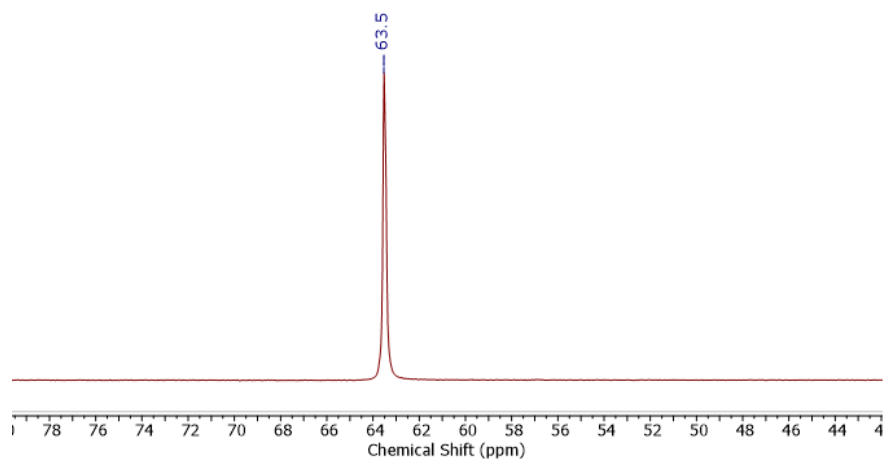
AB Figure 7 Stacked plot of the ¹H NMR spectra (600 MHz, CD₂Cl₂, 25 to -90 °C) for the addition of two equivalents of TEPO to **GeCl₂-dioxane**.



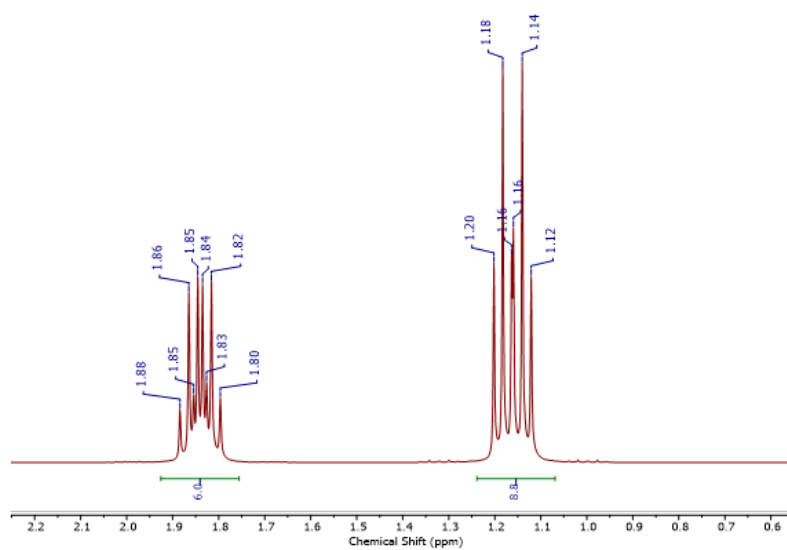
AB Figure 8 Stacked plot of the ³¹P{¹H} NMR spectrum (243 MHz, CD₂Cl₂, 25 to -90 °C) for the addition of TEPO to **[Ge([12]crown-4)₂][OTf]₂**.



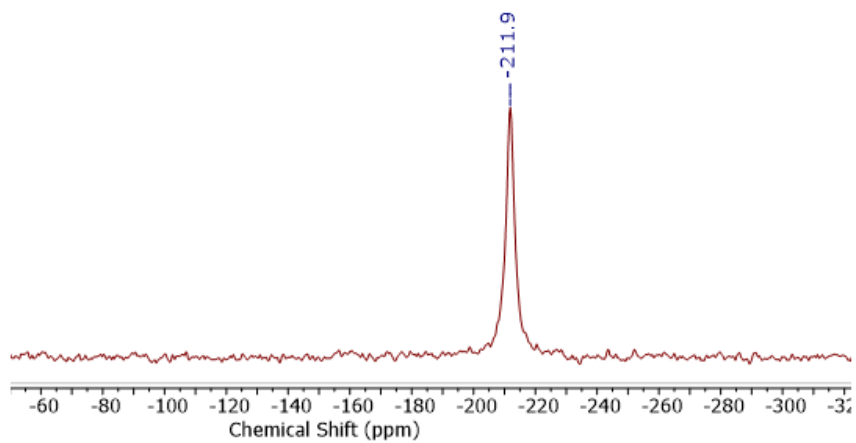
AB Figure 9 Stacked plot of the ^1H NMR spectra (600 MHz, CD_2Cl_2 , 25 to $-80\text{ }^\circ\text{C}$) for the addition of two equivalents of TEPO to $[\text{Ge}([\text{12}]\text{crown-4})_2][\text{OTf}]_2$.



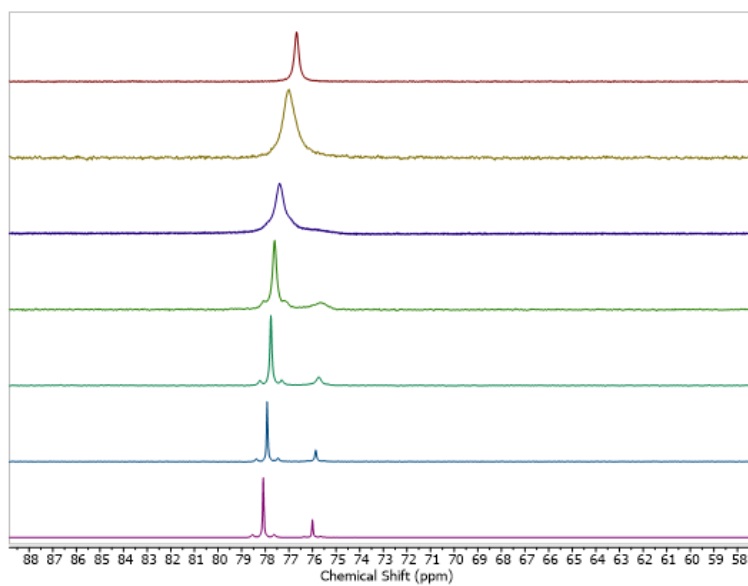
AB Figure 10 $^{31}\text{P}\{^1\text{H}\}$ NMR spectrum (162 MHz, CD_2Cl_2 , $25\text{ }^\circ\text{C}$) for the addition of two equivalents of TEPO to SnCl_2 .



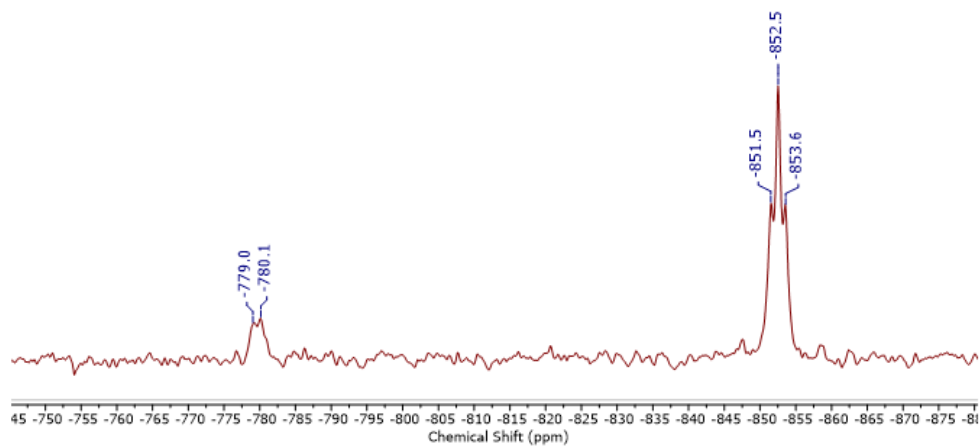
AB Figure 11 ^1H NMR spectrum (400 MHz, CD_2Cl_2 , 25 °C) for the addition of two equivalents of TEPO to SnCl_2 .



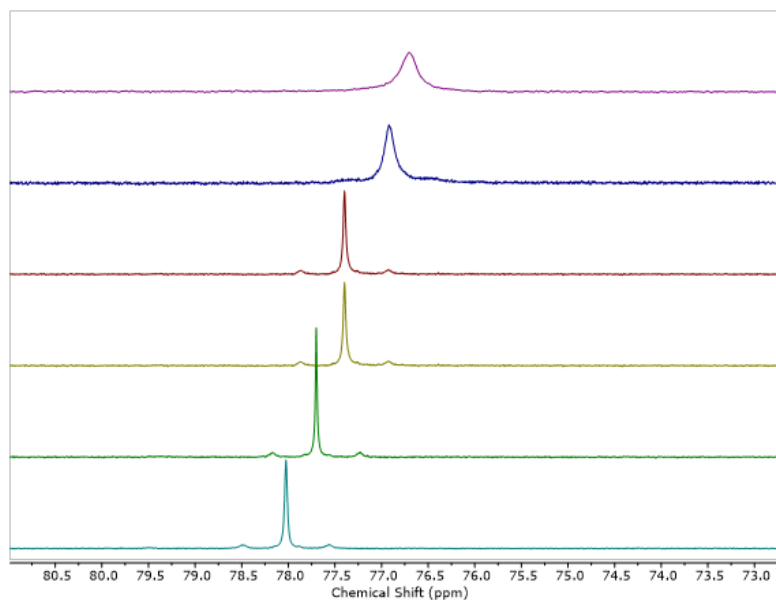
AB Figure 12 ^{119}Sn NMR spectrum (149 MHz, CD_2Cl_2 , 25 °C) of the addition of two equivalents of TEPO to SnCl_2 . $\text{Cr}(\text{acac})_3$ was used as a relaxation agent.



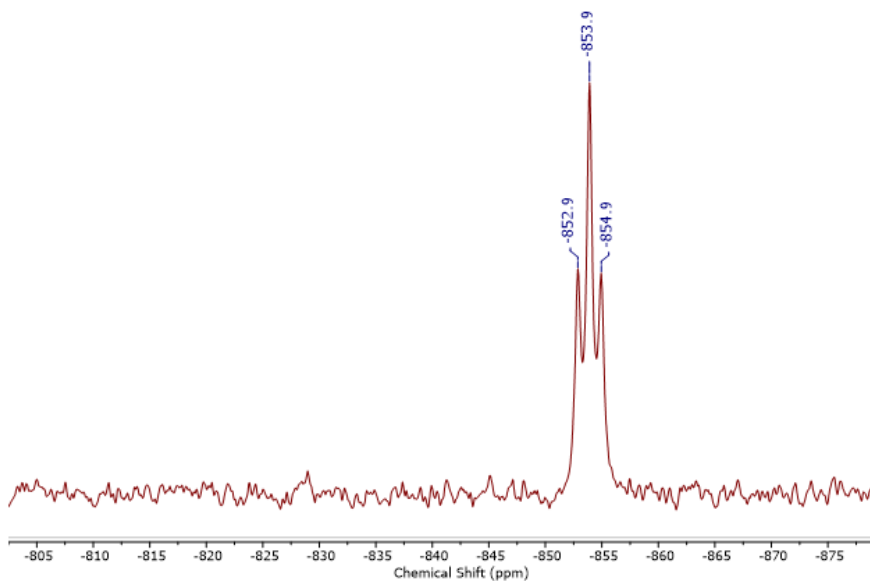
AB Figure 13 Stacked plot of the $^{31}\text{P}\{^1\text{H}\}$ NMR spectrum (243 MHz, CD_2Cl_2 , 25 to -90°C) for the addition of two equivalents of TEPO to $\text{Sn}(\text{OTf})_2$.



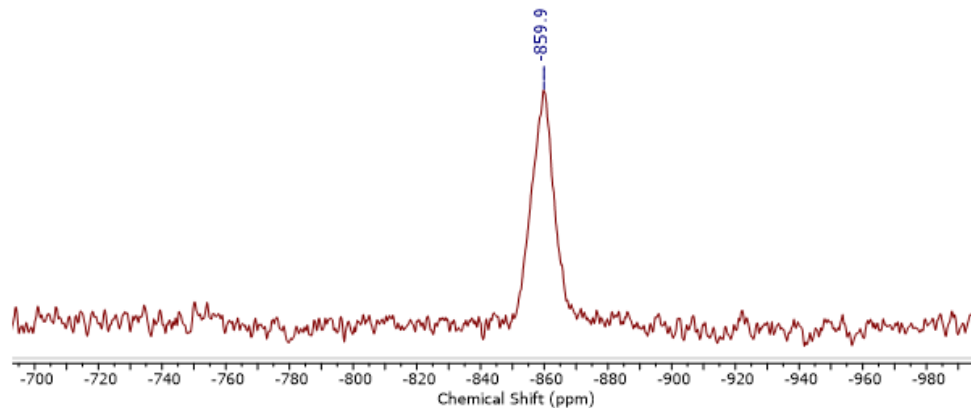
AB Figure 14 $^{119}\text{Sn}\{^1\text{H}\}$ NMR spectrum (224 MHz, CD_2Cl_2 , -80°C) for the addition of two equivalents of TEPO to $\text{Sn}(\text{OTf})_2$.



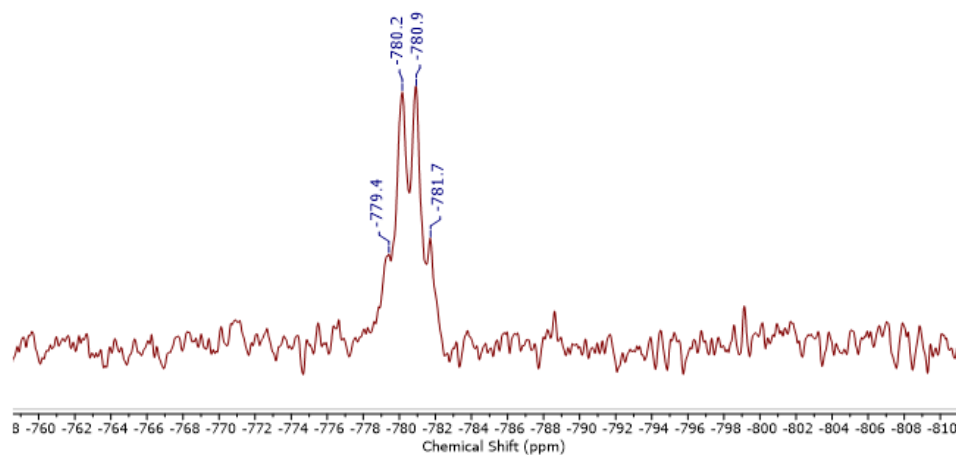
AB Figure 15 Stacked plot of the $^{31}\text{P}\{^1\text{H}\}$ NMR spectrum (243 MHz, CD_2Cl_2 , 25 to -90 $^\circ\text{C}$) for the addition of two equivalents of TEPO to $\text{Sn}(\text{OTf})_2$ and 5 mg of $\text{Cr}(\text{acac})_3$.



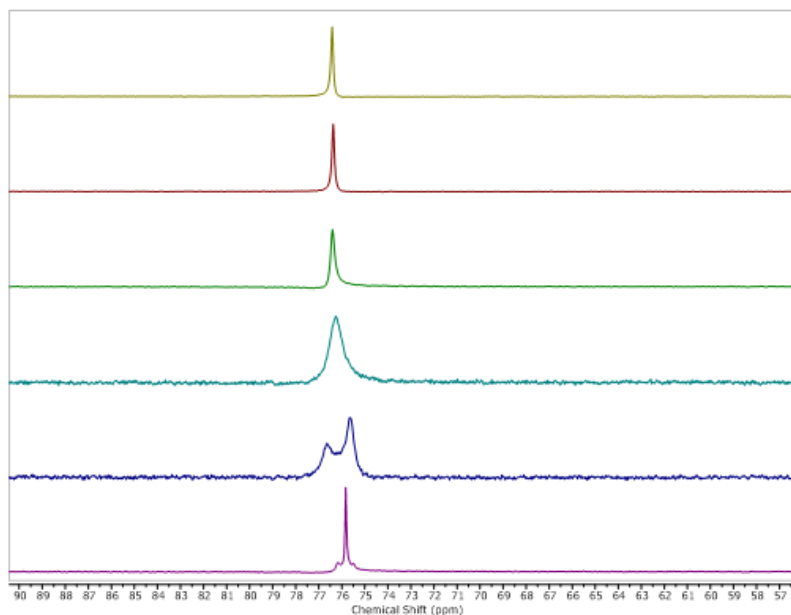
AB Figure 16 $^{119}\text{Sn}\{^1\text{H}\}$ NMR spectrum (224 MHz, CD_2Cl_2 , -80 $^\circ\text{C}$) for the addition of two equivalents of TEPO to $\text{Sn}(\text{OTf})_2$ and 5 mg of $\text{Cr}(\text{acac})_3$.



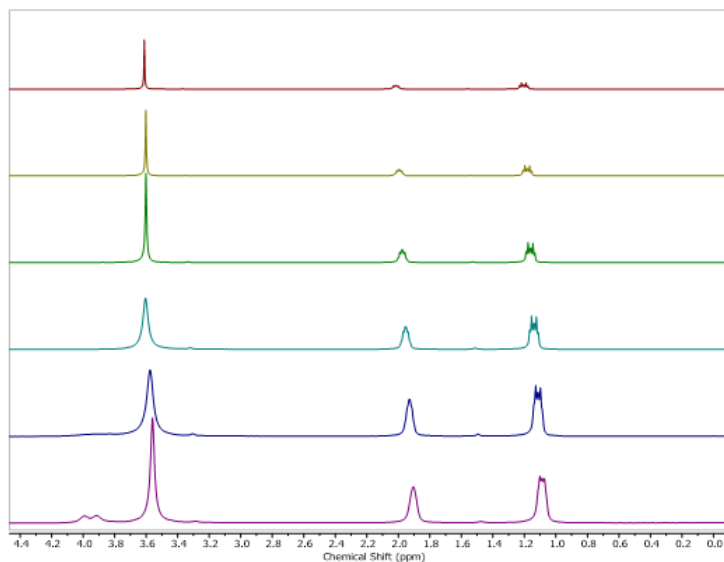
AB Figure 17 $^{119}\text{Sn}\{^1\text{H}\}$ NMR spectrum (189 MHz, CD_2Cl_2 , -80°C) for the addition of two equivalents of TEPO to $\text{Sn}(\text{OTf})_2$ and 5 mg of $\text{Cr}(\text{acac})_3$.



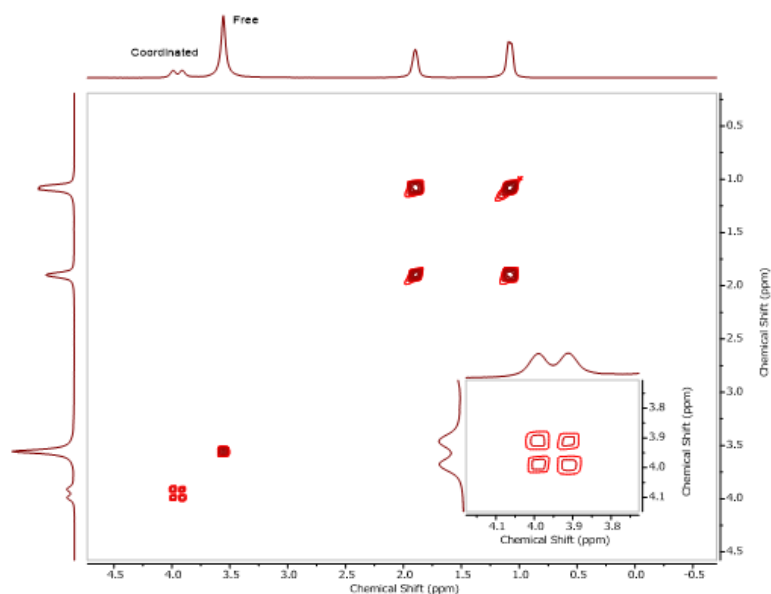
AB Figure 18 $^{119}\text{Sn}\{^1\text{H}\}$ NMR spectrum (224 MHz, CD_2Cl_2 , -80°C) for the addition of two equivalents of TEPO to $[\text{Sn}(\text{[12]crown-4})_2][\text{OTf}]_2$.



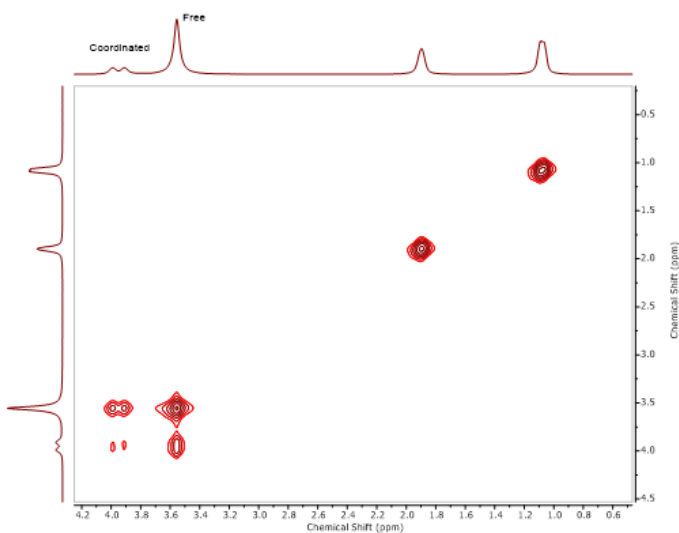
AB Figure 19 Stacked plot of the $^{31}\text{P}\{^1\text{H}\}$ NMR spectrum (243 MHz, CD_2Cl_2 , 25 to -90 °C) for the addition of two equivalents of TEPO to $[\text{Sn}([\text{12}]\text{crown-4})_2][\text{OTf}]_2$.



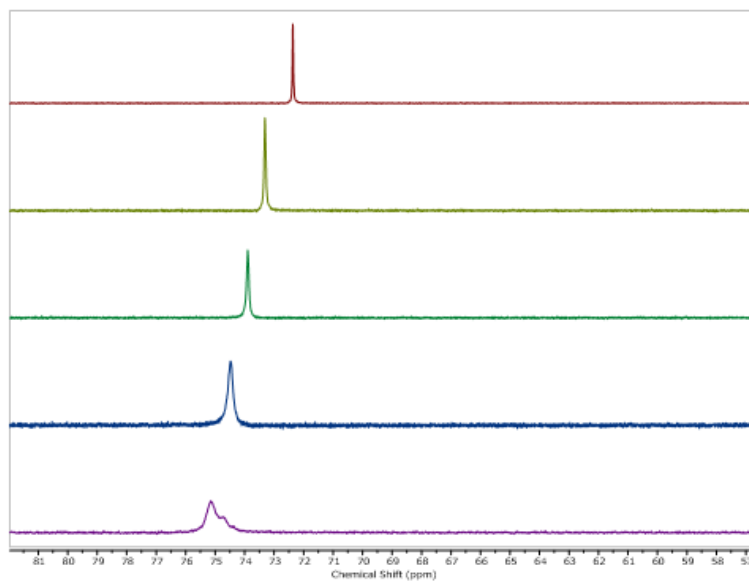
AB Figure 20 Stacked plot of the ^1H NMR spectra (600 MHz, CD_2Cl_2 , 25 to -80 °C) for the addition of two equivalents of TEPO to $[\text{Sn}([\text{12}]\text{crown-4})_2][\text{OTf}]_2$.



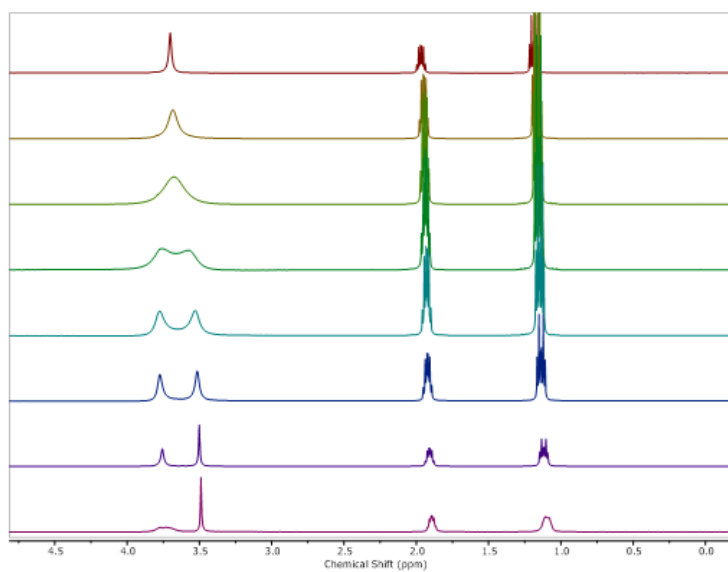
AB Figure 21 ^1H - ^1H COSY spectrum (600 MHz, CD_2Cl_2 , $-90\text{ }^\circ\text{C}$) of $[\text{Sn}([\text{12}]\text{crown-4})_2][\text{OTf}]_2$ and two equivalents of TEPO showing correlation between the two most upfield signals, confirming these signals are derived from one crown ether ring as opposed to two individual crown ether molecules.



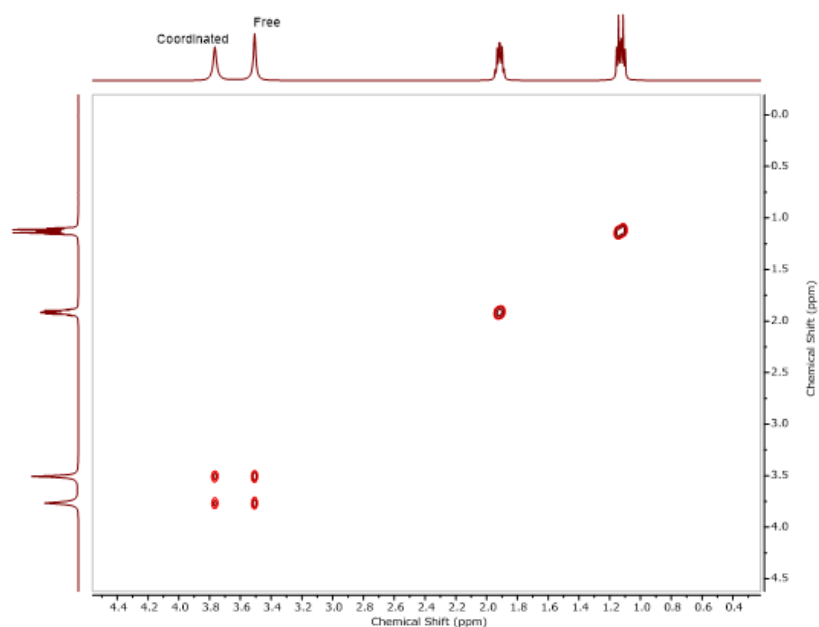
AB Figure 22 ^1H - ^1H EXSY spectrum (600 MHz, CD_2Cl_2 , $-50\text{ }^\circ\text{C}$) of $[\text{Sn}([\text{12}]\text{crown-4})_2][\text{OTf}]_2$ and two equivalents of TEPO showing exchange between the free and coordinated crown ether molecules.



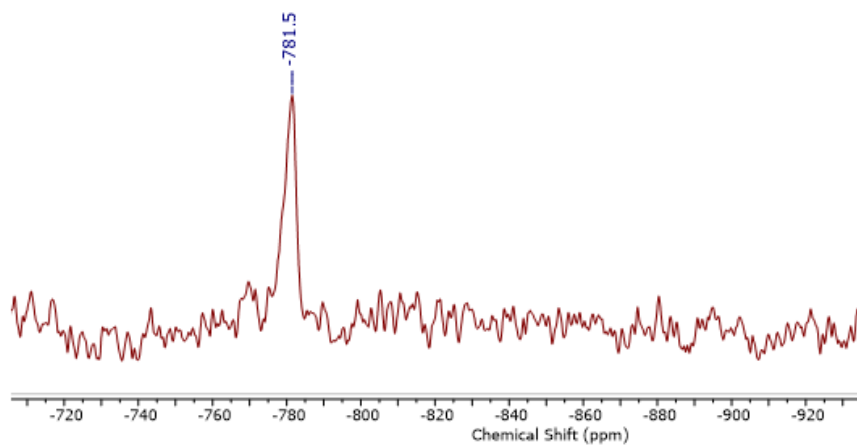
AB Figure 23 Stacked plot of the $^{31}\text{P}\{^1\text{H}\}$ NMR spectrum (243 MHz, CD_2Cl_2 , 25 to -90 °C) for the addition of two equivalents of TEPO to $[\text{Sn}([\mathbf{18}\text{crown-6}][\text{OTf}]_2)$.



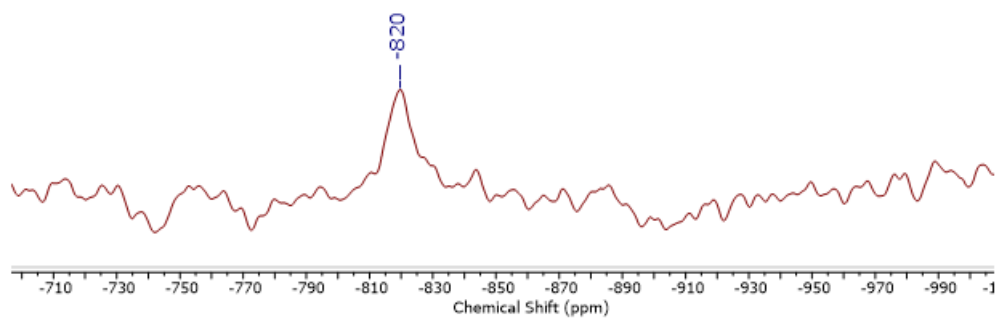
AB Figure 24 Stacked plot of the ^1H NMR spectra (600 MHz, CD_2Cl_2 , 25 to -80 °C) for the addition of two equivalents of TEPO to $[\text{Sn}([\mathbf{18}\text{crown-6}][\text{OTf}]_2)$.



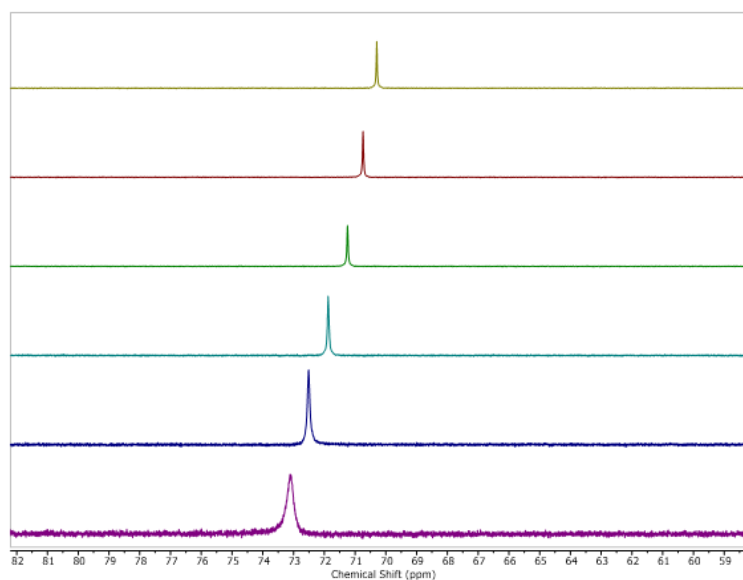
AB Figure 25 ^1H - ^1H EXSY spectrum (600 MHz, CD_2Cl_2 , $-50\text{ }^\circ\text{C}$) of $[\text{Sn}([\mathbf{18}]\text{crown-6})][\text{OTf}]_2$ and two equivalents of TEPO showing exchange between the free and coordinated crown ether molecules.



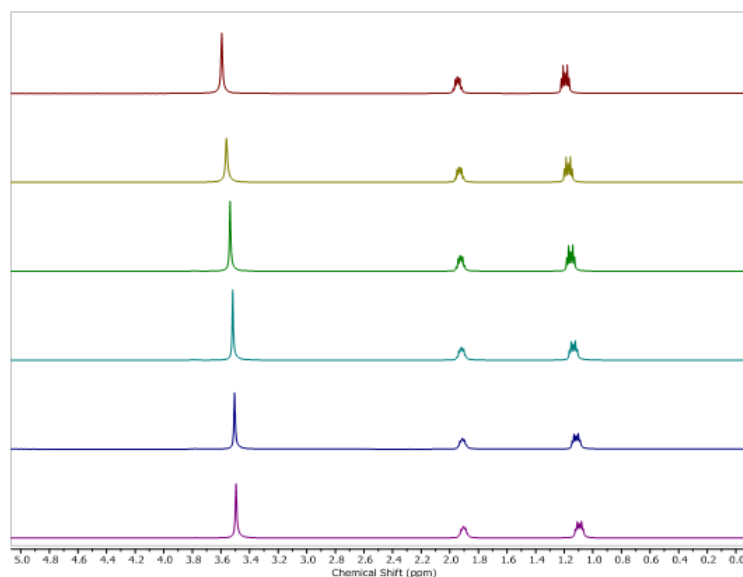
AB Figure 26 $^{119}\text{Sn}\{^1\text{H}\}$ NMR spectrum (224 MHz, CD_2Cl_2 , $-80\text{ }^\circ\text{C}$) for the addition of two equivalents of TEPO to $[\text{Sn}([\mathbf{18}]\text{crown-6})][\text{OTf}]_2$.



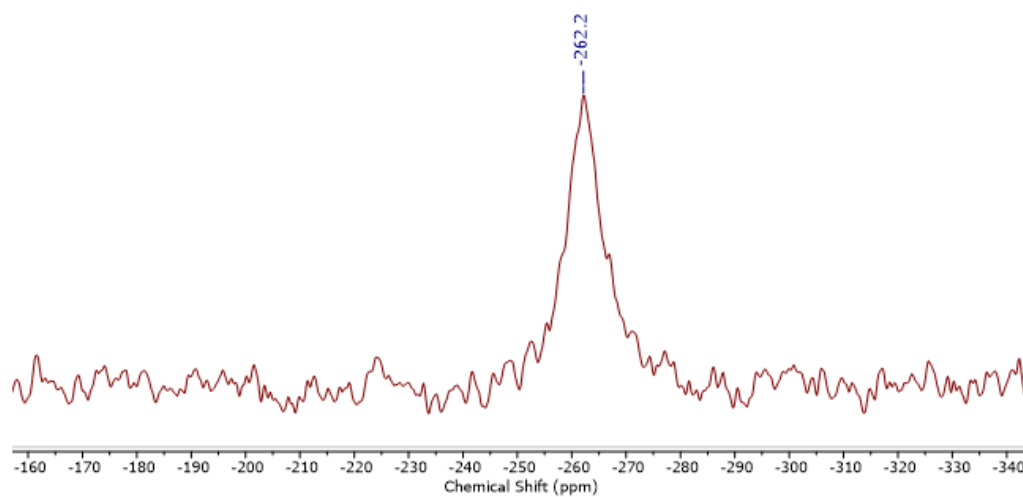
AB Figure 27 $^{119}\text{Sn}\{^1\text{H}\}$ NMR spectrum (149 MHz, CD_2Cl_2 , 25 °C) for the addition of two equivalents of TEPO to $[\text{Sn}(\text{[18]crown-6})][\text{OTf}]_2$.



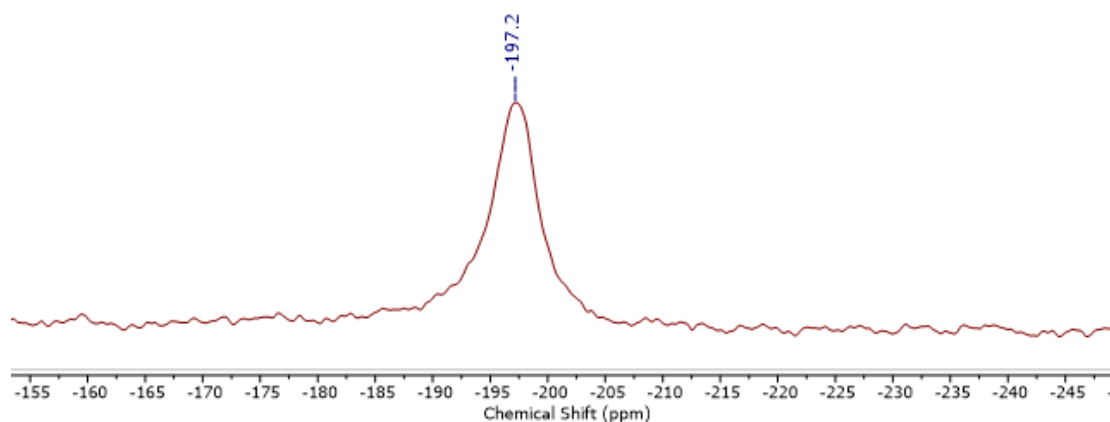
AB Figure 28 Stacked plot of the $^{31}\text{P}\{^1\text{H}\}$ NMR spectrum (243 MHz, CD_2Cl_2 , 25 to -90 °C) for the addition of two equivalents of TEPO to $[\text{SnCl}(\text{[18]crown-6})][\text{SnCl}_3]$.



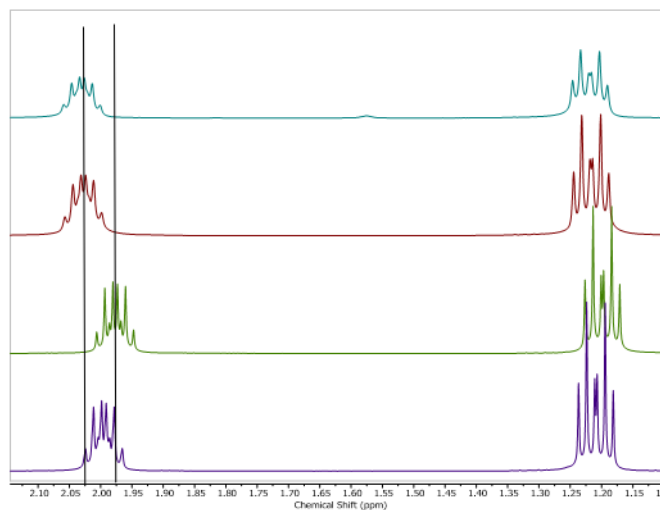
AB Figure 29 Stacked plot of the ¹H NMR spectra (600 MHz, CD₂Cl₂, 25 to -80 °C) for the addition of two equivalents of TEPO to [SnCl([18]crown-6)][SnCl₃].



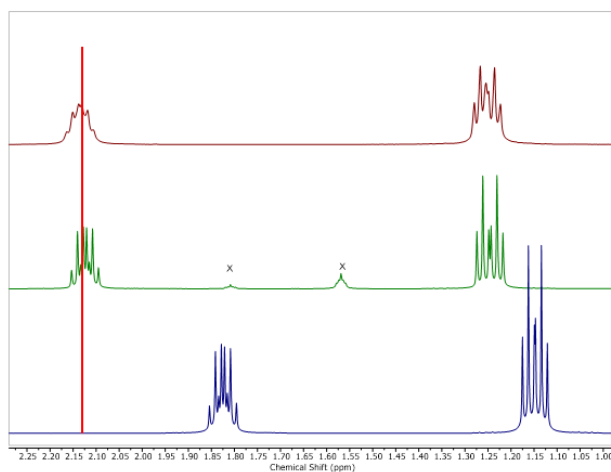
AB Figure 30 ¹¹⁹Sn{¹H} NMR spectrum (224 MHz, CD₂Cl₂, -80 °C) for the addition of two equivalents of TEPO to [SnCl([18]crown-6)][SnCl₃].



AB Figure 31 $^{119}\text{Sn}\{^1\text{H}\}$ NMR spectrum (149 MHz, CD_2Cl_2 , 25 °C) for the addition of two equivalents of TEPO to $[\text{SnCl}(\text{[18]crown-6})][\text{SnCl}_3]$.

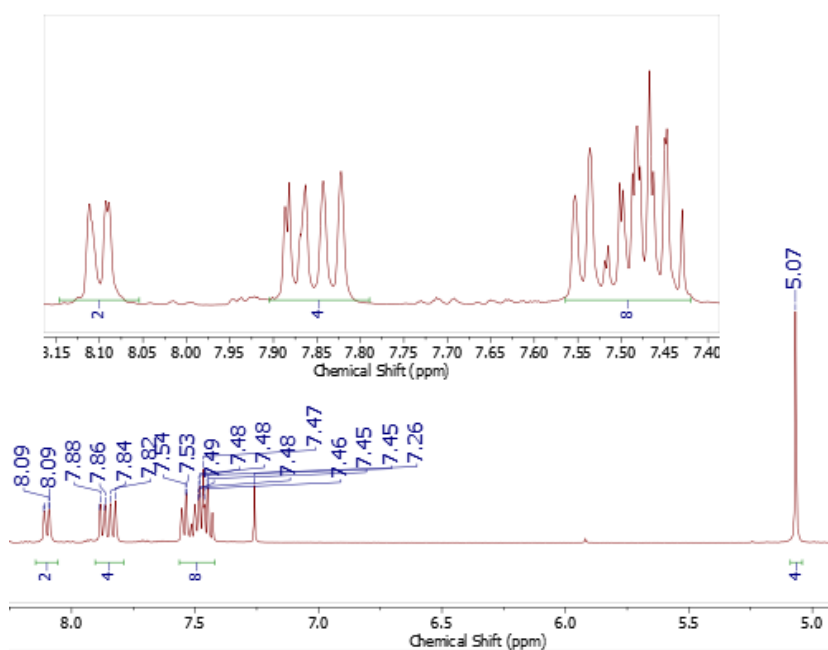


AB Figure 32 Stacked plot of the ^1H NMR spectra (600 MHz, CD_2Cl_2 , 25 to -80 °C) for the addition of two equivalents of TEPO a) $[\text{Sn}(\text{[12]crown-4})_2][\text{OTf}]_2$ b) $\text{Sn}(\text{OTf})_2$ c) $[\text{Sn}(\text{[18]crown-6})][\text{OTf}]_2$ and d) $[\text{SnCl}(\text{[18]crown-6})][\text{SnCl}_3]$.

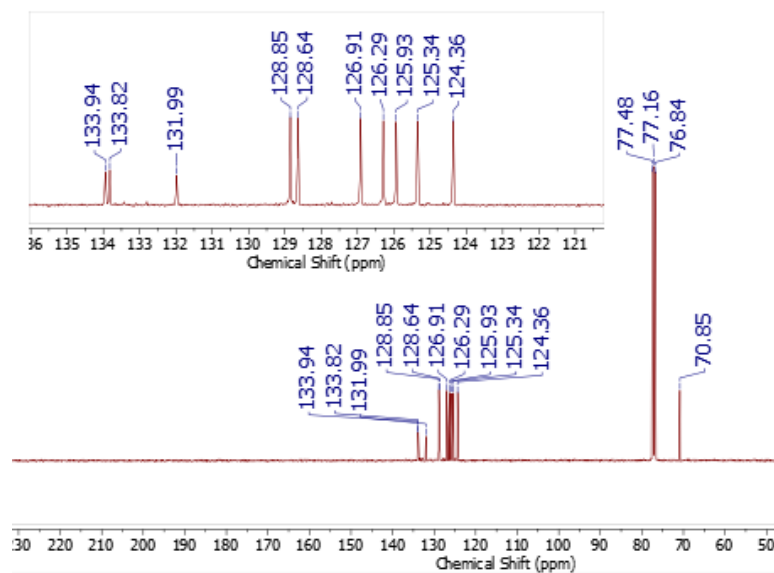


AB Figure 33 Stacked plot of the ^1H NMR spectra (600 MHz, CD_2Cl_2 , 25 to $-80\text{ }^\circ\text{C}$) for the addition of two equivalents of TEPO a) $[\text{Ge}([\mathbf{12}]\text{crown-4})_2][\text{OTf}]_2$ b) $[\text{Ge}([\mathbf{18}]\text{crown-6})][\text{OTf}]_2$ and c) $\text{GeCl}_2 \cdot \text{dioxane}$. Trace amounts of THF and polymerized THF (denoted by X) are present from the synthesis of $[\text{Ge}([\mathbf{18}]\text{crown-6})][\text{OTf}]_2$.

Appendix C: Supplementary Material for Chapter 4

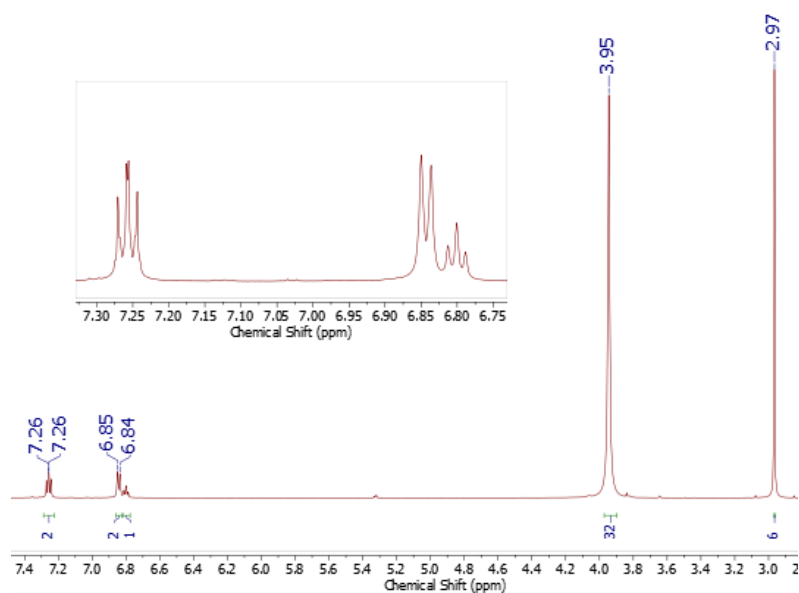


AC Figure 1 ¹H NMR spectrum (400 MHz, CDCl₃) of bis(naphthyl) ether.

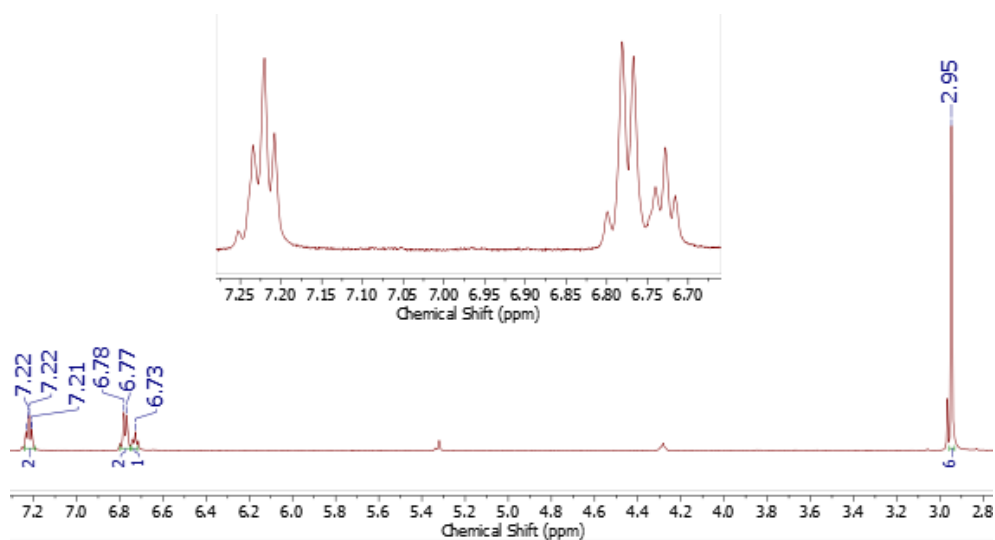


AC Figure 2 ¹³C{¹H} NMR spectrum (101 MHz, CDCl₃) of bis(naphthyl) ether.

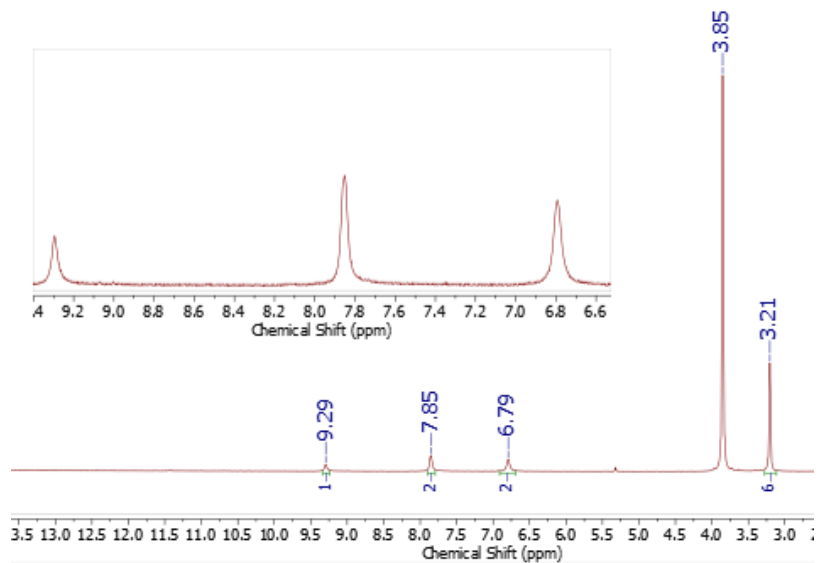
Appendix D: Supplementary Material for Chapter 5



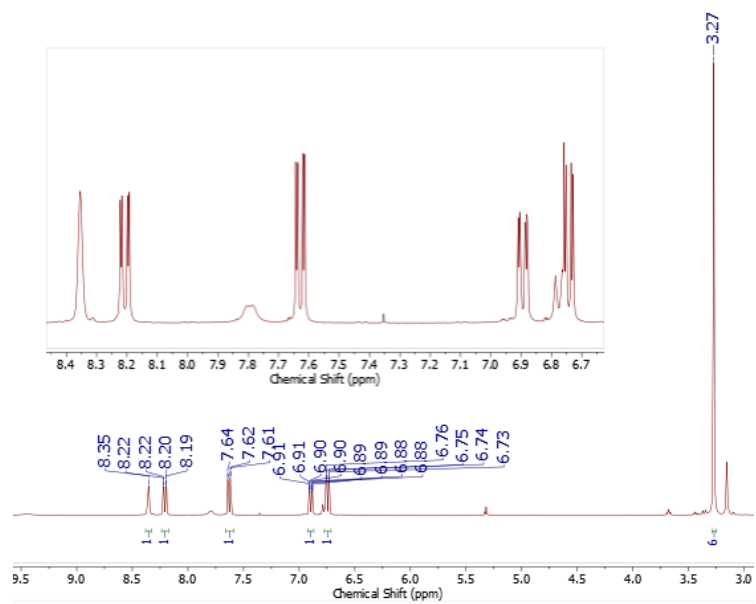
AD Figure 1 ¹H NMR spectrum (400 MHz, CD₂Cl₂) of the addition of *N,N*-dimethylaniline to [Ge([12]crown-4)₂][OTf]₂.



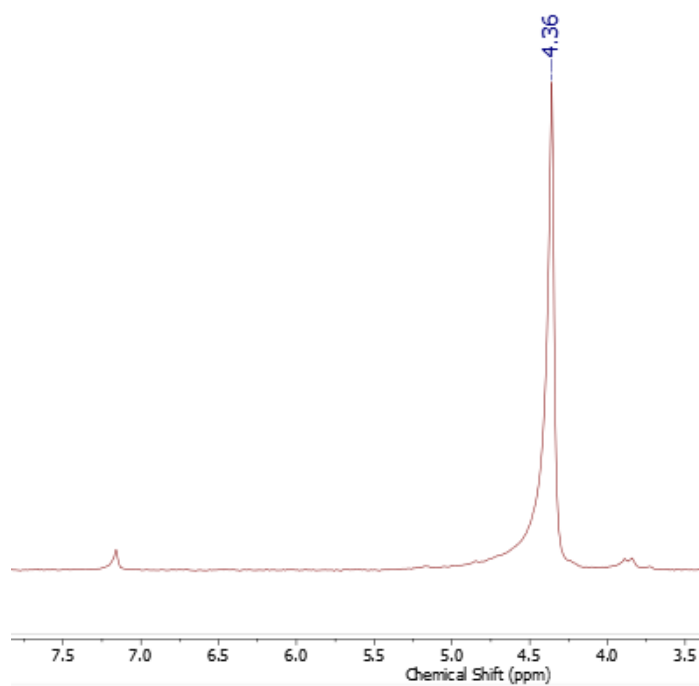
AD Figure 2 ¹H NMR spectrum (400 MHz, CD₂Cl₂) of the addition of *N,N*-dimethylaniline to B(C₆F₅)₃.



AD Figure 3 ^1H NMR spectrum (400 MHz, CD_2Cl_2) of the addition of *N,N*-dimethylaniline to $[\text{Ge}([\mathbf{12}]\text{crown-4})_2][\text{OTf}]_2$.



AD Figure 4 ^1H NMR spectrum (400 MHz, CD_2Cl_2) of the addition of *N,N*-dimethylaniline to $\text{B}(\text{C}_6\text{F}_5)_3$.



AD Figure 5 ^2H NMR spectrum (92 MHz, C_6H_6) of the 1,1'-[oxybis(methylene)]bis[4-methyl-benzene].

Appendix E: Copyright Permissions for Articles/Figures

NH bond activation of ammonia and amines by ditetrelenes: key insights into the stereochemistry of nucleophilic addition

S. L. McOnie, G. A. Özpınar, J. L. Bourque, T. Müller and K. M. Baines, *Dalton Trans.*, 2021, Advance Article , DOI: 10.1039/D1DT03739K

To request permission to reproduce material from this article, please go to the Copyright Clearance Center request page.

If you are an author contributing to an RSC publication, you do not need to request permission provided correct acknowledgement is given.

If you are the author of this article, you do not need to request permission to reproduce figures and diagrams provided correct acknowledgement is given. If you want to reproduce the whole article in a third-party publication (excluding your thesis/dissertation for which permission is not required) please go to the Copyright Clearance Center request page.

Read more about how to correctly acknowledge RSC content.

JOHN WILEY AND SONS LICENSE
TERMS AND CONDITIONS

Dec 02, 2021

This Agreement between University of Western Ontario -- Sarah McOnie ("You") and John Wiley and Sons ("John Wiley and Sons") consists of your license details and the terms and conditions provided by John Wiley and Sons and Copyright Clearance Center.

License Number

5200941136295

License date

Dec 02, 2021

Licensed Content Publisher

John Wiley and Sons

Licensed Content Publication

Angewandte Chemie International Edition

Licensed Content Title

Cationic Crown Ether Complexes of Germanium(II)

Licensed Content Author

Paul A. Rugar, Rajoshree Bandyopadhyay, Benjamin F. T. Cooper, et al

Licensed Content Date

Jun 25, 2009

Licensed Content Volume

48

Licensed Content Issue

28

Licensed Content Pages

4

Type of use

Dissertation/Thesis

Requestor type

University/Academic

Format

Electronic

Portion

Figure/table

Number of figures/tables

5

Will you be translating?

No

Title

Small Molecule Activation and Catalysis by Low Valent Main Group Compounds

Institution name

University of Western Ontario

Expected presentation date

Mar 2022

Portions

I would like to reuse Figures 1-5 which are solid state structures of compounds relevant to my thesis to show the coordination environment in the crown ether complexes

Requestor Location

University of Western Ontario
6-145 John Street

London, ON N6A 1N7
Canada
Attn: University of Western Ontario

Publisher Tax ID

EU826007151

Total

0.00 CAD

Terms and Conditions

TERMS AND CONDITIONS

This copyrighted material is owned by or exclusively licensed to John Wiley & Sons, Inc. or one of its group companies (each a "Wiley Company") or handled on behalf of a society with which a Wiley Company has exclusive publishing rights in relation to a particular work (collectively "WILEY"). By clicking "accept" in connection with completing this licensing transaction, you agree that the following terms and conditions apply to this transaction (along with the billing and payment terms and conditions established by the Copyright Clearance Center Inc., ("CCC's Billing and Payment terms and conditions"), at the time that you opened your RightsLink account (these are available at any time at <http://myaccount.copyright.com>).

Terms and Conditions

- The materials you have requested permission to reproduce or reuse (the "Wiley Materials") are protected by copyright.

- You are hereby granted a personal, non-exclusive, non-sub licensable (on a stand-alone basis), non-transferable, worldwide, limited license to reproduce the Wiley Materials for the purpose specified in the licensing process. This license, and any CONTENT (PDF or image file) purchased as part of your order, is for a one-time use only and limited to any maximum distribution number specified in the license. The first instance of republication or reuse granted by this license must be completed within two years of the date of the grant of this license (although copies prepared before the end date may be distributed thereafter). The Wiley Materials shall not be used in any other manner or for any other purpose, beyond what is granted in the license. Permission is granted subject to an appropriate acknowledgement given to the author, title of the material/book/journal and the publisher. You shall also duplicate the copyright notice that appears in the Wiley publication in your use of the Wiley Material. Permission is also granted on the understanding that nowhere in the text is a previously published source acknowledged for all or part of this Wiley Material. Any third party content is expressly excluded from this permission.
- With respect to the Wiley Materials, all rights are reserved. Except as expressly granted by the terms of the license, no part of the Wiley Materials may be copied, modified, adapted (except for minor reformatting required by the new Publication), translated, reproduced, transferred or distributed, in any form or by any means, and no derivative works may be made based on the Wiley Materials without the prior permission of the respective copyright owner. For STM Signatory Publishers clearing permission under the terms of the STM Permissions Guidelines only, the terms of the license are extended to include subsequent editions and for editions in other languages, provided such editions are for the work as a whole in situ and does not involve the separate exploitation of the permitted figures or extracts, You may not alter, remove or suppress in any manner any copyright, trademark or other notices displayed by the Wiley Materials. You may not license, rent, sell, loan, lease, pledge, offer as security, transfer or assign the Wiley Materials on a stand-alone basis, or any of the rights granted to you hereunder to any other person.
- The Wiley Materials and all of the intellectual property rights therein shall at all times remain the exclusive property of John Wiley & Sons Inc, the Wiley Companies, or their respective licensors, and your interest therein is only that of having possession of and the right to reproduce the Wiley Materials pursuant to Section 2 herein during the continuance of this Agreement. You agree that you own no right, title or interest in or to the Wiley Materials or any of the intellectual property rights therein. You shall have no rights hereunder other than the license as provided for above in Section 2. No right, license or interest to any trademark, trade name, service mark or other branding ("Marks") of WILEY or its licensors is granted hereunder, and you agree that you shall not assert any such right, license or interest with respect thereto

- NEITHER WILEY NOR ITS LICENSORS MAKES ANY WARRANTY OR REPRESENTATION OF ANY KIND TO YOU OR ANY THIRD PARTY, EXPRESS, IMPLIED OR STATUTORY, WITH RESPECT TO THE MATERIALS OR THE ACCURACY OF ANY INFORMATION CONTAINED IN THE MATERIALS, INCLUDING, WITHOUT LIMITATION, ANY IMPLIED WARRANTY OF MERCHANTABILITY, ACCURACY, SATISFACTORY QUALITY, FITNESS FOR A PARTICULAR PURPOSE, USABILITY, INTEGRATION OR NON-INFRINGEMENT AND ALL SUCH WARRANTIES ARE HEREBY EXCLUDED BY WILEY AND ITS LICENSORS AND WAIVED BY YOU.
- WILEY shall have the right to terminate this Agreement immediately upon breach of this Agreement by you.
- You shall indemnify, defend and hold harmless WILEY, its Licensors and their respective directors, officers, agents and employees, from and against any actual or threatened claims, demands, causes of action or proceedings arising from any breach of this Agreement by you.
- IN NO EVENT SHALL WILEY OR ITS LICENSORS BE LIABLE TO YOU OR ANY OTHER PARTY OR ANY OTHER PERSON OR ENTITY FOR ANY SPECIAL, CONSEQUENTIAL, INCIDENTAL, INDIRECT, EXEMPLARY OR PUNITIVE DAMAGES, HOWEVER CAUSED, ARISING OUT OF OR IN CONNECTION WITH THE DOWNLOADING, PROVISIONING, VIEWING OR USE OF THE MATERIALS REGARDLESS OF THE FORM OF ACTION, WHETHER FOR BREACH OF CONTRACT, BREACH OF WARRANTY, TORT, NEGLIGENCE, INFRINGEMENT OR OTHERWISE (INCLUDING, WITHOUT LIMITATION, DAMAGES BASED ON LOSS OF PROFITS, DATA, FILES, USE, BUSINESS OPPORTUNITY OR CLAIMS OF THIRD PARTIES), AND WHETHER OR NOT THE PARTY HAS BEEN ADVISED OF THE POSSIBILITY OF SUCH DAMAGES. THIS LIMITATION SHALL APPLY NOTWITHSTANDING ANY FAILURE OF ESSENTIAL PURPOSE OF ANY LIMITED REMEDY PROVIDED HEREIN.
- Should any provision of this Agreement be held by a court of competent jurisdiction to be illegal, invalid, or unenforceable, that provision shall be deemed amended to achieve as nearly as possible the same economic effect as the original provision, and the legality, validity and enforceability of the remaining provisions of this Agreement shall not be affected or impaired thereby.
- The failure of either party to enforce any term or condition of this Agreement shall not constitute a waiver of either party's right to enforce each and every term and condition of this Agreement. No breach under this agreement shall be deemed waived or excused by either party unless such waiver or consent is in writing signed by the party granting such waiver or consent. The waiver by or consent of a party to

a breach of any provision of this Agreement shall not operate or be construed as a waiver of or consent to any other or subsequent breach by such other party.

- This Agreement may not be assigned (including by operation of law or otherwise) by you without WILEY's prior written consent.
- Any fee required for this permission shall be non-refundable after thirty (30) days from receipt by the CCC.
- These terms and conditions together with CCC's Billing and Payment terms and conditions (which are incorporated herein) form the entire agreement between you and WILEY concerning this licensing transaction and (in the absence of fraud) supersedes all prior agreements and representations of the parties, oral or written. This Agreement may not be amended except in writing signed by both parties. This Agreement shall be binding upon and inure to the benefit of the parties' successors, legal representatives, and authorized assigns.
- In the event of any conflict between your obligations established by these terms and conditions and those established by CCC's Billing and Payment terms and conditions, these terms and conditions shall prevail.
- WILEY expressly reserves all rights not specifically granted in the combination of (i) the license details provided by you and accepted in the course of this licensing transaction, (ii) these terms and conditions and (iii) CCC's Billing and Payment terms and conditions.
- This Agreement will be void if the Type of Use, Format, Circulation, or Requestor Type was misrepresented during the licensing process.
- This Agreement shall be governed by and construed in accordance with the laws of the State of New York, USA, without regards to such state's conflict of law rules. Any legal action, suit or proceeding arising out of or relating to these Terms and Conditions or the breach thereof shall be instituted in a court of competent jurisdiction in New York County in the State of New York in the United States of America and each party hereby consents and submits to the personal jurisdiction of such court, waives any objection to venue in such court and consents to service of process by registered or certified mail, return receipt requested, at the last known address of such party.

WILEY OPEN ACCESS TERMS AND CONDITIONS

Wiley Publishes Open Access Articles in fully Open Access Journals and in Subscription journals offering Online Open. Although most of the fully Open Access journals publish open access articles under the terms of the Creative Commons Attribution (CC BY)

License only, the subscription journals and a few of the Open Access Journals offer a choice of Creative Commons Licenses. The license type is clearly identified on the article.

The Creative Commons Attribution License

The Creative Commons Attribution License (CC-BY) allows users to copy, distribute and transmit an article, adapt the article and make commercial use of the article. The CC-BY license permits commercial and non-

Creative Commons Attribution Non-Commercial License

The Creative Commons Attribution Non-Commercial (CC-BY-NC) License permits use, distribution and reproduction in any medium, provided the original work is properly cited and is not used for commercial purposes.(see below)

Creative Commons Attribution-Non-Commercial-NoDerivs License

The Creative Commons Attribution Non-Commercial-NoDerivs License (CC-BY-NC-ND) permits use, distribution and reproduction in any medium, provided the original work is properly cited, is not used for commercial purposes and no modifications or adaptations are made. (see below)

Use by commercial "for-profit" organizations

Use of Wiley Open Access articles for commercial, promotional, or marketing purposes requires further explicit permission from Wiley and will be subject to a fee.

Further details can be found on Wiley Online

Library <http://olabout.wiley.com/WileyCDA/Section/id-410895.html>

Other Terms and Conditions:

v1.10 Last updated September 2015

Questions? customercare@copyright.com or +1-855-239-3415 (toll free in the US) or +1-978-646-2777.

ELSEVIER LICENSE
TERMS AND CONDITIONS

Dec 02, 2021

This Agreement between University of Western Ontario -- Sarah McOnie ("You") and Elsevier ("Elsevier") consists of your license details and the terms and conditions provided by Elsevier and Copyright Clearance Center.

License Number

5200940534463

License date

Dec 02, 2021

Licensed Content Publisher

Elsevier

Licensed Content Publication

Journal of Organometallic Chemistry

Licensed Content Title

Crown ether complexes of tin(II) trifluoromethanesulfonate

Licensed Content Author

Rajoshree Bandyopadhyay, Benjamin F.T. Cooper, Aaron J. Rossini, Robert W. Schurko, Charles L.B. Macdonald

Licensed Content Date

Apr 1, 2010

Licensed Content Volume

695

Licensed Content Issue

7

Licensed Content Pages

7

Start Page

1012

End Page

1018

Type of Use

reuse in a thesis/dissertation

Portion

figures/tables/illustrations

Number of figures/tables/illustrations

3

Format

electronic

Are you the author of this Elsevier article?

No

Will you be translating?

No

Title

Small Molecule Activation and Catalysis by Low Valent Main Group Compounds

Institution name

University of Western Ontario

Expected presentation date

Mar 2022

Portions

I would like to use Figures 1-3, which are the solid state structures of compounds relevant to my thesis to show the coordination environment in the crown ether complexes.

Requestor Location

University of Western Ontario

London, ON

Canada

Attn: University of Western Ontario

Publisher Tax ID

GB 494 6272 12

Total

0.00 CAD

Terms and Conditions

INTRODUCTION

1. The publisher for this copyrighted material is Elsevier. By clicking "accept" in connection with completing this licensing transaction, you agree that the following terms and conditions apply to this transaction (along with the Billing and Payment terms and conditions established by Copyright Clearance Center, Inc. ("CCC"), at the time that you opened your Rightslink account and that are available at any time at <http://myaccount.copyright.com>).

GENERAL TERMS

2. Elsevier hereby grants you permission to reproduce the aforementioned material subject to the terms and conditions indicated.

3. Acknowledgement: If any part of the material to be used (for example, figures) has appeared in our publication with credit or acknowledgement to another source, permission must also be sought from that source. If such permission is not obtained then that material may not be included in your publication/copies. Suitable acknowledgement to the source must be made, either as a footnote or in a reference list at the end of your publication, as follows:

"Reprinted from Publication title, Vol /edition number, Author(s), Title of article / title of chapter, Pages No., Copyright (Year), with permission from Elsevier [OR APPLICABLE SOCIETY COPYRIGHT OWNER]." Also Lancet special credit - "Reprinted from The Lancet, Vol. number, Author(s), Title of article, Pages No., Copyright (Year), with permission from Elsevier."

4. Reproduction of this material is confined to the purpose and/or media for which permission is hereby given.

5. Altering/Modifying Material: Not Permitted. However figures and illustrations may be altered/adapted minimally to serve your work. Any other abbreviations, additions, deletions and/or any other alterations shall be made only with prior written authorization of Elsevier Ltd. (Please contact Elsevier's permissions helpdesk here). No modifications can be made to any Lancet figures/tables and they must be reproduced in full.

6. If the permission fee for the requested use of our material is waived in this instance, please be advised that your future requests for Elsevier materials may attract a fee.

7. Reservation of Rights: Publisher reserves all rights not specifically granted in the combination of (i) the license details provided by you and accepted in the course of this licensing transaction, (ii) these terms and conditions and (iii) CCC's Billing and Payment terms and conditions.

8. License Contingent Upon Payment: While you may exercise the rights licensed immediately upon issuance of the license at the end of the licensing process for the transaction, provided that you have disclosed complete and accurate details of your proposed use, no license is finally effective unless and until full payment is received from you (either by publisher or by CCC) as provided in CCC's Billing and Payment terms and conditions. If full payment is not received on a timely basis, then any license preliminarily granted shall be deemed automatically revoked and shall be void as if never granted. Further, in the event that you breach any of these terms and conditions or any of CCC's Billing and Payment terms and conditions, the license is automatically revoked and shall be void as if never granted. Use of materials as described in a revoked license, as well as any use of the materials beyond the scope of an unrevoked license, may constitute copyright

infringement and publisher reserves the right to take any and all action to protect its copyright in the materials.

9. Warranties: Publisher makes no representations or warranties with respect to the licensed material.

10. Indemnity: You hereby indemnify and agree to hold harmless publisher and CCC, and their respective officers, directors, employees and agents, from and against any and all claims arising out of your use of the licensed material other than as specifically authorized pursuant to this license.

11. No Transfer of License: This license is personal to you and may not be sublicensed, assigned, or transferred by you to any other person without publisher's written permission.

12. No Amendment Except in Writing: This license may not be amended except in a writing signed by both parties (or, in the case of publisher, by CCC on publisher's behalf).

13. Objection to Contrary Terms: Publisher hereby objects to any terms contained in any purchase order, acknowledgment, check endorsement or other writing prepared by you, which terms are inconsistent with these terms and conditions or CCC's Billing and Payment terms and conditions. These terms and conditions, together with CCC's Billing and Payment terms and conditions (which are incorporated herein), comprise the entire agreement between you and publisher (and CCC) concerning this licensing transaction. In the event of any conflict between your obligations established by these terms and conditions and those established by CCC's Billing and Payment terms and conditions, these terms and conditions shall control.

14. Revocation: Elsevier or Copyright Clearance Center may deny the permissions described in this License at their sole discretion, for any reason or no reason, with a full refund payable to you. Notice of such denial will be made using the contact information provided by you. Failure to receive such notice will not alter or invalidate the denial. In no event will Elsevier or Copyright Clearance Center be responsible or liable for any costs, expenses or damage incurred by you as a result of a denial of your permission request, other than a refund of the amount(s) paid by you to Elsevier and/or Copyright Clearance Center for denied permissions.

LIMITED LICENSE

The following terms and conditions apply only to specific license types:

15. Translation: This permission is granted for non-exclusive world English rights only unless your license was granted for translation rights. If you licensed translation rights you may only translate this content into the languages you requested. A professional translator

must perform all translations and reproduce the content word for word preserving the integrity of the article.

16. Posting licensed content on any Website: The following terms and conditions apply as follows: Licensing material from an Elsevier journal: All content posted to the web site must maintain the copyright information line on the bottom of each image; A hyper-text must be included to the Homepage of the journal from which you are licensing at <http://www.sciencedirect.com/science/journal/xxxxx> or the Elsevier homepage for books at <http://www.elsevier.com>; Central Storage: This license does not include permission for a scanned version of the material to be stored in a central repository such as that provided by Heron/XanEdu.

Licensing material from an Elsevier book: A hyper-text link must be included to the Elsevier homepage at <http://www.elsevier.com> . All content posted to the web site must maintain the copyright information line on the bottom of each image.

Posting licensed content on Electronic reserve: In addition to the above the following clauses are applicable: The web site must be password-protected and made available only to bona fide students registered on a relevant course. This permission is granted for 1 year only. You may obtain a new license for future website posting.

17. For journal authors: the following clauses are applicable in addition to the above:

Preprints:

A preprint is an author's own write-up of research results and analysis, it has not been peer-reviewed, nor has it had any other value added to it by a publisher (such as formatting, copyright, technical enhancement etc.).

Authors can share their preprints anywhere at any time. Preprints should not be added to or enhanced in any way in order to appear more like, or to substitute for, the final versions of articles however authors can update their preprints on arXiv or RePEc with their Accepted Author Manuscript (see below).

If accepted for publication, we encourage authors to link from the preprint to their formal publication via its DOI. Millions of researchers have access to the formal publications on ScienceDirect, and so links will help users to find, access, cite and use the best available version. Please note that Cell Press, The Lancet and some society-owned have different preprint policies. Information on these policies is available on the journal homepage.

Accepted Author Manuscripts: An accepted author manuscript is the manuscript of an article that has been accepted for publication and which typically includes author-

incorporated changes suggested during submission, peer review and editor-author communications.

Authors can share their accepted author manuscript:

- immediately
 - via their non-commercial person homepage or blog
 - by updating a preprint in arXiv or RePEc with the accepted manuscript
 - via their research institute or institutional repository for internal institutional uses or as part of an invitation-only research collaboration work-group
 - directly by providing copies to their students or to research collaborators for their personal use
 - for private scholarly sharing as part of an invitation-only work group on commercial sites with which Elsevier has an agreement
- After the embargo period
 - via non-commercial hosting platforms such as their institutional repository
 - via commercial sites with which Elsevier has an agreement

In all cases accepted manuscripts should:

- link to the formal publication via its DOI
- bear a CC-BY-NC-ND license - this is easy to do
- if aggregated with other manuscripts, for example in a repository or other site, be shared in alignment with our hosting policy not be added to or enhanced in any way to appear more like, or to substitute for, the published journal article.

Published journal article (JPA): A published journal article (PJA) is the definitive final record of published research that appears or will appear in the journal and embodies all value-adding publishing activities including peer review co-ordination, copy-editing, formatting, (if relevant) pagination and online enrichment.

Policies for sharing publishing journal articles differ for subscription and gold open access articles:

Subscription Articles: If you are an author, please share a link to your article rather than the full-text. Millions of researchers have access to the formal publications on ScienceDirect, and so links will help your users to find, access, cite, and use the best available version.

Theses and dissertations which contain embedded PJAs as part of the formal submission can be posted publicly by the awarding institution with DOI links back to the formal publications on ScienceDirect.

If you are affiliated with a library that subscribes to ScienceDirect you have additional private sharing rights for others' research accessed under that agreement. This includes use

for classroom teaching and internal training at the institution (including use in course packs and courseware programs), and inclusion of the article for grant funding purposes.

Gold Open Access Articles: May be shared according to the author-selected end-user license and should contain a CrossMark logo, the end user license, and a DOI link to the formal publication on ScienceDirect.

Please refer to Elsevier's posting policy for further information.

18. For book authors the following clauses are applicable in addition to the above: Authors are permitted to place a brief summary of their work online only. You are not allowed to download and post the published electronic version of your chapter, nor may you scan the printed edition to create an electronic version. Posting to a repository: Authors are permitted to post a summary of their chapter only in their institution's repository.

19. Thesis/Dissertation: If your license is for use in a thesis/dissertation your thesis may be submitted to your institution in either print or electronic form. Should your thesis be published commercially, please reapply for permission. These requirements include permission for the Library and Archives of Canada to supply single copies, on demand, of the complete thesis and include permission for Proquest/UMI to supply single copies, on demand, of the complete thesis. Should your thesis be published commercially, please reapply for permission. Theses and dissertations which contain embedded PJAs as part of the formal submission can be posted publicly by the awarding institution with DOI links back to the formal publications on ScienceDirect.

Elsevier Open Access Terms and Conditions

You can publish open access with Elsevier in hundreds of open access journals or in nearly 2000 established subscription journals that support open access publishing. Permitted third party re-use of these open access articles is defined by the author's choice of Creative Commons user license. See our open access license policy for more information.

Terms & Conditions applicable to all Open Access articles published with Elsevier:

Any reuse of the article must not represent the author as endorsing the adaptation of the article nor should the article be modified in such a way as to damage the author's honour or reputation. If any changes have been made, such changes must be clearly indicated.

The author(s) must be appropriately credited and we ask that you include the end user license and a DOI link to the formal publication on ScienceDirect.

If any part of the material to be used (for example, figures) has appeared in our publication with credit or acknowledgement to another source it is the responsibility of the user to ensure their reuse complies with the terms and conditions determined by the rights holder.

Additional Terms & Conditions applicable to each Creative Commons user license:

CC BY: The CC-BY license allows users to copy, to create extracts, abstracts and new works from the Article, to alter and revise the Article and to make commercial use of the Article (including reuse and/or resale of the Article by commercial entities), provided the user gives appropriate credit (with a link to the formal publication through the relevant DOI), provides a link to the license, indicates if changes were made and the licensor is not represented as endorsing the use made of the work. The full details of the license are available at <http://creativecommons.org/licenses/by/4.0>.

CC BY NC SA: The CC BY-NC-SA license allows users to copy, to create extracts, abstracts and new works from the Article, to alter and revise the Article, provided this is not done for commercial purposes, and that the user gives appropriate credit (with a link to the formal publication through the relevant DOI), provides a link to the license, indicates if changes were made and the licensor is not represented as endorsing the use made of the work. Further, any new works must be made available on the same conditions. The full details of the license are available at <http://creativecommons.org/licenses/by-nc-sa/4.0>.

CC BY NC ND: The CC BY-NC-ND license allows users to copy and distribute the Article, provided this is not done for commercial purposes and further does not permit distribution of the Article if it is changed or edited in any way, and provided the user gives appropriate credit (with a link to the formal publication through the relevant DOI), provides a link to the license, and that the licensor is not represented as endorsing the use made of the work. The full details of the license are available at <http://creativecommons.org/licenses/by-nc-nd/4.0>. Any commercial reuse of Open Access articles published with a CC BY NC SA or CC BY NC ND license requires permission from Elsevier and will be subject to a fee.

Commercial reuse includes:

- Associating advertising with the full text of the Article
- Charging fees for document delivery or access
- Article aggregation
- Systematic distribution via e-mail lists or share buttons

Posting or linking by commercial companies for use by customers of those companies.

20. Other Conditions

v1.10

Questions? customercare@copyright.com or +1-855-239-3415 (toll free in the US) or +1-978-646-2777.

Order Date

24-Dec-2021

Order License ID

1171730-1

ISSN

0300-9246

Type of Use

Republish in a thesis/dissertation

Publisher

CHEMICAL SOCIETY,

Portion

Image/photo/illustration

LICENSED CONTENT

Publication Title

Journal of the Chemical Society. Dalton transactions

Article Title

Stereochemical activity of lone pairs. The crystal and molecular structures of the salts of chloro(1,4,7,10,13,16-hexaoxacyclo-octadecane)tin(II). Calculation of macrocyclic cavity size by force field methods

Author/Editor

CHEMICAL SOCIETY (GREAT BRITAIN), ROYAL SOCIETY OF CHEMISTRY (GREAT BRITAIN)

Date

01/01/1972

Language

English

Country

United Kingdom of Great Britain and Northern Ireland

Rightsholder

Royal Society of Chemistry

Publication Type

Journal

Start Page

1543

Issue

8

REQUEST DETAILS

Portion Type

Image/photo/illustration

Number of images / photos / illustrations

1

Format (select all that apply)

Electronic

Who will republish the content?

Academic institution

Duration of Use

Life of current edition

Lifetime Unit Quantity

Up to 499

Rights Requested

Main product

Distribution

Worldwide

Translation

Original language of publication

Copies for the disabled?

No

Minor editing privileges?

No

Incidental promotional use?

No

Currency

CAD

NEW WORK DETAILS

Title

Small Molecule Activation and Catalysis by Low Valent Group 14 Complexes

Instructor name

Sarah McOnie

Institution name

University of Western Ontario

Expected presentation date

2022-03-07

ADDITIONAL DETAILS

Order reference number

N/A

The requesting person / organization to appear on the license

University of Western Ontario

REUSE CONTENT DETAILS

Title, description or numeric reference of the portion(s)

Figure 1

Editor of portion(s)

Drew, Michael G. B.; Nicholson, David G.

Volume of serial or monograph

1

Page or page range of portion

1543

Title of the article/chapter the portion is from

Stereochemical activity of lone pairs. The crystal and molecular structures of the salts of chloro(1,4,7,10,13,16-hexaoxacyclo-octadecane)tin(II). Calculation of macrocyclic cavity size by force field methods

Author of portion(s)

Drew, Michael G. B.; Nicholson, David G.

Issue, if republishing an article from a serial

8

Publication date of portion

1986-01-01

CCC Terms and Conditions

1. Description of Service; Defined Terms. This Republication License enables the User to obtain licenses for republication of one or more copyrighted works as described in detail on the relevant Order Confirmation (the "Work(s)"). Copyright Clearance Center, Inc. ("CCC") grants licenses through the Service on behalf of the rightsholder identified on the Order Confirmation (the "Rightsholder"). "Republication", as used herein, generally means the inclusion of a Work, in whole or in part, in a new work or works, also as described on the Order Confirmation. "User", as used herein, means the person or entity making such republication.
2. The terms set forth in the relevant Order Confirmation, and any terms set by the Rightsholder with respect to a particular Work, govern the terms of use of Works in connection with the Service. By using the Service, the person transacting for a republication license on behalf of the User represents and warrants that he/she/it (a) has been duly authorized by the User to accept, and hereby does accept, all such terms and conditions on behalf of User, and (b) shall inform User of all such terms and conditions. In the event such person is a "freelancer" or other third party independent of User and CCC, such party shall be deemed jointly a "User" for purposes of these terms and conditions. In any event, User shall be deemed to have accepted and agreed to all such terms and conditions if User republishes the Work in any fashion.
3. Scope of License; Limitations and Obligations.
 1. All Works and all rights therein, including copyright rights, remain the sole and exclusive property of the Rightsholder. The license

created by the exchange of an Order Confirmation (and/or any invoice) and payment by User of the full amount set forth on that document includes only those rights expressly set forth in the Order Confirmation and in these terms and conditions, and conveys no other rights in the Work(s) to User. All rights not expressly granted are hereby reserved.

2. **General Payment Terms:** You may pay by credit card or through an account with us payable at the end of the month. If you and we agree that you may establish a standing account with CCC, then the following terms apply: Remit Payment to: Copyright Clearance Center, 29118 Network Place, Chicago, IL 60673-1291. Payments Due: Invoices are payable upon their delivery to you (or upon our notice to you that they are available to you for downloading). After 30 days, outstanding amounts will be subject to a service charge of 1-1/2% per month or, if less, the maximum rate allowed by applicable law. Unless otherwise specifically set forth in the Order Confirmation or in a separate written agreement signed by CCC, invoices are due and payable on "net 30" terms. While User may exercise the rights licensed immediately upon issuance of the Order Confirmation, the license is automatically revoked and is null and void, as if it had never been issued, if complete payment for the license is not received on a timely basis either from User directly or through a payment agent, such as a credit card company.
3. Unless otherwise provided in the Order Confirmation, any grant of rights to User (i) is "one-time" (including the editions and product family specified in the license), (ii) is non-exclusive and non-transferable and (iii) is subject to any and all limitations and restrictions (such as, but not limited to, limitations on duration of use or circulation) included in the Order Confirmation or invoice and/or in these terms and conditions. Upon completion of the licensed use, User shall either secure a new permission for further use of the Work(s) or immediately cease any new use of the Work(s) and shall render inaccessible (such as by deleting or by removing or severing links or other locators) any further copies of the Work (except for copies printed on paper in accordance with this license and still in User's stock at the end of such period).
4. In the event that the material for which a republication license is sought includes third party materials (such as photographs, illustrations, graphs, inserts and similar materials) which are identified in such material as having been used by permission, User is responsible for identifying, and seeking separate licenses (under this Service or otherwise) for, any of such third party materials; without a separate license, such third party materials may not be used.

5. Use of proper copyright notice for a Work is required as a condition of any license granted under the Service. Unless otherwise provided in the Order Confirmation, a proper copyright notice will read substantially as follows: "Republished with permission of [Rightsholder's name], from [Work's title, author, volume, edition number and year of copyright]; permission conveyed through Copyright Clearance Center, Inc. " Such notice must be provided in a reasonably legible font size and must be placed either immediately adjacent to the Work as used (for example, as part of a by-line or footnote but not as a separate electronic link) or in the place where substantially all other credits or notices for the new work containing the republished Work are located. Failure to include the required notice results in loss to the Rightsholder and CCC, and the User shall be liable to pay liquidated damages for each such failure equal to twice the use fee specified in the Order Confirmation, in addition to the use fee itself and any other fees and charges specified.
6. User may only make alterations to the Work if and as expressly set forth in the Order Confirmation. No Work may be used in any way that is defamatory, violates the rights of third parties (including such third parties' rights of copyright, privacy, publicity, or other tangible or intangible property), or is otherwise illegal, sexually explicit or obscene. In addition, User may not conjoin a Work with any other material that may result in damage to the reputation of the Rightsholder. User agrees to inform CCC if it becomes aware of any infringement of any rights in a Work and to cooperate with any reasonable request of CCC or the Rightsholder in connection therewith.
4. Indemnity. User hereby indemnifies and agrees to defend the Rightsholder and CCC, and their respective employees and directors, against all claims, liability, damages, costs and expenses, including legal fees and expenses, arising out of any use of a Work beyond the scope of the rights granted herein, or any use of a Work which has been altered in any unauthorized way by User, including claims of defamation or infringement of rights of copyright, publicity, privacy or other tangible or intangible property.
5. Limitation of Liability. UNDER NO CIRCUMSTANCES WILL CCC OR THE RIGHTSHOLDER BE LIABLE FOR ANY DIRECT, INDIRECT, CONSEQUENTIAL OR INCIDENTAL DAMAGES (INCLUDING WITHOUT LIMITATION DAMAGES FOR LOSS OF BUSINESS PROFITS OR INFORMATION, OR FOR BUSINESS INTERRUPTION) ARISING OUT OF THE USE OR INABILITY TO USE A WORK, EVEN IF ONE OF THEM HAS BEEN ADVISED OF THE POSSIBILITY OF SUCH DAMAGES. In any event, the total liability of the Rightsholder and CCC (including their respective employees and directors) shall not exceed the total amount actually paid by User

for this license. User assumes full liability for the actions and omissions of its principals, employees, agents, affiliates, successors and assigns.

6. Limited Warranties. THE WORK(S) AND RIGHT(S) ARE PROVIDED "AS IS". CCC HAS THE RIGHT TO GRANT TO USER THE RIGHTS GRANTED IN THE ORDER CONFIRMATION DOCUMENT. CCC AND THE RIGHTSHOLDER DISCLAIM ALL OTHER WARRANTIES RELATING TO THE WORK(S) AND RIGHT(S), EITHER EXPRESS OR IMPLIED, INCLUDING WITHOUT LIMITATION IMPLIED WARRANTIES OF MERCHANTABILITY OR FITNESS FOR A PARTICULAR PURPOSE. ADDITIONAL RIGHTS MAY BE REQUIRED TO USE ILLUSTRATIONS, GRAPHS, PHOTOGRAPHS, ABSTRACTS, INSERTS OR OTHER PORTIONS OF THE WORK (AS OPPOSED TO THE ENTIRE WORK) IN A MANNER CONTEMPLATED BY USER; USER UNDERSTANDS AND AGREES THAT NEITHER CCC NOR THE RIGHTSHOLDER MAY HAVE SUCH ADDITIONAL RIGHTS TO GRANT.

7. Effect of Breach. Any failure by User to pay any amount when due, or any use by User of a Work beyond the scope of the license set forth in the Order Confirmation and/or these terms and conditions, shall be a material breach of the license created by the Order Confirmation and these terms and conditions. Any breach not cured within 30 days of written notice thereof shall result in immediate termination of such license without further notice. Any unauthorized (but licensable) use of a Work that is terminated immediately upon notice thereof may be liquidated by payment of the Rightsholder's ordinary license price therefor; any unauthorized (and unlicensable) use that is not terminated immediately for any reason (including, for example, because materials containing the Work cannot reasonably be recalled) will be subject to all remedies available at law or in equity, but in no event to a payment of less than three times the Rightsholder's ordinary license price for the most closely analogous licensable use plus Rightsholder's and/or CCC's costs and expenses incurred in collecting such payment.

8. Miscellaneous.

1. User acknowledges that CCC may, from time to time, make changes or additions to the Service or to these terms and conditions, and CCC reserves the right to send notice to the User by electronic mail or otherwise for the purposes of notifying User of such changes or additions; provided that any such changes or additions shall not apply to permissions already secured and paid for.
2. Use of User-related information collected through the Service is governed by CCC's privacy policy, available online here:<https://marketplace.copyright.com/rs-ui-web/mp/privacy-policy>
3. The licensing transaction described in the Order Confirmation is personal to User. Therefore, User may not assign or transfer to any other person (whether a natural person or an organization of any kind) the license created by the Order Confirmation and these terms and

conditions or any rights granted hereunder; provided, however, that User may assign such license in its entirety on written notice to CCC in the event of a transfer of all or substantially all of User's rights in the new material which includes the Work(s) licensed under this Service.

4. No amendment or waiver of any terms is binding unless set forth in writing and signed by the parties. The Rightsholder and CCC hereby object to any terms contained in any writing prepared by the User or its principals, employees, agents or affiliates and purporting to govern or otherwise relate to the licensing transaction described in the Order Confirmation, which terms are in any way inconsistent with any terms set forth in the Order Confirmation and/or in these terms and conditions or CCC's standard operating procedures, whether such writing is prepared prior to, simultaneously with or subsequent to the Order Confirmation, and whether such writing appears on a copy of the Order Confirmation or in a separate instrument.
5. The licensing transaction described in the Order Confirmation document shall be governed by and construed under the law of the State of New York, USA, without regard to the principles thereof of conflicts of law. Any case, controversy, suit, action, or proceeding arising out of, in connection with, or related to such licensing transaction shall be brought, at CCC's sole discretion, in any federal or state court located in the County of New York, State of New York, USA, or in any federal or state court whose geographical jurisdiction covers the location of the Rightsholder set forth in the Order Confirmation. The parties expressly submit to the personal jurisdiction and venue of each such federal or state court. If you have any comments or questions about the Service or Copyright Clearance Center, please contact us at 978-750-8400 or send an e-mail to support@copyright.com.

Dear Sir/Madam

Thank you for your correspondence requesting permission to reproduce content from a Taylor & Francis Group content from our Journal in your thesis to be posted on your University's repository.

We will be pleased to grant the permission without fee on the condition that you acknowledge the original source of publication and insert a reference to the Journal's web site: www.tandfonline.com

This permission does not cover any third party copyrighted work which may appear in the material requested. Please ensure you have checked all original source details for the rights holder.

Please note that this licence **does not allow you to post our content on any third-party websites.**

Please note permission does not provide access to our article, if you are affiliated to an institution and your institution holds a subscription to the content you are requesting you will be able to view the article free of charge, if your institution does not hold a subscription or you are not affiliated to an institution that has a subscription then you will need to purchase this for your own personal use as we do not provide our articles free of charge for research.

Thank you for your interest in our Journal.

With best wishes,

Journal Permissions

Journals, Taylor & Francis Group

Permissions e-mail: permissionrequest@tandf.co.uk

Web: www.tandfonline.com

+ 4 Park Square, Milton Park, Abingdon, OX14 4RN

(+44 (0)20 8052 0600

Taylor & Francis is a trading name of Informa UK Limited,
registered in England under no. 1072954

P Before printing, think about the environment.

Information Classification: General

From: Sarah McOnie

Sent: 24 December 2021 02:49

To: Academic UK Non Rightslink <permissionrequest@tandf.co.uk>

Subject: gpss20: Silylation of electrophilic alkynes

Permissions Request

Type of use: Academic

Article title: Silylation of electrophilic alkynes

Article DOI: 10.1080/10426507.2021.2012473

Author name: Sarah L. McOnie & Kim M. Baines

Journal title: Phosphorus, Sulfur, and Silicon and the Related Elements

Volume number: *

Issue number: *

Year of publication: *

Name: Sarah McOnie

Street address:

Town: London

Postcode/ZIP code: Country: Canada

Email:

Telephone:

Intended use: To be used in your Thesis?

Are you requesting the full article?: Yes

Which University?: University of Western Ontario

Title of your Thesis?: Small Molecule Activation and Catalysis by Low Valent Group 14

Compounds

University repository URL: <https://ir.lib.uwo.ca/etd/>

Is this a “Closed” or “Open” deposit?: open

Additional comments:

Curriculum Vitae

Name:	Sarah McOnie
Post-secondary Education and Degrees:	The University of Western Ontario London, Ontario, Canada 2016-2022 PhD Mount Allison University Sackville, New Brunswick, Canada 2012-2016 B. Sc.
Honours and Awards:	NSERC CG-SM 2016-2017 NSERC USRA 2015
Related Work Experience	Teaching Assistant The University of Western Ontario 2016-2021 <i>Courses:</i> Introductory Chemistry I & II Organic Chemistry I Organic Chemistry for the Life Sciences Inorganic Structure and Bonding Organic and Inorganic Structure Elucidation Elucidation of Organic and Bioorganic Mechanisms Teaching Assistant Mount Allison University 2012-2016 <i>Courses:</i> Introductory Chemistry, Introductory Physical Chemistry, Introductory Biochemistry, Experiential Synthetic Chemistry
Relevant Coursework	Advanced NMR Spectroscopy Catalysis Bioorganic Chemistry and Methods

X-ray Crystallography
Organometallic Bond Activation

Publications:

McOnie, S. L.; Özpınar, G. Bourque, J. L.; Müller, T.; Baines, K. M.. “NH bond activation of ammonia and amines by ditetrelenes: key insights into the stereochemistry of nucleophilic addition” *Dalton Trans.*, **2021**, *50*, 17734-17750.

McOnie, S. L.; Baines, K. M. “Silylamination of Electrophilic Alkynes” *Phosphorus, Sulfur*, **2021**, doi: 10.1080/10426507.2021.2012473

Lucier, B. E. G.; Terskikh, V. V.; Guo, J.; Bourque, J. L.; **McOnie, S. L.;** Ripmeester, J. A.; HuaNg, Y. ; Baines, K. M. ” Chlorine-35 Solid-State Nuclear Magnetic Resonance Spectroscopy as an Indirect Probe of the Oxidation Number of Tin in Tin Chlorides” *Inorg. Chem.*, **2020**, *59*, 13651-13670.

Tashkandi, N. Y.; **McOnie, S. L.;** Bourque, J. L.; Baines, K. M. “The Diverse Reactivity of Isocyanides Towards Disilenes”, *Angew. Chem. Int. Ed.*, **2019**, *58*, 3167-3172

Conference Abstracts

McOnie, S.L.; Baines, K. M. “Lewis acidity and Mechanistic Insights into, Hydrosilylation Catalyzed by Cationic Group 14 Crown Ether Complexes”, CCCE 2021, August 18, 2021, Zoom conference (Oral)

McOnie, S.L.; Baines, K. M. “Mechanistic Insights into Hydrosilylation Catalyzed by Cationic Group 14 Crown Ether Complexes”, International Symposium on Silicon, July 5th, 2021. Zoom conference. (Poster)

McOnie, S.L.; Baines, K. M. “Mechanistic Insights into Hydrosilylation Catalyzed by Cationic Group 14 Crown Ether Complexes”, Physical Organic Mini-symposium, November 3, 2020, Zoom conference. (Oral)

McOnie, S.L.; Baines, K. M. “Hydrosilylation Catalyzed by Low Valent, Cationic Group 14 Crown Ether Complexes”, 102nd Canadian Chemistry Conference and Exhibition, June 4, 2019, Quebec City, QC. (Poster)

McOnie, S. L.; Baines, K.M. “Amine Functionalization by Ditetrelenes”, 101st Canadian Chemistry Conference and Exhibition, May 30, 2018, Edmonton, Canada. (Poster)

McOnie, S. L.; Baines, K.M. “Amine Functionalization by Ditetrelenes” Inorganic Discussion Weekend, November 4, 2017, Toronto, Canada. (Poster)

McOnie, S. L.; Tashkandi, N. Y.; Bourque, J. L. Baines, K. M. Isocyanides and Disilenes: New Chemistry from an Old Reaction. Short oral presentation presented at the International Symposium on Silicon, August 9, 2017, Ji’nan, China. (Oral and poster) Awarded a second-place prize.

McOnie, S. L.*; Tashkandi, N. Y.; Bourque, J. L.; Baines, K. M. “The Addition of Isocyanides to Disilenes: New Chemistry from an Old Reaction”. August 9, 2017.; 100th Canadian Chemistry Conference and Exhibition, May 30, 2017, Toronto, ON. (Poster)

McOnie, S. L.*; Briand, G. “(Dithiolato)bismuth Alkoxides for the Ring Opening Polymerization of Cyclic Esters”. 99th Canadian Chemistry Conference and Exhibition, June 7, 2016, Halifax, NS. (Poster)

